UNIVERSITA' DEGLI STUDI DI VERONA

DEPARTMENT OF

SURGERY, DENTISTRY, PAEDIATRICS AND GYNAECOLOGY

GRADUATE SCHOOL OF

LIFE AND HEALTH SCIENCE

DOCTORAL PROGRAM IN

CARDIOVASCULAR SCIENCE

WITH THE FINANCIAL CONTRIBUTION OF

UNIVERSITY OF VERONA

Cycle / year XXXIII / 2017

TITLE OF THE DOCTORAL THESIS

Role of sympathetic neurons in the control of cardiac cells

S.S.D. MED/11

Coordinator: Prof. GIOVANNI BATTISTA LUCIANI

Signature _____

Supervisor: Prof. GIUSEPPE FAGGIAN

Signature _____

Tutor: Prof. MARCO MONGILLO

Signature _____

Tutor: Prof. JULIA GORELIK

Signature _____

Tutor: Dr.ssa. TANIA ZAGLIA

Signature _____

Tutor: Dr. J. SANCHEZ-ALONSO-MARDONES

Signature _____

PhD candidate: LOLITA DOKSHOKOVA

Signature _____

Role of sympathetic neurons in the control of cardiac cells

Lolita Dokshokova
PhD thesis
Verona,
ISBN 12324-5678-910

University of Verona
Research Office – National and International PhD programmes
ph: 045.802.8608 – fax 045.802.8411 – Via Giardino Giusti 2 – 37129 Verona

ABSTRACT

This work focuses on the functional interaction of cardiac sympathetic neurons (SN) with resident myocardial cell types, including cardiomyocytes (CM) and cardiac fibroblasts (CF). The narration is organized in four main paragraphs, each with a specific introduction, relative methods and discussion. The first part describes the results achieved in the development of an improved culture method to promote maturation of primary CMs from neonatal rat hearts, which has yielded an optimized cell model suited for the study of CM-SN interaction. The second part focuses on the investigation of the functional effects of SN activation on co-cultured cardiomyocytes and the role of specific intercellular communication sites on SN-CM communication, including the subtype specific activation of β1 or β2 adrenoreceptors. The third part investigates the role of such specific contact sites on neurotrophin-mediated "retrograde" signaling between CMs and SNs. In the fourth part the determinants of SN-CF communication are studied, with a focus on the role of sympathetic neurotransmitters in the regulation of cardiac fibroblast proliferation and differentiation.

The heart is constructed by the ordered displacement of multiple cell types, including cardiomyocytes, endothelial and smooth muscle cells, fibroblasts, and immune resident cells. The heart is innervated by sensory, sympathetic, and parasympathetic neurons, which interact with and influence all cells in the tissue. Given the plethora of implications in myocardial biology, the identification of molecular mechanisms involved in the crosstalk between cardiac sympathetic nerves and cardiomyocytes, cardiac fibroblasts, or vascular cells, has a fundamental importance in understanding both normal and pathologic heart function.

Rationale of Chapter I: To understand better the communications between cardiomyocytes (CMs) and other cell types of the heart, we had to improve the existing experimental model of cultured neonatal rat CMs in vitro. The primary culture of neonatal rat cardiomyocytes is a frequently used model system to study morphology, biochemical/molecular biological and electrophysiological characteristics of the contractile heart cell. The success of this preparation has

derived from a number of advantages of the isolation of cardiomyocytes from the neonatal heart compared to isolation from adult hearts. Firstly, the preparation of neonatal cardiomyocytes is cheaper, less time-consuming and cells are handled like a common cell line. The isolation normally gives reasonable cell numbers, which can easily maintain in culture for relatively long times (up to 2-3 wks). Secondly, the cells are amenable to genetic manipulation using plasmid transfection or viral infection.

Together with these practical advantages, the culture of neonatal cardiomyocytes has several limitations. One of the problems is the purity of the preparation: contamination with non-cardiomyocytes is common, and dividing cells, mainly fibroblast, may impact on cell behaviour. Second, the intrinsic biology of neonatal CMs should be considered. The intracellular architecture, which in freshly isolated adult cardiomyocytes is highly organized and replicates that of native cells in the heart, is still immature in neonatal CMs. As such, the main intracellular Ca^{2+} store, the sarcoplasmic reticulum (SR), which is central to the excitation-contraction coupling at the base of the activation of cardiac contraction, appears in neonatal CMs with a perinuclear distribution and does not develop terminal specializations (i.e. terminal cisternae, dyads) as in the fully mature cells.

Aim of the Chapter I: To promote the maturation of neonatal CMs in order to preserve neonatal cellular plasticity in a more reliable and translatable cellular model which would replicate some of the characteristics of the cells isolated from adult hearts.

Results of Chapter I: By modifying the culture conditions in the neonatal CM preparation, through the removal of new-born serum and addition of a combination of growth factors typically used in adult CMs culture such as insulin, transferrin and sodium selenate, we obtained more highly differentiated cells, yet retaining the experimental flexibility of the model.

Neonatal CMs cultured with this “New” medium display higher sarcomere organization and develop regular distributed RyR2 clusters. The regular sarcomere deposition is accompanied by mitochondria allocated along the sarcomeres, where they are found in closer interaction with the SR.

Functionally, the organization of SR Ca^{2+} release units were supported by the dynamics of spontaneous Ca^{2+} release events, i.e. Ca^{2+} sparks, which were smaller and faster, more like Ca^{2+} sparks typical of mature and fully differentiated cells.
The distribution of mitochondria across the sarcomeres was similarly accompanied by functional consequences in terms of Ca^{2+} signalling. Activation of contraction associated Ca^{2+} transients was accompanied, in the cells cultured in "Standard" medium, by little elevation of mitochondrial Ca^{2+} levels, which were instead much higher in New cells. This behaviour is in line with a more developed Ca^{2+} signalling system in the modified culture conditions.
These culture conditions had additional changes suggesting a more "mature" phenotype, notably, the receptor expression level, with an increased expression of βeta-2 Adrenoreceptor (β2AR), supported by the functional imaging data.
Neonatal cardiomyocytes cultured under these new conditions show morphological, molecular and functional characteristics suggestive of a more advanced developmental stage, and may thus represent valuable in different scenarios, including basic and applied cardiovascular research.

Rationale of Chapter II: The Autonomic Nervous System (ANS) plays a crucial role in the maintenance of the homeostasis of all organs including heart. ANS is divided into two branches: the sympathetic and the parasympathetic system. The textbook view on cardiac physiology states that the cardiac sympathetic nervous system (SNS) modulates heart activity by norepinephrine (NE) which, once discharged by sympathetic neurons (SNs), diffuse into the myocardial interstitium. However, this view on the neurogenic control of heart functions does not completely fit with the physiologic requirements of the system, which needs that modulation of heart activity occurs rapidly, efficiently and in a repeatable way. In addition, this model fails to explain how the SNS can modulate heart activity through a wide range of actions spanning from the modulation of heart rate on a beat-to-beat basis and the regulation of cell size, in basal conditions, to the maximal chronotropic response, during the fight or flight response. On the contrary, these concepts fit well with the idea that NE is released in a restricted intercellular domain, as occurring in a synapse.

The sympathetic nervous system regulates cardiac function through the activation of β1 and β2 adrenergic receptors. Previous work from the laboratory of Kobilka has shown that at junctional sites between neurons and cardiomyocytes, β1AR are predominantly accumulated, and β2AR are transiently present. Unfortunately, the functional aspect of these transformations is still unknown.

Aims of Chapter II: To compare the Ca^{2+} dynamics of intercellular communication between sympathetic neurons and cardiomyocytes and determine their response upon local activation of an individual neuron.

To assess the role of β1 and β2 adrenergic receptors in the process of neuronal activation of neonatal cardiomyocytes.

Results of Chapter II: In this work, we used sympathetic neuron/cardiomyocyte co-cultures to investigate the dynamics of neuro-cardiac communication in a multi-cellular monolayer with complex interactions. The activation of sympathetic neurons with the Ach receptor agonist, nicotine, showed modulation of Ca^{2+} signalling, consistent with the inotropic effect of βAR stimulation, in interacting co-cultured cardiomyocytes. To gain more insight on neuro-cardiac communication, we used precise positioning of a drug-delivering pipette with a SICM system to perfuse nicotine locally on a single neuron in the culture. Interestingly, upon single neuron activation, only 22.5% of surrounding cardiomyocytes had βAR dependent Ca^{2+} modulation, a fraction compatible with that of cardiomyocytes interacting with a single neuron. This is in line with our previous demonstration that signalling between sympathetic neuron and cardiomyocytes occurs via direct interaction at the Neuro Cardiac Junction (NCJ), and that the synapse confines signalling to the cells in direct contact.

Our experiments show that the effects of neuronal activation on Ca^{2+} dynamics are predominantly due to β1AR stimulation. Interestingly, limiting the effect of neuronally-released NE to β2AR decreased calcium transient amplitude. This is in line with previous results showing that β2AR have a modest effect on Ca^{2+} dynamics (E Devic *et al.*, 2001), and with the receptor dynamic internalization and reappearance away from the neuro-cardiac membrane patch.

Collectively, this data shows how the neuronal distribution network determines what cells will receive sympathetic input and is in line with the concept of synaptic

communication. When translated to the heart, it supports that the dense innervation of the myocardium is necessary to achieve simultaneous modulation of Ca^{2+} signalling in all cardiomyocytes in the tissue.

Rationale of Chapter III: The sympathetic neurons require neurotrophins for their survival, differentiation, and healthy development. Neurotrophins are a family of secreted proteins which include nerve growth factor (NGF), brain-derived neurotrophic factor (BDNF), neurotrophin 3 (NT3) and neurotrophin 4/5 (NT4/5). NGF is considered the most important for the survival, innervation, and differentiation of sympathetic neurons.

It has been shown that myocytes can produce NGF (Shelton and Reichardt, 1984) which binds tyrosine kinase receptor TrkA and upregulates prosurvival genes. Given that the NCJ may also allow neurons to operate in a synapse, it is important to understand if retrograde myocyte to neuron trophic signalling, which is key for their growth and survival, may also take place at this contact sites.

Aim of Chapter III: To study the role of neuro-cardiac junction (NCJ) on sympathetic neuron survival and cardiac innervation.

Results of Chapter III: In this work, we investigated the role of retrograde signalling from CMs to SNs, and how it is crucial for neuronal survival and development. We provided morphologic evidence of NGF in CMs and TrkA NGF receptors in contacting neuronal varicosities. Also, we showed that retrograde trophic signalling between myocyte and neuron, which is key for their growth and survival, also takes place at this contact sites.

This hypothesis is firstly supported by the evidence that in heart sections, the high-affinity NGF receptor TrkA is found in correspondence to the neuronal varicosities. The distance between neuron and cardiomyocyte membranes is typically within 0.5 microns. Complementary to the NGF-sensing apparatus, immunostaining for NGF in myocardial sections showed the presence of the neurotrophin in CMs, mirroring the position of the presynaptic neuronal processes. These results indicate that in the heart the key molecular players of heart-neuron signalling are preferentially localized at the NCJ, supporting that the myocyte may locally release neurotrophin to the TrkA expressing neuronal ending.

We further showed in an in vitro model system, that junctional contact sites between the neuron and CM develop and grow in time by an NGF dependent mechanism. The observation guiding subsequent experiments was the remarkable effect that the co-culture with cardiomyocytes had on NGF dependency of SNs. NGF withdrawal from the culture medium of SNs cultured alone leads to shrinkage of the varicosities and death of most cells. However, in co-culture with CMs, neurons developed mature processes even in the absence of exogenous NGF and developed ramifications and intercellular contacts. Cardiomyocyte conditioned medium by itself fail to sustain neuronal survival, which was identical to that observed upon NGF removal. Together with the very low NGF concentration measured in the co-culture medium, suggest that intercellular NGF signalling may take place at localized signalling compartments in the close proximity between CM and SN.

Rationale of Chapter IV: Cardiac fibroblasts (CFs) are key cellular regulators of the highly dynamic myocardial extracellular matrix (ECM), which impacts on heart structure and function in both normal and pathologic conditions. CF-dependent ECM deposition and degradation have been attributed to the effects of a variety of factors, some of which take part to pathologic ECM remodelling and interstitial fibrosis, which compromises heart mechanics and predisposes to arrhythmias. There is a growing interest in identifying strategies to prevent CF activation. Based on the literature showing that CFs express sympathetic neurotransmitter receptors (Meszaros *et al.*, 2000), we test the hypothesis that the cardiac SNs are regulators of CFs biology in vivo.

Aims of Chapter IV: To compare the dynamics of intercellular communication between SNs and CFs.

To define the role of sympathetic neurotransmitters in the regulation of cardiac fibroblast proliferation and differentiation.

To analyse the effect of removing sympathetic neurons on the tissue fibrotic response upon myocardial infarction.

Results of Chapter IV: The analysis of the cell-to-cell interaction site, which was performed with SICM, an advanced methodology offering the unique advantage of reconstructing the surface profile of living cells non-invasively, has uncovered

significant differences between the neuronal interaction with CMs. Remarkably, the volume of the varicosities interacting with CF was smaller than the average volume of CM-interacting ones.

By establishing a structured contact with target cells at the NCJ, neuron-cardiomyocyte communication occurs rapidly, at high efficiency and potently. The morphologic aspects of the SN/CF interaction support that neuro-fibroblast interaction is underlain by different properties. Our experiments assaying signalling coupling between SN and CF show that the effect of neuronal activation on cAMP responses of connected CF support that intercellular SN-CF signalling does not follow the same dynamics. In fact, neuronal activation did not evoke significant activation of βAR responses in CF.

Our evidence indicates that the unconventional sympathetic neurotransmitter, Neuropeptide Y (NPY), has a role in regulating cardiac fibroblast proliferation and differentiation. It is well known that activation of the SNS occur immediately after myocardial infarction and is maintained elevated throughout the cardiac postischemic remodelling. It is remarkable, in line with the evidence accrued in vitro, that ablation of SN responses was effective in reducing the extent of myocardial fibrotic remodelling. The evidence thus supports that sympathetic neurons play a maladaptive role in the fibrotic response to myocardial ischemia. The condition associated with sympathetic neuron activation, input by NPY might stimulate fibroblast proliferation and fuel myocardial fibrosis. Complementarily, these results suggest that interfering with sympathetic neurotransmitter receptors different from the commonly used adrenergic receptor blockers might alleviate the degree of postischemic myocardial remodelling.

Table of Contents

ABBREVIATIONS

AraC	1-β-D-Arabinofuranosylcytosine
cAMP	Cyclic Adenosine monophosphate
CF	Cardiac fibroblasts
CM	Cardiomyocyte
CREB	Cyclic AMP responsive element binding
DAPI	4',6-diamidino-2-phenylindole
DBH	Dopamine β-hydroxylase
DM	Differentiating medium
DMEM	Dulbecco's Modified Eagle Medium
DTT	Dithiothreitol
Edn3	Endothelin-3
EdnrA	Endothelin receptor type A
EDTA	Ethylenediaminetetraacetic acid
ELISA	Enzyme-linked immunosorbent assay
ERK	Extracellular signal regulated kinase
FBS	Fetal bovine serum
FDM	First day medium
FRET	Fluorescence resonance energy transfer
Gs	G stimulatory
HS	Horse serum
IF	Immunofluorescence
IP_3	Inositol 1,4,5-triphosphate
KO	Knock out
L-DOPA	L-3,4-dihydroxyphenylanine
MCS	Multiple cloning site
MI	Myocardial infarction
NCX	Na^{2+}/Ca^{2+} exchanger
NE	Norepinephrine
NGF	Nerve growth factor
NMJ	Neuromuscular junction

NCJ	Neurocardiac junction
NPY	Neuropeptide Y
NT	Neurotrophin
P/S	Penicillin/streptomycin
PBS	Phosphate buffered saline
PCR	Polymerase chain reaction
PFA	Paraformaldehyde
PH	Phenylephrine
PI3K	Phosphatidylinositol 3-kinase
PKA	Protein kinase A
PLCγ	Phospholipase Cγ
RT-qPCR	Real time quantitative PCR
RyR	Ryanodine receptor
S.E.M.	Standard error of the mean
SCG	Superior cervical ganglia
SDM	Second day medium
SERCA	Sarco/endoplasmic reticulum Ca^{2+}-ATPase
SGN	Sympathetic ganglia neuron
SN	Sympathetic neurons
EM	Electron microscopy
TOH	Tyrosine hydroxylase
TRITC	Tetramethylrhodamine
TX-100	Triton X-100
NCJ	Neuro-cardiac junction
NRVM	Neonatal rat ventricular myocyte

CHAPTER I

"DEVELOPMENT OF A PROTOCOL FOR *IN VITRO* MATURATION OF NEONATAL CARDIOMYOCYTES"

Index

1. INTRODUCTION I

1. The heart: structure and function

1.1 Gross anatomy

The heart, thanks to its contractile activity, provides the blood enriched in oxygen and nutrients to all cells of the organism. The mammalian heart is divided in two main sections: i) the right one sustains the pulmonary circulation, ii) while the left one is responsible for the systemic circulation. Both sections contain two chambers named respectively *atrium*, and *ventricle*. The right (RA) and the left (LA) atria constitute the heart *base*, while the two ventricles fuse at the levels of the cardiac *apex*. Right and left atria are divided by the inter-atrial septum, while the interface between atria and ventricles is delimited by the atrioventricular (AV) valves (i.e. the tricuspid valve for the right section and the mitral valve for the left section), which guarantee unidirectional flow of the blood from the atria to the ventricles. The semilunar valves are located at the interface between the ventricles and great arteries and ensure blood flow from the ventricle to the arteries (**Fig.1.1**).

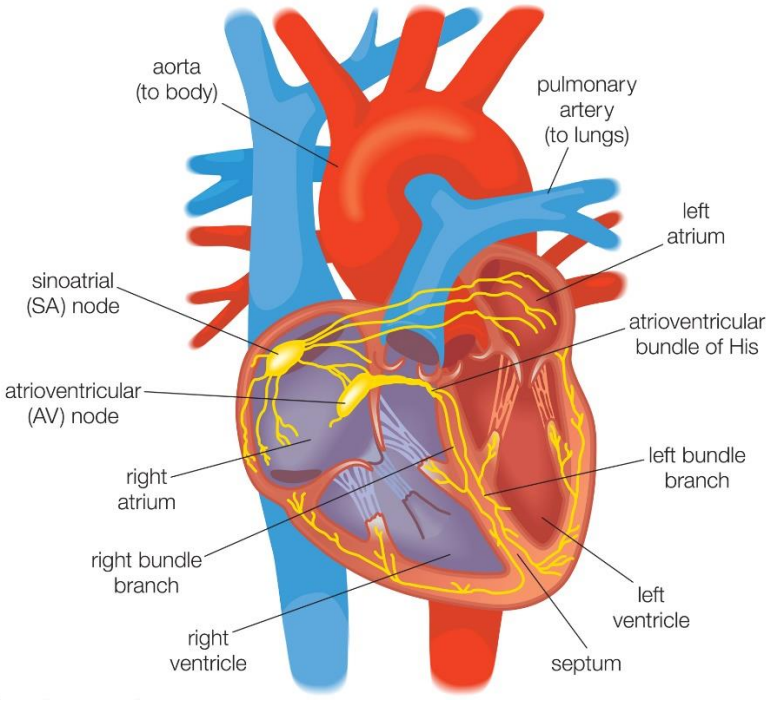

Fig.1.1 Gross anatomy of the heart (Encyclopædia Britannica, Inc 2010).

The larger cusps of the mitral and tricuspid valves are bound to fibrous structures called *chordae tendineae*, which link the valve leaflet to papillary muscles, projecting into the right and left ventricular cavities (Becker and De Wit, 1979) and are functional to the maintenance of correct valve plane during the heart cycle. At the level of the right stream, the pulmonary valve, consisting of three fibrous cusps that close during the diastole towards the lumen of the artery, enables flow of blood to the lungs. Here, the blood is oxygenated and subsequently transported, through four pulmonary veins, into the left atrium that is connected to the LV *via* the mitral valve. The LV is surrounded by a thick muscular wall, whose contraction pumps blood into the aorta, the main artery warranting transport of the oxygenated blood to all peripheral body districts (Netter, 2019). Right and left ventricles are separated by the inter-ventricular septum (Katz, 2011).

The cardiac wall is formed by three portions (Brutsaert, 1989), here listed from the outer to the inner:

1. the *epicardium*, a layer of squamous epithelial cells;
2. the *myocardium*, the thicker portion, responsible for contractile activity;
3. the *endocardium*, a layer of endothelial cells delimiting the lumen of the cardiac chambers.

1.2 Cytoarchitecture of the myocardium

The myocardium is an involuntary, striated muscle constituting the main tissue mass of the heart walls. Microscopically, we can look at the structure of myocardium. Most of the cells of the myocardium are the single cardiac muscle cells, namely *cardiomyocytes*. The cardiomyocytes are held together by extracellular matrix, secreted by *fibroblasts*. In addition, the myocardium tissue contains the cardiac conduction system carries electrical signals rapidly, and the coronary arteries bring nutrients and oxygen to the muscle cells, respectively. All these structures will be discussed in detail below.

1.2.1 The cardiomyocytes: ultrastructure

Cardiomyocytes (CMs) account for about 70% of the total cardiac volume and can be classified in two sub-types:

1. *the working cardiomyocytes*, which constitute the large majority of total CMs and are responsible for mechanical contraction. They are represented in the atria and the ventricular walls;
2. *the cardiomyocytes of the conduction system*, including the nodal cells of the Sino Atrial Node (SAN) and the Atrial Ventricular Node (AVN), the His bundle cells, the left and right branches and the distal portion the Purkinje Fiber (PF) network (Bailey, Lathrop and Pippenger, 1977). These cells are responsible for the origin and propagation of electrical signals and the synchronization of ventricular contraction.

The **working CMs** can be subdivided into atrial, smaller in size, and ventricular CMs. Moreover, inside the ventricular walls three subtypes of CMs can be distinguished for their different electrophysiological properties (Antzelevitch *et al.*, 1991; Moseley *et al.*, 1993). These cells are organized into three juxtaposed layers with different orientation which, starting from the outer to the inner part of the heart wall, are called: *subepicardium* (EPI), *midmyocardium* (MID) and *subendocardium* (ENDO). Recent studies performed in the murine heart, using diffusion tensor cardiovascular magnetic resonance (DTI) (Moseley *et al.*, 1993; Basser, Mattiello and LeBihan, 1994), allowed to precisely define CM orientation. While in the EPI and ENDO regions, the CM long axis is aligned parallel to the 'base-to-apex' direction, CMs of the MID have an orientation which progressively changes from the EPI to the ENDO regions (Jiang *et al.*, 2004; Schmitt *et al.*, 2009; Brunello *et al.*, 2013; Angeli *et al.*, 2014) (**Fig.1.2**).

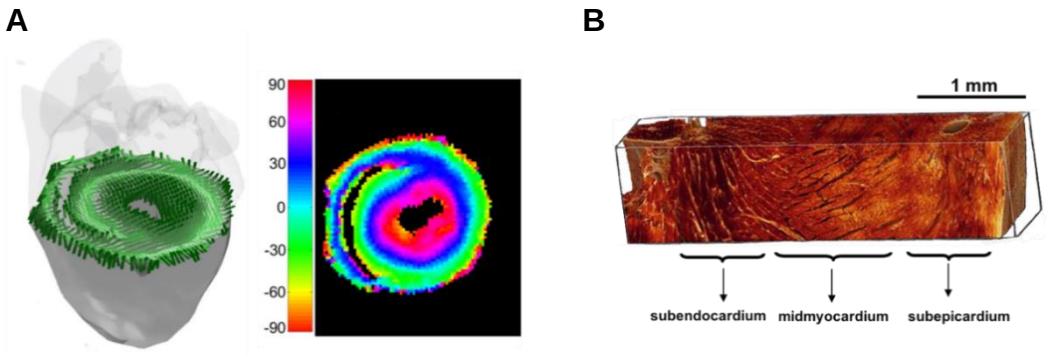

Fig.1.2 A. 3D reconstruction of the myocardial fiber orientation in the ventricles of mouse heart, obtained with DTI (left panel). False colour map indicating the angle formed by the intersection of the long axis of CMs and the transversal plane (right panel). **B.** 3D reconstruction of a ventricular myocardial section showing the complex cytoarchitecture of the tissue with highlighted the three regions composing the ventricular wall (Sands *et al.*, 2005; Healy, Jiang and Hsu, 2011).

Independently from their orientation and ventricular location, working CMs have an extremely organized structure and display common features. In comparison with skeletal muscle cells, CMs are narrower and much shorter, being about 25 µm wide and 100 µm long. CMs are often branched and contain from one to three nuclei located inside the cell. CMs are delimited by a plasma membrane, called *sarcolemma,* which forms regularly distributed deep invaginations, known as T-tubules (transverse tubules). Thanks to these invaginations, membrane depolarisation penetrates quickly throughout the cell, allowing voltage dependent Ca^{2+} influx to simultaneously activate 'Ca^{2+}-induced Ca^{2+} release' in multiple cell portions, by mechanisms that will be discussed in detail below.

Inside the CM, the 60% of the cell volume is occupied by myofibrils, whose fundamental contractile unit is represented by the 'sarcomere'. Electron microscopy (EM) analysis allowed to identify the sarcomere, as described by alternance of bright and dark bands characterized by a peculiar protein composition. A dark line, called *Z line* delimits the sarcomere, which is included between two successive Z lines. Thin filaments, identified as lighter bands, I bands at EM, connect the Z lines toward the sarcomere centre, which appears as a dark band, called *A band*, constituted by contractile proteins organized in thick filaments.

The thick filaments of the sarcomere are constituted by *myosin*, a complex protein in which three portions can be identified: i) the head, consisting of two heavy chains and two light chains and endowed with ATPase activity; ii) the joint, which changes conformation during the contractile cycle and iii) the tail, consisting of four light chains. Thin filaments are made up of two actin units and the interacting proteins tropomyosin and troponin complex [Troponin T (TnT), Troponin I (TnI) and Troponin C (TnC)] and are organized in such a way as to prevent, in basal conditions, the interaction of myosin with actin (Braunwald, Ross and Sonnenblick,

1967). As stated above, the confines of the sarcomere are delimited by the Z lines, which are occupied by the Z disks, constituted by a complex protein apparatus, including α-actinin, ZASP, desmin, titin and the tropomyosin complex, which contributes to maintaining the sarcomere structure (**Fig.1.3-1.4**). The mechanism of contraction bases on the sliding of the Z bands, dragged by the movement of the thin filaments of actin, towards the center of the sarcomere (*line M*). The trigger igniting the sarcomere contraction is the second messenger, Ca^{2+} (**Fig.1.5**).

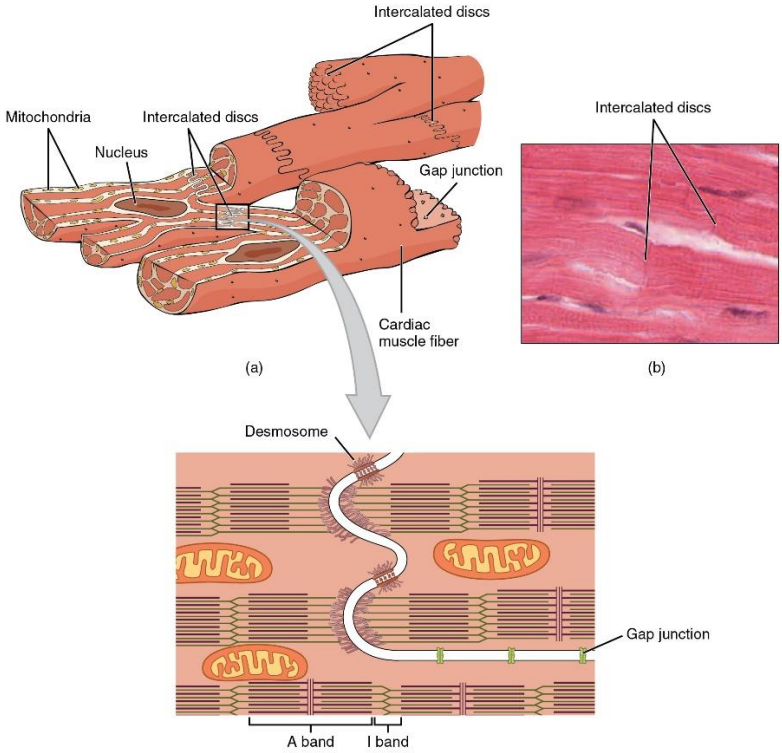

Fig.1.3 Anatomical illustration of Cardiac muscle. Cardiac muscles are striated and contain intercalated discs. The intercalated disks connecting the ends of adjoining cardiac myocytes contain desmosomes that link adjacent cells mechanically and gap junctions (Betts, 2017).

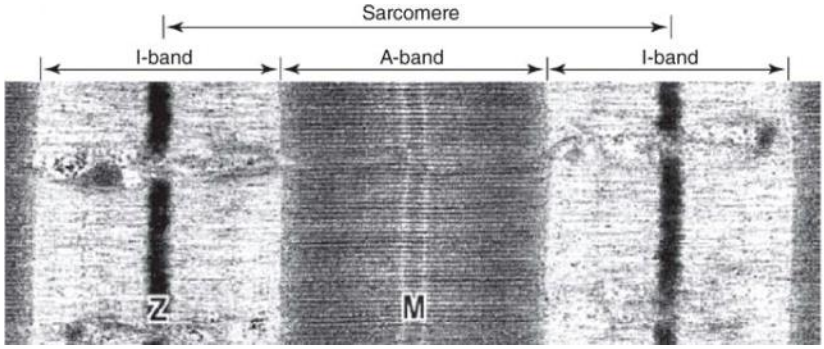

Fig. 1.4 Electron microscopy image of the muscle sarcomere (Henderson *et al.*, 2017).

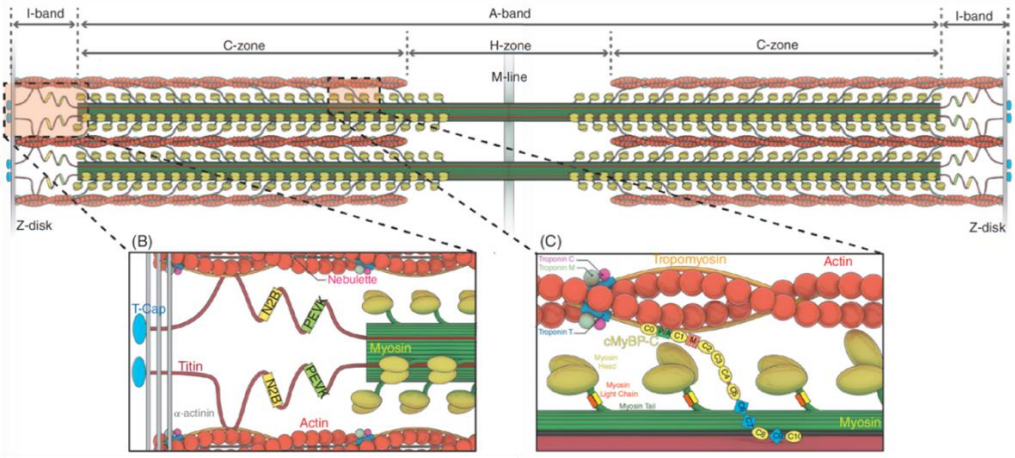

Fig. 1.5 Diagram illustrating the distribution of myofilaments and accessory proteins within a sarcomere. The titin molecules extend from the Z disc to the M line. Part of titin molecule is closely associated with a myosin thick filament the rest is elastic and changes length as the sarcomere contracts and relaxes. The actin filaments are coated with tropomyosin and are capped at both ends. Tropomodulin caps the minus end of the actin filaments at the Z disc, which also contains α-actinin (Lin, Song and Sadayappan, 2017).

1.2.2 Cardiomyocyte contraction: the excitation-contraction coupling

Differently from the skeletal muscle, the heart contracts autonomously, independently for neuronal inputs. The electrical stimulus which triggers heart contraction originates for specific cells, called *pacemaker cells*, which organize into the SAN, localized in the posterior RA wall, at the insertion of the superior cava vein (Tsien, 1979). The pacemaker cells, as all the cell of the conduction system, possess an intrinsic capacity of spontaneous depolarization, which is called automaticity. Since the SAN cells exhibit the fastest spontaneous depolarization

rate among all conductive CMs, this structure takes the lead and initiates heart depolarization waves. After been propagated to both atria, the depolarization wave reaches the AV insulating region and can only propagate through the AVN, where it is slowed by the connexin-45 (Cx45) expressing nodal cells. The Atria-Ventricular activation delay is fundamental for the correct sequence of contraction of atria and ventricles. Once passed through the AVN, the depolarization wave reaches the His bundle in the IVS, where it divides into the RBB and LBB, which propagate the electrical impulse to the distal part of the PF network, which is, in turn, interspersed throughout the ventricles and contact the working ventricular CMs (**Fig.1.6**).

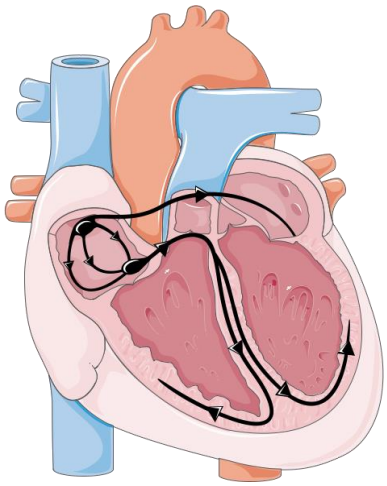

Fig.1.6 The cardiac conduction system (Katz, 2011).

At the end of the activating action potential (AP), each heart cell is re-polarized by the action of a complex set of currents, restoring the membrane potential at its baseline value (Katz, 2011). The rhythmic depolarization of the heart, described above, precedes every heartbeat and it is defined as sinus rhythm. Depolarization waves following different paths result in arrhythmic beats also known as ectopic or extra-systolic beats, causing the so-called premature ventricular contractions (PVC). Repetitive PVCs define arrhythmias, which originate when such aberrant depolarizations are sustained and thus overcome the sinus rhythm (Xie *et al.*, 2010; Myles *et al.*, 2012). Arrhythmias can be divided, based on their location, into: supraventricular (arising from atria and nodal cells) or ventricular and, based on

their effect on heart rate (HR), into tachycardia (increasing HR) or bradycardia (decreasing HR) (Priori *et al.*, 2015).

The process starting from the depolarizing wave triggering an AP and culminating in CM contraction, is called *Excitation-Contraction Coupling* (ECC) (Bers, 2002) and is represented in **Fig.1.7**.

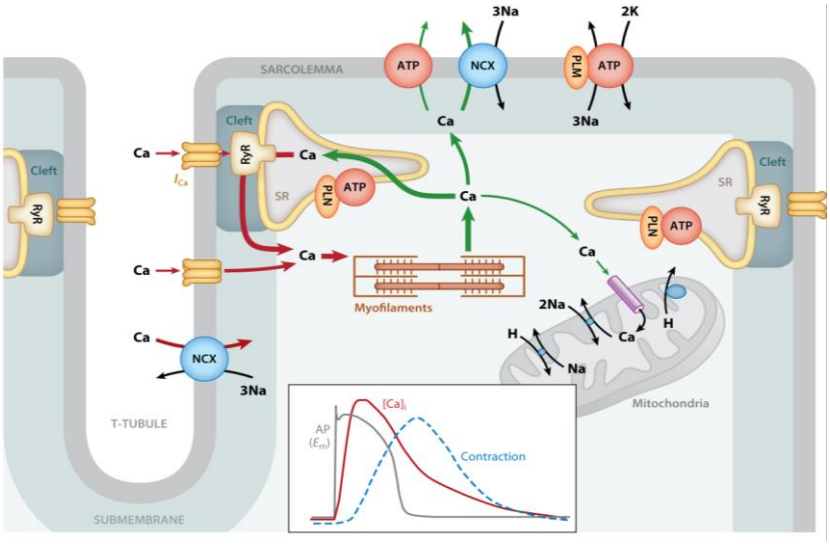

Fig.1.7 The role of Ca^{2+} in the ECC. Ca^{2+} supply is indicated in red, while the removal in green (Bers, 2002).

In detail, once reached the working CMs, the depolarization wave induces opening of L-type Ca^{2+} channels (LTCC), located in the T-tubules. The resulting Ca^{2+} influx into the cytoplasm opens of the intracellular Ca release channel RyR2, with a massive Ca^{2+} release from the SR. Ca^{2+} release from the SR is a passive flux which follows the concentration gradient with the low cytosolic [Ca^{2+}] (Fabiato, 1983). The elevated $[Ca^{2+}]_i$ in the cytosol allows sarcomere shortening. Interestingly, release of Ca^{2+} from the SR through a single RyR2 channel cluster does not cause a global increase in cytosolic Ca^{2+} but generates individual "elementary" Ca^{2+} release events, known as *Ca^{2+} spark* (Cheng, Lederer and Cannell, 1993). Features of these Ca^{2+} sparks, such as amplitude, duration and area, depend on RyR2, whose function is tightly regulated. Indeed, several proteins are known to bind the channels, mediating stabilization (Wehrens *et al.*, 2003; Lehnart *et al.*, 2006) or increasing flux (triadin, junction). Post-translational modifications of RyR2 also modulate the channel activity: indeed, its phosphorylation, either by CaMKII or

PKA, increases the channel open probability and the resulting release of Ca^{2+}, participating to the mechanism of positive inotropy caused by βAR (Lehnart *et al.*, 2004). SR-derived Ca^{2+} binds to TnC activating a conformational change in the troponin-tropomyosin complex and allowing actomyosin interaction. Once attached, myosin, with ATP dependent conformational change, pulls the actin filaments into the sarcomere centre, thus leading to sarcomere shortening. The interaction between myosin and actin occurs as long as cytosolic Ca^{2+} concentration remains elevated. At the end of contraction, Ca^{2+} is sequestered back into the SR by an ATP-dependent Ca^{2+} pump (SERCA2 ATPase), thus lowering cytosolic [Ca^{2+}] and removing Ca^{2+} from TnC. Troponin I, thanks to the conformational change of troponin complex induced by reduced intracellular [Ca^{2+}], is once again able to inhibit the actin-binding site on myosin, so that the initial sarcomere length is restored (Huxley, 1969). Ca^{2+} re-uptake, from the cytosol to the SR, is essential to restore the starting conditions before a new AP fires. In the adult CM, approximately 75-80% of cytosolic Ca^{2+} re-enters into the SR, the remaining is extruded from the cell *via* NCX (Na^{+}-Ca^{2+} Exchanger) (19-24%) or taken up by the mitochondria (1%) (Williams *et al.*, 2013). Ca^{2+} re-uptake from SR is mediated by SERCA, in an ATP-requiring process, as Ca^{2+} is transported against its concentration gradient. An essential regulator of SERCA2 is the interacting protein phospholamban (PLB), that keeps the pump in a low Ca^{2+} sensitivity state, thus slowing the re-uptake rate. Such inhibitory effect of PLB is reversed by its phosphorylation by PKA or CaMKII, whose effect is faster relaxation and increased SR load. Ca^{2+} extrusion from the cell is primarily exerted by NCX, located on the plasma membrane. By transporting 3 Na^{+} across the membrane in exchange for a single Ca^{2+} ion, NCX is an electrogenic mechanism of efflux, that generates an inward depolarizing current consequent to Ca^{2+} efflux. This depolarizing current is usually small and impacts on the membrane potential only for few millivolts, however, in the failing heart, or during cytosolic Ca^{2+} overload, can cause dangerous arrhythmic phenomena (Reuter *et al.*, 2005).

1.3 The cardiac syncytium

The contraction of ventricular CMs occurs in a synchronous and simultaneous way. This is ensured by the fact the cardiac muscle is a functional syncytium in which CMs are tightly connected mechanically and electrically to each other, thanks to specialized structures called intercalated disks (ID) (Weidmann, 1966; Weingart, 1974; Hoyt, Cohen and Saffitz, 1989; Franke *et al.*, 2006; Veeraraghavan, Poelzing and Gourdie, 2014). Three types of cell junction make up an intercalated disc: gap junctions (GJ), desmosomes (DS) and, fascia adherens (FA) (**Fig.1.8**).

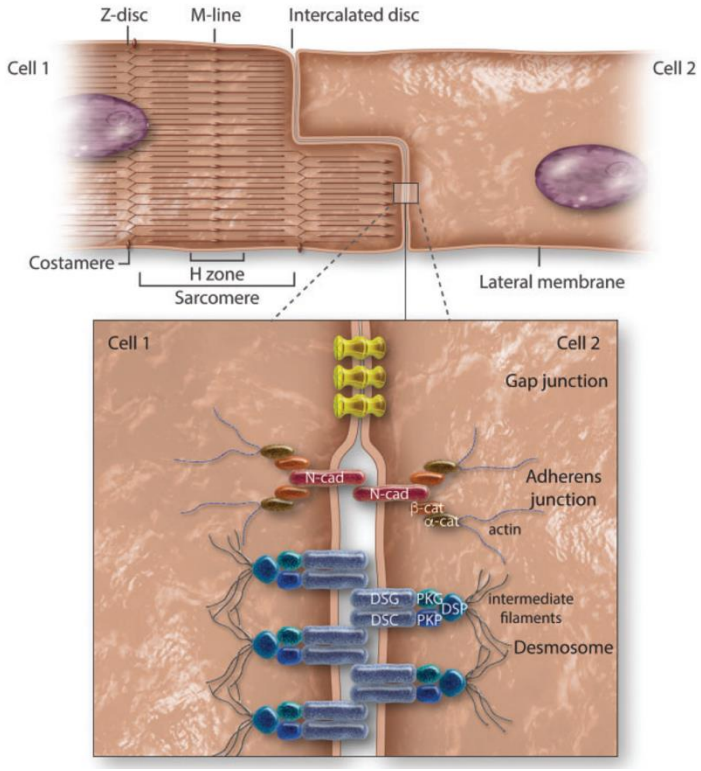

Fig.1.8 Organization of cardiomyocyte intercalated disks (Vermij, Abriel and van Veen, 2017).

- **Gap junctions**: these are specialized intercellular connections between channel-forming proteins on two adjacent cardiac cells, allowing electrical coupling. The rapid conductance of depolarization across cardiomyocytes allows the heart to function and contract as a coordinated unit called syncytium
- **Macula adherens**: this junctional complex directly attaches to the intermediate filaments and causes the cells to adhere tightly to a group. These specialized cell structures are also known as desmosomes.

- **Fascia adherens (or *fasciae adherents*)**: these are majorly the anchoring regions for actin.

Gap junctions. The electrical connection between adjacent CMs is operated by GJ non-selective channels which allow ions and small molecules to diffuse freely between the cytosol of connected CMs. These channels reduce internal electrical resistance, thus creating a functional syncytium in which all CMs are electrically coupled (Peters, 1996). GJs are constituted by proteins called connexins (Cx), which are arranged in hexamers at the sarcolemma to form a non-selective channel known as connexon, which represents half of the complete GJ (Franke *et al.*, 2006) (**Fig.1.9**).

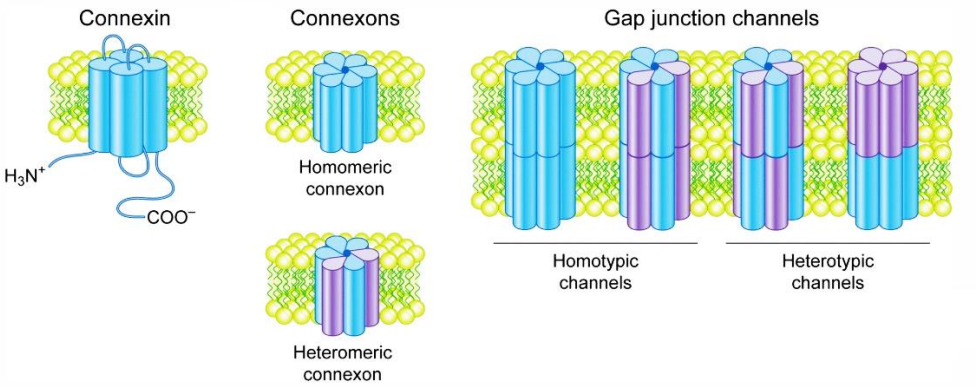

Fig.1.9 Gap junction channels (Totland *et al.*, 2020).

In the heart many different connexin isoforms are described, the most abundant being: connexin 43 (Cx43), connexin 40 (Cx40) and connexin 45 (Cx45). GJs formed by the different isoforms of connexin present different permeability to ions, thus conducting electrical impulse with different efficiency. Since GJs are the links between each single CM, this means that the speed of propagation of electrical *stimuli* is determined by the connexin type expressed (Gros *et al.*, 1994). Cx43 is the most abundant and it is expressed by all working CMs and the distal PFs; Cx40 is expressed in atrial working CMs, in coexistence with Cx43, and in PFs; Cx45 is expressed almost exclusively in SAN and AVN, while a very low expression was also detected in PFs (Van Kempen *et al.*, 1996; Kirchhoff *et al.*, 2000; Miquerol *et al.*, 2010).

Desmosomes allow the cardiac muscle to sustain the contractile activity for the entire lifespan. DS are multiprotein complexes involved in intercellular junctions in tissues subjected to mechanical stress, such as epithelium and cardiac muscle. They anchor the intermediate filaments of the cytoskeleton to the cytoplasmic membrane. Structurally, DS are made up of two main regions: an extracellular central domain (ECD), or "desmoglea", which has a key role in cell adhesion and a dense and symmetrical cytoplasmic plaque, which develops along the plasma membrane. Each plate is in turn divided into an outer dense plate (ODP) and an internal plate (IDP) onto which intermediate filaments (IF) are inserted. The region between the IDP and the IF is called the satellite zone (**Fig. 1.10**) (North, Hargreaves and McKendrick, 1999).

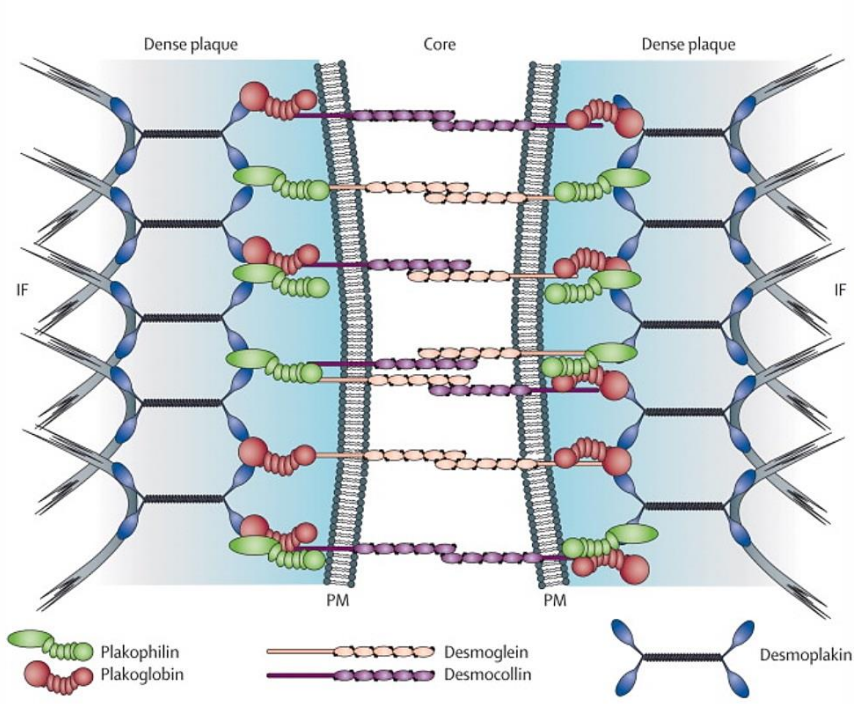

Fig. 1.10 Schematic representation of DS components (Basso *et al.*, 2009).

The proteins that make up DS are part of three families: i) the **desmosomal cadherins,** which include desmoglein (DSG) and desmocollin (DSC); ii) the **armadillo protein,** which include plakoglobin (JUP) and plakophilin (PKP) and, iii) desmoplakin (DSP) which is part of the **plakin family**. The desmosomal cadherins, desmocollins and desmogleins, are type I membrane glycoproteins, consisting of an intracellular C-terminal domain located in the ODP and an

extracellular domain involved in cell-cell adhesion and binding with Ca^{2+} ions (Basso *et al.*, 2009). Armadillo proteins are characterized by a central motif of variable repetitions, called arm, flanked by the C- and T-terminal domains. These proteins are located in the ODP and are involved in the assembly of DS and their adhesion activity (they mediate the contact between plakins and desmosomal cadherins).

Among the plakins, DSP plays an important role in CM junctions. DSP consists of an N-terminal domain located in the ODP, while the C-terminal domain is found in the IDP, thus allowing the contact between IF and the other proteins that characterize DS (Gallicano, 2001).

Fascia adherens. The adherens junctions (AJs) are a form of cell–cell adhesion structure observed in a variety of cell types. These structures are made up by the transmembrane protein E-cadherin, and the intracellular components, p120-catenin, β-catenin and α-catenin. The extracellular regions of these proteins mediate adhesion of cells to their neighbours, while the intracellular regions interact with an array of proteins (Meng and Takeichi, 2009). AJs display dual properties of robustness and plasticity. In multicellular organisms, they support both strong cell–cell adhesion and rapid cell–cell contact remodelling during development and wound healing. The core components of AJ are clusters of cadherin molecules, which mediate cell–cell adhesion through homophilic interactions in *trans*. Interactions of cadherins with the actin cytoskeleton are essential for providing both stability and plasticity to AJ. Cadherins regulate the turnover of actin by regulating its polymerization and anchor tensile acto-myosin networks at the cell cortex. In turn, actin regulates cadherin turnover by regulating its endocytosis and actomyosin networks exert forces driving remodelling of cell–cell contacts. The interplay between AJ and contractile acto-myosin networks has striking outcomes during epithelial morphogenesis. Their integrated dynamics result in different morphogenetic patterns shaping tissues and organs (Collinet and Lecuit, 2013).

1.4 Cardiac postnatal development: structural and functional differences between neonatal and adult cardiomyocytes

In the very first weeks after birth, the heart undergoes dramatic changes during differentiation of rat CMs, which lose the replicative capacity and continuing their growth through physiological hypertrophy. In order to maximize their contractile performance, and to fulfil the increasing perfusion demand of the growing organism, neonatal CMs face a profound process of maturation to the adult phenotype, characterized by alterations in sarcomere structure, energetic metabolism and Ca^{2+} handling (Anmann *et al.*, 2014). The hypertrophic process that leads neonatal CMs to acquire the size of adult cells includes synthesis and assembly of new sarcomeres, to maintain the contractile efficiency in a bigger cell. Concomitantly, several studies reported a switch in the expression of the two myosin isoforms: in mouse hearts, while neonatal cells predominantly express β-myosin, adult CMs express α-myosin (Lyons *et al.*, 1990). Changes in the proportion of myosin heavy chain (MHC) isoforms seem to be directly related to the degree of mechanical performance and efficiency of the heart as it switches from fetal to postnatal circulation. In the need of adapting cardiac performance to increasing perfusion requests, developing CMs tune their metabolism, increasing the efficiency of ATP production and its availability for contraction and relaxation. Many studies (Bass *et al.*, 2001) show that postnatal development of neonatal CMs is characterized by a switch from glycolic to oxidative metabolism. Indeed, if neonatal CMs mainly rely on glucose as main energetic source, up to 90% of ATP provided in adult CMs is obtained by oxidation of fatty acids. This process, triggered by the elevation of O_2 content, from uterus to external environment, ensures a higher efficiency of ATP production: in fact, if each glucose molecule yields 2 ATP molecules via anaerobic glycolysis, the same amount of carbon atoms undergoing oxidative phosphorylation yield 36 ATP molecules.

Oxidative phosphorylation consists in sequential reduction-oxidation reactions, in which electrons flow from a donor to an acceptor molecule, such as oxygen, through energy releasing processes. These reactions take place into mitochondria, where four enzymatic complexes that guide electron flow towards a fifth complex, known as ATP synthase, are localized in the inner mitochondrial membrane (IMM).

Remarkably, this process also grants the maintenance of efficient mitochondrial homeostasis, as the concomitant proton exclusion from the mitochondrial matrix sustains the negative mitochondrial membrane potential. Consistent with the increased energetic request and ATP production in adult CMs, compared to neonatal, a hallmark of CM postnatal development is represented by the increase in mitochondrial population (from 25% to 35%) (Piquereau *et al.*, 2010). Variations in mitochondria not only regard their quantity but, interestingly, their intracellular distribution: if neonatal cells display almost exclusively perinuclear mitochondria, in adult CMs at least three "sub-populations" can be distinguished, depending on their localization. Beside perinuclear mitochondria, also sub-sarcolemma and inter-myofibrillar mitochondria can be observed. The formation of different mitochondrial sub-population is part of a more complex "cellular program" whose aim is the compartmentalization of intracellular signalling and optimization of energetic resources, acted primarily by the creation of specialized structure (Piquereau *et al.*, 2010). This sophisticated mechanism, which marks the development from immature to mature CM and includes cytoskeletal reorganization and formation of communication points between organelles, includes several players such as T-tubules, SR, myofibrils and mitochondria. With the purpose to minimize waste of ATP, in adult CMs, the players involved in its production and consumption are tightly coupled: indeed, mitochondria are found juxtaposed to myofibrils, SR, and sarcolemma. These complexes are called Intracellular Energy Units (ICEUs) and represent the basic organization pattern of energy metabolism in adult CMs. The metabolic feedback within the single ICEUs is acted by phosphoryl transfer pathways, such as creatine kinase (the predominant, in CMs), adenylate kinase and direct ADP/ATP channeling. These enzymes, especially creatine kinase, have been found to increase in protein content during cardiac development to adulthood (Hoerter, Kuznetsov and Ventura-Clapier, 1991). In addition to the changes in cellular metabolism, CMs development is also accompanied to modifications in intracellular Ca^{2+} handling. During postnatal development the main intracellular Ca^{2+} store, the SR, reaches its complete maturation and becomes central to the Ca^{2+} fluxes that accompany cardiac contractions. In CM of neonatal hearts, the SR is composed by several vesicles

containing a limited amount of Ca^{2+} and, only in adult hearts, the SR is found in its typical structure made of well-defined "cisternae". Moreover, the Ca^{2+}-related proteins (e.g. SERCA, PLB, RyR2) regulating the release and re-uptake of Ca^{2+} from the SR, and thus the oscillation of its cytoplasmic concentration in the adult hearts, are increasingly expressed and correctly placed in the SR membrane only during postnatal development. In addition, CMs develop T-tubules, which are membrane invaginations that regularly cross the cytoplasm from one cell side to the other. These peculiar structures are enriched in ion channels, including LTCC, which are positioned with their intracellular side facing the RyR2 Ca^{2+} release channel on the SR cisternae; the juxtaposed T-tubular and SR membrane form the so called "dyads" (Seki *et al.*, 2003). These morphological differences between the subcellular structures in neonatal vs. adult CMs carry important functional differences and thus, the mechanism of excitation-contraction coupling differs between neonatal and adult CMs. This is of particular interest given that neonatal CMs are a widely used cellular model in cardiac research for their amenability to cell culture and genetic manipulation. Fetal and neonatal CMs have longer lasting contractions and their activation relies mostly on the influx of Ca2+ from the extracellular space. The Ca^{2+} cycle, during activation including both the influx and the efflux of the ion, occurs across the plasma membrane and is accompanied by depolarizing currents. The entry of Ca^{2+} from the extracellular space is mediated, also in this case, by the L-type Ca^{2+} channels located in plasma membrane. During diastole, Ca^{2+} is extruded from the CMs mainly through NCX and Plasma Membrane Ca^{2+} Pump ATPase (PMCA) (Carafoli, 1991; Carafoli, Garcia-Martin and Guerini, 1996).

1.5 Limitations of conventional cultured neonatal CMs

The neonatal rat cardiomyocyte culture was established by Harary and Farley in 1963 (Harary and Farley, 1963). The original procedure underwent a series of modifications and relatively standard protocols are now commonly employed.

The primary culture of neonatal rat cardiomyocytes is a frequently used model system to study morphology, biochemical/molecular biological (i.e. gene regulation, protein expression and localization) and electrophysiological

characteristics of the contractile heart cell. Success of this preparation has derived from a number of advantages of the isolation of cardiomyocytes from the neonatal heart compared to isolation from adult hearts. Firstly, the preparation of neonatal cardiomyocytes is cheaper, does not require optimization and a dedicated setup, it less time-consuming and cells are handled like a common cell line. The isolation normally gives reasonable cell numbers (approximately 1,5/2M cells/heart), which can easily maintain in culture for relatively long times (up to 2-3 wks). Secondly, the cells are amenable to genetic manipulation using plasmid transfection or viral infection.

Together with these practical advantages, the culture of neonatal cardiomyocytes has several limitations, some of which may be overcome, others which must be considered when using such model for cardiovascular research:

one of the problems is the purity of the preparation: contamination with non-cardiomyocytes is common, and dividing cells, mainly fibroblast, may impact on cell behaviour especially with the time in culture. In most experiments, it is likely that more than 20/30% of contaminating fibroblasts may disturb the analysis.

A second order of problems is intrinsic in the biology of neonatal cardiomyocytes. These cells are yet immature, and as such, the intracellular architecture, which in freshly isolated adult cardiomyocytes is highly organized and replicates that of native cells in the heart, is still immature. As such, the main intracellular Ca^{2+} store, the sarcoplasmic reticulum (SR), which is central to the excitation-contraction coupling at the base of the activation of cardiac contraction, appears in neonatal cardiomyocytes with a perinuclear distribution, and does not develop terminal specializations (i.e. terminal cisternae, dyads). The functional correlate of this aspect is that neonatal cardiomyocytes mostly use L-type Ca^{2+} channel ion entry to supply Ca^{2+} necessary for contraction. In addition, the sarcomeres, precisely organized in longitudinal, parallel repeats in adult cells are found along various directions in the neonatal cell. Furthermore, as was mentioned before, while three different populations of mitochondria can be identified in adult cardiomyocytes, based on their location (perinuclear, subsarcolemmal, intermyofibrillar) and shape (elongated vs. rounded), in neonatal cells mitochondrial subsets are not distinguished, and most of the organelles show a perinuclear radial displacement

resembling that of cultured fibroblasts. Mitochondrial tethering to intracellular Ca^{2+} release channels is similarly incomplete, with likely changes in the control of mitochondrial Ca^{2+} homeostasis.

All these characteristics indicate that while for some studies the advantages of cultured neonatal cardiomyocytes overcome their limitations, and are a suitable experimental model, improvements of the cell phenotype and maturation is needed to allow the detailed analysis of e.g. sarcomere dynamics, cytosolic and mitochondrial Ca^{2+} signalling.

2. AIM OF THE STUDY I

Optimize the culture conditions to promote the maturation of neonatal CMs in order to preserve neonatal cellular plasticity in a more reliable and translatable cellular model which can replicate some of the characteristics of the cells isolated from adult hearts.

3. METHODS I

3.1 Animal models

We used CMs isolated from neonatal (P1-P3) Sprague-Dawley rat hearts. All experimental procedures were performed according to the European Commission guidelines and have been approved by the local ethical committee and the Italian authority (Ministero della Salute), in compliance of Italian Animal Welfare Law (Law n.116/1992 and subsequent modifications), as well as of the guidelines of UK Home Office Animal (Scientific Procedures) Act of 1986 in London, UK.

3.2 Primary culture of neonatal cardiomyocytes

Cultured neonatal CMs were obtained from newborn (P1-P3) rat hearts. Rats were sacrificed by cervical dislocation and hearts quickly removed. Atria were carefully excised, then ventricles were collected in a 50 mL tube half-filled with ice-cold ADS Buffer 1x (**Tab.1**). Under a sterile hood, ventricles were washed to remove excess of blood then minced in a 10 cm Petri dish, placed on ice, in 5mL of ADS in order to obtain heart fragments around 1 mm^3. Mechanically minced ventricles were then transferred into a 50 mL sterile tube with a 5 mm magnetic stir bar. ADS Buffer was completely removed and replaced with 6 mL of Digestion Buffer (**Tab.1**) and positioned on a magnetic stirrer inside a water-bath at 37°C. The first cycle of 10 minutes (min.) allows to remove damaged cells so the supernatant was discarded at the end of this time. Another 6 mL of Digestion Buffer were added to the heart pieces for 20 min. always at 37°C on a stirrer. The supernatant of this cycle was then transferred to a 15 mL tube containing 1 mL of Horse Serum in order to block the enzymatic activity then centrifuged at 1250 rpm for 5 min. The supernatant was removed, and cells were re-suspended in 2.5 mL of first day medium (**Tab.1**) and maintained in the incubator until the digestion cycles were completed. Non-digested heart pieces repeated the digestion step previously described; usually a total of 8-10 cycles are required to complete the enzymatic digestion of 10 hearts. At the end of the digestion cycles, isolated cells were mixed and seeded in a 10 cm Petri dish (BD Falcon) and maintained in the incubator at 37°C for 1 hour. This pre-plating allows to separate CMs from cardiac fibroblasts that are characterized by faster adhesion to the dish. After the pre-plating step, cell

suspension, enriched in CMs, were collected in a new 50 mL tube. The total number of cells obtained was determined diluting cells in 0.2% Trypan Blue and counting viable cells in a Bürker chamber. CMs were then plated on laminin-coated glass coverslips (1.8 μg/100 mm^2) at a density of 470 cells/mm^2 for live imaging and immunofluorescence analysis, and of 550 cells/mm^2 for protein and RNA extraction. Then, 24 hours after isolation, cells were washed by ADS Buffer and the medium was replaced on the second day medium (**Tab.1**).

For the aim of this chapter two types of mediums Standard or New (see **Tab.1**) were used for all the experiments.

Table 1. Solutions and Medium used in this study.

ADS Buffer	
Components	**Concentration**
NaCl	106 mM
Hepes	20 mM
KCl	0.8 mM
$MgSO_4 \cdot 7H_2O$	5.3 mM
Glucose	0.4 mM
	5 mM
	pH 7.4

Digestion Buffer	
Collagenase A (Roche)	0.45 mg/mL
Pancreatin (SIGMA-Aldrich)	1.2 mg/mL
	in ADS Buffer

First Day Medium ("New Protocol")	
Component	**Concentration (v:v)**
MEM	88.8%
Fetal Bovine Serum (FBS, Gibco)	10%
Non-Essential Amino Acids (NEAA, Gibco)	0.1%
Penicillin/Streptomycin (P/S, Gibco)	1%
BrdU (100 μM in DMSO, SIGMA-Aldrich)	0.1%

Second Day Medium ("New Protocol")	
Component	**Concentration (v:v)**
MEM	98.8%
Insulin-Transferrin-Selenite (ITS, Gibco)	0.1%
Non-Essential Amino Acids (NEAA, Gibco)	0.1%
Penicillin/Streptomycin (P/S, Gibco)	1%

First day medium ("Standard protocol")	
Component	**Concentration (v:v)**
DMEM 25 mM-Hepes (Gibco)	67 %
M-199 (Gibco)	17.5%
Horse Serum (Gibco)	10%
Newborn Calf Serum (Gibco)	5 %
L-Glutamine (200 mM) (Gibco)	1%
Pen/Strep (Gibco)	1%

Second day medium ("Standard protocol")	
Component	**Concentration (v:v)**
DMEM 25 mM-Hepes (Gibco)	75 %
M-199 (Gibco)	17 %
Horse Serum (Gibco)	5%
Newborn Calf Serum (Gibco)	0.5 %
L-Glutamine (200 mM) (Gibco)	1%
Pen/Strep (Gibco)	1%

3.3 Immunofluorescence analysis on cultured cells

Cultured CMs, processed with the standard our new protocol, were fixed with formaldehyde 3.7% in 1X PBS (v/v, SIGMA Aldrich) for 30 min. at 4°C. After fixation cells were washed 3 times for 10 min. in 1X PBS, followed by cell permeabilization in PBS, supplemented with 1% BSA for 5 min. at room temperature. After washing in PBS, cells were incubated with the primary antibody diluted in PBS, supplemented with 1% for 2 hours at 37°C in a humidified chamber. At the end of the incubation with the primary antibody, cells were washed in PBS and then incubated with the appropriate secondary antibody, diluted in PBS, supplemented with 1% BSA, for 30 min. at 37°C. Nuclei were counterstained with DAPI (1:5000, v/v in PBS 1X) for 5 min. at room temperature. Finally, the coverslips were mounted with Elvanol over a glass slide (Vetrotecnica) and analysed at the confocal microscope Leica SP5 for morphological and

morphometric analyses. The primary and secondary antibodies used in this study are listened in **Table 3**.

Table 2. Solutions used in this study.

PBS 1X	
Component	**Concentration**
NaCl	137 mM
KCl	27mM,
KH2PO4	15 mM,
Na2HPO4·2H2O	9 mM
	in H2O, pH 7.0

Fixation solution	
Component	**Concentration (v:v)**
H2O	45%
Methanol	45%
Acetic acid	10%

Elvanol	
Component	**Concentration (v:v)**
PBS 1X	70ml
Polyvinyl alcohol (P-8136 Sigma)	10g
Glycerol	30ml
NaN3 1M	1ml

Table 3. Primary and secondary antibodies used in this study.

Secondary antibody	**Supplier**	**Dilution**
Anti-rabbit 488	Alexia Fluor	1:1000
Anti-mouse 546	Alexia Fluor	1:1000

Primary antibody	**Supplier**	**Dilution**	**Host**
α-actinin	Sigma	1:200	Mouse
dystrophin	Abcam	1:300	Rabbit
RyR2	Sigma	1:200	Rabbit
Tom20	Santa Cruz	1:100	Rabbit
Serca2a	Life Technologies	1:500	Mouse

3.4 Morphometric analyses

The images of ‘standard’ and ‘new’ CMs, acquired with a confocal microscope (see 3.3), were analysed using ImageJ software and the shape descriptors tool provided.

Different morphological parameters were considered: i) the mean CM area; ii) the ratio between the area occupied by sarcomeres and the total cellular area; iii) the aspect ratio (major axis/minor axis); iv), the roundness (4*area/π* major axis2; this coefficient is an index of the circumference like, shape of the cell); v), the solidity (effective area/convex area; being "convex area" the area of the polygon that best fits in), and vi) the plot profile (analysis of the intensity of fluorescence/pixel along a determined segment). For each experiment, twelve images were acquired and analysed. Both CM types ("Standard" *vs.* "New") were compared to isolated adult CMs.

3.5 In vitro transmission electron microscopy (TEM)

For *in vitro* TEM, cells were seeded directly on the plastic of 6-well plates, previously laminin-coated. Samples were fixed in 0.1M sodium cacodylate, supplemented with 2.5% glutaraldehyde, at pH 7.2 for 40 min. at 4°C and washed twice for 30 min. with 0.2M sucrose in 0.1M sodium cacodylate, at pH 7.2, maintaining cells on ice. After fixation, samples were processed in the TEM facility at the Department of Biology, University of Padova. Post-fixation was done in 0.1 M sodium cacodylate, supplemented with 1% osmium tetroxide, pH 7.2, for 2 hours at 4°C. Samples were then dehydrated in alcoholic solutions containing increasing ethanol concentration (50% for 15 min., 70% for 30 min., 90% for 30 min. and 100% for 90 min.), incubated with propylene oxide for 45 min. and embedded in epoxy resin. Resin embedding was performed with three successive 45 min. long incubations with different solutions of acetone/resin (2:1, 1:1 and 1:2) and incubating cells with 100% resin for 1 hour. Then fresh resin was added. Polymerization was performed with 3 repeated 24 hours incubations at 37°C, 45°C and 60°C. The resin was extracted from the wells and sections were cut, stained with 1% toluidine blue and observed at the light microscope. Sections of selected fields were stained with uranyl acetate, 50% ethanol and Reynolds lead citrate and examined with a FEI Tecnai 12 electron microscope.

3.6 RT-qPCR

Reverse transcription-polymerase chain reaction (RT-PCR) involves the same process as ordinary polymerase chain reaction (PCR) — cycling temperature to amplify nucleic acids.

The difference between PCR and RT-PCR is that in the first case there is amplification only deoxyribonucleic acids (DNA), and in the second case there is the amplification of ribonucleic acids (RNA) through the formation of complementary DNA (cDNA) by using specialized enzymes, known as reverse transcriptase (RT). By using specific primers, it is possible to control the exact part of cDNA which will be amplified.

RNA Extraction

The cells were washed two times in PBS 1X, and then covered by TripleXtractor (GB23, GRiSP) for 5 minutes and scraped from the bottom of the petri dish. After this step it is possible to store the mixture at the -80°C. If cells were frozen then they were incubated for 5 minutes at RT. The 100 µl of chloroform were added for each 500 µl of TripleXtractor, then the tubes with mixture were several times turned upside down to shuffle components properly and incubated for 2-3 minutes at RT. The columns were centrifuged at 12000 g for 15 minutes at 4°C and aqueous phase from the top were transferred into new tube.

Based on the amount of TripleXtractor which was used for cell extraction for each 500µl of TripleXtractor were added 250 µl of 100% isopropanol to the aqueous phase and incubated at RT for 10 minutes. After that the mixtures were centrifugated at 7500 g for 5 minutes at 4°C. The supernatant was removed, and the pellet was washed with 500 µl of 75% ethanol for every 500 µl of TipleXtractor used. The tubes were vortexed briefly and centrifugated at 7500 g for 5 min at 4°C. The supernatant was removed, and tubes were kept open under the laboratory fume hood till pellet got dry. After that the RNA were resuspended in 50 µl of RNAse/DNAse free H2O and mixed by pipette for proper RNA resuspension. The RNA was quantified by spectrophotometer NanoDrop2000 (Thermo Fisher Scientific). For the next step 400 ng of RNA needed, to calibrate RNA from

different samples the volume of needed RNA was calculated and RNAse/DNAse free H2O were added to obtain a final volume of 11.5 µl.

Reverse transcription of RNA

For each sample were prepared the first mix consisted by 11.5 µl of extracted RNA 400 ng, 1 µl of deoxynucleotide triphosphate (dNTPs) 10 mM, 1 µl of Random Primers mix 3 µg/µl. As positive control was used glyceraldehyde 3-phosphate dehydrogenase (GAPDH), and as negative control was used RNAse/DNAse free H2O. The tubes with mixes were placed in Thermal Cycler 2720 (Applied Biosystems) with 65°C for 5 minutes and then tubes were placed into ice for 2 minutes. Meanwhile were prepared the second mix consisted 4 µl Reverse Transcriptase Buffer 5x (18057018, Thermo Fisher Scientific), 1 µl of Dithiothreitol (DTT) 0.1M, 1 µl of RNAse out, 0.5 µl of Reverse Transcriptase. Then two mixes were mingled together and centrifuged to ensure all liquid is collected at the bottom of each tube, then again placed in Thermal Cycler 2720 (Applied Biosystems) with running program being used the next order: 5 minutes at 25°C) ⇒ 60 minutes at 50°C ⇒ 15 minutes at 70°C. After the program was completed, 30 µl of RNAse/DNAse free H2O was added to the tubes which already contained cDNA and were ready to use for PCR amplification.

Quantitative PCR (qPCR) or Real Time PCR

This step is used to detect and quantify nucleic acids for numerous applications. In standard PCR, DNA is amplified by 3 repeating steps: denaturation, annealing and elongation. In dye-based qPCR due to fluorescence labelling it is possible to quantify the amount of the amplified DNA by measuring proportional increases of fluorescence signal during each cycle as DNA replicates, according DNA is quantified in “real time”. In this work were used SYBR® Green is the most commonly used dye for non-specific detection. The dye emits at 520 nm and fluorescence emitted can be detected and related to the amount of targeted DNA.

To perform qPCR for each gen sample were prepared 5µl of SYBR Green 2x (Applied Biosystems) and 0.2 µl of primers mix 50 µM, consisted of synthetic primers - chemically synthesized oligonucleotides of DNA, which was customized

to a specific site determined by gene of interest from the cDNA sequence. The primer mix was including forward (FW) from 5' to 3'(→) direction primer and reverse (RV) which extend from 3'(←) primer. The qPCR white plate was carefully placed on the clean surface, which was pre-washed by RNAseZAP (Sigma-Aldrich). The wells were loaded by 5 µl of SYBR Green and primers mixture and then at the same wells were added 5 µl of cDNA diluted in RNAse/DNAse free H2O in 1:5 ratio respectively. As already noted, for each gen of interests were used a positive and negative control GAPDH and RNAse/DNAse free H2O. For each well the fresh filtered tips were used, and once plate was fully loaded the transparent seal was applied on the top of plate. The plate was shortly spun and placed in the Quant Studio 5 (Applied Biosystems) with running program being used the next order:

- denaturation: 95°C for 3 minutes
- 40 cycles of → denaturation at 95°C for 15 seconds;
  → primers annealing and extension at 64°C for 45 seconds.

The cycle quantification (Cq) value were analysed. It is the PCR cycle number at which sample's reaction curve cross the threshold line. The threshold is the point at which a reaction reaches a fluorescent intensity above background levels. Cq value tells how many cycles it took to detect a real signal from the samples, so it is possible to inverse these values too the amount of target nucleic acid, and correlate to the number of target copies in your sample. Lower Cq values (below 29 cycles) indicate high amounts of target sequence. Higher Cq values (above 38 cycles) indicate lower amounts of target nucleic acid. Delta-Delta Cq or the Livak normalization method was used. The primers used in this study are listened in **Table4**.

Table 4. Primers used in this study.

Primers	Supplier
Fw_rat GARGH	CACCATCTTCCAGGAGCGAG
Rev_rat GARGH	GGCGGAGATGATGACCCTTT
Fw_rat αAR 1a	GGTTGCTTCGTCCTCTGCT
Rev_rat αAR 1a	GAAATCCGGGAAGAAAGACC
Fw_rat αAR 1b	CCCTTCTTCATCGCTCTCC
Rev_rat αAR 1b	GGATTGAGGCAGCTGTTGA

Fw_rat αAR 1d	TTCTTCTTCGTCCTGCCTCT
Rev_rat αAR 1d	AGCGGGTTCACACAGCTATT
Fw_rat βAR 1	AGAGCAGAAGGCGCTCAAG
Rev_rat βAR 1	AGCCAGCAGAGCGTGAAC
Fw_rat βAR 2	TGCTATCACATCGCCCTTC
Rev_rat βAR 2	ACCACTCGGGCCTTATTCTT

3.7 Western Blotting

Protein extraction

The culture medium was removed from the plate and cells were washed with ice-cold sterile PBS. Cells were then incubated with ice-cold RIPA buffer (200µl for 50000 cells) (**Tab.5**) for 5 minutes, and whole cell protein lysates were collected, by scraping the culture dish, in a 1.5 ml tube, maintained on ice for 1 hour, and centrifuged at 12000 rpm for 10 minutes at 4°C. The supernatant was collected, and proteins were denatured at 70°C for 10 minutes, during constant mixing at 1250 rpm. Protein concentration was quantified by using the Bradford assay, as recommended by the manufacturer, subsequently validated with a Coomassie blue staining. Protein extracts were then aliquoted and stored at -80°C.

Electrophoresis

Gel electrophoresis is commonly used to separate biological molecules depending on their different molecular weights. To this purpose, 20 µg to 60 µg of protein extracts were added with a proper volume of Loading Buffer (**Tab.5**) and loaded on a 4-12% polyacrylamide gel (Life Technologies). The electrophoretic run was performed for 90 minutes at 100mV in 3-(N-morpholino) propanesulfonic acid (MOPS) buffer (Life Technologies). To test the quality of protein extracts, once the electrophoresis was completed, the polyacrylamide gel was stained with SimplyBlueTM SafeStain for 30 minutes at room temperature. The dye was fixed using the fixing solution described in (**Tab.5**) for 30 minutes at room temperature, followed by gel incubation in destaining solution (**Tab.5**) (1hour at room temperature). The dye emission of the stained gel was analysed with a luminometer Hyper processor (Amersham Biosciences).

Protein transfer

Proteins were then transferred on a methanol-activated polyvinylidene fluoride (PVDF) membrane (GE Healthcare, 0.2 μm porosity) by using Transfer Buffer (**Tab.5**) at 4°C, 400 mA for 90 minutes. After transfer, membranes were usually stained with Ponceau-red dye (SIGMA-Aldrich) to verify transfer efficiency and quality.

Membrane incubation with antibodies

Membranes were saturated in 0.1% Tween 20-Tris Buffered Saline (TTBS) (**Tab.5**) supplemented with 5% milk for at least 1 hour at room temperature, to reduce non-specific binding of the primary antibody to the membrane. After incubation with the primary antibody, membranes were washed with 0.1% TTBS 3 times for 10 minutes. The adequate Horse Radish Peroxidase (HRP) conjugated secondary antibody was incubated for 90 minutes at room temperature; other 3 washes were then performed. Finally, for the detection of immunoreactivity, we used the chemiluminescent HRP substrate (ECL Plus, Pierce). Chemiluminescence detection was performed with ImageQuant Las 4000 mini (GE Healthcare). Quantitative analysis of immunoreactivity, as a correlate of protein expression was performed by image analysis with Image J (National Institutes of Health, Bethesda, MD).

The antibodies used in WB are listened in **Table 2**.

Table 5. Solutions used in this study.

Loading Buffer	
Component	**Concentration (v:v)**
SDS 1%,	84%
Sample Buffer 1X	30%
DTT	6%

Destaining solution	
Component	**Concentration (v:v)**
H2O	88%
Methanol	5%
Acetic acid	7%

Lysis Buffer	
Component	**Concentration**
Tris	50mM
NaCl	150mM
MgCl2	10mM
DTT	0,5mM
EGTA	1mM
Glycerol	10%
SDS	2%
Triton	2%
Anti-phosphatase	1X
Anti-protease	1X
	in H2O, pH 7,5

Relaxation Buffer	
Component	**Concentration**
PFA 4%	25mM
PBS 1X	72mM
KCl	2,5mM

RIPA Buffer	
Component	**Concentration**
Tris	65 mM
NaCl	150 mM
Sodium Deoxycholate	0.025%
Np-40	1%
EDTA	1mM
Anti-phosphatase (Roche)	1X
Anti-protease (Roche)	1X

Rosso Ponceau	
Component	**Concentration (v:v)**
Red Ponceau	0.5%
Acetic acid	1%
	in H2O

Transfer buffer	
Component	**Concentration (v:v)**
Methanol	20%
NuPAGE Transfer Buffer 20X (Invitrogen)	5%
NuPAGE Antioxidant (Invitrogen)	0.05 %
H2O	75%

TTBS 0.1%	
Component	**Concentration**
Tris Base – HCl (pH 7.6)	50mM
NaCl	150 mM
Tween20	0.1%

3.8 Live imaging of Ca^{2+} dynamics

Neonatal CMs were loaded with the fluorescent Ca^{2+} indicator Fluo4-AM (1.5 µMol/L) for 20 minutes at 37°C, washed in Tyrode solution (in mM/L, 125 NaCl, 5 KCl, 1 Na3PO4, 1 MgSO4, 5.5 glucose, 1.8 CaCl2, 20 HEPES, pH 7.4) for 10 min at 37°C to let de-esterification of the dye. The coverslip was held in the cell chamber and placed at the confocal microscope (Leica TCS SP5), equipped with a oil immersion x40 objective (NA1.4). CMs were electrically stimulated at 1 Hz through parallel platinum field electrodes at RT. Cells were stimulated for one minute prior to imaging Ca^{2+} sparks, which were recorded after ceasing pacing. The line-scan mode was used to increase temporal resolution. Fluo-4 fluorescence was excited with the 488-nm line of an argon laser, and emission was selected through a 525/40mn bandpass filter. Images were acquired using the proprietary software LAS AF (Leica Microsystems), and analysed using the "SparkMaster" plugin in ImageJ (Wayne Rasband, NIH Bethesda USA), a program for automated Ca^{2+} spark analysis in confocal line-scan images, (Picht *et al.*, 2007). The program provides histograms of individual spark parameters such as Amplitude, Full Width at Half Maximum (FDHM) and Full Duration at Half Maximum (FDHM).

3.9 Live imaging of cAMP dynamics

To study the cAMP dynamics in living cells we used the FRET-sensor Epac-S^{H187} (Klarenbeek *et al.*, 2015).

FRET-based imaging experiments were performed in 4–15 days culture. Cells were infected 48 hours before the experiment using an adenoviral construct expressing S^{H187} gene. The virus was applied for 24 hours (it was kindly gifted by Prof. Kostantinos; 1µl of virus in 2 ml of culture medium) then washed out and replaced by fresh culture medium. During live imaging experiment, cells were maintained in Tyrode solution (in mM/L, 125 NaCl, 5 KCl, 1 Na^3PO^4, 1 $MgSO^4$, 5.5 glucose, 1.8

$CaCl^2$, 20 HEPES, pH 7.4) at RT. Imaging was performed with an inverted Olympus IX50 microscope, equipped with 40x oil immersion objective (1.3 NA); Cells were illuminated through a 430/40nm bandpass filter, and emission was acquired in two separate channels centred at 480/25 and 545/40 nm, for detection of CFP fluorescence and sensitized emission of YFP, respectively. To activate the cAMP production in cardiomyocytes cells were superfused with norepinephrine (NE) at 10 nM and 100 nM. Stimulation of cAMP synthesis with Forskolin (FK) and inhibition of phosphodiesterase with 3-Isobutyl-1-methylxanthine (IBMX) were used to elicit maximal cAMP accumulation and determine the sensor dynamic range. The analysis was performed with ImageJ, and changes of cAMP were measured in the cell cytosol by measuring the ratio between 480 nm and 545 nm fluorescence emission signals upon excitation at 430nm, after background subtraction.

3.10 Statistical analysis

All data are expressed as the mean ± SEM. Experimental groups were compared using unpaired (paired when appropriate) T-test. $P < 0.05$ was considered statistically significant.

4. RESULTS I

4.1 *In vitro* cardiomyocyte maturation: choosing the right medium

To develop a new protocol able to induce maturation of neonatal CMs, we focused on the composition of the media, maintaining the traditional technique to isolate cells from neonatal rat hearts (as described in Methods). Differently from the Standard medium, which is mainly constituted by DMEM (Dulbecco's Modified Eagle Medium), our New medium is based on MEM (Minimum Essential Medium). The lower glucose content (5 mM *vs.* 25 mM) led us to choose MEM as mainly constituent of both first and second day medium, to maintain cells in a glucose concentration similar to the physiologic (Pradhan et al. 2010). Considering that the fetal serum tends to maintain cells in an undifferentiated state, we decided to lower the total serum content in both the first and the second day medium (from 15% in Standard medium to 10% in New medium, in first day medium, and from 5.5% to 0%, in second day medium respectively). Additionally, we replaced horse serum (HS) with fetal bovine serum (FBS), thus reducing the amount of nutrients and growth factors. On the other hand, we added a combination of growth factors typically used in adult CM culture, such as insulin, transferrin and sodium selenate, known to preserve and enhance sarcomere arrangement of the cells. We assessed the effects of these modifications of culture conditions (from Standard to New protocol) on the cellular structural and functional phenotype, by using morphologic, morphometric, molecular and biochemical analyses.

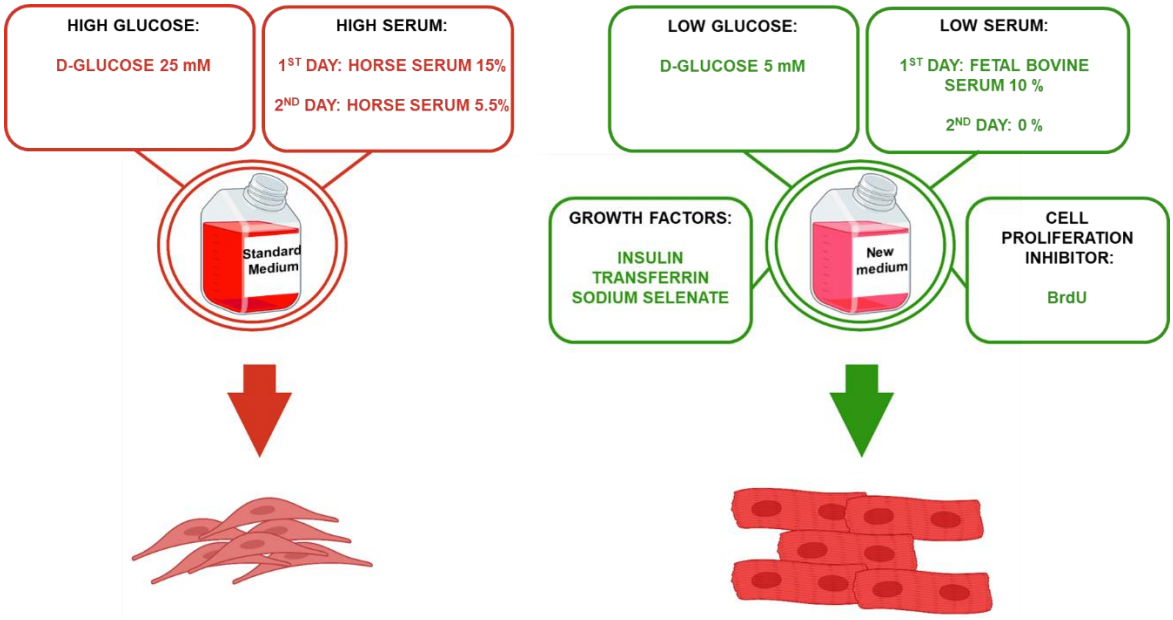

Fig.1.11 The key difference between the "Standard" and "New" protocols for neonatal CM culture. For the detailed protocol see Table1.

4.2 The new protocol of cardiomyocyte culture reduces fibroblast proliferation.

Although the standard procedure to obtain neonatal CMs includes steps to increase the CM fraction and its purity, among the several cell populations present in the tissue fragments, a small number of cells able to divide inevitably contaminates the preparation, especially in long-term cultures. Cardiac fibroblasts, which are not perfectly removed during preparation, have this potential and, upon differentiation into myofibroblast, increase collagen synthesis and secretion, establishing direct cell-cell coupling with CM. Both the direct interaction and the paracrine communication with CMs has the potential to induce CM de-differentiation (Nielsen *et al.*, 2009). With this in mind, we aimed at minimizing the stimuli that would promote fibroblast growth, which was already decreased by the reduction of glucose and the removal of serum in the culture medium, by adding from the first day after cell separation, the anti-proliferative agent bromodeoxyuridine (5-Bromo-β'-deoxyuridine, BrdU). BrdU is a thymidine-analogue that, once incorporated into newly synthetized DNA, inhibits cell division. Its effect on CM is negligible, given the very low mitotic index of these cells in culture. To assess the percentage of contaminating fibroblasts and, therefore, the purity of Standard *vs.* New CM culture, we performed IF analysis with specific markers to identify CMs. Double staining with an antibody specific for the sarcomeric protein α-actinin and the nuclear marker DAPI, allows to identify the CM fraction (positive for α-actinin) from the other cells present in the culture (positive to DNA-intercalated DAPI). Confocal microscopy showed that the non-CM cellular population was significantly decreased in cultures following the treatment with BrdU (CM fraction, New protocol: 85±5 *vs.* Standard protocol: 65±8, in %) (**Fig.1.12 A**).

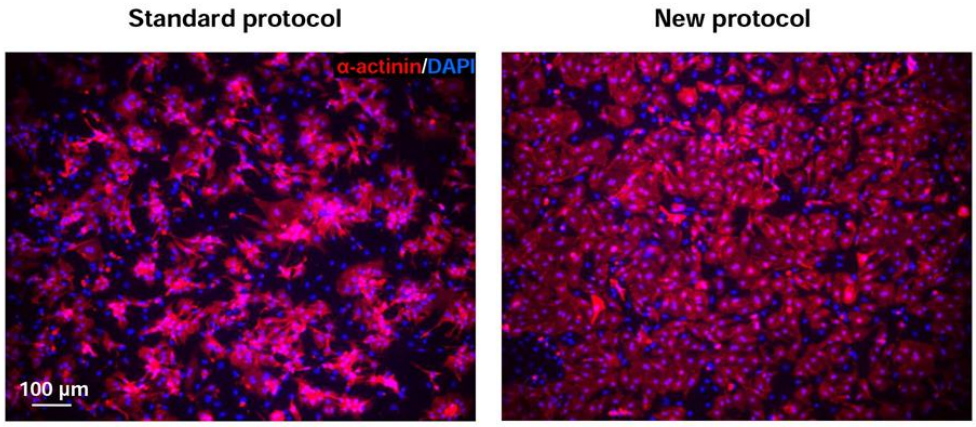

Fig.1.12 Establishment of a novel protocol to increase the purity of cultured neonatal cardiomyocytes. Representative IF image of rat neonatal CMs cultured with the Standard (left panel) and the New protocol (right panel). Cells were stained an antibody to α-actinin. Nuclei were counterstained with DAPI. This procedure allowed to estimate the percentage of "non-cardiomyocyte" nuclei among the total cells in the coverslip, providing a percentage of CM purity.

To investigate the effect of this treatment, equal number of cells were plated at the same density in Standard *vs.* New medium and, after 5 days, fixed and processed for WB. Immunoreactivity for α-actinin and SERCA2A resulted increased in New neonatal CMs, as compared to Standard CMs (**Fig.1.13**).

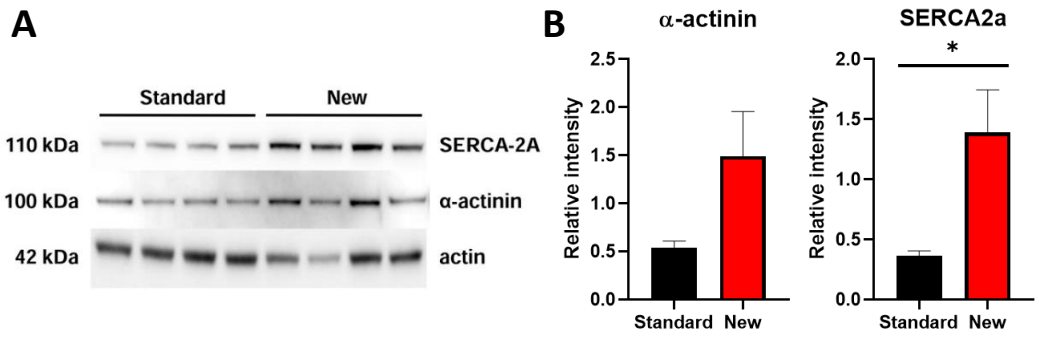

Fig.1.13 Analysis of cells cultured with different medium. A) WB analysis of protein extracts from CMs cultured with the Standard vs. New protocol. **B)** Histogram of western blot results, which represents relative intensity of α-actinin (0.5±0.1, 1.5±0.5) and SERCA2a (0.4±0.1, 1.4±0.4) normalised to actin for Standard and New CMs respectively. (n=3 replicates, error bars represent SEM).

This data suggests that the addition of anti-proliferative agent, BrdU, in the culture medium is useful to reduce the number of proliferating cardiac fibroblasts in culture, thus enhancing CM purity in culture and, at the same time, lowering the de-differentiative effect that fibroblast have on cultured CMs. In further support of this, while dystrophin localizes into the cytoplasm of neonatal CMs, CMs cultured with the modified protocol show a partial distribution of dystrophin along the sarcolemma (**Fig.1.14**).

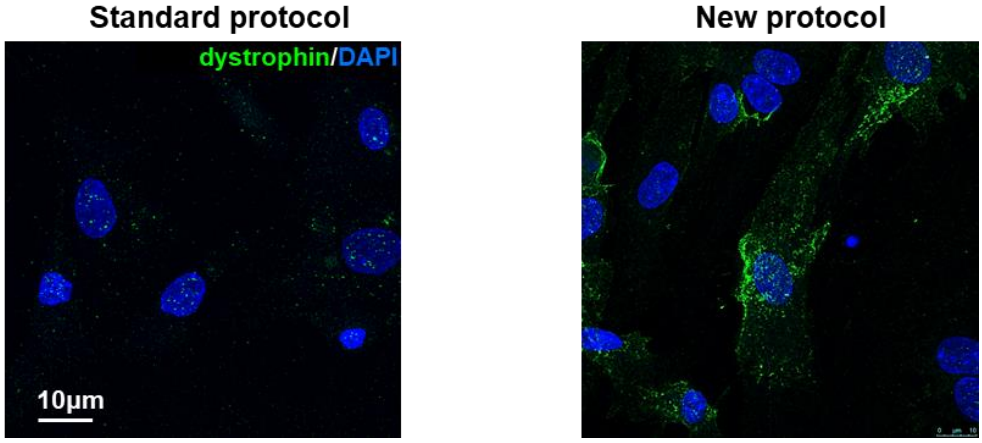

Fig.1.14 Neonatal CMs cultured with New medium display partial distribution of dystrophin protein around the perimeter of cells, while there is no signal from Standard ones. IF analysis on rat neonatal CMs cultured with the Standard (left panel) and the New protocol (right panel). Cells were stained an antibody to dystrophin. Nuclei were counterstained with DAPI.

4.3 Morphologic and morphometric characterization of cultured cardiomyocytes.

To assess the effect of the new culture protocol on CM structure, we immuno-stained the cells with an antibody specific for α–actinin and compared the size and shape of Standard *vs.* New CMs. The most evident difference between the two conditions regarded the size and shape of CMs, which showed a more regular and compact morphology, with homogeneous distribution along the surface with the New culture conditions. Conversely, CMs cultured with the traditional protocol tended to group in clusters showing radial ramifications that resulted in an irregular shape (**Fig.1.15**).

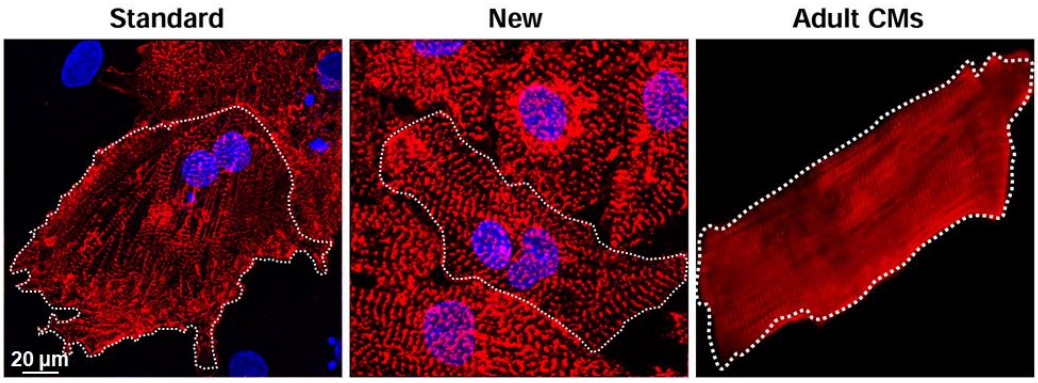

Fig.1.15 Neonatal cardiomyocytes cultured with the new protocol are more similar in shape to adult CMs. Confocal IF analysis on cultured rat neonatal CMs processed with the Standard (left) or New (right) protocol, as well as freshly isolated rat adult CMs. Cells were stained with an antibody to α-actinin. Nuclei were counterstained with DAPI. The white lines delineate the cellular profile.

These initial qualitative observations were followed by quantitative analyses on images acquired at the confocal microscope and analysed using ImageJ. The measurement of the mean cellular area showed that the CMs cultured following the New protocol were bigger, as compared to CMs cultured with the Standard protocol (CMs area: Standard: 800.8±28.2 *vs.* New: 1017.9±25.7, in μm^2) (**Fig.1.16 A**). Once fully developed, the adult CM is characterized by a compact cylindrical shape and, when isolated and plated, it adheres to the coverslip displaying a regular-rectangular shape, with an evident major axis and the absence of invaginations

(**Fig.1.15**, right image). To determine if the New protocol affected CMs morphology, we analysed the confocal images with specific plugins running in ImageJ, to evaluate several shape factors, including:

i) Aspect Ratio

ii) Roundness

iii) Solidity.

As reference, we performed the same analysis on adult CMs previously isolated in the laboratory.

Aspect Ratio (AR). This parameter is the ratio between the long and short axis of the cell. The ratio is highest in rod-shaped cells, such as isolated adult CMs. The analysis, performed in Standard, New neonatal and adult CMs, revealed that neonatal CMs cultured following the New protocol showed higher AR, with values closer to those of adult CMs than that of Standard neonatal cells (**Fig.1.16 B**).

Roundness. This coefficient is an index of the circumference-like shape of the cell. The mathematic formula is: $4*\text{area}/\pi*\text{major axis}^2$. Contrarily to AR, this parameter was chosen as indicator of less differentiated cells. The measurements performed showed that Standard neonatal CMs had higher roundness as compared to New neonatal CMs thus suggesting that, this latter cell type was more differentiated than the former. Consistently, adult CMs had the lowest roundness parameter, being mature (**Fig.1.16 C**).

Solidity. This parameter represents the ratio between the total cellular and the convex area, being this latter the area of the polygon that best fits in. Solidity indicates the degree of regularity of the perimeter. A regular perimeter, determined by absence of ramifications, is typical of adult mature CMs. Analysis of solidity showed higher values for New neonatal CMs as compared to Standard CMs, thus indicating a more regular and mature shape in the cells cultured following the newly developed protocol (**Fig.1.16 D**).

Globally this set of data demonstrates, with unbiased quantification methods, that, compared to Standard protocol for neonatal CMs preparation, the New conditions yield more elongated cells, with regular membranes, and allow obtain a morphologic phenotype more closely resembling that of CMs isolated from the adult heart.

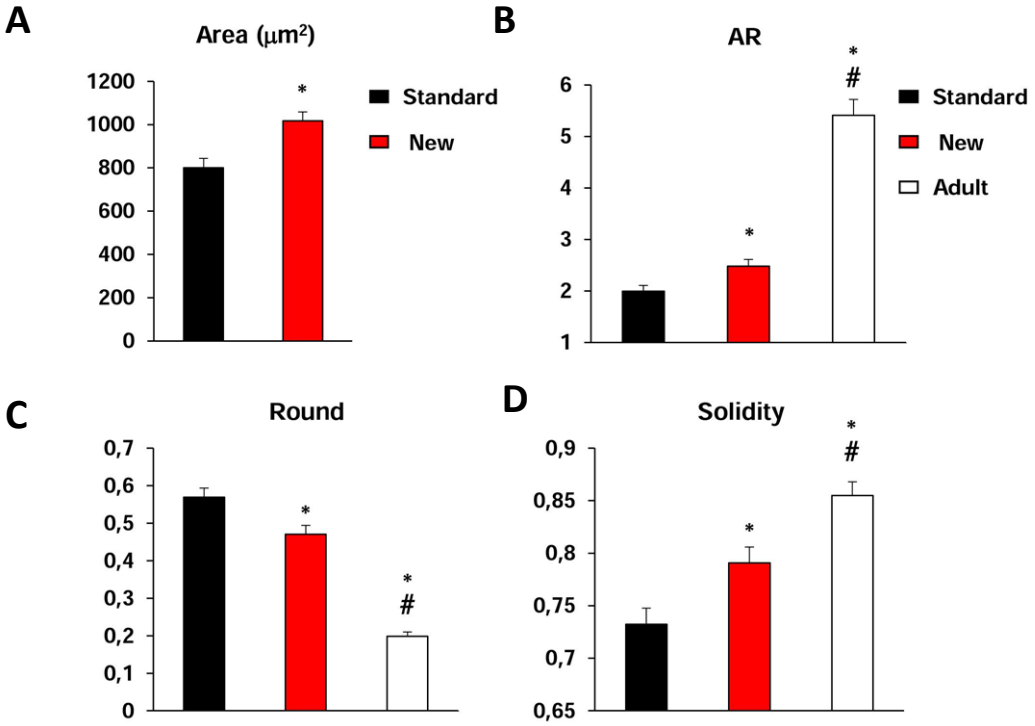

Fig.1.16 A) Evaluation of cell area measured in neonatal CMs cultured with Standard and New protocol. **B-D)** Morphometrical analyses (Aspect Ratio, Round, Solidity) performed on neonatal CMs cultured with the standard protocol (black bars) vs. the New protocol (Red bars) vs. adult CMs (white bars). (n=100 CMs per group, 3 cultures. *, $p<0.05$; ** $p<0.01$. * is referred to Standard CMs, # is referred to New neonatal CMs, bars represent SEM).

4.4 Analysis of sarcomere structure on cultured cardiomyocytes

The regular organization of contractile units in sequentially displaced sarcomeres is a hallmark of mature CMs. In the cells obtained from neonatal hearts, sarcomeres are not fully developed yet, and distribute roughly radially along the multiple cell membrane elongations, which may co-exist in different directions. To determine whether the New protocol may impact on sarcomere organization, we evaluated the distribution profile of α–actinin in cultured CMs. The images of CMs incubated with anti-α–actinin antibody were acquired at high detail with confocal microscopy and analysed with ImageJ (**Fig.1.17 A**). The degree of organization of α–actinin was estimated by fluorescence measurement along a hand-traced line paralleling the cellular major axis. The graphs in **Fig.1.17 B** show the plot of fluorescence intensity profile: as intensity of the fluorescence reflects immunoreactivity, intensity peaks are located in correspondence of Z-lines delimiting the sarcomere. While the fluorescence intensity profile observed in Standard neonatal CMs was irregular, in both peak intensity and frequency, New neonatal CMs showed increased organization and the peaks of fluorescence intensity were at a regular distance (about 1.6±0.07 μm). The analysis on adult CMs demonstrated perfect repetition of fluorescence peaks, detected at the regular distance of (1.8±0.04 μm). This data suggests that the New protocol promotes, in neonatal CMs, the organization of contractile apparatus, hallmark of mature adult CMs.

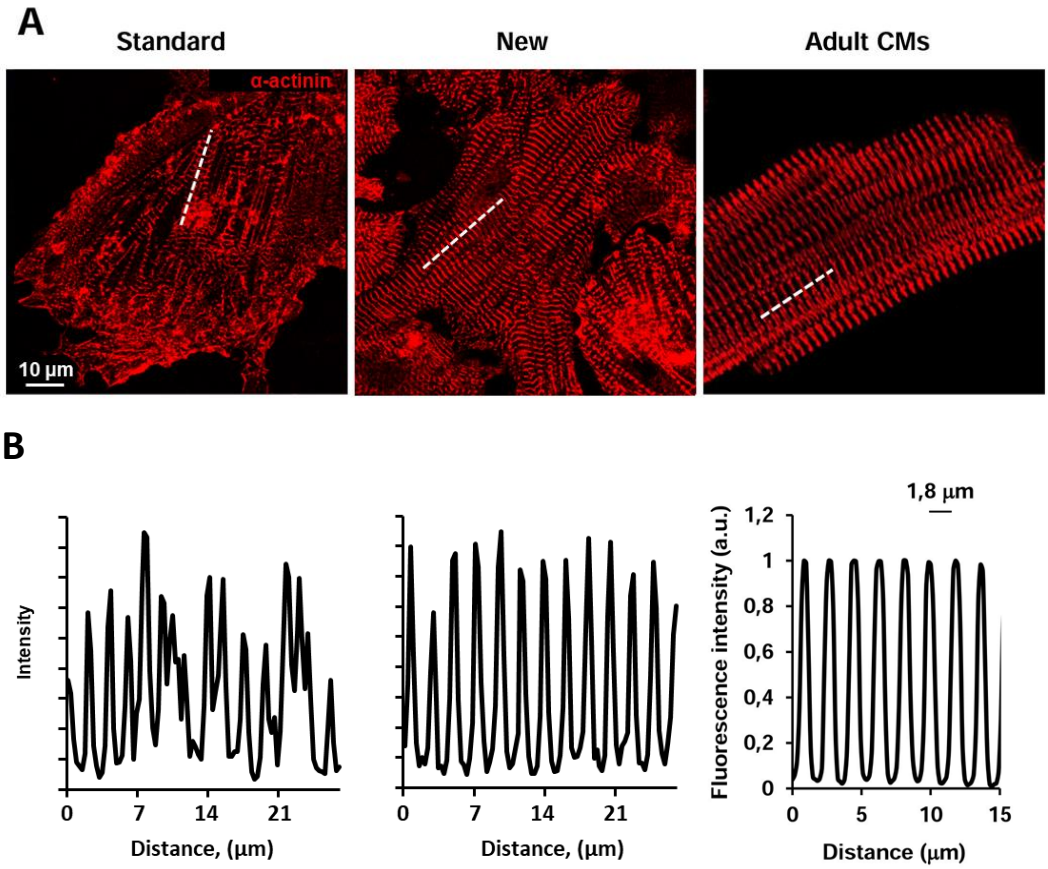

Fig.1.17 Neonatal cardiomyocytes cultured with the novel protocol display higher sarcomere organization. A) Representative Confocal IF images of neonatal CMs cultured with Standard or New protocol, as well as adult CMs, all stained with an antibody to α-actinin, to mark sarcomere structure. **B)** Fluorescence intensity analysis ("plot profile") of sarcomere α-actinin signal along the dashed line in (A) showed a more regular signal in New CMs compared to Standard ones, resembling the perfectly localized signal detected in adult CMs. (n=10 CMs per group).

4.5 Analysis of mitochondria on cultured cardiomyocytes

As previously described, one important difference between neonatal and adult CMs is represented by the displacement of the mitochondrial population. Indeed, neonatal mitochondria are almost exclusively found in the perinuclear region; conversely, the mitochondrial network observed in adult CMs shows three well-defined sub-populations: perinuclear, inter-myofibrillar and sub-sarcolemmal. We thus decided to investigate mitochondrial distribution by performing morphological analyses, using confocal IF analysis. IF staining performed on neonatal CMs cultured with the Standard and New protocol revealed that TOM20, a protein found in the Outer Mitochondrial Membrane (OMM), was different in the two experimental models. In Standard neonatal CMs, mitochondria were found in the typical perinuclear distribution, while New CMs showed mitochondria well positioned throughout the cell, in peripheral as well as inter-myofibrillar and sub-sarcolemmal regions (**Fig.1.18**).

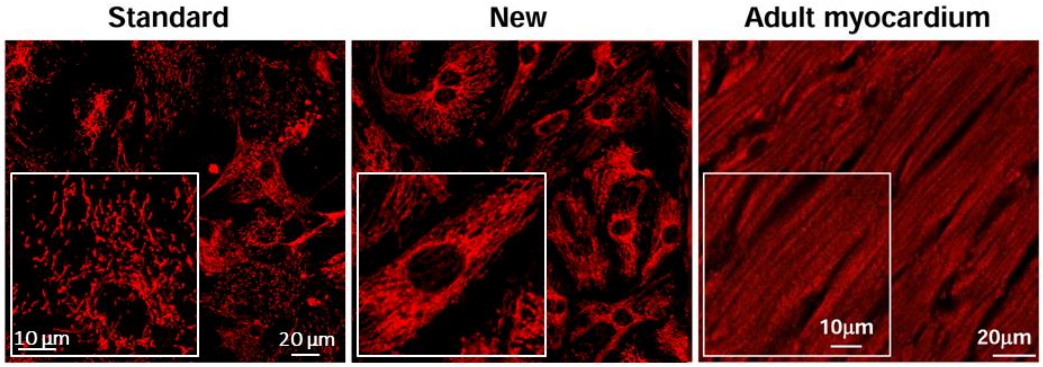

Fig.1.18 Neonatal cardiomyocytes cultured with the novel protocol display increased ultrastructural organization. Representative confocal IF images of neonatal CMs cultured with Standard or New protocol, as well as from a heart cryosection, all stained with an antibody to TOM20, to detect mitochondria.

Additionally, TEM images were analysed. Interestingly, New CMs displayed a higher organized structure, with mitochondria tightly placed along sarcomeres and SR cisternae. In line with this, mitochondria occupied a percentage of the total cellular area that was higher in New CMs (area mito/total area: Standard: 14.3±3.8 *vs.* New: 21.3±2.1, in %, (**Fig.1.19**).

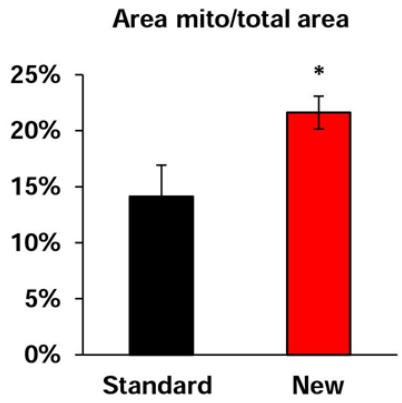

Fig.1.19 Measurement of the ratio between the area occupied by mitochondria and the total cellular area in Standard and New CMs. (n=20 CMs per condition; *, $p<0.05$, bars represent SEM).

Moreover, a light increase of electron density, which did not reach statistical significance, suggested a more developed oxidative phosphorylation system (OXPHOS) machinery (**Fig.1.20**).

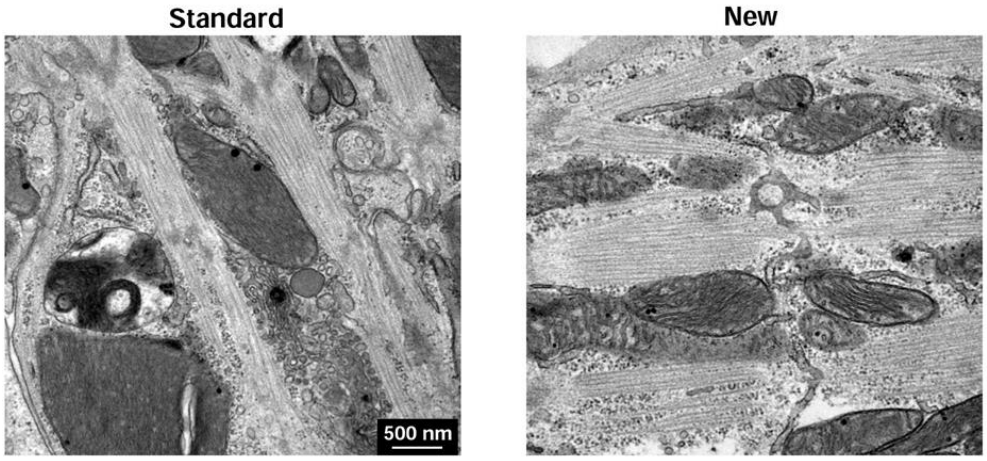

Fig. 1.20. Transmission electron Microscopy (TEM) images performed on Standard and New neonatal cultured CMs.

These preliminary observations are now object of further investigations, to achieve statistical power.

4.6 Characterization of spontaneous contraction frequency and RyR2 distribution on neonatal cultured cardiomyocytes

During de-differentiation, cultured neonatal ventricular CMs express an electrophysiological phenotype similar to sinoatrial node (SAN) pacemaker cells (Eghbali *et al.*, 2005), showing spontaneous rhythmic depolarizations. Conversely, working CMs isolated from adult heart do not show spontaneous activity and only contract in response to electrical depolarization. Spontaneous contraction frequency (SCF) represents therefore an indicative parameter of the maturation state of neonatal CMs. To measure SCF in Standard *vs.* New CMs, cells were placed on the stage of a bright field microscope (Olympus CK30), where short movies (1 minute) were recorded and contractions determined by analysis of the digital sequences. The analysis of SCF in Standard *vs.* New CMs showed that, after 5 days of culture, Standard CMs spontaneously contract, synchronously, at higher frequency than New CMs (SCF, Standard CMs: 0.45±0.07 *vs.* New CMs: 0.02 0.01, in Hz) (**Fig.1.21**).

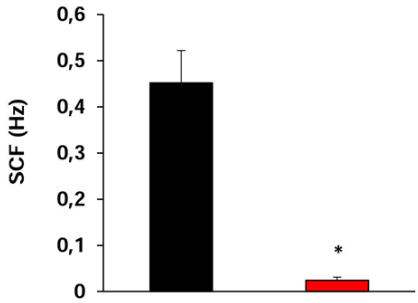

Fig.1.21 Neonatal cardiomyocytes cultured with the novel protocol display decreased spontaneous contraction frequency. Quantification of spontaneous contraction frequency (SCF) in Standard and New neonatal CMs, measured both at bright field and with real-time imaging of Ca^{2+} dynamics. (n=20 CMs per group; from 3 different isolations; * $p<0.05$, bars represent SEM)

Among the molecular components involved in CICR, RyR2 has a central role in controlling Ca^{2+} release from the SR and impacts on the rate of spontaneous depolarizations in pacemaker cells. During postnatal development, RyR2 expression increases and the protein achieves its mature distribution appearing in clusters localized along lines parallel to Z-bands in correspondence to the terminal SR cisternae. To analyse RyR2 expression and distribution in New neonatal CMs

IF analysis was performed. Image analysis showed that New CMs had a significant increase in RyR2 signal, showing fluorescence clusters repeated along the Z-band, with an intercluster distance similar to that of adult cells (**Fig.1.22**).

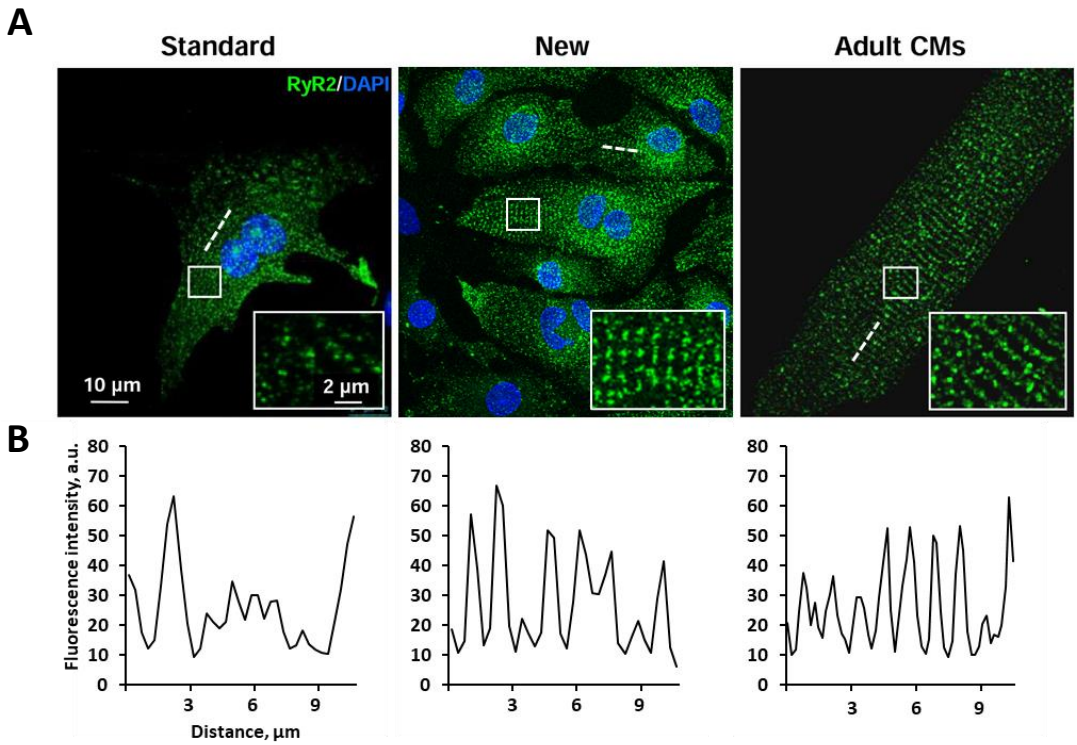

Fig. 1.22 Neonatal cardiomyocytes cultured with the novel protocol display improved RyR2 distribution. A) Representative Confocal IF images on neonatal CMs cultured with Standard or New protocol, as well as adult CMs, all stained with antibody to RyR2. **B)** Plot profile of RyR2 signal along the dashed line in (A) showed a more regular signal in New CMs compared to Standard ones.

4.7 Ca^{2+} signalling in neonatal rat cardiomyocytes

The highly ordered distribution of RyR2 (**Fig.1.23**) in correspondence of the sarcomere Z-bands, suggests that the channel may form Ca^{2+} release Units (CRUs), analogous of those of the adult cardiomyocytes. Stochastic opening of RyR2 within a CRUs in unstimulated cells is associated with a spatially confined and transient Ca^{2+} elevation known as "Ca^{2+} spark". These events are detectable with fluorescent Ca^{2+} probes such as fluo-4 (see Methods) in live cell imaging with microscopes endowed with high-temporal and spatial resolution.

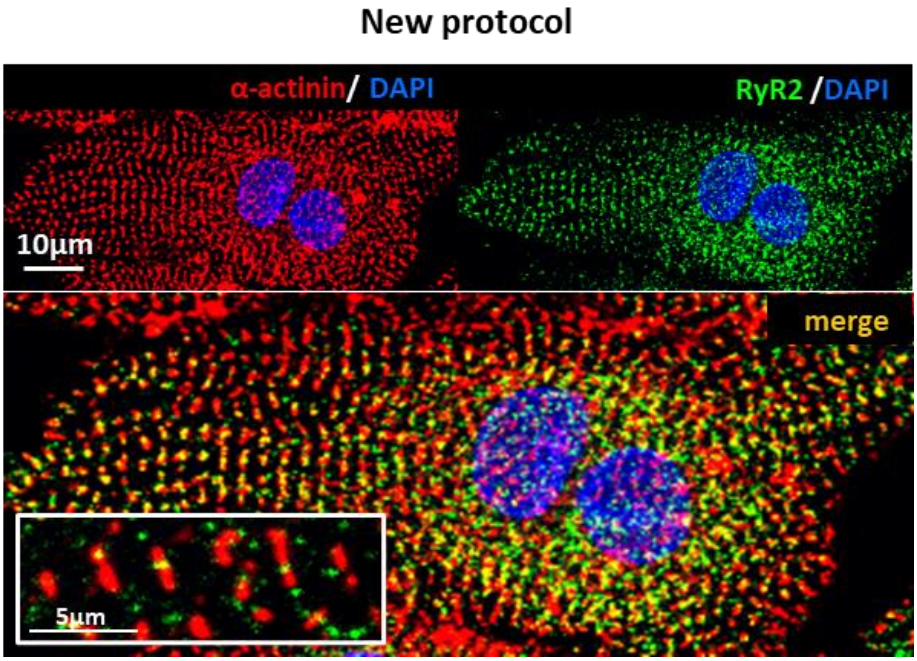

Fig. 1.23 The highly ordered distribution of RyR2 suggest forming Ca^{2+} release Units (CRUs) similar to adult CMs. Representatives confocal IF image of a neonatal CM cultured with New protocol, stained with α-actinin and RyR2. Nuclei were counterstained with DAPI.

We thus used fast-scan confocal Fluo-4 imaging to compare the kinetics of spontaneous Ca^{2+} sparks between cells cultured with the Standard vs. New protocols. Interestingly, the analysis of kinetic parameters of the local "diastolic" Ca^{2+} transients showed that, while Standard cardiomyocytes display large prolonged macro-sparks and travelling Ca^{2+}, New CMs had faster and smaller subcellular Ca^{2+} transients, which were confined to a narrower region (FWHM, Standard CMs: 4.2±0.5 *vs*. New CMs: 2.3±0.2, in µm; FDHM, Standard CMs:

88±10 vs. New CMs: 33±4, in ms) (n=20 per group, from 3 different isolations) (**Fig.1.24**) (see Methods).

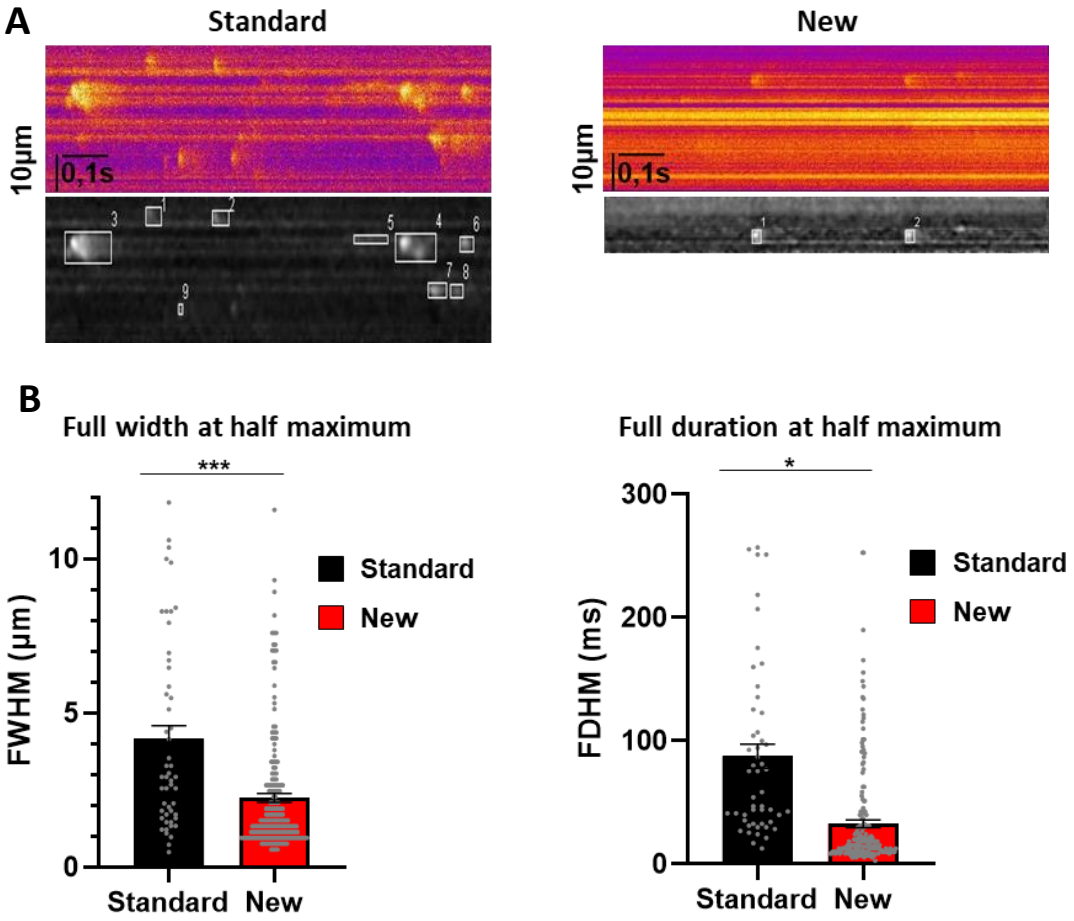

Fig.1.24 Ca^{2+} sparks are smaller and faster in CMs cultured with the New protocol. **A)** Representative traces of line scanning traces of Ca^{2+} events in living CMs loaded with FLUO4-AM and detected events of the same traces after Spark Master analysis. **B)** Spark analysis data recapitulating the width and duration at half maximum of a single Ca^{2+} event in neonatal CMs cultured with New vs Standard protocol. (n=20 per group; *, $p<0.05$; ***$p<0.001$, bars represent SEM)

The difference in RyR2 distribution and the effect of spontaneous Ca^{2+} release events in Standard vs. New CMs is in line with the predicted effect of the assembly of functionally independent CRUs in the cells treated with our "new" developed culture protocol.

4.8. Characterization of contraction - associated cytosolic Ca^{2+} transients in Standard vs New CMs.

We next aimed to determine, in the two different culture conditions, the properties of global Ca^{2+} elevations associated to the activation of Ca^{2+} induced-Ca^{2+} release, which reflect the series of biochemical events underlying coupling between membrane depolarization and cell contraction (E-C coupling).

To this aim, Fluo-4 loaded CMs were imaged during field stimulation, as obtained by applying a short (10ms) 1V/cm voltage step, delivered with platinum electrodes connected with a square wave electrical stimulator (Harvard Apparatus, Boston, MA). Given that, as described above (see 4.6), New CMs display reduced spontaneous contractions as opposed to the cells in the Standard conditions. Cell were paced to analyse Ca^{2+} dynamics in comparable conditions during electrically induced contractions.

The average amplitude of intracellular Ca^{2+} elevations elicited by cell stimulation at 1 Hz, was indistinguishable between Standard and New CMs (**Fig.1.25).** In the first few evoked beats after stimulation started, the amplitude of Ca^{2+} oscillations increased progressively in the New cardiomyocytes, and remained, after roughly 10 s onwards, regular and identical between consecutive beats (Amplitude of intracellular Ca^{2+}: Standard CMs: 910±44 a.u. vs New CMs: 818±76 a.u.).

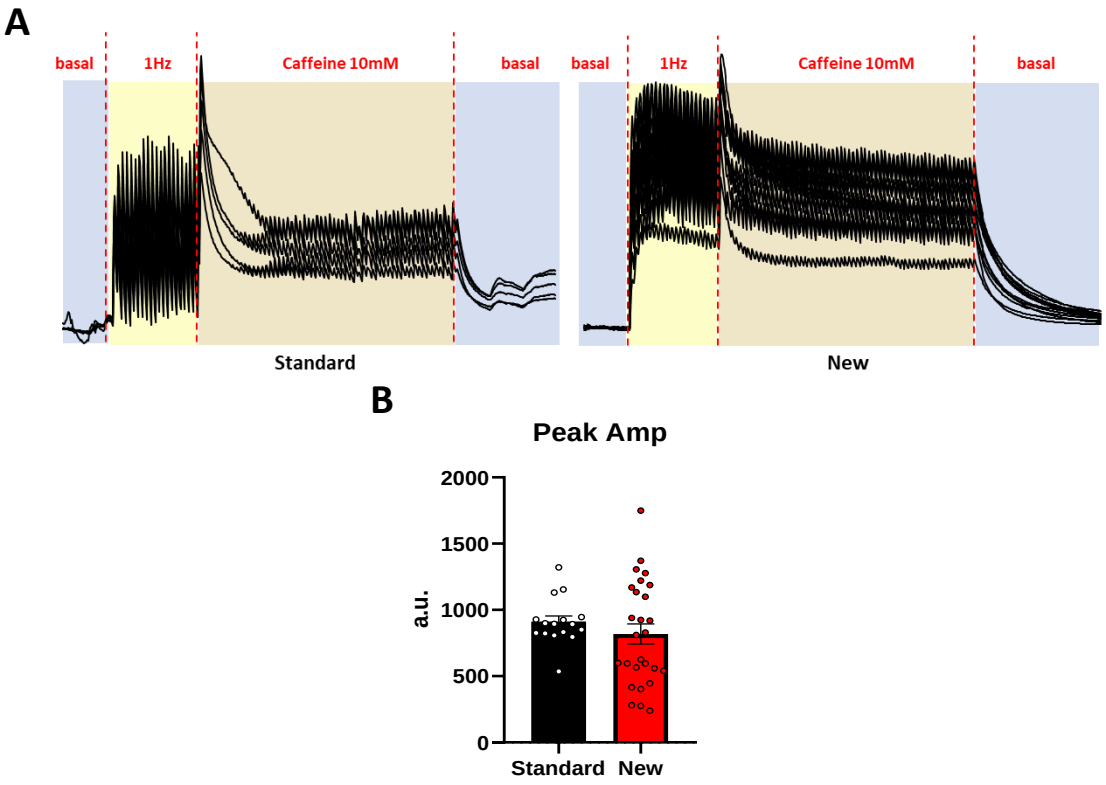

Fig.1.25 A) Cytosolic [Ca^{2+}] transients in Standard (left) and New (right) CMs stimulated at 1 Hz. **B)** Amplitude analysis of intracellular Ca^{2+} elevations elicited by cell stimulation at 1 Hz in Standard vs New CMs . (N=16 cells for Standard, 27 cells for New, from 3 different isolations, error bars represent SEM).

Caffeine was used to rapidly open RyR2 channels and estimate the content of releasable SR Ca^{2+}, which resulted in a transient Ca^{2+} increase of the same entity in New vs. Standard cells, suggesting that the SR is loaded with Ca^{2+} to the same extent **(Fig.1.26).** Notably, in the presence of Caffeine, electrical pacing caused increases in the ion concentration which was more elevated in Standard than in New cells, suggesting that the contribution of RyR2 independent cytosolic Ca^{2+} increase (e.g. Ca^{2+} entry through LTCC) was more pronounced in the former conditions.

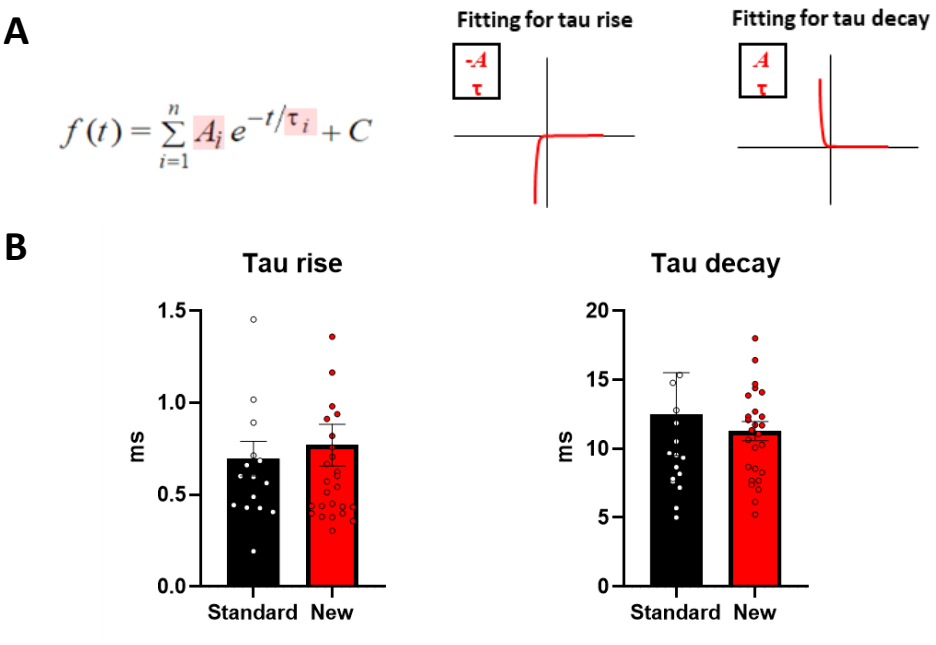

Fig.1.26 A) Exponential Fit was used to calculate Tau rise and Tau decay of cytosolic calcium transient. **B)** Summary graph of Tau rise:0.7±0.1 ms; 0.8±0.1, Tau decay:13±3, 11±1 ms for Standard vs New CMs respectively. (N=16 cells for Standard, 27 cells for New, from 3 different isolations, error bars represent SEM).

4.9. Pacing induced mitochondrial Ca^{2+} uptake in Standard vs. New cardiomyocytes.

The mitochondrial Ca^{2+} uptake channel complex (MCUC) is distributed on CM mitochondria of adult cells, facing the RyR2 Ca^{2+} release channels on the SR. With the notion that mitochondria are found, in the New CMs, in subcellular distribution more similar to adult cells. We aimed to quantitate with fluorescence imaging the kinetics of mitochondrial Ca^{2+} uptake evoked by electrically stimulated contractions. To this aim, cells were transduced with the mitochondrial Ca^{2+} sensor mtGCamp6, and Ca^{2+} changes were recorded using FRET imaging microscopy. Ca^{2+} levels in the mitochondrial matrix oscillated simultaneous to cell pacing (and, see 4.8, cytoplasmic Ca^{2+} transients). After starting cell pacing, the levels of $mtCa^{2+}$ transient were steady in the cells in Standard conditions, while they increased promptly and progressively in New cells (see **Fig.1.27**).

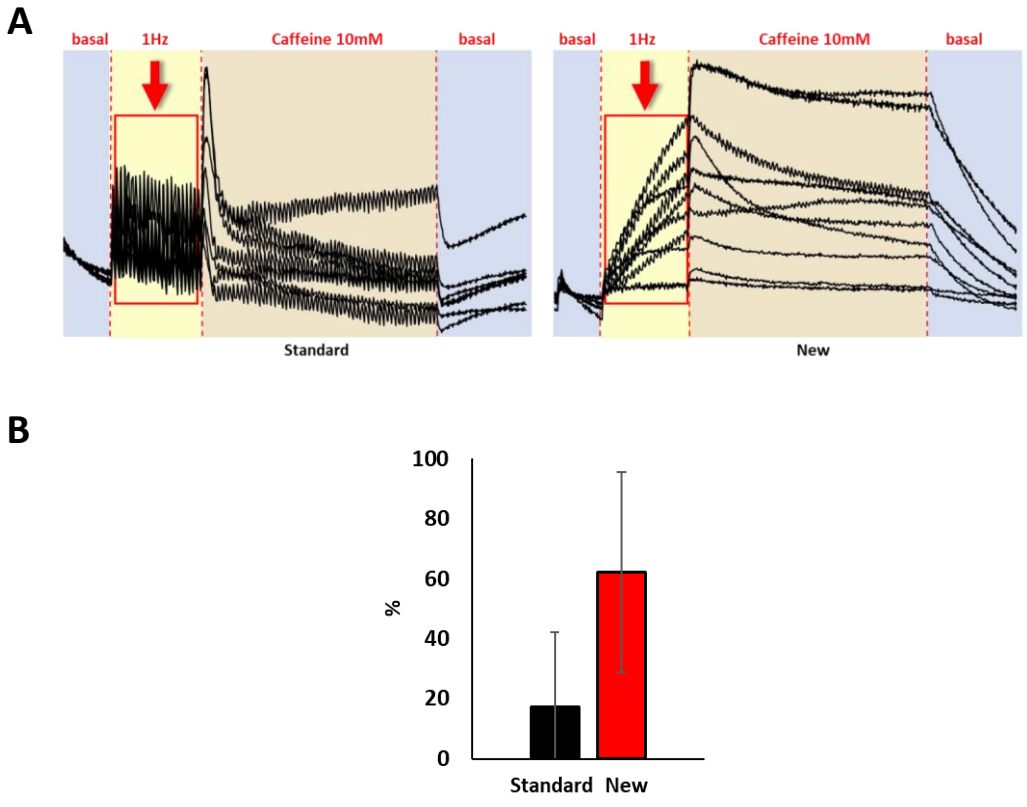

Fig.1.27 A) Mitochondrial [Ca2+] transients in Standard (left) and New (right) CMs stimulated at 1 Hz. **B)** The percentage of cells, where mitochondrial calcium goes up after stimulation. (N=47 cells for Standard, 112 cells for New, from 3 different isolations, error bars represent SD).

This behaviour could suggest "tighter" coupling between Ca^{2+} releasing RyR2 and MCUC in New cells. We tested then the effect of stimulating SR Ca^{2+} release from RyR2 with rapid Caffeine (20mM) application, which resulted in a faster $mtCa^{2+}$ uptake in New vs Standard cells (**Fig.1.28**).

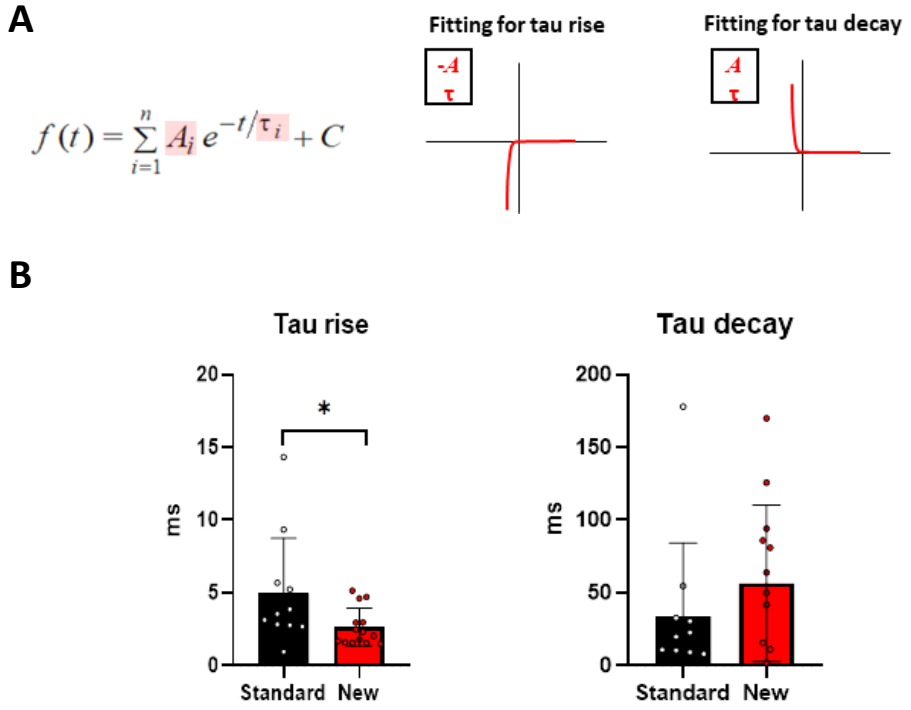

Fig.1.28 A) Exponential Fit was used to calculate Tau rise and Tau decay of mitochondrial calcium transient. B) Summary graph of Tau rise: 4.9±1.1, 2.6±0.3 ms; Tau decay: 34±15, 57±15 ms for Standard vs New CMs respectively. (N=47 cells for Standard, 112 cells for New, error bars represent SEM).

Altogether, the results of these experiments suggest that changes in the subcellular distribution of mitochondria in the cardiomyocytes cultured with the "New" protocol (see above and Fig. 1.16, 1.20) are accompanied by adaptation in the regulation of mitochondrial Ca^{2+}, which may likely reflect on metabolic function.

4.10 Characterization of cAMP signalling in neonatal rat cardiomyocytes

The cellular response to beta-adrenoceptor activation is mediated by intracellular signalling mediated by the cAMP/PKA pathway, elicited by interaction of the receptor-coupled Gs alpha protein with adenylyl cyclase.

To compare the effect of adrenergic receptor activation in living cardiomyocytes, the changes in intracellular [cAMP] upon treatment with the adrenergic agonist Norepinephrine (NE) were assayed using the fluorescent cAMP Epac-S^{H187} biosensor (see Methods), expressed in CMs cultured with Standard or New protocol by adenovirus infection. Cells were stimulated during image acquisition with a epifluorescence microscope and NE was applied to the cell bathing solution at 10nM or 100 nM. At the end of each experiment, combined stimulation with the adenylyl cyclase activator Forskolin (50µM) and the phosphodiesterase inhibitor, IBMX (50µM) was used to induce maximal cAMP accumulation, sensor saturation and quantitate the fluorescence dynamic range. As shown in **Fig.1.29**, the response to low dose of NE (10nM) was similar in cells cultured in New or Standard conditions. At 100nM the increased cAMP achieved on New cells was significantly higher than on Standard cells (Proportional increase of CFP/YFP fluorescence intensity in CMs cultured %: at NE 10 nM, Standard 23±4 vs. New 22±3; at 100 nM Standard 31±2 vs. New 53±7).

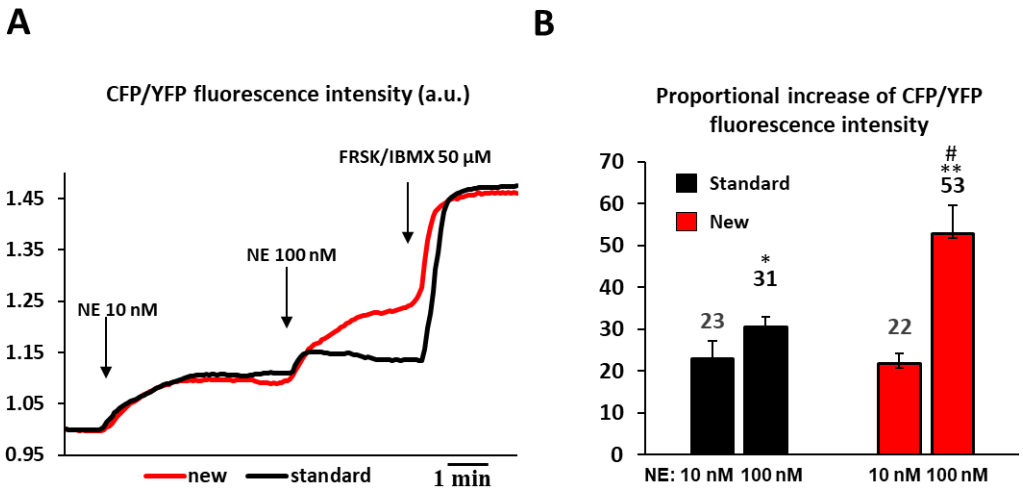

Fig1.29 Cardiomyocytes cultured in new medium display more mature cAMP signalling. A) Representative traces of cAMP kinetics, measured on neonatal CMs cultured with Standard (black curve) vs. New (red curve) conditions, stimulated with NE at the concentration of 10 and 100 nM. As positive control, cells were treated with forskolin (FRSK) and IBMX both at the concentration of 50 mM. (B) Proportional increase after NE 10nM and NE 100 nM of CFP/YFP (480nm/545nm) fluorescence intensity in CMs cultured with New vs. Standard protocol, calculated on maximal response elicited by FRSK/IBMX administration. (n=20 CMs per group. *, $p<0.05$; **, $p<0.01$. * is referred to group-matched NE 10 nM stimulated CMs, # is referred to NE concentration-matched CMs).

While several factors may have a role in determining such non-linear differences between adrenoceptor responses in New vs. Standard CMs, this behaviour might be due to increased β2AR isotype expression level in New cells. In fact, given that the affinity of NE is highest for β1AR, stimulation at 10nM would primarily activate β1AR, while β2ARs are only properly activated at 100nM NE. Measurements performed with selective receptor type stimulation would more accurately reflect such biology, and they should be considered in future studies.

To get insight into the mechanisms causing different responses to adrenoceptor stimulation in New vs. Standard cells, we performed RT-qPCR to quantify the expression level of the main adrenoceptor subtypes. As shown in **Fig.1.30**, cells cultured with the New protocol had significantly higher expression of α1AR, β1AR

and β2AR, with very variable upregulation of β1AR throughout the different samples, and rather coherent upregulation of β2AR.

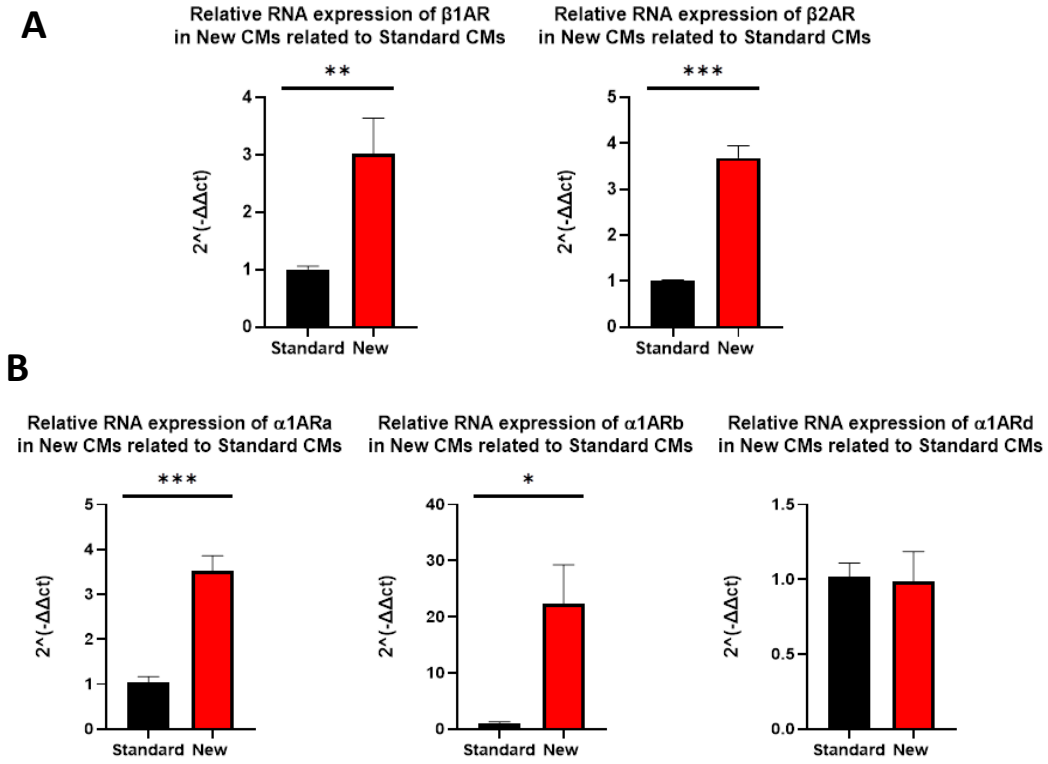

Fig.1.30 CMs cultured with New medium display higher relative RNA expression of βARs and α1ARa and α1ARb than in CMs cultured with Standard medium. Quantitative real-time PCR were performed on CMs cultured with New or Standard medium and relative RNA expression levels of **A)** β1/2ARs and **B)** α1AR1a/b/d were calculated by semi-quantitative analysis. Results were normalized for GAPGH mRNA expression. Data are presented as the level of RNA expression in New CMs in each with respect to corresponding to RNA expression in Standard CMs.

These experiments suggest increased β2AR expression, that the New protocol leads to changes in the β1/ β2 AR ratio and, therefore, in the cellular response to adrenergic agonists.

5. DISCUSSION I

Cultured neonatal rat cardiomyocytes are a commonly used as an *in vitro* model system for molecular and cellular biology studies in cardiovascular sciences. Developed in the 1963 the isolation protocol (Harary and Farley, 1963) has seen a rather limited number of refinement and changes along the years, and as such, it has substantially remained unchanged ever since (Sreejit, Kumar and Verma, 2008). The protocol changes, which were invented include shortening the processing time, reducing number of growth supplements (Sreejit, Kumar and Verma, 2008) and using of chemical reagents to inhibit nonmyocyte proliferation (Simpson and Savion, 1982).

The aspects more influential in the success of neonatal rat ventricular myocytes (NRVM) culture have been: i) the ease of preparation, ii) the amenability to genetic modifications, through viral or plasmid induced expression of exogenous genes (Louch, Sheehan and Wolska, 2011), iii) the relatively good similarity between the mechanisms of second messenger and genetic regulation when compared to those of freshly isolated adult cardiomyocytes (Janowski *et al.*, 2006; Quaife-Ryan *et al.*, 2017), iv) the easy preservation in culture, which enables performing long term experiments (Louch, Sheehan and Wolska, 2011).

Despite these clear advantages, one must be aware of significant differences between the neonatal cardiomyocyte biology and that of the adult cardiomyocyte, or the mature heart cell. As mentioned before, in the first days after birth, cardiomyocytes, which retain a limited dividing capacity, undergo a complex series of differentiative changes including modification in cell structure, organization of sarcomeric proteins in well-ordered structures, development of excitation contraction coupling mechanisms mediated by extracellular and intracellular Ca^{2+} cross-talk, or energetic metabolism changes (Anmann *et al.*, 2014; Guo and Pu, 2020).

As already was mentioned earlier, excitation-contraction coupling in mature CMs is mediated by the entry of limited amount of Ca^{2+} ions through L-type Ca2+ channels, triggering the release of larger amount of Ca^{2+} from the sarcoplasmic reticulum (SR). The molecular system allowing such "Ca^{2+} induced Ca^{2+} release" to be finely tuned, requires organization of the sarcoplasmic reticulum and

development of SR Ca^{2+} *release units* formed by regularly distributed clusters of RyR2 Ca^{2+} release channels and L-type channels on the membrane.

In NRVM, the immature cell structure does not support formation of Ca^{2+} release units, and the SR is not fully involved in Ca^{2+} ion exchange, which relies mostly on Ca^{2+} entry from membrane Ca^{2+} channels. RyR2 is distributed throughout the cell matrix, reflecting the distribution of the developing ER/SR (Louch, Koivumäki and Tavi, 2015).

The standard medium, which commonly used is based ether on DMEM high glucose or M-199, or combination of both with additional horse or newborn serum and antibiotics such as penicillin/streptomycin (Salameh and Dhein, 2005; Louch, Sheehan and Wolska, 2011; Ehler, Moore-Morris and Lange, 2013). We created novel medium for maturation of the neonatal CMs. By modifying the culture conditions in the neonatal CM preparation, through removal of newborn serum and addition of a combination of growth factors typically used in adult CMs culture such as insulin, transferrin and sodium selenate, we obtained more highly differentiated cells, yet retaining the experimental flexibility of the model.

Neonatal cardiomyocytes cultured with the New medium display higher sarcomere organization, and remarkably, develop regularly distributed RyR2 clusters along the transversal Z lines of the sarcomere. The regular sarcomere deposition is accompanied by the dislocation of mitochondria along the sarcomeres, in *interfibrillary* displacement, where they are found in closer interaction with the SR. Functionally, the organization of SR Ca^{2+} release units were supported by the spatio-temporal dynamics of spontaneous Ca^{2+} release events, i.e. Ca^{2+} sparks, which were smaller and faster, more similar to Ca^{2+} sparks typical of mature and fully differentiated cells.

The distribution of mitochondria across the sarcomeres was similarly accompanied by functional consequences in terms of Ca^{2+} signalling. Activation of contraction associated Ca^{2+} transients was accompanied, in the Standard cells, by little elevation of mitochondrial Ca^{2+} levels, which were instead much higher in New cells. This behaviour is in line with the more developed Ca^{2+} signalling system in the modified culture conditions.

The New cells had additional changes suggesting a more “mature” phenotype, notably, the receptor expression level, with the increased expression of β2AR, supported by the functional imaging data.

The mechanisms linking the modified culture conditions to the structural and functional changes found in the cultured cardiomyocytes have not been investigated in detail. One likely major factor contributing to better maturation of the cultured cells is the removal of newborn serum. Interestingly, however, it was recently reported (Isu *et al.*, 2020), that addition of FFA to the culture medium promotes the development of intracellular organelles and SR, supporting that the metabolic factors present in the modified cell medium may thus act as important players in the development of more differentiated neonatal cardiomyocytes.

With these experiments, we can conclude that neonatal cardiomyocytes cultured with the New medium protocol show morphological, molecular and functional characteristics suggestive of a more advanced developmental stage, and may thus represent valuable in different scenarios, including basic and applied cardiovascular research.

CHAPTER II

"DYNAMICS OF SYMPATHETIC NEURON- CARDIOMYOCYTE COMMUNICATION"

Index

4.2 Optical recording of cytosolic Ca^{2+} in neonatal CMs during sympathetic neurons activation

4.3 Optical recording of cytosolic Ca^{2+} in neonatal cardiomyocytes during local activation of single neuron by nicotine

4.4 Characterization of calcium transient in cardiomyocyte/neurons cultures in the presence of β1 or β2 adrenergic receptor antagonists

5. DISCUSSION II

1. INTRODUCTION II

1. Cardiac autonomic innervation

1.1 General organization of the ANS

The Autonomic Nervous System (ANS) plays a crucial role in the maintenance of the homeostasis of all organs, as it finely tunes functions, spanning from the modulation of blood pressure to the control of gastrointestinal responses to food intake, contraction of the urinary bladder, and thermoregulation (Guyton and Hall, 2006). Interestingly, all these actions are regulated independently from the voluntary control, and as such, the ANS is defined as an involuntary system (Karemaker, 2017).

The ANS operates through a two-neuron series, including: i) **pre-ganglionic neurons**, whose cell bodies originate from the lateral horn of the grey matter of the spinal cord, which establish a synaptic contact with ii) **post-ganglionic neurons**, whose cell bodies are organized in peripheral ganglia and directly innervate the effector tissues with their terminal portions (Karemaker, 2017).

The ANS comprises two branches which differ both for their fine anatomy and function: i) the Parasympathetic Nervous System (PNS) and ii) the Sympathetic Nervous Systems (SNS). These two branches are simultaneously represented in the majority of body tissues, and exert opposite effects, resulting in the precise control of organ homeostasis. While the PNS predominates during resting conditions, the SNS is activated during the “fight or flight” response or exercise stresses (Guyton and Hall, 2006).

The preganglionic neurons of the PNS originate from several cranial nerve nuclei and from the sacral segments of the spinal cord (S_2-S_4). The long axons of the parasympathetic neurons establish synaptic contacts with postganglionic neurons, whose cell bodies are organized in ganglia close to- or embedded into the effector tissues. As a consequence, the axons of the postganglionic neurons are normally shorter (Guyton and Hall, 2006).

Parasympathetic neurons enclosed in different nerves are targeted to specific organs, and, in detail, among the cranial nerves, the oculomotor nerve (III) innervates the eyes; the facial nerve (VII) innervates the lacrimal gland, the salivary

glands and the *mucus* membranes of the nasal cavity; the glossopharyngeal nerve (IX) innervates the parotid (salivary) gland; and the *vagus* nerve (X) innervates the viscera of the thorax and the abdomen (i.e. heart, lungs, stomach, pancreas, small intestine, the upper half of the large intestine, and liver). As matter of fact, most PNS fibers (about 75%) are in the *vagus* nerve.

The preganglionic neurons that arise from the sacral region of the spinal cord form the pelvic nerves. Parasympathetic neurons participating in these nerves innervate the viscera of the pelvic cavity (i.e. lower half of the large intestine and organs of the renal and reproductive systems) (**Fig.2.1**).

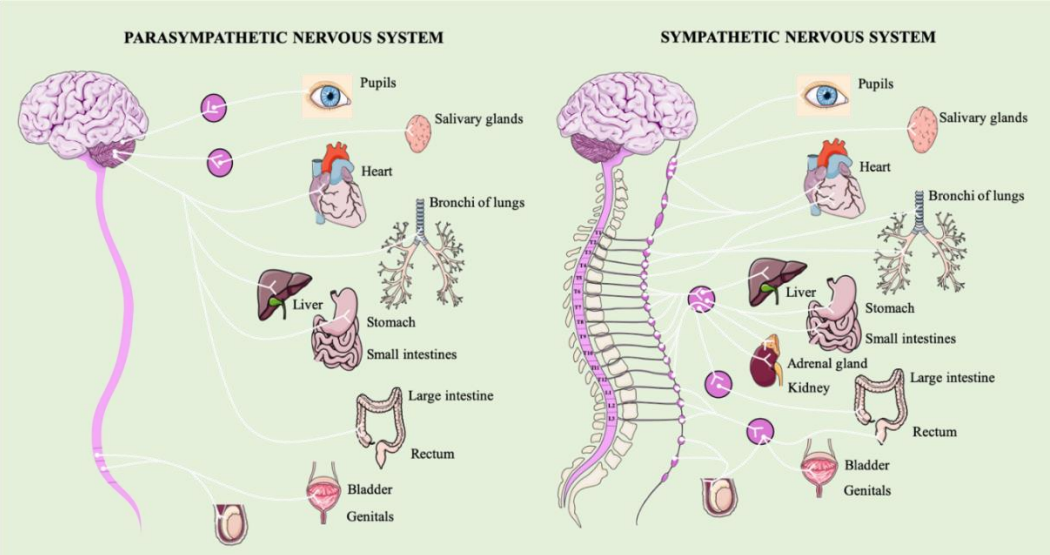

Fig.2.1 Organization of the Autonomic Nervous System.

On the contrary, the preganglionic neurons of the SNS originate from the thoracic and lumbar regions of the spinal cord (segments T_1 through L_2) and establish synaptic contacts with several postganglionic neurons found in the sympathetic ganglia (SG) chains, which consist of 22 ganglia running along either side of the spinal cord. From these ganglia, localized at distance from the targets, long axons originate and innervate the effector tissues (Guyton and Hall, 2006). Other preganglionic neurons exit the spinal cord and pass through the ganglion chain without synapsing with a postganglionic neuron. Instead, the axons of these neurons travel more peripherally and synapse with postganglionic neurons in one of the sympathetic collateral ganglia. These ganglia are located about halfway between

the central nervous system and the effector tissue. In addition, a subset of preganglionic neurons is directed to the adrenal medulla. The cells of this gland have the same embryonic origin of the neural tissue and, in fact, function as modified postganglionic neurons. Instead of releasing neurotransmitters directly on the effector organ, they release them in the bloodstream, thus functioning as long-range neuroendocrine systems. An important feature of this system, which is quite distinct from the parasympathetic, is that the postganglionic neurons of the sympathetic system travel within each of the 31 pairs of spinal nerves. Interestingly, 8% of the fibers that constitute a spinal nerve are sympathetic. This allows for the dense distribution of sympathetic nerve fibers to most effector organs, including the skin, its blood vessels and sweat glands. In fact, most innervated blood vessels in the entire body, primarily arterioles and veins, receive only sympathetic nerve fibers. Therefore, vascular tone and sweating are only regulated by the sympathetic system (**Fig.2.1**).

1.2 Gross anatomy of the heart innervation

Among the different organs, the heart is densely innervated by both the parasympathetic and the sympathetic branches of the ANS.

As stated above, the parasympathetic and the sympathetic branches of the ANS work in a reciprocal fashion to regulate heart activity by finely modulating heart rate (HR) (chronotropy), at the level of the SAN, and the conduction velocity (dromotropy), at the level of the conduction system. In addition, the SNS modulates heart contractility, by regulating the force of contraction (inotropy) and relaxation (lusitropy), at the level of ventricular myocardium (Zipes, 2008).

The ***parasympathetic neurons*** derive from cardiac neural crest cells, which migrate into the developing heart and form cardiac ganglia located at the base of the atria. From these ganglia, postganglionic cardiac parasympathetic neurons extend to the SAN, the AVN, the atria and heart's blood vessels, while the innervation of ventricular myocardium is limited. Parasympathetic neurons release acetylcholine (ACh) as a neurotransmitter.

On the other hand, ***sympathetic neurons*** (SNs) develop from trunk neural crest cells, which migrate and form sympathetic ganglia where they proliferate and

differentiate into mature neurons. The cell bodies of the postganglionic SNs innervating the heart mainly organize in the middle-cervical and stellate ganglia, with the superior cervical and the 4th to 6th thoracic ganglia contributing to a little extent. From these ganglia, SNs extend their projections from the base of the heart throughout all the myocardium (Mitchell, 1953; Kimura, Ieda and Fukuda, 2012; McCully *et al.*, 2013; Fukuda *et al.*, 2015) (**Fig.2.2**). Cardiac SN processes have a peculiar structure, which is quite different from other peripheral neurons, such as the motoneuron. Indeed, they show the typical "pearl and necklace" morphology, characterized by regular varicosities corresponding to the neurotransmitter releasing sites and contacting the target cells. Although SNs release a number of molecules (e.g. adenosine triphosphate, serotonin and histamine), the two main sympathetic neurotransmitters are norepinephrine (NE) and neuropeptide Y (NPY), which are stored in different vesicles (Fukuda *et al.*, 2015). Effects of SN activation on CMs mainly involve NE. NPY seems to have a minor impact in the short-term effects (seconds), while it seems to have a role in the long term (days) in the regulation of CM ion currents (Protas and Robinson, 1999; Protas *et al.*, 2003).

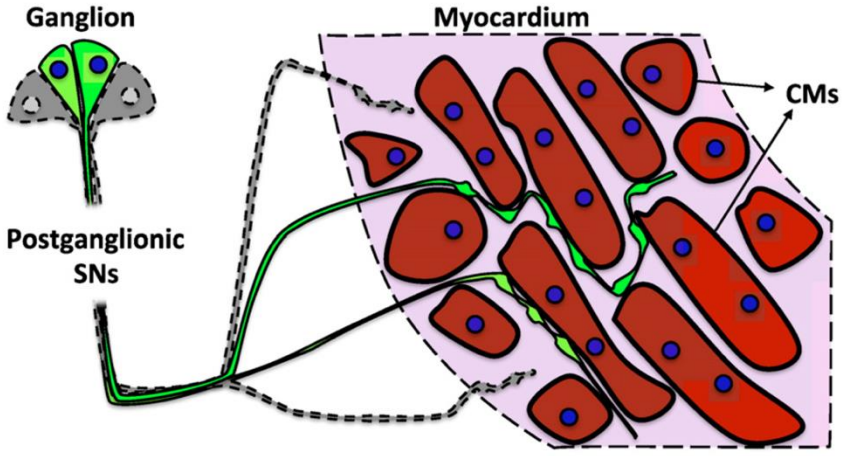

Fig. 2.2 Anatomy of heart innervation (Franzoso, Zaglia and Mongillo, 2016).

1.3 Sympathetic Neurotransmitters

1.3.1 Norepinephrine

Norepinephrine (NE) is a catecholamine synthesized starting from L-tyrosine, thanks to the activity of three enzymes. Among which tyrosine hydroxylase (TOH), converts tyrosine to L-3,4-dihydroxyphenylanine (L-DOPA), then dopamine β-

hydroxylase (DBH) hydroxylates dopamine to produce NE. These proteins are usually used in immunohistochemical and biochemical assays as SN markers (Franzoso, Zaglia and Mongillo, 2016). NE operates by binding to the adrenergic receptors (ARs), which are G protein-coupled receptor (GPCR), expressed on the CM membrane. GPCRs contain seven transmembrane α-helices and a large cytosolic C-terminal loop. The ligand-binding sites include hydrophobic regions made up by α-helices, while the G proteins-binding sites include both transmembrane α-helices and the intracellular domain (Clapham and Neer, 1997; Luttrell, 2006; Katz, 2011). There are different isoforms of NE receptors: α-adrenoceptors (α-ARs) and β-adrenoceptors (βARs). Alpha-ARs associate with trimeric G_q protein activating the phospholipase C (PLC)/Ca^{2+} downstream signalling pathway, while βARs associate with G_s proteins activating adenosine monophosphate (cAMP), protein kinase A (PKA), the exchange protein activated by cAMP (EPAC), and PI3K/Akt (Franzoso, Zaglia and Mongillo, 2016). As concerns βARs, β1ARs couple to trimeric G_s protein, while β2ARs with G_s and G_i proteins, the latter having a negative inotropic effect (E Devic *et al.*, 2001). The signal is switched off reducing the extracellular NE concentration thanks to NE uptake by the neuron through the NE transporter (NET), NE catabolism and cessation of intracellular signalling cascade.

1.3.2 Neuropeptide Y

Neuropeptide Y (NPY) is the result of post-translational modifications of the pre-pro-NPY, composed of 97 amino acids. The mature NPY consists of 36 amino acids. There are six known receptors for NPY (Gericke *et al.*, 2009); the Y1, Y2 and Y5 isoforms are the more expressed in the myocardium (Pellieux *et al.*, 2000). NPY and NE are both released by sympathetic nerve terminals upon sympathetic stimulation (Yang *et al.*, 2008), and both of them operate acute and long-term cardiac effects. NPY administration in spontaneously beating guinea pig hearts operates positive inotropic and chronotropic effects. NPY long term effects include regulation of CM ion channel expression and consequently of their electrophysiological properties (Franzoso, Zaglia and Mongillo, 2016). NPY acts through $G_{i/o}$ proteins triggering two events: PLC activation and inhibition of

adenylyl cyclase (AC). PLC activation mediates proliferative pathways downstream to Y1 receptors. It leads to the increase of intracellular Ca^{2+}, mainly by extracellular Ca^{2+} influx, but possibly also by mobilization of intracellular Ca^{2+} stores. This activates PKC, which stimulates the Ras– Raf–MEK–MAPK cascade, and CaMKII, which facilitates this process by its direct interactions with Raf-1. Moreover, the possibility that CaMKII also acts via inhibition of AC (Wong *et al.*, 2001), cannot be excluded. A decrease in AC activity and cAMP level inhibits PKA thus blocking its inhibitory effects on the Ras–Raf proteins. This pathway can be activated by both Y1 and Y5 receptors, but it is particularly important at low concentrations of NPY, where Y5 receptor-dependent PKA inhibition provides an additional amplification signal, compensating for a lower Y1 receptor-induced increase in Ca^{2+} (Pons *et al.*, 2008).

It has been demonstrated that, in addition to activate CMs, NPY operates a variety of effects on all the myocardial cell types, including cardiac fibroblasts and MSCs (as discussed below). It has been demonstrated that NPY induces their proliferation and differentiation into adipocytes, *in vitro* (Yang *et al.*, 2008; Gericke *et al.*, 2009). NPY receptors are highly expressed also in the endothelium and vascular smooth muscle cells (VSMCs), in fact it has been demonstrated to be a key regulator of the vascular tone, mediating vasoconstriction (Dumont and Quirion, 2006). In addition, NPY stimulate VSMC proliferation *via* Y1 receptors (Zukowska-Grojec and Vaz, 1988; Pons *et al.*, 2008).

1.4 Cardiac sympathetic innervation pattern

The myocardium starts to be innervated by SNs in the early post-natal weeks and axonal sprouting is guided by the balance between chemoattractant neurotrophins (e.g. nerve growth factor, NGF (Levi-Montalcini and Angeletti, 1968); neurotrophin-3, NT-3) and chemorepellent factors (e.g. semaphorin-3A, Sema-3A) released by target myocardial cells. SN axons penetrate the myocardium, following blood vessels, an intermediate target, that express NT-3. The neurotrophins NGF and NT-3 signal through the same receptors: the tropomyosin receptor kinase A (TrkA) and the p75 neurotrophin receptor (p75), to coordinate distinct phases of SN development (Kuruvilla *et al.*, 2004). NT-3, released by

vascular smooth muscle cells, activates TrkA expressed on sympathetic axons, allowing axonal extension along the vasculature. As axons approach the heart, and begin to acquire CM-derived NGF, the ensuing retrograde NGF/TrkA signalling promotes cell survival, anabolic responses and expression of p75. The increase in p75, in turn, diminishes axonal responsiveness of TrkA to NT-3, enabling NGF to become the dominant axonal growth factor, allowing stable contacts between CMs and SNs (Lockhart, Turrigiano and Birren, 1997). Chemorepellent factors, such as Sema-3A, instead interfere with neuronal process growth, causing their retraction, and inhibit the interaction of the neuron with the target cells (Franzoso, Zaglia and Mongillo, 2016). In the mouse heart, it is described that, in the embryonic stages, Sema-3A is expressed homogeneously by CMs of the ventricles, while during the postnatal development, it was observed a gradual decrease in the expression of Sema-3A that starts in the subepicardial CMs and progresses to the subendocardial ones. Indeed, it has been demonstrated that mice lacking Sema-3A show hyperinnervation of the myocardium and an unbalance of the innervation pattern, while mice overexpressing Sema-3A show an almost denervated myocardium and are subjected to increased mortality due to sudden cardiac death (SCD) (Chen *et al.*, 2007).

When the developmental process is completed, the balance between chemoattractant and chemorepellent factors generate a well-defined pattern of innervation in the heart. The characterization of cSN topology was initially obtained by the analysis of thin heart sections in which SN processes were identified by antibodies specific for enzymes involved in NE biosynthesis, such as TOH and DBH. This analysis allowed to demonstrate that, in the murine heart, SNs heterogeneously among the four chambers, with the highest density of nerve fibers in the atria, followed by the RV and LV. Moreover, inside the ventricular walls there is a decreasing gradient of SN density from the epicardium to the endocardium (Randall *et al.*, 1968; Ieda *et al.*, 2007). In line with these results, we recently estimated one SN process every two CMs in the sub-epicardium, while the density appeared decreased in the sub-endocardial regions. Interestingly, such innervation pattern is species-specific, as in the rat SN density is similar in the sub-epicardial and sub-endocardial regions, while in the rabbit, pig and human hearts, SNs are

highly represented in the sub-endocardial myocardium (Pianca *et al.*, 2019). Although the results presented above provided important advances in the study of heart innervation, they were not designed to define the 3-D topology of the cardiac sympathetic network. To achieve this goal, Freeman *et al.*, 2014 used two-photon fluorescence microscopy, combined with computer-assisted image analyses, to determine the morphology of SN circuits in intact hearts isolated from transgenic mice with SN specific expression of Green Fluorescent Protein (GFP) under the DBH promoter. This approach allowed to generate, although in small cardiac volumes, the first 3-D reconstruction of the cardiac SN network. Such analysis showed that, contrary to common belief, SN arborisation within the myocardium is so dense and intertwined that each CM is simultaneously contacted by different neuronal processes, all of which establish multiple neuro-muscular contacts at the regularly displaced neuronal varicosities (**Fig.2.3**).

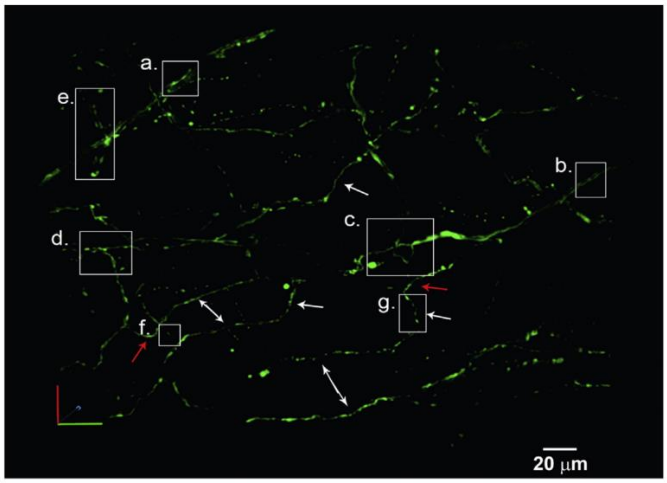

Fig.2.3 3-D reconstruction of the cardiac SN network in a tissue block from a GFP transgenic mouse (Freeman *et al.*, 2014).

In addition, while the inspection of thin tissue sections surmised that some CMs are innervated and some others are not, the 3-D reconstruction of the neuronal tree revealed that SNs are represented in the heart with a density much higher than expected.

1.5 Modulation of cardiomyocyte activity by sympathetic neurons

The textbook view of the cardiac SNS is best represented by the acute activation of neuronal discharge of NE in the 'fight-or-flight' reaction to both intrinsic (hemodynamic, emotional) and extrinsic (fear, pain) stressors (Jansen et al. 1995). However, it is worth reminding that SNs control heart functions, even in resting conditions (Lombardi et al. 1996), by continuously tuning heart rate (HR) on a beat-to-beat basis heart rate variability (HRV). In addition, previously our lab and others demonstrated that cardiac SNs control long-term signalling mechanisms involved in transcriptional control, cell division and regulation of cell size (Ogawa *et al.*, 1992; Cao *et al.*, 2000; Li *et al.*, 2004; Ieda *et al.*, 2007; Zaglia *et al.*, 2013).

For the ***acute responses***, the increase in contraction force of CMs is exerted by SNs at the level of the working CMs. Neuronally-released NE binds to CM βAR leading to a cascade of downstream events: the activation of $G\alpha_s$, which in turns activates AC, the enzyme responsible for the production of the second messenger cyclic-AMP (cAMP). cAMP activates its main effector, the protein kinase A (PKA), that phosphorylates the L-type Ca^{2+} channels and the RyR2, enhancing the CICR and resulting in the increase of the cytoplasmic Ca^{2+} content. This increase leads to an augmented sarcomere contraction during systole. PKA activity is also essential in the control of Ca^{2+} reuptake in the SR during diastole. Indeed, through the phosphorylation of phospholamban (PLB), which positively modulates the activity of SERCA, it increases the speed of cytosolic Ca^{2+} clearance, thus resulting in the shortening of Ca^{2+} transient (**Fig.2.4**) (Opie, 2004). This allows CMs to be prone to increase the frequency of contraction.

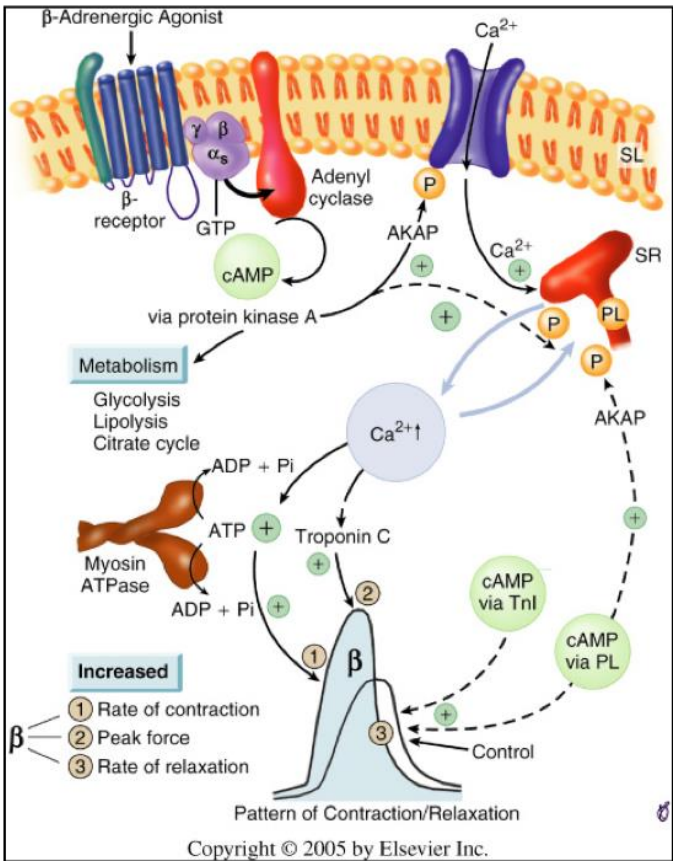

Fig.2.4 Signalling pathways underlying SN-dependent control of CM contraction (Opie, 2004).

The frequency of heart contraction, which is dictated by SAN depolarization, is positively modulated by SNs innervating SAN cells. The SAN is the physiological pacemaker of the heart and SAN cells spontaneously depolarize through the activation of several different ion channels. The depolarization of these cells starts with the opening of no specific cation channels, called hyperpolarization-activated cyclic-nucleotide gated channels (HCN), which is opened when the membrane potential is below -60/-70 mV and carry an inward depolarizing current called I_f. Then the L-type Ca^{2+} channels open and contribute to depolarize the cell. Moreover, the Ca^{2+} entered in the cytosol is extruded by NCX that, by exchanging each Ca^{2+} with three molecules of Na^+, generate an additional inward current. The repolarization, instead, is ensured by two K^+ channels, which carry I_k and $I_{k,Ach}$ currents. $I_{k,Ach}$ is modulated by parasympathetic neurons, while I_k is controlled by SNS. SNs, innervating the SAN, accelerate its depolarization rate through the

release of NE and activation of βARs in nodal cells. This leads to the increase of cAMP through the $G\alpha_s$/AC pathway, which is able directly to positively modulate HCN opening and thus increase I_f. Moreover, cAMP mediated activation of PKA results in the phosphorylation of L-type Ca^{2+} channels and I_k channels, which increase depolarization and repolarization currents respectively, leading to the shortening of nodal cell action potential duration. These effects ultimately result in the increase of depolarization frequency of SAN that determines an increase in HR (**Fig.2.5**).

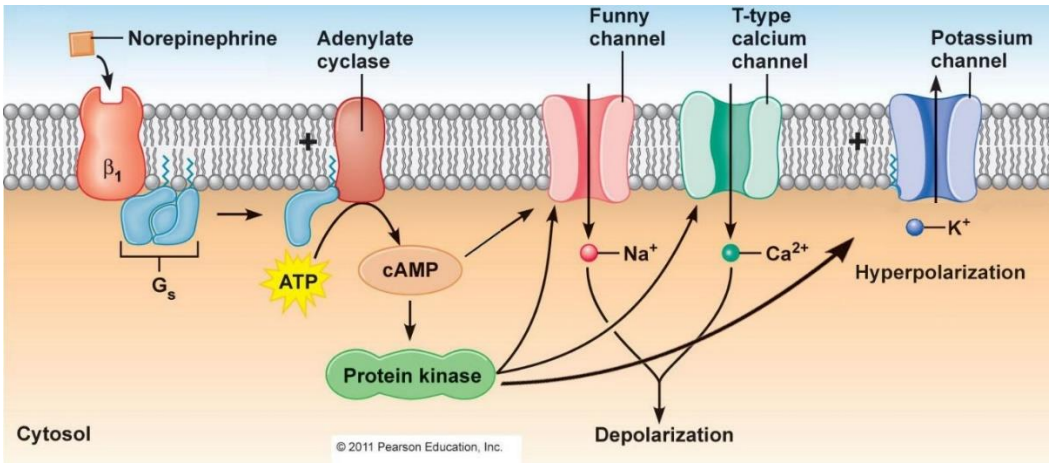

Fig.2.5 Signalling pathways underlying neurogenic control of heart activity (Reece, 2011)

The activation of the ANS (both sympathetic and parasympathetic branches) generates changes in HR, that are seen in the ECG traces as variations in the distance between two consecutive QRS complexes, a phenomenon which is defined HRV. The measure of HRV offers the possibility to quantify the amount of activation of the ANS in a specific situation.

Another important extrinsic modulator of heart activity is constituted by the release of catecholamines from the adrenal glands into the circulatory system, which reaches the heart and activates βARs of CMs exerting a positive inotropic and chronotropic effect. This is the result of endocrine signalling, which simultaneously targets various organs eliciting a systemic response in cases of elevated stress.

For the *long-term effects*, we recently demonstrated that cSN activity is required to maintain the correct cardiac mass. In detail, we demonstrated that NE discharged by SNs activate a signalling pathway downstream to CM β2ARs (β2AR/Akt/Foxo-

3a) which represses the expression of ubiquitin ligases, thus inhibits proteolysis, and promotes protein synthesis (Zaglia *et al.*, 2014) (**Fig.2.6**).

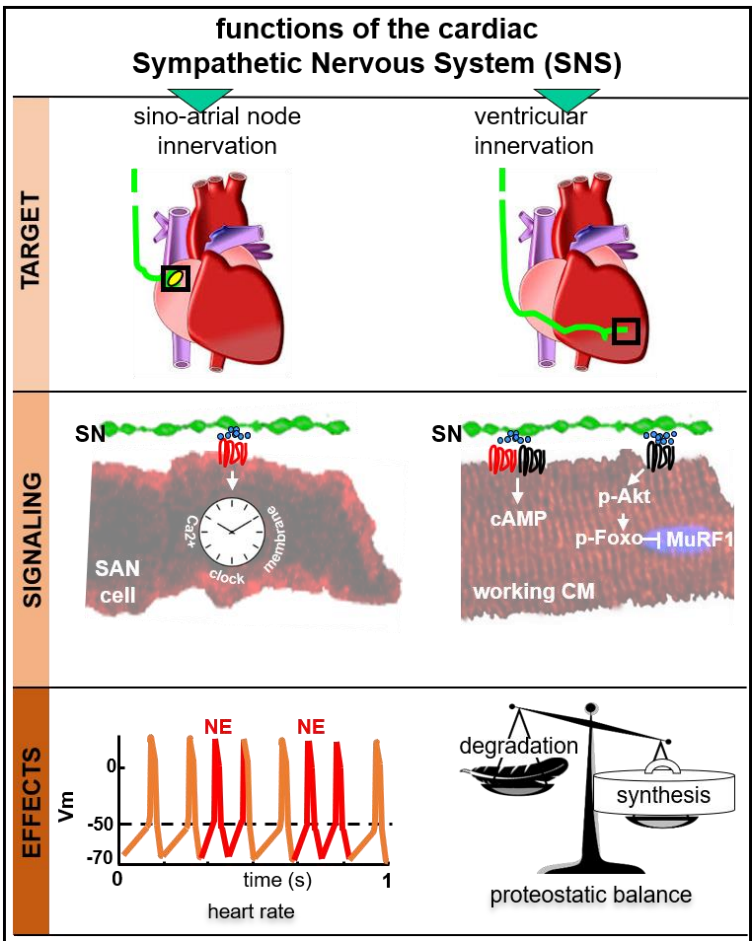

Fig.2.6 Effects of acute and chronic cardiac sympathetic neuron activity (Zaglia and Mongillo, 2017).

1.6 The 'cardiac synapse' and the dynamics of neuro-cardiomyocyte communication

The textbook view on cardiac physiology states that the cardiac SNS modulates heart activity by norepinephrine (NE) which, once discharged by SNs, diffuse into the myocardial *interstitium*. However, this view on the neurogenic control of heart functions does not completely fit with the physiologic requirements of the system, which needs that modulation of heart activity occurs rapidly, efficiently (with low neurotransmitter release by the SN) and in a repeatable way. In addition, this model fails to explain how the SNS may modulate heart activity through a wide range of actions spanning from the modulation of heart rate on a

beat-to-beat basis and the regulation of cell size, in basal conditions, to the maximal chronotropic response, during the fight or flight response. On the contrary, these concepts fit well with the idea that NE is released in a restricted intercellular domain, as occurring in a synapse. The theory of 'the cardiac synapse' has been debated for a long time. Briefly, several researchers failed to detect structured neuromuscular contacts in the heart (FAWCETT and SELBY, 1958; PRICE *et al.*, 1959; Kisch, 1961; NAPOLITANO *et al.*, 1965), and subscribed the concept whereby neurotransmitters, released by activated SN varicosities, diffuse in wide gaps between nerve processes and cellular targets (Grillo, 1966). In contrast, other colleagues described the existence of contacts between unmyelinated SN processes and the CM surface, and the polarization of neurotransmitter vesicles on the side of neuronal varicosities facing the CM. These works suggested that, although in the absence of pre- or post-synaptic specializations, autonomic varicosities establish, with target cells, junctions, where neuromuscular transmission occurs, and that neurotransmitters 'act on discrete pools of specialized subsynaptic receptors' (BAXTER and NISBET, 1963; Trautwein and Uchizono, 1963; Thaemert, 1969; Landis, 1976; Klemm, Hirst and Campbell, 1992; Choate, Klemm and Hirst, 1993; Prando *et al.*, 2018). The conflicting results described above can be explained by the elevated biologic variability between hearts from different species (amphibians *vs.* mammals), and from the inspection of different heart regions (atria *vs.* ventricles), where both the target cells (i.e. CMs) and the innervating SNs display different properties (Zaglia and Mongillo, 2017). Confocal immunofluorescence (IF) analysis of murine ventricular sections, revealed selective accumulation of βARs, specific adaptor/scaffold proteins of the βAR signalling pathway (e.g. SAP97, AKAP79), and cell–cell interaction molecules (e.g. cadherin, β-catenin), in the 'post-synaptic' CM membranes at the contact site with the 'pre-synaptic' neuronal varicosities (O G Shcherbakova *et al.*, 2007). These latter results prompted the study of the mechanisms underlying neuro-cardiac communication. This aspect of neuro-cardiac physiology was mainly investigated *in vitro*, and the first study showed that functional synaptic contacts are developed in co-cultures between SNs and CMs (Conforti, Tohse and Sperelakis, 1991) and that the development of such 'synapses' is directly regulated by NGF (Lockhart, Turrigiano and Birren, 1997;

Lockhart, 2000). In keeping with the cardiac effects of SNS activation, functional assays *in vitro* demonstrated that 'sympathetic innervation improves the contractility of isolated CMs', and accelerates spontaneous beating rate, thus 'indicating that autonomic innervation directly contributes to the modulation of cardiac function' (Lloyd and Marvin, 1990; Michaelevski and Lotan, 2011; Zaika, Zhang and Shapiro, 2011; Takeuchi *et al.*, 2012) and supported that, in disease state, such as hypertension, SNs have a direct role in the disease-associated alterations of myocyte responsiveness to catecholamines (Larsen, Lefkimmiatis and Paterson, 2016). The concept that SNs directly activate CM βARs has recently been confirmed by Wengrowski *et al.*, 2015 who used SN optogenetics in isolated perfused hearts and demonstrated that neuronal photostimulation increased HR and contraction force, and susceptibility to arrhythmic events. Remarkably, the concept whereby SNs communicate directly to target CMs, through 'neuro-cardiac synapses' applies also to the human context, as synaptic neuro-effector contacts were demonstrated in co-cultures between human induced pluripotent stem cell-derived (hiPSC) SNs and CMs, as well as between rat SNs and hiPSC CMs (Takeuchi *et al.*, 2013; Oh *et al.*, 2016; Sakai *et al.*, 2017). In support of a 'synaptic' neuro-cardiac communication, by combining *in vivo* and *in vitro* ultrastructural and IF analyses, with high-resolution imaging of cAMP dynamics in SN-CM co-cultures, and pharmacological assays, Prando *et al.*, 2018 have demonstrated that SNs communicate "synaptically" with target CMs, by discharging NE into a tight intercellular cleft, where high NE concentration is reached at the expense of the release of a low number of neurotransmitter vesicles (Prando *et al.*, 2018). Altogether, these results support the notion whereby cSNs regulate acute heart function by communicating to target CMs in a synaptic fashion. This working model fits well with the requirements of the sympathetic nervous inputs to modulate heart function in an efficient, rapid, and repeatable way. Interestingly, this communication modality is also at the base of the long-term SN-dependent cardiac effects, as demonstrated by the direct correlation, in different mammalian hearts, between SN density and CM size: CM volume is higher in highly innervated heart regions (Pianca *et al.*, 2019). Taken altogether the notions presented above whetted the interest for a deeper comprehension of the molecular mechanisms underlying

neuro-cardiac communication.

Recently, since cardiac SNs are unevenly distributed throughout the myocardial walls, it was investigated by Pianca *et al.* (2019) the hypothesis that CM size distribution reflects the topology of neuronal density. In line with the trophic effect of SNs, and with local neuro-cardiac communication, CMs, directly contacted by SNs in co-cultures, were larger than the non-targeted ones. This property reflects the distribution of CM size throughout the ventricles of the intact mouse heart, in which cells in the outer myocardial layers, which were contacted by more neuronal processes, were larger than those in the less innervated subendocardial region. Such differences disappeared upon genetic or pharmacological interference with the trophic SN/CM signalling axis. This data suggests that both the acute and chronic influence of SNs on cardiac function and structure is enacted because of the establishment of specific intercellular neuro-cardiac junction sites.

2. AIMS OF THE STUDY II

To compare the Ca^{2+} dynamics of intercellular communication between sympathetic neurons and cardiomyocytes and determine their response upon local activation of an individual neuron.

To assess the role of β_1 and β_2 adrenergic receptors in the process of neuronal activation of neonatal cardiomyocytes.

3. METHODS II

3.1 Animal models

We here used CMs isolated from neonatal (P1-P3) Sprague-Dawley rat hearts. All experimental procedures were performed according to the European Commission guidelines and have been approved by the local ethical committee and the Italian authority (Ministero della Salute), in compliance of Italian Animal Welfare Law (Law n.116/1992 and subsequent modifications), as well as of the guidelines of UK Home Office Animal (Scientific Procedures) Act of 1986 in London, UK.

3.2 Primary culture of neonatal cardiomyocyte

Cultured neonatal cardiomyocytes (CMs) were obtained from newborn (P1-P3) rat hearts and isolated following the protocol described previously (see **Methods of Chapter I**).

Based on the previous results, only the New protocol of cultured medium was used as was described in Chapter I (see **Tab.1 of Chapter I**).

3.3 Superior cervical ganglia neuron isolation

Neurons were isolated according to the protocol by Zareen, N. et al. (2009). Superior cervical ganglia were collected from neonatal rats at the age from 1 to 3 days old. Pups were rapidly decapitated and the superior cervical ganglion, which is found close to the carotid artery at the point of bifurcation, was gently detached and placed in a culture dish containing cold Complete Medium (MEM 85%; HS 10%; FBS 5%). After ganglia settled down, the medium was removed, and tissue were resuspended in 0.25% trypsin solution with ethylenediaminetetraacetic acid (EDTA) and placed in a 37 ˚C water-bath for 30-35 minutes. After that 8-10 mL of Complete Medium were added to neutralize the trypsin and centrifuged at 300 rpm for 2 minutes. Once the supernatant was removed, ganglia were resuspended in 1 mL of cultured medium. The neuron cells were dissociated by triturating the ganglia with passage in fire-polished glass pipettes with increasingly small diameters (approximately 2/3 to 1/2 mm). After undissociated tissues settled to the bottom, medium with cells was collected. Neurons were seeded at glass coverslips coated with laminin (0.1 $\mu g/mm^2$) at the density of 20 cells/mm^2.

In this work, neurons were cultured with the same medium as neonatal cardiomyocytes (see **Tab.1 of Chapter I**) with addition 100ng/mL neuron growth factor (NGF). Every 48 hours half of the medium in each well was refreshed.

3.4 Co-cultures of SNs and CMs

Freshly isolated rat neonatal cardiomyocytes and sympathetic neurons were mixed at 1:50 ratio (Neurons : CMs) and seeded on glass coverslips coated with laminin 0.1 μg/mm^2 at the density of 470 cells/mm^2 for cardiomyocytes and 10 cells/mm^2 for neurons respectively.

Co-cultures were cultured with the "New protocol" (see **Tab.1 of Chapter I**) "first day" medium, with additional 100 ng/mL nerve growth factor (NGF) and after 24 hours the medium was replaced with the "second day" culture medium and then was refreshed every 48 hours.

3.5 Immunofluorescence analysis

Cardiomyocyte-sympathetic neuron (CM/SN) co-culture were stained following the protocol described earlier (see **Methods of Chapter I**). The primary and secondary antibodies used in this study are listed in **Table6**.

Table 6. Primary and Secondary antibody used in this study.

Target	Supplier	Dilution	Host species
α-actinin	Sigma	1:200	Mouse
TOH	Sigma	1:1000	Rabbit
Anti-rabbit 488	Alexia Fluor	1:1000	Goat
Anti-mouse 546	Alexia Fluor	1:1000	Goat

3.6 Live imaging Ca^{2+} dynamics in CM-SN co-cultures

Optical recording of cytosolic calcium release was performed on neonatal cardiomyocytes and cardiomyocytes co-cultured with neurons. On the 4th day culturing cells were washed with Hank's Balanced Salt Solution (HBSS) and further HBSS with HEPES 2.38 g/L and Sodium Bicarbonate 0.35 g/L was used for the experiments. Cells were loaded with the fluorescence calcium dye fluo-4 at the concentration 1.5 μMol/L for 20 minutes at 37℃ and then 10 min in dye-free

solution to allow complete de-esterification. The release of intracellular calcium was recorded with a digital camera (MICAM Ultima) and performed on the inverted fluorescence microscope, (Nikon) equipped with oil immersion x63 objective. During the experiment, the temperature was constant at around 35℃. The cells were electrically stimulated at a frequency of 0.5 Hz at 30V. After baseline recordings, Nicotine (1μM) was added to the bath to activate neurons in both cardiomyocytes co-cultured with neurons and in cardiomyocytes alone to take into account any nicotine effect on cardiomyocytes by itself. The analysis of data was done by the MiCAM analysis software (BV_Analyse v11.08).

3.7 Combination of live imaging Ca^{2+} dynamics and Scanning Ion Conductance Microscopy (SICM) in CM-SN co-cultures.

Scanning Ion Conductance Microscopy (SICM) is a contactless method of imaging based on scanning a sample using an electrolyte loaded nanopipette, by measuring the ion current formed by resistance established between the cell and pipette, depending on their reciprocal distance. The tip size of the pipette was 300 nm (80-100MΩ), pulled from the borosilicate glass capillary (IntraCel BF100-50-7.5) by a laser puller (ItraCel, Sutter Instrument Co, P-2000). The pipette manipulator operates vertical movements of the pipette along the Z direction towards the cell surface and is regulating by the current=resistance=distance pipette/cell. Cells were bathed in (145 KCl, 1 MgCl2, 1 CaCl2, 2 EGTA, 10 Glucose, 10 HEPES, all mM/L, pH 7.4) solution, while the pipette was filled by internal solution (145 KCl, 2 MgCl2, 5 HEPES, all in mM/L pH 7.4). Through analysis with the software routine IonView, the electrical signal was converted into a topographic image of the scanned surface. The topological characteristics such as Volume, Surface area, Surface contact and Height were calculated by SCIM Image viewer (Novak *et al.*, 2009).

SICM additionally provide local stimulation of live cells (Nikolaev *et al.*, 2006, 2010). Local stimulation was achieved by applying pressure to the pipette while constantly superfusing the cells with buffer solution. Pressure application resulted in the delivery of ~1 μM of nicotine solution onto the cell surface and did not cause any membrane deformations. Local application ensured activation of a single soma.

CMs were loaded with fluo-4 (1.5 µMol/L, 20 min). After the localized delivery of nicotine (1µMol) to the soma of single neuron, the response from cardiomyocytes stimulated at 0.5 Hz 30 V were recorded. The analysis of data was done by the MiCAM analysis software (BV_Analyse v11.08).

3.8 Live imaging of Ca^{2+} dynamics during β1/β2 adrenergic receptor blocking.

Sympathetic neurons were activated by applying 1µMol nicotine in the bath. Then the response from CM stimulated at 0.5 Hz with 30 V was recorded while CGP-20712 (0.3µMol) or ICI-118551 (50 nMol) antagonists were present in the bath. The analysis of data was done by the MiCAM analysis software (BV_Analyse).

3.9 Statistical analysis

All data are expressed as the mean ± SEM. Experimental groups were compared using unpaired (paired when appropriate) either ANOVA tests or T-test $P < 0.05$ was considered statistically significant.

4. RESULTS II

4.1 Optimization of the sympathetic neuron-cardiomyocyte co-culture method.

The first task in the study of sympathetic neuron-cardiomyocyte communication was to select the most suited *in vitro* model system. We established the co-culture of neonatal rat sympathetic ganglia neuron and neonatal rat ventricular cardiomyocytes. We refined the cell culture procedure to increase neuronal and cardiomyocyte cell yield and quality (see **Methods Chapter II**). Based on the previous studies, the ratio 1:50 neurons:cardiomyocytes was selected to approximate the neuronal network density in the monolayer to that of intact heart (Prando *et al.*, 2018).

The schematics of isolation and Bright Field image of the co-culture are shown in **Fig.2.7**

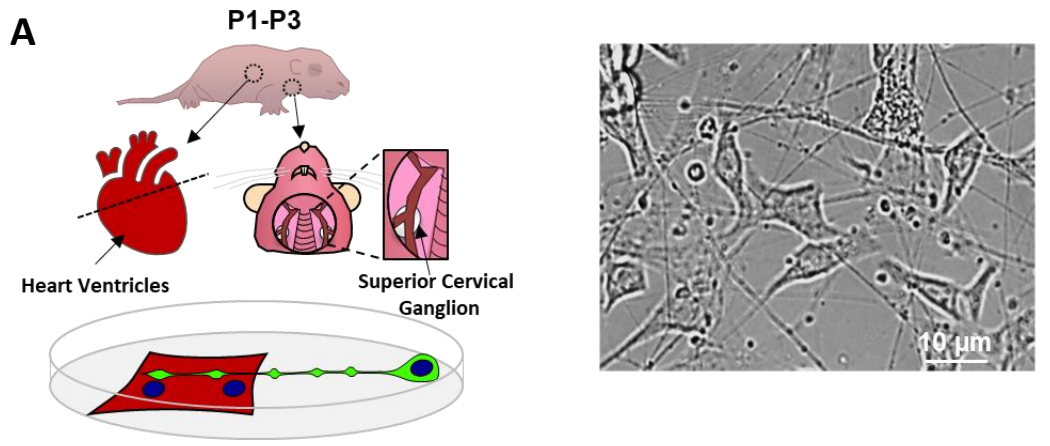

Fig.2.7 Establish sympathetic neuron-cardiomyocyte co-culture: choosing the right parameters *in-vitro* cultivation to reproduce similar physiological condition of intact heart. A) The isolation scheme and bright field image of SNs and CMs plated at a density ratio of 1:50 (SN:CM). **B)** Representative immunostaining images of 3 days co-cultures. Anti-tyrosine hydroxylase (green), anti-α-actinin (red), and DAPI (blue).

Sympathetic neurons and CMs were identified upon labelling the co-culture with anti-tyrosine hydroxylase (TOH) for the neurons and anti-α-actinin antibodies for the CMs, showing that in the first 72 hours, distinctive enlargements with high TOH immunoreactivity developed along the neuronal process and were recognized as neuronal varicosities. As previously demonstrated, (Prando *et al.*, 2018) specialized neuro-cardiac junctions connect the neuronal varicosities to the CM and represent the sites of extracellular neuromuscular signalling. Given that the effect of NE released by the neurons on cardiomyocyte function features centrally the increase in cytoplasmic Ca^{2+} transients, we analysed the effect of neuronal activation in the co-culture monolayer by recording CM Ca^{2+} fluctuations.

4.2 Optical recording of cytosolic Ca^{2+} in neonatal CMs during sympathetic neurons activation.

The excitation-contraction coupling machinery, which in cardiomyocytes regulates Ca^{2+} influx, release from the SR and efflux, is a fundamental process controlling cardiomyocyte contractility. Neuronal release of NE, through activation of α and β adrenergic receptor cascade reactions causes increased function of L-type Ca^{2+} channels, Ryanodine Receptors (RyR2) and SERCA pumps, resulting in increased cytosolic calcium and contraction rate and force.

To verify whether specific functional coupling was in place between sympathetic neurons and cardiomyocytes in the co-culture, we performed Ca^{2+} imaging experiments in cells loaded with the Ca^{2+} indicator Fluo-4-AM, during electrically stimulation at 0.5Hz. (see **Method Chapter II**). To activate neuronal release of NE, we stimulated nicotinic acetylcholine receptors by applying 1μM of nicotine in the bath. Nicotine increases rapidly the contraction-associated calcium transient amplitude in CM co-cultured with neurons by 36% ($p<0.001$ versus CM monoculture without SN exposed to 1um nicotine) (**Fig.2.8**). Notably, such increase was recorded in all cardiomyocytes in the field of view, which was expected and not against the neuro-junctional coupling hypothesis, given that nicotine application stimulates NE release from all neurons in the dish, which are in contact with nearly all cardiomyocytes.

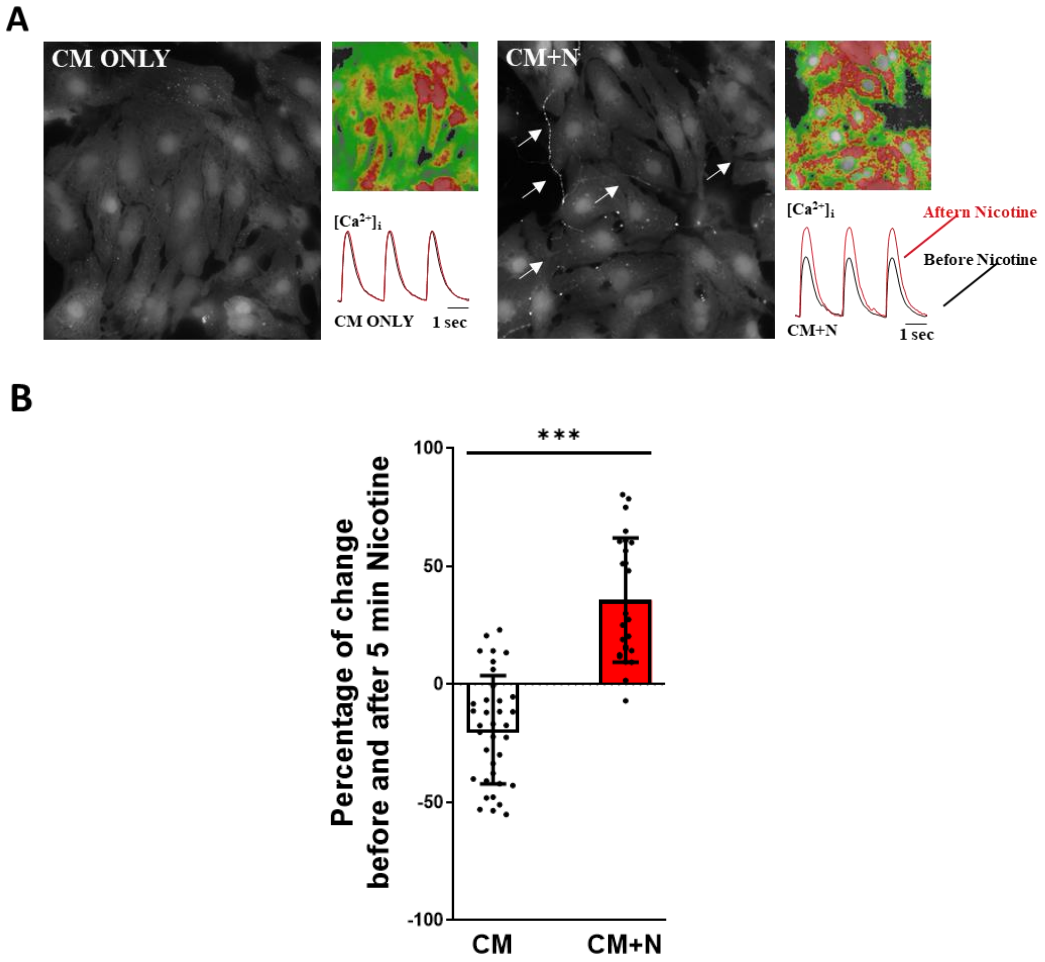

Fig.2.8 Optical recording of cytosolic Ca^{2+} in neonatal CMs during sympathetic neurons activation by nicotine. A) Representative images of cardiomyocytes with fluo-4 dye under fluorescent light and cardiomyocytes calcium transient traces before and after 1µM of nicotine application in CMs cultured alone or with SNs. **B)** Summary graph of the changes in calcium transient after nicotine application (CM only: -19±4 vs CM+SN: 36±5, in %; ***p<0.001, from 5 different isolations)

4.3 Optical recording of cytosolic Ca^{2+} in neonatal cardiomyocytes during local activation of single neuron by nicotine.

To investigate with more precise experimental control the activation of SN, we used an advanced equipment (Scanning Ion Conductance Microscopy (SICM)) allowing localized drug delivery in cell culture (Nikolaev *et al.*, 2010). By combining SICM and optical recording of Ca^{2+} fluctuations, we were able to determine the effect of activating a single neuron on contacted cardiomyocytes.

The experiment is briefly designed as follows:

Once a neuronal soma is found, a nanopipette (30MΩ) is positioned above its highest point (**Fig.2.9 A-B**).

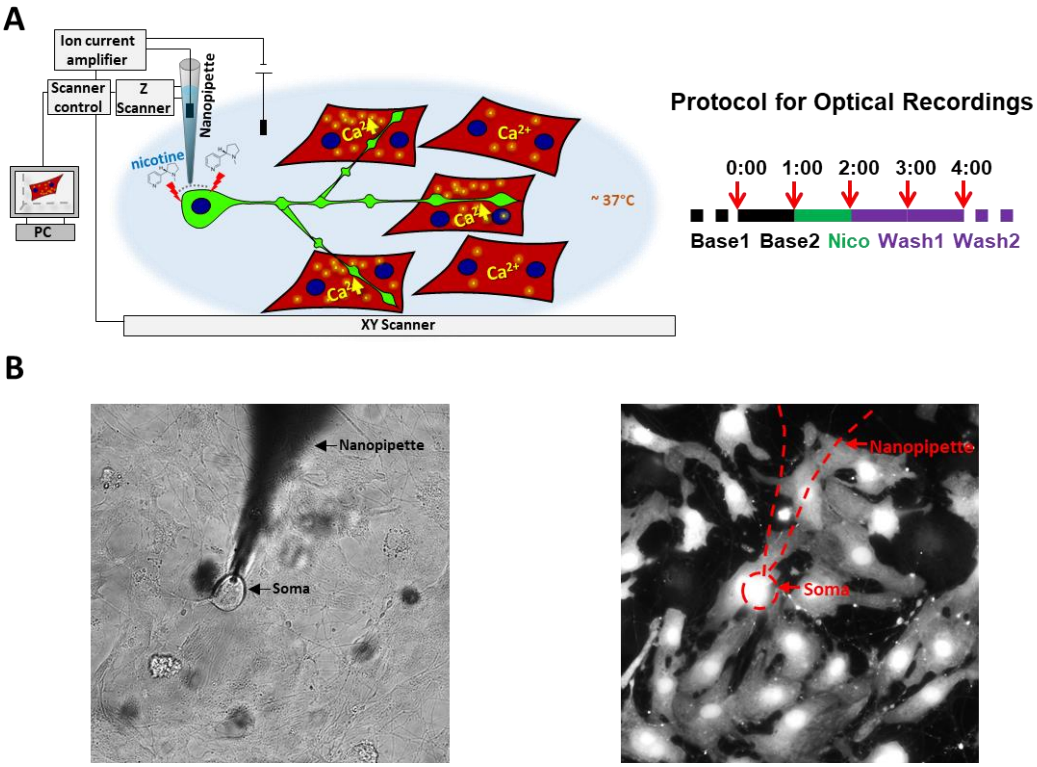

Fig.2.9 Combination of optical recording of cytosolic Ca^{2+} in neonatal cardiomyocytes and SICM. A) Scheme of localized nicotine delivery by SICM to a single neuron; protocol of optical recordings of Ca2+ in contact CMs. **B)** Brightfield image showing the neuronal soma and the nanopipette (left) and the corresponding fluo-4 image of the CM+SN co-culture.

A double release application (by positive pressure and by voltage) is used to release nicotine from the internal solution in the nanopipette during 1 minute. Calcium

transients under pacing stimulation (0.5Hz) from the CM surrounding this neuron were recorded before, during and after the application of nicotine. In 22.2% of the CMs in the field of view, the amplitude of Ca^{2+} transients was increased by single neuron stimulation to an extent similar to that of global neuronal stimulation. Once the nicotine stimulation ended, transients from the responding CM recovered to baseline levels (**Fig.2.10**).

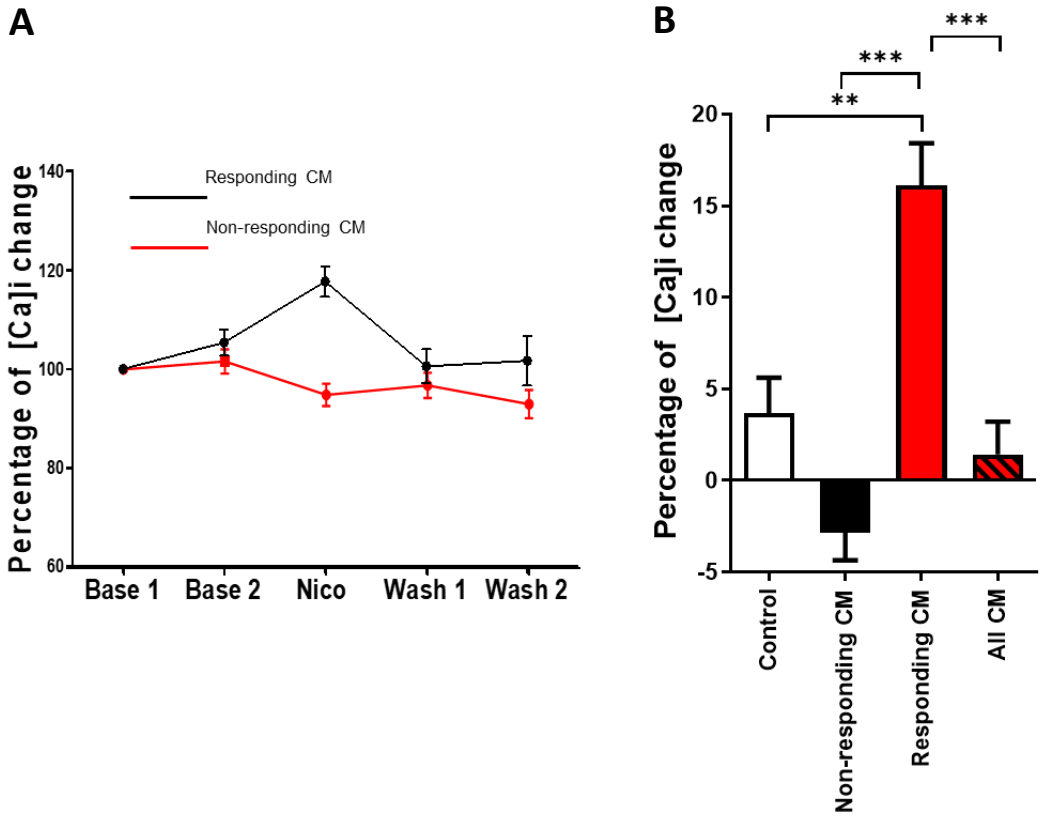

Fig.2.10 Optical recording of cytosolic Ca^{2+} in neonatal CMs during local activation of single neuron by nicotine. A) Percentage of Ca^{2+} change in "responding" (black) and "non-responding" (red) CMs before (base1/2), during (nico) and after (wash1/2) the application of nicotine. **B)** Summary graph (Control CMs: 4±2%, Non-responding CMs: -3±2%, Responding CMs: 16±2%, All CMs: 1±%2; **, $p<0.01$; ***, $p<0.001$). All data are expressed as mean ± standard of the mean (SEM).

The immunofluorescence analysis on the same coverslips, the fraction of CMs in the monolayer which responded to the neuronal stimulation is on the same order of magnitude of that of cells contacted by the branches of a single neuron. This is in line with the neuro-cardiac junctional coupling hypothesis we have proposed. We

previously shown that neuronal stimulation of the cAMP response in cardiomyocytes in co-culture is regulated by neurons in direct contact (Prando *et al.*, 2018).

These experiments extend the observation to downstream effects mediated by beta-AR activation, and allows to visualize the communication network that one neuron may establish through branching and ramifications.

Current work continues the characterization the synaptic communication and functional interaction between sympathetic neurons and CMs. Our results correspond with the idea that CMs and neurons require direct contact for efficient communication.

4.4 Characterization of calcium transient in cardiomyocyte/neurons cultures in the presence of β1 or β2 adrenergic receptor antagonists.

As described above, activation of the sympathetic nervous system operates through NE release into the synaptic cleft between neuron and CM and interacting with the "postsynaptic" β-adrenoceptors (βAR).

β1AR and β2AR play different roles in the regulation of cardiac contractility, which could be sustained by compartmentation of signalling in a receptor-specific way. In neonatal myocytes, activate β1AR leads to a PKA-dependent increase in the contraction rate, and the increase of intracellular Ca^{2+}. Activated β2AR seem to play a biphasic effect on the contraction rate that is independent of PKA activation (Devic *et al.*, 2001), and exert negative inotropic effects at high dose, possibly mediated by a Gs/Gi switch (Paur *et al.*, 2012).

It was previously shown that neuro-cardiac junctional sites display reorganization of the post-synaptic membrane protein distribution, which include β1and β2 adrenoceptors (O G Shcherbakova *et al.*, 2007).

To achieve deeper understanding of the individual role of β1 or β2 adrenergic receptors in neuro-cardiac communication, we used subtype specific beta-AR antagonists, namely CGP-20712 (antagonist to β1), ICI-118551 (antagonist to β2). Calcium imaging was used in neonatal cardiomyocytes co-cultured with neurons, stimulated by 1uM nicotine. The recordings were done under pacing stimulation (0.5Hz) in the presence of ICI-118551 (50 nM) to block β2AR, or CGP-20712 (0.3 μM) to block β1AR.

Fig.2.11 Scheme of β1 or β2 blocking in the CMs co-cultured with neurons and calcium transient traces before and after 1μM of nicotine application in CMs cultured with SNs.

The data shows that neuronal stimulation of β1AR (in presence of the β 2AR blocker) increases cardiomyocyte calcium transient amplitude (Percentage of Ca^{2+} change, CM only: -7±4 vs CM+SN: 6±4, in %; $p<0.05$). Stimulation of β2AR had the opposite effect on Ca2+ dynamics, decreasing transient amplitude (Percentage of Ca2+ change, CM only: 6±1 vs CM+SN: -14±5, in %; $p<0.05$).
Interestingly, β1AR stimulation elicits a smaller increase in Ca^{2+} amplitude when β2AR is blocked (Percentage of Ca2+ change, CM+SN while β2 blocked: 6±4 vs CM+SN general response: 36±5, in %; $p<0.05$).

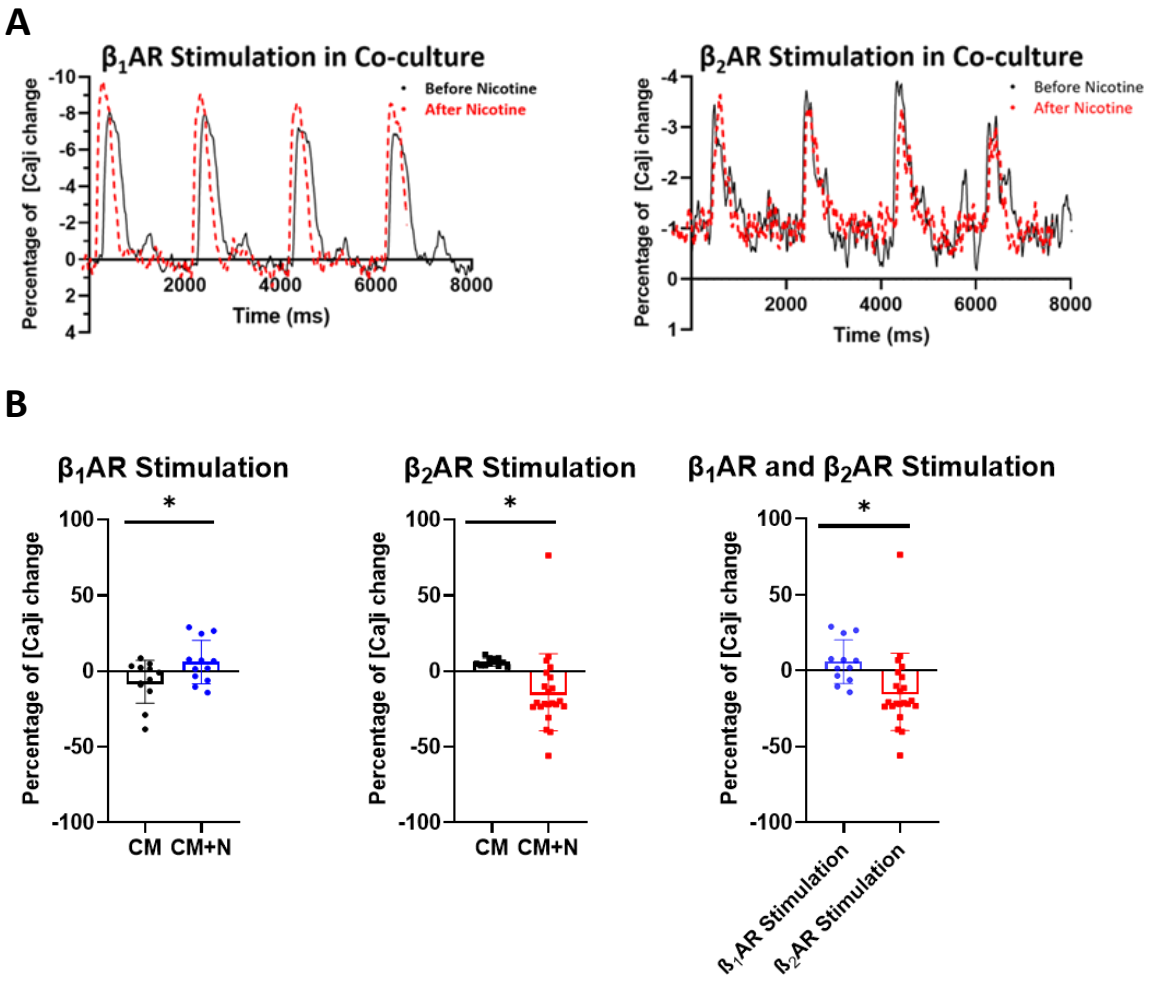

Fig.2.12 Characterization of calcium transient in CMs co-cultured with neurons, stimulated by nicotine in the presence of β1 or β2 adrenergic receptors blockers. **A)** Calcium transient traces before and after 1μM nicotine application in CMs cultured with SNs under β1 or β2AR stimulation. **B)** Summary graph of the changes in calcium transient after β1AR stimulation (left), after β2AR stimulation (middle) (, and the comparison between β1AR and β2AR stimulation (right).

5. DISCUSSION II

In this work, we used sympathetic neuron/cardiomyocyte co-cultures to investigate the dynamics of neuro-cardiac communication in a multi-cellular monolayer with complex interactions. Collectively, the experiments allow deeper insight into the neurogenic regulation of CM function. Our finding is in agreement with work of (Haass and Kübler, 1997), the activation of sympathetic neurons with the Ach Receptor agonist, nicotine, showed modulation of Ca^{2+} signalling, consistent with the inotropic effect of βAR stimulation, in interacting co-cultured CMs. The global effect of neuronal activation may seem in favour of diffuse adrenergic signalling from neuron to CM, and somewhat against direct neuro-cardiomyocyte coupling. It has to be taken into account, however, that neurons in the culture branch in different directions and establish multiple contacts with different CMs. This implies that in a field of view of 125×125 micron, all cells are likely contacted by one or more neurons, and the global effect of neuronal stimulation follows the dense innervation of the cell monolayer. (Freeman *et al.*, 2014; Zaglia and Mongillo, 2017)

To gain more insight on neuro-cardiac communication, we used precise positioning of a drug-delivering pipette with a SICM system to perfuse nicotine locally on a single neuron in the culture. Interestingly, upon single neuron activation, only 22.5% of surrounding cardiomyocytes had βAR dependent Ca^{2+} modulation, a fraction compatible with that of cardiomyocytes interacting with a single neuron. This is in line with our previous demonstration (Prando *et al.*, 2018) that signalling between sympathetic neuron and cardiomyocytes occurs via direct interaction at NCJ, and that the synapse confines signalling to the cells in direct contact.

Previous work from the Kobilka's lab has shown that at junctional sites between neurons and cardiomyocytes, β1AR are predominantly accumulated, and β2AR are transiently present (O G Shcherbakova *et al.*, 2007).

Our experiments show that the effects of neuronal activation on Ca^{2+} dynamics are predominantly due to β1AR stimulation. Interestingly, limiting the effect of neuronally-released NE to only β2AR stimulation decreased the calcium transient amplitude. This is in line with (E Devic *et al.*, 2001) showing that β2AR have a modest effect on Ca^{2+} dynamics , and with the receptor dynamic internalization and reappearance away from the neuro-cardiac membrane patch.

Interestingly, even if β2AR were ineffective in regulating Ca^{2+} dynamics, blockade of β2AR blunted the response to NE. The specific blockers were used at a concentration granting specificity. (Baker, 2005)

While more experiments are needed to infer the molecular mechanisms responsible for this effect, some speculations can be made. Given that β2AR stimulation has no effect on Ca^{2+} transient amplitude, the difference from β1AR response cannot be due to removal of β2AR dependent effects on Ca^{2+} dynamics. It could be explained with the idea that β1AR signalling depends on β2AR stimulation, as it has been suggested that β2AR compartmentalizes β1AR signalling at the nanoscale local domains (Yang *et al.*, 2019). (Hua-Qian Yang et al., 2019)

Collectively, data shows how the neuronal distribution network determines what cells will receive the sympathetic input and is in line with the concept of synaptic communication (Takeuchi *et al.*, 2013; Wengrowski *et al.*, 2015; Oh *et al.*, 2016; Sakai *et al.*, 2017; Prando *et al.*, 2018). When translated to the heart, it supports that the dense innervation of the myocardium is necessary to achieve simultaneous modulation of Ca^{2+} signalling in all cardiomyocytes in the tissue.

CHAPTER III

"THE NEURO-CARDIAC JUNCTION DEFINES AN EXTRACELLULAR MICRODOMAIN REQUIRED FOR NEUROTROPHIC SIGNALLING"

Index

4.1 The key molecular players of NGF signalling are predominantly found at the neuro-cardiac interaction sites

4.2 Local NGF release by cardiomyocytes sustains survival of the contacted sympathetic neuron

4.3 The neuro-cardiac interaction is required for TrkA activation and NGF uptake in the neuron

5 DISCUSSION III

1. INTRODUCTION III

1.1 Neurotrophins

Neurotrophins are a family of secreted proteins required for survival, differentiation, and development of different subtypes of neurons. The mammalian neurotrophins consist of nerve growth factor (NGF), brain-derived neurotrophic factor (BDNF), neurotrophin 3 (NT3) and neurotrophin 4/5 (NT4/5). NGF was the first neurotrophin identified, described by Rita Levi Montalcini in the 1950s as a soluble factor inducing sympathetic neuron hypertrophy and fiber outgrowth, after mouse sarcoma tumour implantation close to the spinal cord in the developing chicken embryo (Levi-Montalcini and Hamburger, 1951). Starting from such seminal discovery, it is now clear that NGF, NT3 and BDNF play important roles in the regulation of survival and differentiation of the peripheral neurons. In particular NT3 is expressed by the peripheral nervous system during embryogenesis and impacts on perinatal neural development of sensory and sympathetic neurons (Wyatt *et al.*, 1999). Remarkably, both neuronal types depend on NT3 for their survival and differentiation and become dependent on NGF only at later stages of postnatal development (Lewin and Mendell, 1993). BDNF also acts as a target-derived survival factor for a subtype of dorsal root ganglia neurons and other sensory neurons (Michael *et al.*, 1997). Despite the pro-survival effects of neurotrophins on peripheral neurons, neither NGF nor BDNF seem crucial for the survival of central neurons (Lessmann, Gottmann and Malcangio, 2003). This can be explained by the overlapping role of neurotrophins on neurons that may trophic input of more neurotrophins (**Fig.3.1**). In support of this concept, the effects of BDNF and NT3 on hippocampal neuronal survival are brought to light only when interference with both neurotrophins is achieved (Minichiello and Klein, 1996).

Since NGF is the most important neurotrophin determining differentiation, target organ innervation and survival of the sympathetic nervous system, the study of molecular physiology of NGF signalling, in neurons and heart cells, may provide new insights in diseases characterized by altered innervation.

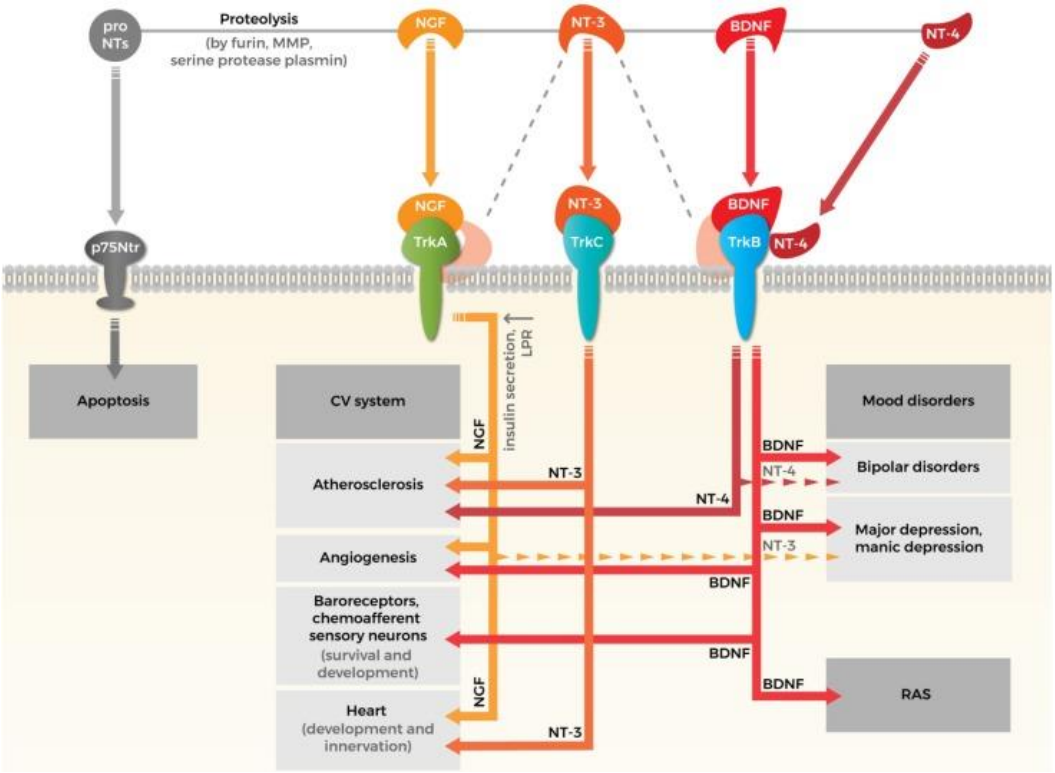

Fig.3.1 Crossroads of neurotrophins in cardiovascular system and psychopathology. (László et al. 2019)

1.2 NGF synthesis

NGF is synthesized from either two transcripts that originate from alternative splicing (Bierl *et al.*, 2005) of the NGF gene and differ in an exon. As many other neurotrophins, NGF is expressed as a pre-pro-protein giving rise to 2 pre-pro-isoforms: a 34KDa (variant A) and a 27 kDa (variant B) isoforms. Once the protein translocates to the endoplasmic reticulum, the pre-peptide is cleaved producing 32 kDa and 25 kDa NGF fragments, namely variant A and B respectively. In the endoplasmic reticulum, pro-neurotrophins can spontaneously establish non-covalently linked dimers between the same or different variants. The pro-NGF is transported to the Golgi apparatus, where it is cleaved by the pro-protein convertases (e.g. furin) to produce the mature 13 kDa NGF protein. In addition to pro-domain cleavage, NGF processing includes N-linked glycosylation of pro-domain residues and sulfation of these N-linked oligosaccharides. The glycosylation has is required for efficient neurotrophin expression, exit from the

endoplasmic reticulum, and escape from intracellular degradation (Seidah *et al.*, 1996).

Since its discovery, NGF function was described first in controlling organ innervation by sympathetic and sensory neurons (Maxwell Cowan *et al.*, 1984). Its mRNA and protein can be found in innervated organs (e.g. submandibular glands, heart, lung, liver, kidney, spleen), where it is produced in low amounts (Shelton and Reichardt, 1984). Its release is crucial for organ innervation so that the degree of sympathetic innervation of an organ correlates with the amount of NGF that it produces (Korsching and Thoenen, 1983).

1.3 NGF signalling pathways

NGF binds to two distinct classes of receptors: the generic low affinity p75 neurotrophin receptor (p75NTR) and the specific high-affinity tyrosine kinase receptor TrkA (Toni, Dua and Van Der Graaf, 2014). The first receptor belongs to the tumour necrosis factor receptor family and binds to all neurotrophins with nanomolar affinity. p75NTR is a transmembrane glycoprotein with a cytoplasmic portion containing a death domain analogous to that described in many other apoptosis-inducing receptors. Its ectodomain comprises four cysteine reach repeats, all of which are required for an efficient NGF binding. The biological function of the p75NTR depends on the neurotrophin that it binds as well as on the presence of the TrkA receptor at the surface of the cell (Wiesmann and De Vos, 2001). For instance, TrkA affinity to NGF is increased by the presence of p75NTR, thus enhancing the pro-survival neurotrophin effect in SNs (Epa, Markovska and Barrett, 2004). On the other hand, p75NTR stimulation by NGF in cells expressing p75NTR but not TrkA leads to neuronal apoptosis (Frade, Rodriguez-Tebar and Barde, 1996).

TrkA receptors bind NGF with picomolar affinity. Being a tyrosine kinase receptor, TrkA undergoes dimerization and subsequent tyrosine phosphorylation on several residues in the cytoplasmic domain (e.g. Tyr674, Tyr675) upon NGF binding. These events are followed by activation of downstream TrkA-mediated signalling pathways (**Fig.3.2**), which include ERK1/ERK2, that act on the transcription factors CREB and MEF2; PI3K, that phosphorylates AKT; PLCγ, that produces DAG and

IP3, triggering Ca^{2+} release from the intracellular stores (Harrington and Ginty, 2013). These pathways upregulate pro-survival genes and are responsible for inhibition of apoptosis (Pazyra-Murphy *et al.*, 2009) by preventing activation of the pro-apoptotic transcription factor c-jun and of pro-caspase 3 (Mok, Lund and Campenot, 2009) and BAX translocation to the mitochondria (Putcha, Deshmukh and Johnson, 1999).

TrkA activation involves the production and retrograde transport of an endosome-based signalling platform that is described by the so-called signalling endosome hypothesis (Harrington and Ginty, 2013). The mechanism of endocytosis upon NGF binding can be classified as clathrin-dependent or clathrin-independent. The first form of endocytosis is characterized by the development of complexes that include TrkA, clathrin and AP2 (Howe *et al.*, 2001), while the second process involves the production of macropinocytotic structures that require the presence of the NGF-regulated GTPase (Shao *et al.*, 2002). The early stages of TrkA endocytosis involve the activation of PLCγ and in particular, PI3K, since PI3K inhibition through LY294002 at far distant axons affected retrograde NGF transport (Kuruvilla, Ye and Ginty, 2000). PI3K activation leads to the recruitment of AP2, the RAS related protein RAB5 and dynamin, which is involved in the scission of the endocytic vesicle from the cellular membrane (Harrington and Ginty, 2013). Moreover, long-distance movements of the endosome require disassembly of the actin cytoskeleton that is achieved after activation of Rac1-cofilin pathway, thanks to the stability of NGF-TrkA complex in the acid pH of early endosomes. In comparison to NGF, NT3 can bind to the TrkA and it activates the initial stages of endocytosis, but its labile interaction is interrupted during pH acidification in the endosome and thus NT3 cannot activate the subsequent steps (Harrington *et al.*, 2011). Finally, activated endosomes are transported back to the soma through dynein driven transport system along the microtubules. In these endosomes, TrkA is maintained in a phosphorylated state (Riccio *et al.*, 1997) and PLCγ, PI3K and Erk signalling persist during endosome transport.

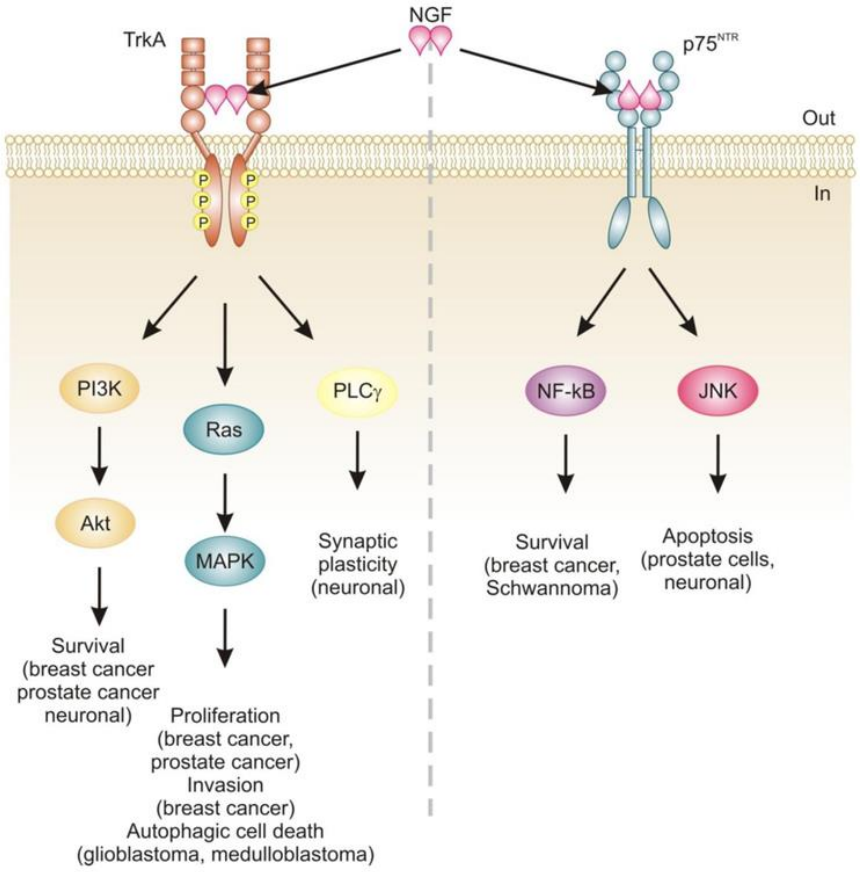

Fig.3.2 Signalling pathways activated by NGF (Molloy, Read and Gorman, 2011).

1.4 NGF structure

Human NGF crystal structure has been presented in complex with human TrkA (Wlesmann *et al.*, 1999). The NGF monomer is characterized by a pair of 2 stranded twisted β sheets with a reverse loop (L3) and a cysteine knot-motif, characterized by 3 disulphide bonds on one end, and 3 β hairpin loops (L1, L2, L4) on the other (**Fig.3.3**). In the dimer, the central β sheets of the two monomers pack against each other and interaction between residues of these two β sheets are responsible for the stabilization of the dimeric structure (Wiesmann and De Vos, 2001).

Like the other neurotrophin receptors, TrkA is a transmembrane protein characterized by an extracellular domain that comprises a leucine-rich domain between two cysteine-rich clusters, followed by two immunoglobulin (Ig)-like domains. These two domains are thought to be involved in NGF binding. TrkA Ig-like domain 5 by itself binds NGF with a similar affinity to the TrkA. TrkA-d5 consists of a β sandwich characterized by two four-stranded sheets. One comprises

strands A, B, E and D, the other strands C, C', F and G (Wiesmann and De Vos, 2001).

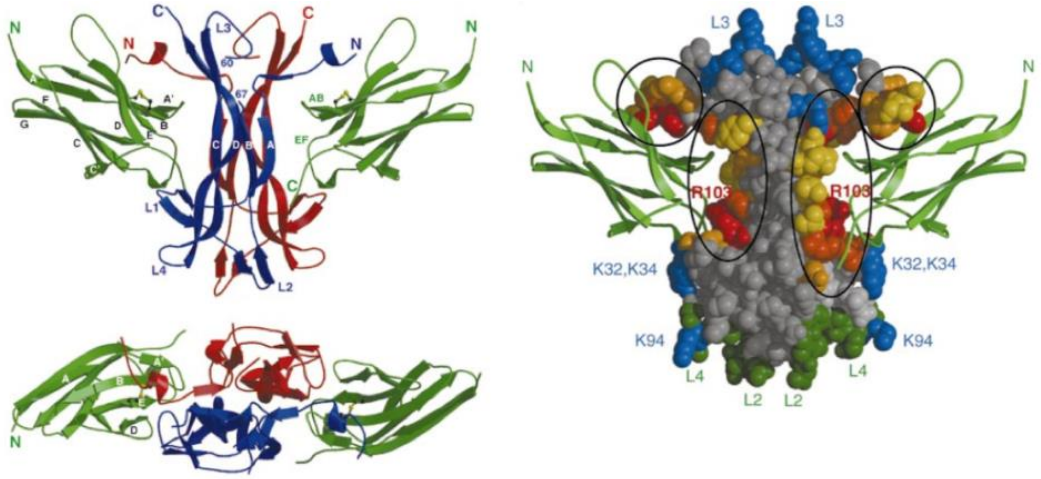

Fig.3.3 NGF structure in complex with domain 5 of TrkA (Wiesmann and De Vos, 2001).

The crystallographic structure of NGF in complex with domain 5 of TrkA shows 2 patches of interaction as represented in Fig.3.3 One patch is considered specific for NGF binding to its receptor, the other one is considered conserved since it is maintained throughout all neurotrophins. Since neurotrophins share a 50% of sequence identity, the presence of both patches allows TrkA binding to many neurotrophins but SN survival only upon NGF binding. For example, in SNs from the superior cervical ganglia, NT3 can interact with NGF receptor and to trigger its phosphorylation but not its retrograde transport and SN survival (Harrington *et al.*, 2011).

The conserved patch is the larger one and involves residues from the AB, C'D and EF loops, the C-terminus of TrkA, the β hairpin loop L1 and residues of the four β-strands of NGF. Arg103 is highly conserved among neurotrophins and its side chain protrudes from NGF to stack against the phenyl group of Phe327 on TrkA, forming a hydrogen bond with the carboxyl group of Asn349 (Wlesmann *et al.*, 1999; Settanni, Cattaneo and Carloni, 2003).

The specific patch is characterized by interactions between the N-terminal residues 2-13 of NGF and the ABED sheet of TrkA and shows small conservation among neurotrophins and receptors. In this interaction patch, residues 6-9 of NGF develop

a helical conformation; His4 and Ile6 are the most important residues involved in the ligand-receptor interaction. Ile6 is in a hydrophobic pocket at the surface of the TrkA with Pro5 and Phe7 contributing to the hydrophobic interactions. His4 and Glu11 increase the strength of the interaction by establishing hydrogen bonds with Ser304 and Arg347 of the 5th domain of TrkA (Wlesmann *et al.*, 1999).

1.5 NGF effects on sympathetic neurons

NGF is produced only in the low amount by the target organs, is required for sympathetic neuronal survival and axonal outgrowth. These observations are supported by the almost complete loss of sympathetic innervation in *NGF*$^{-/-}$ (Crowley *et al.*, 1994) or *TrkA*$^{-/-}$ (Smeyne *et al.*, 1994) mice, and are the basis of the neurotrophic factor theory: according to this hypothesis, the neurons and their ramifications are abundant during the development phase of peripheral innervation. Only the neurons reaching the target organ and establishing contact receive adequate NGF amounts to survive, while the unconnected ones are negatively selected, undergoing apoptosis. This mechanism matches the amount of innervation an organ receives to its size and demand (Harrington and Ginty, 2013).

Consistent with the concept of that neurons receive the required NGF from the peripheral target organs, it has been demonstrated that NGF withdrawal from the SN caused accumulation of phosphorylated c-jun in the cell body that could not be rescued by direct NGF administration at the soma (Mok, Lund and Campenot, 2009). These data support that signalling at the terminal axon is required for neuronal survival. However, it remains to be studied whether NGF signalling requires the establishment of a contact site between the sympathetic neuron and the heart or whether its release in the interstitial space is sufficient to allow pro-survival neurotrophin signalling.

Interestingly, NGF upregulates TrkA expression, influencing neuronal selection in the phase of target organ innervation. This implicates that neurons which are in close contact with the target organs would express more copies of TrkA, and therefore would have a reduced NGF requirement for survival. Conversely, neurons that are not well placed would express lower levels of TrkA and have a higher

requirement of NGF that, when insufficient would result in neuronal death (Deppmann *et al.*, 2008).

There may be another mechanism, through which NGF regulates neuronal selection. It is known that NGF signalling upregulates BDNF and NT4 in SNs. Since SNs do not express the BDNF/NT4 receptor (the TrkB), these neurotrophins act as an agonist of the p75NTR, causing neuronal death (Bamji *et al.*, 1998). This evidence has led to the idea that SNs establish an efficient interaction with the target organ expressing BDNF and NT4, leading to the death of neurons that fail to innervate the target organ in a paracrine manner, while being protected thanks to TrkA upregulation and NGF signalling (Deppmann *et al.*, 2008).

In addition to promoting neuronal survival, other effects of NGF on SGNs were supported by experiments performed on *NGF*$^{-/-}$ and *Bax*$^{-/-}$ mice (Glebova NO, 2004). Bax is part of the apoptotic machinery activated upon NGF withdrawal, and its deletion prevents sympathetic neuronal loss in NGF KO mice. Interestingly, despite neurons grow normally along vessels and reach the target organ in *NGF*$^{-/-}$ and *Bax*$^{-/-}$ mice, sympathetic innervation is absent in the heart and heterogeneously altered in the other organs. This work not only showed that NGF requirement by SNs varies among different organs and that initial sympathetic outgrowth does not depend on NGF, but also suggest that NGF regulates heart innervation independently of its pro-survival activity.

1.6 Other neurotrophins acting on SNs

In addition to NGF, a number of other neurotrophin-like factors have roles in SGNs growth and survival.

Artemin is expressed by smooth muscle cells and its receptor GFRα3 is expressed by SGNs (Honma *et al.*, 2002). Artemin is known to promote axonal growth along the vasculature. As a result, no increase in neuronal apoptosis was detected in SCG of mice KO for either artemin or its receptors at the early stage of development. Increased death was detected when neurons become dependent on target-derived NGF, suggesting that this effect is a secondary consequence of the failure of many neurons to innervate the target organ (Andres *et al.*, 2001).

Endothelin-3 (Edn3) has been reported to be expressed by the external carotid artery and a part of SGNs express its receptor EdnrA. Since axonal growth is completely absent in the external but not in the internal carotid artery of *EdnrA*$^{-/-}$ mice, Edn3 is relevant for axonal growth of a discrete subset of SGNs (Davies, 2009).

NT3 is a neurotrophin expressed and released by the vasculature and SGNs express its receptor (TrkC). NT3 enhances outgrowth of sympathetic processes *in vitro* (Davies, 2009). Consistently, 50% of SNs survived after birth in *NT3*$^{-/-}$ mice (Wyatt *et al.*, 1997; Francis *et al.*, 1999). Moreover, no innervation defects or increased neuronal death was observed in *TrkC*$^{-/-}$ mice (Fagan *et al.*, 1996), suggesting that NT3 effects on SNs are achieved through TrkA signalling rather than TrkC receptor at the early developmental stage. Despite this observation, since neuronal loss in *NT3*$^{-/-}$ or *NGF*$^{-/-}$ mice occurs at the same developmental stage and is not higher in double KO mice when compared to *NGF*$^{-/-}$ mice (Francis *et al.*, 1999), it seems more likely that in *NT3*$^{-/-}$ mice, SNs die because they fail to reach the target organ and do not receive the adequate supply of pro-survival NGF. For this reason, NT3 signalling seems to be important during axonal growth along the vasculature. Moreover, SNs show a developmental change in their responsiveness from NT3 to NGF that is mediated by NGF signalling. When neurons are starting to innervate their target, p75^{NTR} is much lower than TrkA and it is upregulated to similar TrkA levels after birth (Wyatt *et al.*, 1997). Since p75^{NTR} is known to increase TrkA affinity to NGF and to inhibit SN responsiveness to NT3, it seems that p75^{NTR} upregulation is involved in the change of neuronal dependence from NT3 to NGF (Davies, 2009).

Since SGNs do not express TrkB (Fagan *et al.*, 1996), BDNF or NT4/5 do not exert prosurvival effects, but might rather affect neuronal apoptosis through p75^{NTR}, as described before.

1.7 NE-NGF link

The existence of a crosstalk between neurotransmitter and neurotrophin signalling has been proposed in the case of the neuromuscular junction (NMJ), in which on the one hand the motor neuron activates the muscle by releasing acetylcholine and on the other, myofibers signal back to the neuron through the release of the

neurotrophin NT4. In the in vitro model between Xenopus motor neurons and muscles overexpressing NT4, the released of the neurotrophin from myocytes caused potentiation of presynaptic neurotransmitter release and the enhancement of postsynaptic response. Repetitive synaptic activity-induced NT4 release by the myocyte, further potentiating synaptic transmission (Wang and Poo, 1997). A similar role of synaptic potentiation was described for NGF. In this case, the stimulation of neurons in CM-SGN co-cultures caused a rise in CM contraction rate at increasing NGF concentrations. This effect was observed after either acute or chronic NGF stimulation (Lockhart, Turrigiano and Birren, 1997). Increased NGF expression was demonstrated in astrocytoma cells treated with the non-selective β-agonist isoproterenol (Mocchetti *et al.*, 1989), suggesting that in different cell types β-adrenergic and NGF signalling interact. However, neither a similar interplay between NE released by the neuron and postsynaptic NGF expression nor the effect of the interaction between β-adrenergic signalling and NGF dependent signalling has been addressed so far in the neuro-cardiac junction.

2. AIMS OF STUDY III

To study the role of the neuro-cardiac junction (NCJ) on sympathetic neuron survival and cardiac innervation.

3. METHODS III

3.1 Animal models

CMs isolated from neonatal (P1-P3) Sprague-Dawley rat hearts were used. All experimental procedures were performed according to the European Commission guidelines and have been approved by the local ethical committee and the Italian authority (Ministero della Salute), in compliance of Italian Animal Welfare Law (Law n.116/1992 and subsequent modifications), as well as of the guidelines of UK Home Office Animal (Scientific Procedures) Act of 1986 in London, UK.

3.2 Sympathetic Neuron (SN)/Cardiomyocyte (CM) co-cultures.

Rat and murine SN/CM co-cultures were set up, as described in Methods **ChapterII**.

3.3 PC12 cultures

In a subset of experiments, co-cultures were established between rat neonatal CMs and PC12-derived SNs. PC12 cells were maintained in an undifferentiated state in DMEM-H16, supplemented with 10% horse serum, 5% fetal bovine serum, 1% penicillin/streptomycin (all from Thermo Fisher). The SN differentiation medium was made by DMEM-H16, supplemented with 1% horse serum, 0.5% fetal bovine serum, 1% penicillin/streptomycin (all from Thermo Fisher), and 100 ng/mL NGF (Sigma Aldrich).

3.4 Plasmids and siRNA

The TrkA-DsRed2 plasmids was gift from Professors Moses Chao (Addgene). For NGF silencing experiments, we used the siRNA oligonucleotides (Sigma-Aldrich) previously used on mouse cells (si44) (Ogawa et al. 2012), which perfectly matched with the rat NGF mRNA encoding for the 2 transcript variants of the β polypeptide (XM_003749364.1, XM_227525.6). SIC001 was used as a control siRNA (Sigma-Aldrich).

3.5 Cell transfection.

Undifferentiated PC12 cells and CMs were transfected by using lipofectamine 2000 (Thermo Fisher) and TransFectin (Bio Rad), respectively, following the manufacturer instructions. 10 pmol oligonucleotides and 3 μg plasmid were incubated with TransFectin to achieve co-transfection of NGF siRNA and pEGFP.

3.6 Scanning Ion Conductance Microscopy (SICM)

This method was described in the Chapter I.

3.7 Action potentials

Action Potentials (AP) were recorded from sympathetic neurons in co-culture with cardiomyocytes at room temperature in current clamp using the whole-cell patch clamp techniques using an Multiclamp 700B amplifier (Molecular Devices, Sunnyvale, CA, USA) and pClamp 10.0 software. The external solution contained (in mM): 140 NaCl, 3 KCl, 2.5 CaCl2, 1.3 MgCl2, 5 HEPES, 11 Glucose; pH 7.4. Patch pipettes (3.5-5 MOhm) were filled with an internal solution containing (mM): 120 K-gluconate, 0.5 CaCl2, 1 MgCl2, 10 EGTA, 10 HEPES, 10 sucrose, 3 MgATP, 8 NaCl, 0.3 GTP, 20 Phosphocreatine, 5OU creatine phosphokinase; pH 7.2. Resting membrane potential (RMP) was recorded at the beginning of the experiments. For action potential recordings, cells were clamped at -70mV and action potentials were elicited with 5ms and 300ms depolarising current pulses of 50-200 pA. Data were samples at 10 KHz. AP characteristics were analysed using pClamp software (Molecular Devices, San José CA, USA).

3.8 Immunofluorescence analysis

Rodent hearts were harvested from adult rats and mice, fixed in 1% paraformaldehyde (PFA) (v:v in 1X PBS; Sigma Aldrich), and processed as described in (Zaglia *et al.*, 2013). 10 μm thick cryosections were obtained using a cryostat (Leica 1860) and processed for IF, as previously described (Zaglia *et al.*, 2013).

For *in vitro* IF analysis cells were stained followed the protocol described earlier (see Methods of **Chapter I**) The primary and secondary antibodies used in this study are listed in **Table 7.**

Table 7. Primary and Secondary antibody used in this study.

Target	Supplier	Dilution	Hot species
α-actinin	Sigma	1:200	Mouse
cTnI	Invitrogen	1:400	Mouse
TOH	Sigma	1:1000	Rabbit
SNAP25	Abcam	1:200	Mouse
TrkA	Alomone labs	1:200	Rabbit
NGF	Alomone labs	1:200	Rabbit

3.9 Evaluation of the size of SN varicosities.

To analyse the size of TOH or SynI marked sites, ROIs were manually drawn on the maximal projection obtained from the z-stack image series and areas were calculated using ImageJ or Fiji.

Analysis of post-synaptic membrane protein accumulation. The 'ReSlice' tool of ImageJ was used on neuronal boutons and the fluorescence intensity profiles were measured along ROIs manually traced on CM membrane.

3.10 Analysis of TrkA distribution at the neuro-cardiac contacts.

This analysis was performed with a custom-developed routine implemented in Matlab®. ROIs of the SNs and CMs are manually drawn on the IF images of the processes and on the BFs, respectively. The grayscale value of TrkA immunostaining inside the neuronal ROI is then calculated as a function of the distance from CM membranes. To subtract background, only pixels with a greyscale value higher than 50 were considered.

3.11 Assessment of NGF uptake by SNs

Here, we used a low affinity anti-NGF antibody (Abcam) that detected overexpressed neurotrophin and not the endogenous levels. Linear ROIs were traced along processes in BF images and the orthogonal section of both BF and

fluorescent images was obtained. After imposing a threshold to eliminate background, the number of processes with NGF positive vesicles was measured**.**

3.12 Imaging of TrkA-DsRed2 retrograde transport in co-cultures.

Time-lapse fluorescence microscopy was used to assess the TrkA-DsRed2 transport along the neuronal process as an effect of receptor activation by NGF. Imaging experiments were performed 7 days after differentiation with NGF 100 ng/mL. Cells on the coverslip were placed in a culture dish incubator and coupled to a heater controller (Warner Instruments) that kept the temperature at 37°C. A mixture of 5% CO_2, 95% O_2 was blown for atmosphere and pH control. During the imaging experiment, cells were maintained in complete medium without phenol red to avoid background. The culture dish incubator was coupled to the confocal microscope, using the immersion equipped with a 60× objective. For analysis of TrkA-DsRed2 movements along processes, kymographs of the time-lapse images were derived with the ImageJ® plugin kymograph. Vesicle trajectories were manually drawn in a blind manner and the direction and speed of TrkA-DsRed2 dots was quantified.

3.13 ELISA

To estimate NGF concentration in the CM conditioned medium, we used the ChemiKine NGF sandwich ELISA Kit (Chemicon), following the manufacturer's instructions.

3.14 Statistical analysis

All data are expressed as the mean ± SEM. Experimental groups were compared using unpaired (paired when appropriate) ANOVA tests and comparisons between multiple groups were performed using either the Kruskal–Wallis test or T-test $P < 0.05$ was considered statistically significant.

4. RESULTS III

4.1 The key molecular players of NGF signalling are predominantly found at the neuro-cardiac interaction sites

Myocardial neurons, originating from the sympathetic chain ganglia, elongate their processes throughout the heart walls, where they run along and between CMs, showing the typical pearl necklace morphology (**Fig.3.4 A**). In healthy adult rats and mice, similarly shaped and sized neuronal varicosities, which are displaced at regular intervals (1.7±0.2 μm) along the neuronal process and establish close contact with CM membrane (Prando *et al.*, 2018; Pianca *et al.*, 2019).

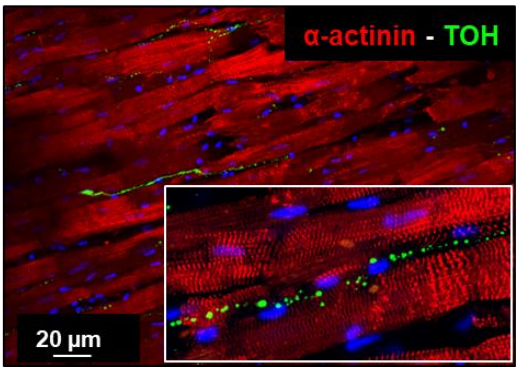

Fig.3.4 Sympathetic neurons varicosities displaced at regular intervals. Confocal IF analysis of heart sections from adult rats, co-stained with antibodies to α-actinin and TOH.

It is well agreed that sympathetic neuron (SN) survival and function are sustained by neurotrophins (mainly NGF), generally provided by the target-innervated organ. While evidence supports that direct communication between active catecholamine releasing varicosities and contacted cardiomyocytes, underlies neurogenic control of heart function, the role of intercellular coupling on cardiac-derived support of neuronal survival has remained neglected.

We thus made the hypothesis that the NCJ may also represent the preferred site for 'CM-to-SN' neurotrophic signalling and used confocal immunofluorescence (IF) to visualize the presence and local distribution of the molecular elements of NGF signalling at the SN-CM contact sites. Sympathetic neuronal processes, identified with an antibody against tyrosine hydroxylase (TOH), showed immunoreactivity for the high affinity NGF receptor (TrkA), which was predominantly detected in

SNAP25 positive varicosities contacting CMs (at intercellular distances included between 0 and 0.5 μm) and not in those distant from the target cell (**Fig.3.5**).

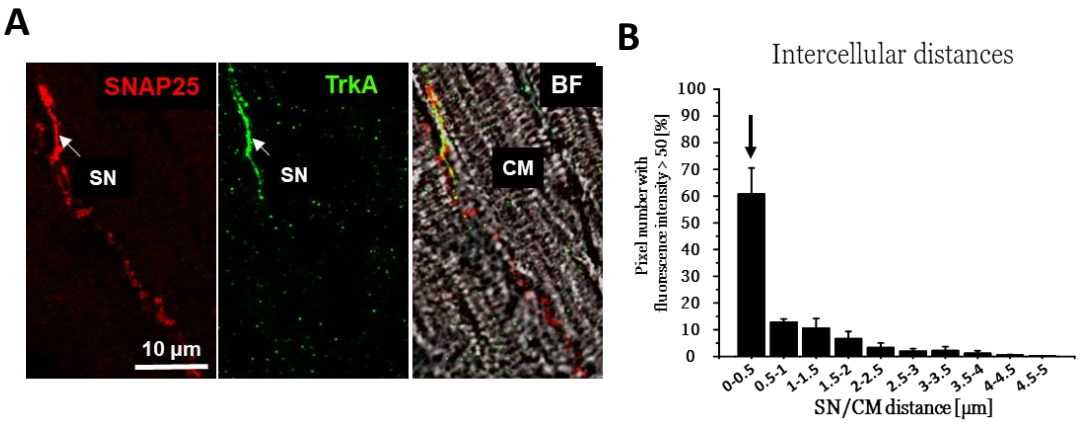

Fig.3.5 The player of NGF signalling are localized at the NCJ. A) Confocal IF analysis of heart sections from adult rats, co-stained with antibodies to SNAP25 (red) and TrkA (green). The right image in panel (A) shows the bright field (BF). **B)** Quantitative analysis of TrkA immunostaining in neuronal processes at different intercellular distances from the CM membrane. The arrow indicates the neuro-cardiac interaction site. Bars represent SEM. (**p<0.01, n=19 confocal images from 3 different rat hearts).

Staining with an antibody specific for NGF demonstrated that the neurotrophin had a vesicular pattern within CMs, and clustered in a roughly 2μm deep submembrane space. Interestingly, in a significant number of neuro-cardiac contacts (about 56%), the NGF-enriched domains mirrored the position of the presynaptic neuronal process, indicating that the membranes of NGF-releasing myocyte and NGF-sensing varicosities face the same restricted domain (**Fig.3.6**). NGF was also detected along the SN process, likely resulting from active neurotrophin signalling initiated by NGF exchange at the intimate interaction site.

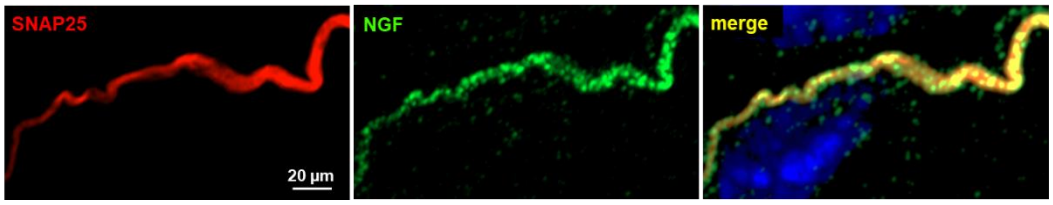

Fig.3.6 NGF mirroring position of SNAP25 in rat heart slices. Confocal IF analysis of adult rat heart sections, co-stained with antibodies to SNAP25 and NGF.

These results suggest that in the heart, CMs sustain SN viability through local NGF release at the neuro-cardiac junction (NCJ).

4.2 Local NGF release by cardiomyocytes sustains survival of the contacted sympathetic neuron

To investigate neurotrophin-mediated communication at the single-cell level, we used an in vitro model system already validated, based on the co-culture between SNs and CMs, which replicates the features of the neuro-myocyte interaction observed in the intact heart, in term of neuronal morphology, expression of lineage markers and exocytosis-related proteins.

After few days in culture, in the presence of NGF, neuronal processes elongated, arborized, and established adhesion with the spontaneously beating CMs (**from Chapter II**). Neurons became mature with time, up to the first two weeks (**Fig.3.7 A-C**). Electrophysiologic analysis of SN at different time points during the culture, showed that maturation also included membrane properties, i.e. action potential.

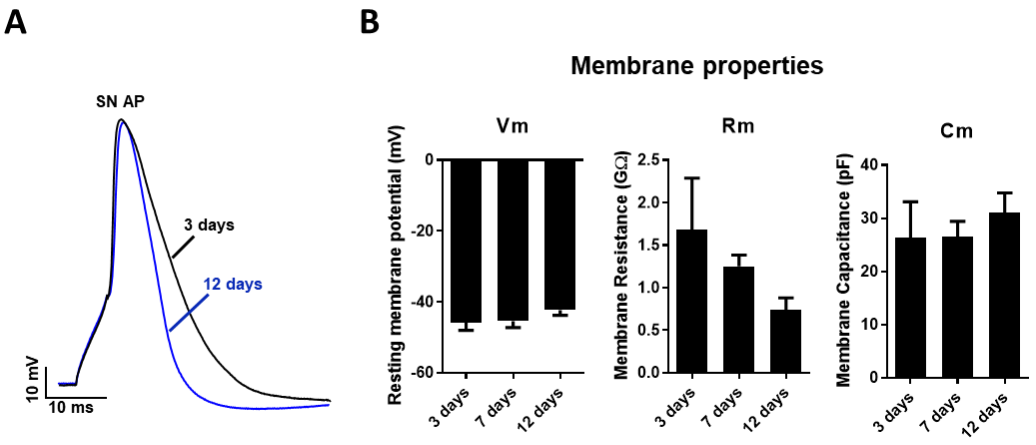

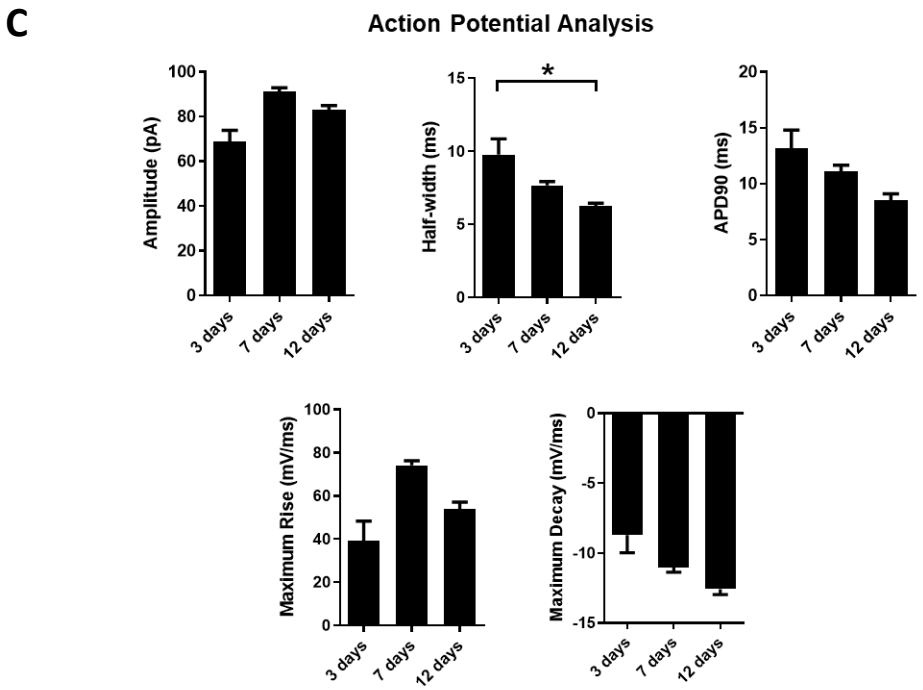

Fig.3.7 Action potential modulation in SNs indicates their maturation in time during co-culture with CMs. A) APs evoked by short pulses applied to the soma (5 ms and 300 ms duration, 50-200 pA amplitude, 10 KHz). **B)** Membrane properties: Resting membrane potential (Vm); -46±2, -46±2, -42±1 mV; Membrane resistance (Rm): 1.7±0.6, 1.3±0.1, 0.7±0.2 GΩ; Membrane Capacitance (Cm): 26±7, 26±3, 31±4 pF, generated at 3, 7 and 12 days respectively. **C)** Action potential characteristics: Amplitude: 69±5, 91±2, 83±2 pA; Half-width: 9.8±1.1, 7.7±0.3, 6.2±0.2 ms; APD90: 13.2±1.7, 11.1±0.5, 8.5±0.6 ms; Maximum Rise: 39±9, 74±2, 54±3 mV/ms; Maximum decay: -8.7±1.2, -11.0±0.3, -12.6±0.4 mV/ms, for 3, 7 and 12 days. N=15cells, *p<0.05, error bars SEM.

As previously demonstrated, when SNs are cultured alone, removal of NGF from the culture medium causes SN degeneration and death (**Fig.3.8 A**).

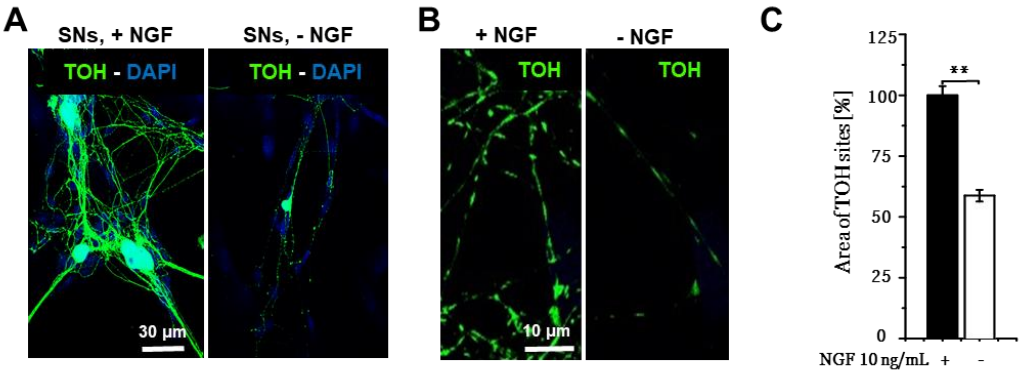

Fig.3.8 Degeneration of SNs in the absence of NGF. A-B) Confocal IF analysis of sympathetic neurons co-cultured in the absence or the presence of NGF. Nuclei were counterstained with DAPI. **C)** Quantitative analyses of the size of TOH-marked sites of SNs cultured in the absence or the presence of NGF in the culture medium. Bars represent SEM (**, $p<0.01$; n=453 varicosities for each group, from three independent cultures).

In addition to promoting cell survival, NGF also had trophic effects on the size of neuronal varicosities, which were larger in NGF-treated, than in NGF-deprived cultures, when neurons were culture alone. (**Fig.3.8 B-C**) (varicosity area: with NGF, 1.40±0.06 *vs.* without NGF, 0.82±0.04, in μm^2, $p<0.01$).

Neuronal death, caused by NGF withdrawal when neurons are culture alone, was reduced in SN-CM cultures at the early stage and almost entirely prevented when NGF was not supplemented externally (**Fig.3.9**), supporting that cardiomyocytes can support neurotrophic input to SNs.

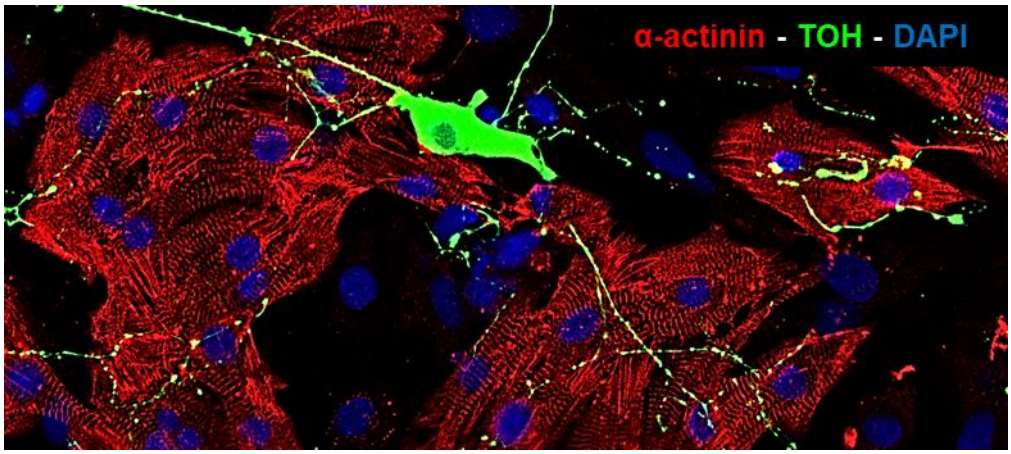

Fig.3.9 Local cardiomyocyte NGF release sustains innervating sympathetic neurons. Representative confocal IF image of SNs-CMs co-culture co-stained with antibodies to α-actinin and TOH.

By using SICM it was possible to evaluate the topographical characteristics of neuronal varicosities, as shown in **Fig.3.10 A-B**.

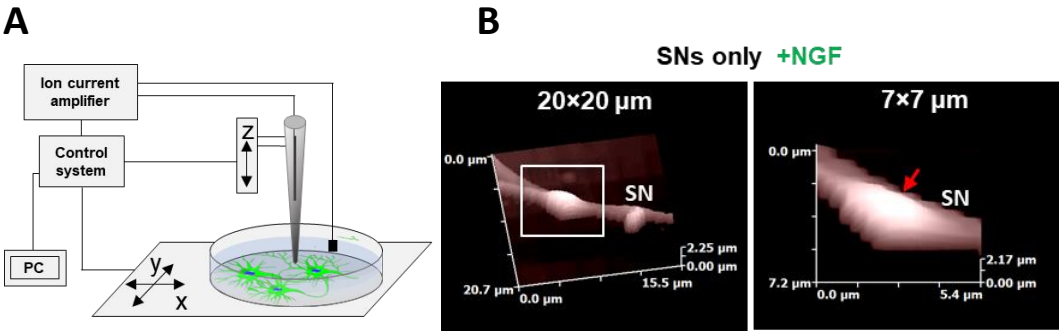

Fig.3.10 Synaptic button scanned by SICM in a pure culture of SN. A) Setup diagram of SICM: A nanoscale pipette serves as a scanning probe allowing the evaluation of the neuronal prosses surface topography. **B)** Representative 20×20 and 7×7 µm SICM surface scans of a sympathetic neuron synapse.

We thus scanned neurocardiac contacts in co-cultures without any addition of external NGF, at different co-culture time points. The results indicate that the varicosities enlarge from day 2 till day 4, then the size is maintained, even without adding NGF to the culture. (**Fig.3.11 A-C**).

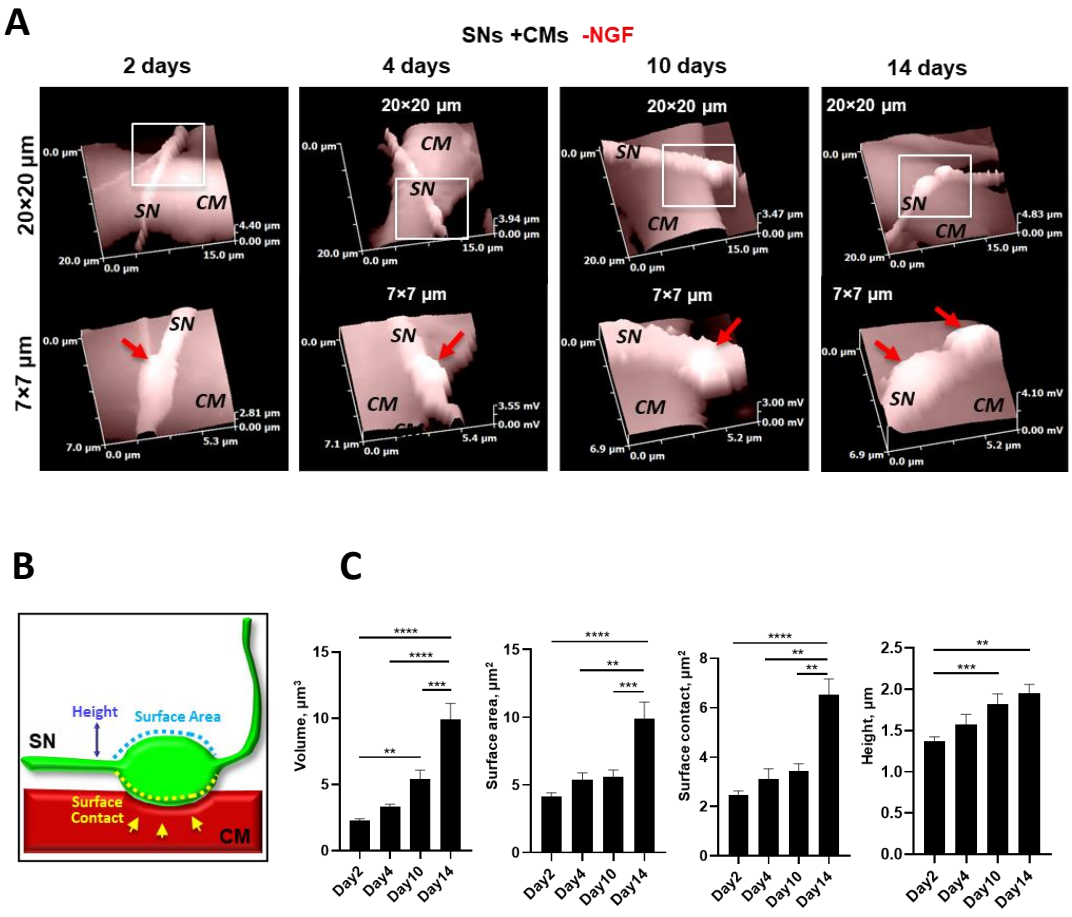

Fig.3.11 Sympathetic neurons co-cultured with CMs without addition of NGF. A) Representative 20×20 and 7×7 µm SICM surface scans of SN-CM contact sites obtained after 2, 4, 10 and 14 days. **B)** Schematic representation and summary graphs of the Volume: 2.3±0.1, 3.3±0.2, 5.391±0.7, 9.9±1.2 μm^3; Surface area: 4.2±0.3, 5.4±0.5, 5.6±0.5, 9.9±1.2 μm^2; Surface contact: 2.5±0.2, 3.1±0.4, 3.4±0.3, 6.5±0.6 μm^2; Height: 1.4±0.1, 1.6±0.1, 1.8±0.1, 2.0±0.1 µm of the neuronal processes were analysed, obtained after 2, 4 10 and 14 days respectively. (N=31 number of contacts, from 5 different isolations *, $p<0.05$, bars represent SEM).

Franzoso *et al*. already assessed the morphometry of neuronal processes in contact with CMs, showing that bigger boutons were developed in these conditions than non-contact processes ones (varicosity area: SNs contacting CMs, 3.28±0.13 vs. SNs not contacting CMs 2.36±0.14, in μm^2) (Unpublished data), further suggesting that CMs may sustain neuronally trophism. This was confirmed by SICM, which

we used to scan SN varicosities in co-cultures maintained in absence or presence of NGF (Volume: 5.1±0.6, 5.2±0.4, μm^3; Surface Area: 6.3±0.5, 7.2±0.4 μm^2; Surface Contact 3.5±0.3, 3.9±0.2, μm^2; Height: 1.8±0.1, 1.8±0.1, µm, for -NGF or + NGF respectively) (**Fig.3.12 A-C).** These results suggest that local CM-NGF release maintain the same size of varicosities as with addition of NGF to the culture, suggesting that CM may provide sufficient neurotrophic input to SNs to sustain neuronal survival and development.

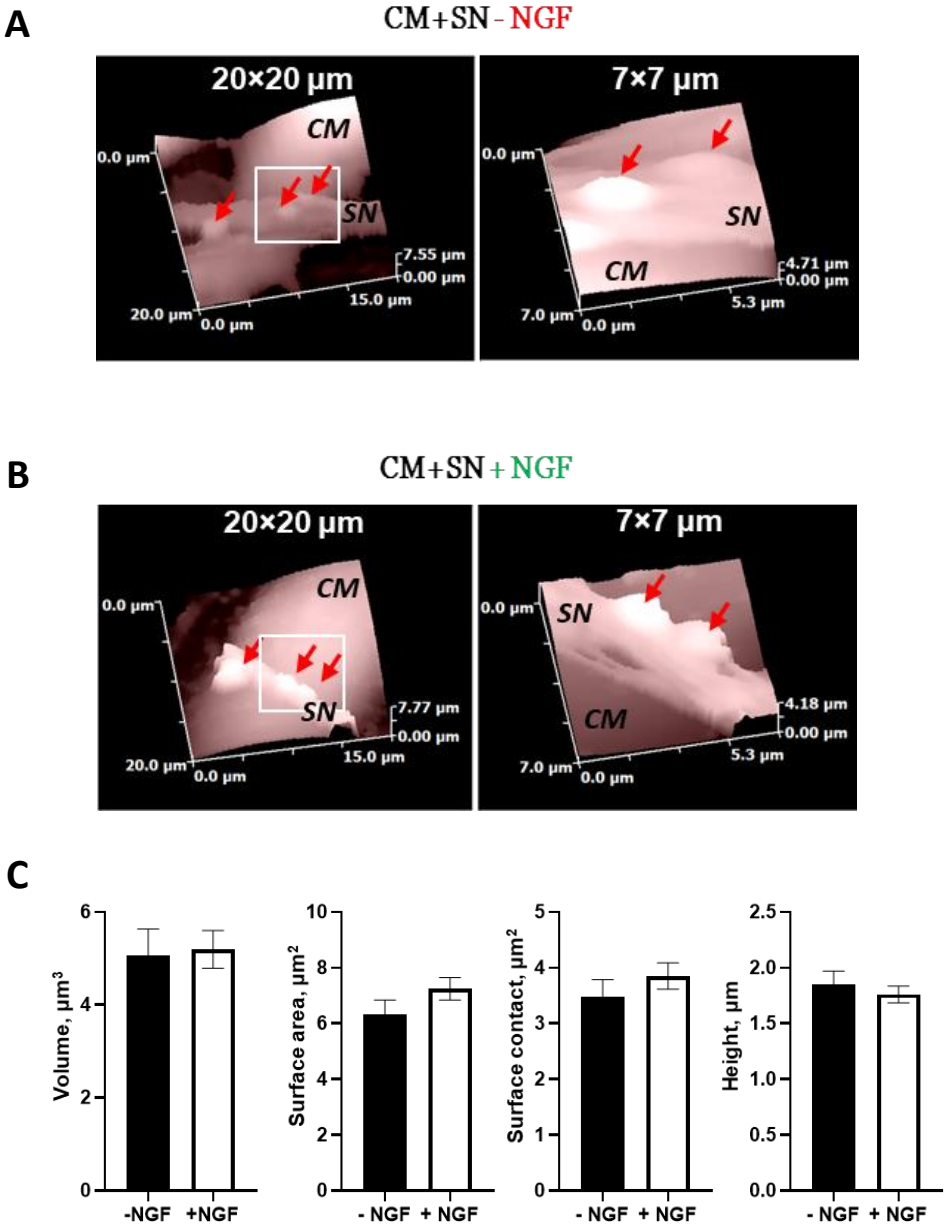

Fig.3.12 Local CM-NGF release maintain the same size of varicosities as with addition of NGF to the co-culture. A-B) Representative 20×20 and 7×7 µm SICM surface scans of SN-CM contact sites obtained in the absence or the presence of NGF **C) S**ummary graphs of the neuronal processes topographical characteristic such as Volume, Surface Area, Surface Contact and Height for -NGF or + NGF respectively. (N=19 number of contacts, bars represent SEM).

In line with this, increased neuronal viability in co-cultures was dependent on CM-released NGF, as silencing of cardiomyocyte with NGF-siRNA44 caused neuronal mortality to similar extent as NGF withdrawal in SNs cultured alone (**Fig.3.13-3.14**).

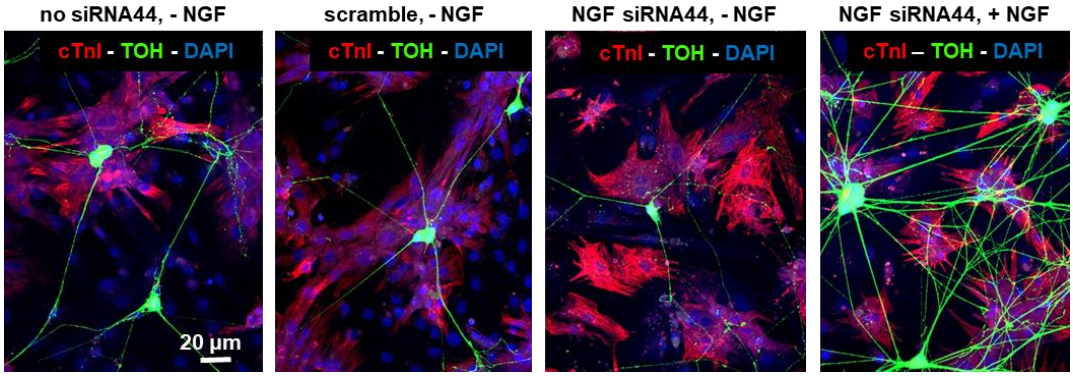

Fig.3.13 Cardiac sympathetic neurons are dependent on CM released NGF. Confocal IF analysis of SN-CM co-cultures transfected with scramble (SIC001) and NGF targeted siRNA44, co-stained with antibodies to cardiac troponin I (cTnI) and TOH. Nuclei were counterstained with DAPI.

Given that CMs produce and release NGF, we tested whether neuronal viability in the co-culture was preserved by the CMs releasing sufficient amounts of the neurotrophin in the medium. To assess this, neurons cultured alone were incubated in culture medium conditioned by cardiomyocytes, which failed to preserve cell viability (**Fig.3.14**). This result agreed with the measure of NGF concentration in the conditioned medium collected from 7-day SN-CMs co-culture without exogenous NGF, which resulted about 1000-fold lower (1.61±1, in pg/ml) than the minimal concentration required for neuronal survival (Lockhart, Turrigiano and

Birren, 1997), suggesting that mechanisms are in place to increase the effective NGF achieved at the neurotrophin receptor.

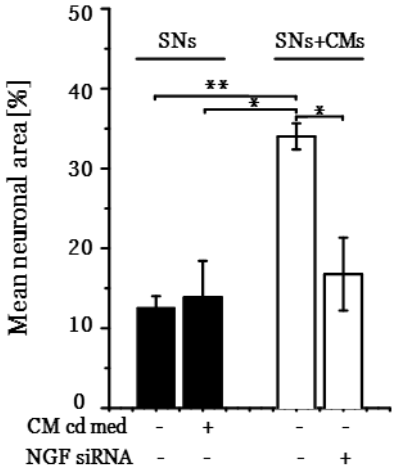

Fig. 3.14 Quantification of Area of neurons i) cultured alone without exogenous NGF in the culture medium (first bar) or treated with CM conditioned medium (second bar), ii) in co-cultures with CMs upon neurotrophin withdrawal (third bar) or NGF-siRNA44 delivery to CMs (fourth bar, error bars represent SEM, *0.01<p<0.05, **p<0.01, on average, 28 images per condition were analysed from 3 independent co-cultures). Upon NGF withdrawal, higher neuronal numbers were measured in co-cultures when compared to SNs alone (neuronal numbers: 34.01 ±1.63% vs. 12.58 ±1.44%, respectively). Treatment of SNs with CM conditioned medium or NGF silencing in co-cultures resulted both in neuronal numbers similar to neurotrophin deprived neurons (neuronal numbers: 13.88 ±4.55% and 16.78 ±4.57%, respectively).

Consistently, co-transfection of siRNA against NGF and GFP, which allowed identify silenced CMs, resulted in the selective decrease in size of those TOH marked varicosities in contact with GFP+/NGF-silenced CMs (**Fig.3.15**) (varicosity area: SNs contacting scramble-CMs, 1.52 ±0.06 *vs.* SNs contacting shNGF-CMs, 1.21 ±0.06, in μm^2). Consistently, decrease in SN varicosity size was prevented by NGF addition to the culture medium.

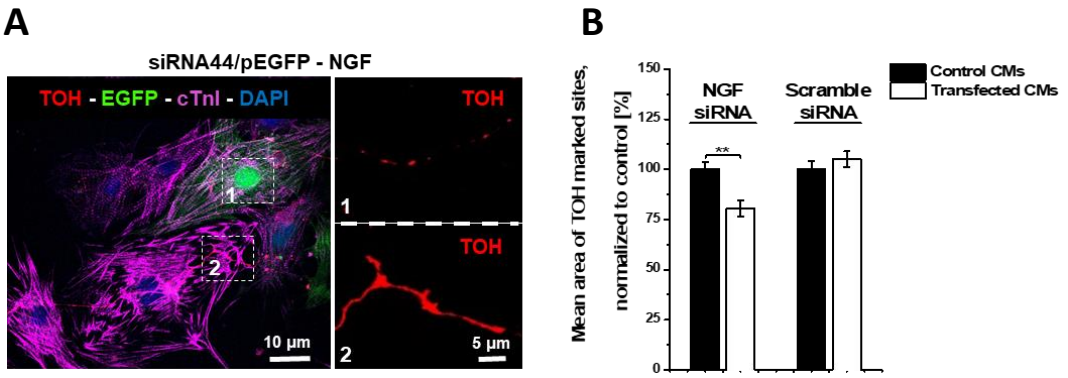

Fig.3.15 Evidence of cell-to-cell NGF mediated signalling. A) Confocal IF analysis of SN-CM co-cultures co-transfected with siRNA against NGF and pEGFP (green signal). Cells were co-stained with antibodies to TOH and cTnI. Nuclei were counterstained with DAPI. **B)** Quantitative analysis of the size of TOH marked sites along processes on GFP positive (shNGF) or negative (control) CMs, in co-cultures undergone shNGF. Bars represent SEM (**, $p<0.01$, n=448 varicosities for each group. Three independent cultures were analysed). Data are normalized to processes on non-transfected CMs of the same cultures.

Our results indicate that CM-released NGF acts on SNs at a concentration sufficient to promote neuronal viability and maturation, *via* direct intercellular interaction, despite NGF is almost undetectable in the culture medium.

4.3 The neuro-cardiac interaction is required for TrkA activation and NGF uptake in the neuron

It has previously been shown that NGF binding to TrkA receptors on the neuronal membrane triggers the endocytosis and retrograde transport of the NGF/TrkA complex to the soma (Hendry *et al.*, 1974) and activates the expression of survival genes (Deppmann *et al.*, 2008). We exploited the retrograde translocation of the NGF-TrkA complexes to functionally assay NGF signalling in CM/SN couples. To this aim, we expressed the fluorescent fusion protein TrkA-DsRed2 in SNs, which was localized on the cell membrane, as well as in intracellular vesicles along the neuronal processes, and used real time confocal microscopy to monitor the speed and direction of the fluorescent protein complex (**Fig.3.16 A-B**).

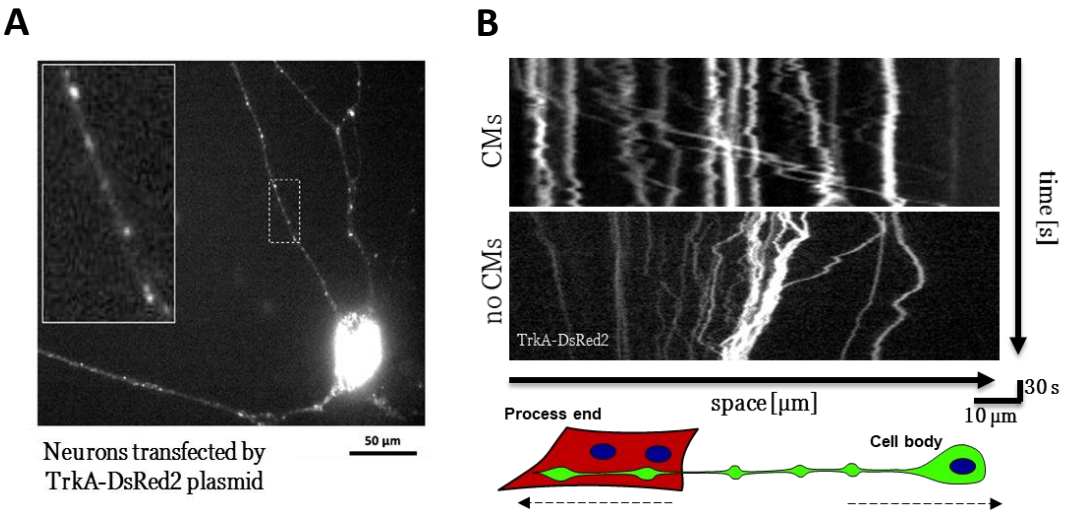

Fig.3.16 TrkA retrograde transport in SNs. A) Representative confocal IF image of cultured SNs transfected with the fused fluorescent protein TrkA-DsRed2. **B)** Kymographs of TrkA-DsRed2 expressing processes on CMs (upper panel) or other cardiac cells (lower panel), without NGF in the culture medium. Vesicles moving to the right side are directed to neuronal soma.

It was shown by Nomura *et al.* (2011) that velocity of TrkA vesicles associated with NGF was remarkably higher than that of TrkA vesicles without NGF. Remarkably, our result demonstrates that the number and speed of TrkA-DsRed2 vesicles retrogradely transported was significantly higher in processes contacting CMs, than in isolated SNs or in those contacting other cell types present in the co-culture (e.g.

cardiac fibroblasts) (retrograde movements in SNs: on CMs, 21.17±10.98 *vs.* on non-myocyte-cells 5.77±1.73, in %; * p<0.05) (**Fig.3.17**).

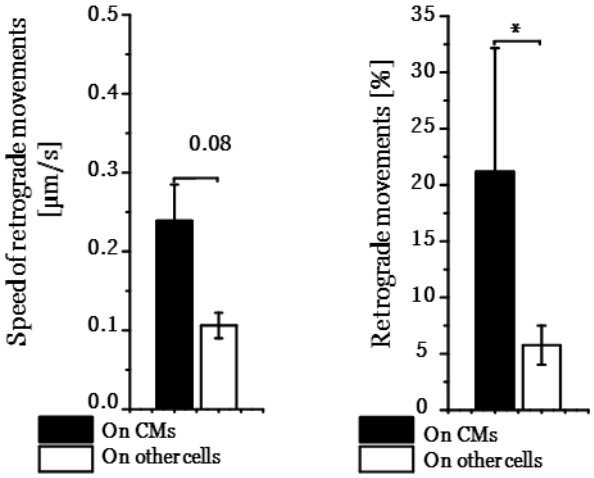

Fig.3.17 Quantification of the number and speed of TrkA-DsRed2 retrograde movements in SN processes contacting CMs vs. SN processing innervating non-myocyte cells. Bars represent SEM (*, p<0.05, n=15 cells for each group; 3 independent cultures were analysed).

These results demonstrate directly that CMs exchange NGF with the contacted neurons, and efficiently activate pro-survival receptor signalling.

Altogether, the data presented above are in line with the generation of a high concentrated NGF domain at the NCJ and suggesting that the neuro-cardiac contact sites form a structurally determined domain, which may direct release of NGF. These results indicate that direct neuro-cardiac contact sites represent functional CM/SN communication units allowing local and efficient intercellular NGF signalling.

5 DISCUSSION III

In this work we investigated the role of retrograde signalling from CMs to SN, and how it is crucial for neuronal survival and development. We provided morphologic evidence of NGF in CMs, and TrkA NGF receptors in contacting neuronal varicosities. We deeply accessed into the molecular physiology of cardio-neuronal communication, by applying advanced imaging methodologies in an *in vitro* model system based on the co-culture sympathetic rat SCG neurons and neonatal CMs.

The evidence that CM establish contact sites with sympathetic neuron varicosities has formed the background of the investigations (Takeuchi *et al.*, 2013; Wengrowski *et al.*, 2015; Oh *et al.*, 2016; Sakai *et al.*, 2017; Prando *et al.*, 2018). We here show that retrograde trophic signalling between myocyte and neuron (Franzoso, Zaglia and Mongillo, 2016), which is key for their growth and survival, also takes place at these contact sites.

This hypothesis is firstly supported by the evidence that in heart sections, the high affinity NGF receptor TrkA is found in correspondence to the neuronal varicosities (Fig. 3.6). The distance between neuron and cardiomyocyte membranes is typically within 0.5 micron. Complementary to the NGF-sensing apparatus, immunostaining for NGF in myocardial sections showed the presence of the neurotrophin in cardiomyocytes, mirroring the position of the presynaptic neuronal processes. These results indicate that in the heart, the key molecular players, of heart-neuron signalling are preferentially localized at the neuro-cardiac junction, supporting that the myocyte may locally release neurotrophin to the TrkA expressing neuronal ending.

We further showed in an in vitro model system, that junctional contact sites between the neuron and cardiomyocyte develop and grow in time with NGF dependent mechanism.

The observation guiding subsequent experiments was the remarkable effect that the co-culture with CMs had on NGF dependency of SNs. While NGF withdrawal from the culture medium of SNs cultured alone, to shrinkage of the varicosities and death of the majority of cells, in co-culture with CMs neurons developed mature processes even in the absence of exogenous NGF and developed ramifications and intercellular contacts. The failure of CM conditioned medium to sustain neuronal

survival, which was identical to that observed upon NGF removal, and the very low NGF concentration measured in the culture medium suggest that intercellular NGF signalling may take place at localized signalling compartments. The NGF concentration measured in the co-culture medium was of about three orders of magnitude lower than that required by neurons to survive in culture, despite their full survival and development. This suggests that the effective NGF concentration activating TrkA receptors is higher, as result of diffusion restricted signalling compartments, like the neuro-cardiac junction. We have previously shown that neuro-cardiac contact sites enable neuro-cardiac signalling to occur efficiently and locally, and the morphologic aspect of the intercellular contact sites suggest the NCJ may play the same effect on NGF signalling.

To investigate on these aspects, we exploited state-of-the-art methods in cell biology, using Scanning Ion Conductance Microscopy to determine the cell topography at the neurocardiac contact site, and Real time confocal imaging of TrkA-DsRED trafficking in co-cultures to functionally assay retrograde NGF signalling.

Scanning Ion Conductance Microscopy allowed to determine the topography of neuro-cardiac contact sites and obtain high resolution details on the membrane displacement of neurons and myocytes. The surface topography of neuronal varicosities at contact sites with cardiomyocytes was characterized, and the elevated spatial resolution of the methodology was used to calculate Surface Area, Surface contact, Height and Volume of the typical neuro-cardiac junction.

Experiments on co-cultures at different time points in development of the NCJ showed that growth of the neuronal varicosity occurs in time and that intercellular contact has the same effect of NGF on the size of varicosities. This suggests that NGF signalling occurs at the contact site regardless of the addition of the neurotrophin in the medium, and that the contacted CM provides enough neurotrophin to activate its trophic effect.

To directly assess NGF signalling dynamics in co-culture, we exploited that signalling is mediated by the NGF receptor TrkA, which gets internalized and translocated, NGF-bound, to the neuronal soma. To test if CMs would release NGF and activated retrograde transport of TrkA on the contacted neurons, we expressed

a fluorescence-labelled TrkA construct in SNs and used real-time confocal microscopy to visualise the TrkA DS vesicle movements. This assay allowed to quantitate the speed and direction of the vesicle translocation. Both parameters were measured in neurons in contact with CMs through specific junctions and in neurons in contact with other cells present in the same culture dish, for instance fibroblasts, although the latter express even higher amount of NGF. Interestingly, the directed movements of TrkA vesicles toward the cell soma were higher in neurons receiving NGF from CMs than from other cells. This is in line with the results of (Pianca *et al.*, 2019), showing that cardiomyocytes establish with neurons more stable contacts than cardiac fibroblasts, whose interaction is transient and dynamic.

Altogether, our study has used multiple methodologies in experimental cardiology, in different models in vitro and ex vivo, to demonstrate that neurotrophic signalling from the heart to sympathetic neurons occurs through localized signalling compartments at the contact points between neuronal varicosities and the CM membrane. The neuro-cardiac junction structure enables CMs to sustain and direct neuronal development with low amounts of NGF. Conditions that increase the intermembrane distance between neuron and myocyte, or reduce NGF synthesis e.g. aging, diabetes (Kaye *et al.*, 2000; Pittenger and Vinik, 2003), which are accompanied to lower efficiency of adrenergic signalling (Ferrara *et al.*, 2014; Fu, Wang and Xiang, 2017), are poised to have reduced NGF signalling efficiency as well, and this will be tested in future experiments.

CHAPTER IV

"SYMPATHETIC NEURON – FIBROBLAST COMMUNICATION. MYOCARDIAL INFARCTION."

Index

1. INTRODUCTION IV

1.1 Fibroblast-SN interaction

The heart is constructed by the ordered displacement of multiple cell types, including CMs, endothelial and smooth muscle cells, fibroblasts and immune resident cells. It is innervated by sensory, sympathetic and parasympathetic neurons, which interact and influence all cells in the tissue. Given the plethora of implications in myocardial biology, the identification of molecular mechanisms involved in the crosstalk between cardiac sympathetic nerves and cardiomyocytes, cardiac fibroblasts or vascular cells, has a fundamental importance in understanding both normal and pathologic heart function.

Cardiac fibroblasts (CFs) are key cellular regulators of the highly dynamic myocardial ECM, which impacts on heart structure and function in both normal and pathologic conditions. CF-dependent ECM deposition and degradation have been attributed to the effects of a variety of intrinsic (e.g. microRNA, trophic and cell death released factors) and extrinsic factors (e.g. hormones, cytokines), some of which take part to pathologic ECM remodelling and interstitial fibrosis, which compromises heart mechanics and predisposes to arrhythmias (Fan *et al.*, 2012). Thus, there is a growing interest in identifying strategies to prevent CF activation. Based on previous results demonstrating a close connection between CFs and SNs (Mias *et al.*, 2013), and current literature showing that CFs express sympathetic neurotransmitter receptors, we will test the hypothesis that *the cardiac SNs are regulators of CFs biology in vivo*. Sympathetic neurotransmitters promote fibroblast proliferation and differentiation, via β2AR and NPY-R (Grässel and Muschter, 2017). In addition, it was observed that in co-cultures, SNs and FBs interact and communicate (Zurn, 1992; Nindl *et al.*, 2004; Mias *et al.*, 2013)although the mechanisms and dynamics of such intercellular interaction are not elucidated.

Looking at the anatomy of the cardiac SNS, with the exclusion of neurons originating in cardiac ganglia, neuronal bodies mainly organize into the stellate ganglia, and long axons travel along blood vessels and reach the epicardium, from where processes distribute in the myocardial interstitium and interact with the

different cardiac cell types. Neuronal interaction with fibroblasts, which can be identified in myocardial sections, has been described in vitro to have different dynamics than that of neurons with cardiomyocytes (Pianca *et al.*, 2019). Neither the morphologic adaptations of the interacting cells, nor the functional communication between SNs and fibroblasts have, however, been studied in detail. SNs mainly discharge two neurotransmitters: NE and NPY, which are stored in different vesicles. FBs express receptors for both neurotransmitters which, have been shown to promote FB proliferation and differentiation (Oben *et al.*, 2003).

Fibroblasts isolated from healthy rat hearts revealed that Pro-Nerve growth factor (NGF) and pro-differentiating mature NGF were abundantly expressed (Mias *et al.*, 2013). As described earlier, NGF is the major trophic factor for sympathetic nerves, not only supporting growth but also survival and differentiation, and promoting cardiac nerve outgrowth during development or in some pathological conditions (Aloe *et al.*, 2016). The level of NGF in the target organ is also directly correlated to sympathetic innervation density, and fibroblasts are thus poised to release neurotrophin and attract neuronal interaction. Consistently, co-culture of PC12 cells with cardiac fibroblasts leads to their differentiation into neurons, and this was prevented by anti-NGF blocking antibodies suggesting a paracrine action of NGF secreted by fibroblasts (Mias *et al.*, 2013).

Activated fibroblasts (myofibroblasts) isolated from myocardial infarction rat hearts exhibited significantly higher mature NGF expression than normal fibroblasts. Within the ischemic area, which lacks cardiomyocytes, tyrosine hydroxylase immunoreactivity was increased and associated with local “anarchic” and immature sympathetic hyperinnervation; notably, tissue norepinephrine content was similar to that of normal cardiac tissue, suggesting depressed sympathetic function (Mias *et al.*, 2013).

1.2 Role of sympathetic neurotransmitters in the regulation of fibroblast proliferation and differentiation

As mentioned above, SNs discharge two main neurotransmitters: NE and NPY.

NE elicits a proliferative effect on cultured rat cardiac fibroblasts which is prevented by the β2-adrenergic blockade. The activation of CREB contributes to

the increase in proliferation (Kwon *et al.*, 2009). The p42/p44MAPK pathway, which was also found to be activated by NE, might as well be involved in the regulation of the comedogenic effect. (Leicht, Greipel and Zimmer, 2000).

Neuropeptide Y (NPY), a 36-amino acid peptide, is a sympathetic neurotransmitter, regulating many physiological and pathophysiological processes in the respiratory system. Crnkovic *et al.* (2014) determined an increased NPYergic innervation within the pulmonary arterial wall and higher expression of the NPY receptor 1 (Y1-receptor) in the lungs of patients diagnosed with pulmonary hypertension; they also demonstrated a vasoconstrictive effect of NPY on lung vessels and a proliferative effect on pulmonary smooth muscle cells. NPY induces proliferation, migration, and increase IL-6 synthesis in fibroblasts. NPY null mice had decreased IL-6 signalling and a reduced proliferation of lung fibroblasts. Additionally, IL-6/STAT3 signalling has been reported to promote differentiation of fibroblast into myofibroblast (Pedroza *et al.*, 2016).

The effect from NE and NPY differ through cell types. Transgenic mice overexpressing NPY in adrenergic neurons have increased level of hepatic triglycerides, fatty acids and cholesterol, which contributed to the development of hepatosteatosis (Ruohonen *et al.*, 2008). It was shown that the sympathetic neurotransmitters, norepinephrine and neuropeptide Y, markedly stimulate the proliferation of activated, myofibroblast-like, hepatic stellate cells. Beta-adrenoceptors also impact on collagen gene expression. Physiologically relevant concentrations of sympathetic neurotransmitters directly modulate the phenotype of hepatic stellate cells. This suggests that targeted interruption of sympathetic nervous system signalling in hepatic stellate cells may be useful in constraining the fibrogenic response to liver injury (Oben *et al.*, 2003).

In the cardiovascular system, there are three known NPY receptors: Y1R, Y2R, and Y5R (McDermott and Bell, 2007). These receptors are expressed in the peripheral and central nervous system, including within the blood vessels, CMs and entero-endocrine cells (Brothers and Wahlestedt, 2010). The cardiac-related NPY receptors have been commonly implicated in pathological states and have been suggested to be prominent players in the pathogenesis of cardiovascular diseases

including hypertension, atherosclerosis, myocardial ischemia/infarction, diabetic, stress and hypertrophic cardiomyopathies, and heart failure (Tan *et al.*, 2018).
Receptors responding to norepinephrine in heart cells are mainly β1, β2, and β3 isotypes. Cardiac fibroblasts express predominantly β2AR, as recently demonstrated with cAMP imaging by Grisan *et al.* (2020).

1.3 SD208 TGF-β inhibitor

The cytokine transforming growth factor β (TGFβ) is a major contributor to fibrogenic responses underlying cardiac interstitial fibrosis.
Both TGFβ1 levels and relative mRNA are significantly increased in cardiac infarct scar and correlated with collagen type I expression and elevated Smad 2, 3, and 4 (Hanna and Frangogiannis, 2019). This suggests that heightened responses to TGFβ may significantly contribute to cardiac fibrosis. TGFβ directly induces collagen production and ECM contraction by fibroblasts, including those isolated from heart tissue (Lijnen and Petrov, 2002). Overexpression of TGFβ in heart, under the control of the albumin promoter, caused myocardial fibrosis. TGFβ1, β3 and LTBP are increased in patients with cardiac fibrosis associated with valve replacement surgery, suggesting the involvement of active TGFβ in cardiac fibrogenesis (Leask, 2007).
Recently Błyszczuk *et al.* (2020) showed that SD208 inhibitor effectively blocked TGFβ1-mediated growth of human fibrotic cardiac microtissues.

1.4 Myocardial infarction

1.4.1 Epidemiology

An estimated 17.9 million people died from cardiovascular diseases in 2016, representing 31% of all global deaths. Of these deaths, 85% are due to heart attack and stroke (World Health Organization or WHO). Acute myocardial infarction is caused by cell necrosis due to significant and sustained ischaemia (Mendis *et al.*, 2011), which is usually, the acute manifestation of atherosclerosis-related coronary heart disease. MI results from either coronary heart disease, which implies

obstruction to blood flow due to plaques in the coronary arteries or, much less frequently, to other obstructing mechanisms (e.g. spasm of plaque-free arteries).

1.4.2 Pathogenesis of MI with a focus on the mechanisms underlying myocardial remodelling

The correct function of cardiac cells, like other cells in the body, is compromised in case of insufficient oxygen supply. A condition of imbalance between the requirement of oxygenated blood by the myocardium and the inability of the coronary circulation to supply it is indicated by the term ischemia. Ischemic heart disease, also called coronary heart disease, is currently the main cause of death in the human population of industrialized countries. More than 90% of individuals affected by this pathology have atherosclerotic occlusions of one or more main branches of the coronary arteries. The part of the myocardium normally perfused by the blocked coronary will no longer receive blood and oxygen, will no longer have a nutrient supply and be incapable of removing of catabolites.

When the perfusion of the myocardium is reduced for more than 20-40 minutes, ischemia leads to cell necrosis. As consequence of the reduced availability of oxygen, oxidative phosphorylation is inhibited and the ATP concentration is lowered (Kalogeris *et al.*, 2012). This leads to an increase in anaerobic glycolysis, which is however unable to compensate for the reduced ATP, but leads to an increase in the concentration of pyruvate and then lactate, with consequent tissue acidosis (Chan *et al.*, 2018).

Ischemia inevitably leads to injury of intracellular organelles. Mitochondria undergo damage caused by reactive oxygen species (free radicals), which in addition to having a critical role in the pathogenesis of infarction, play a chemotactic function for leukocytes (Grisham and Granger, 1988).

Alterations in the pumps and proteins associated with the membrane of the sarcoplasmic reticulum, contribute to raise cytoplasmic calcium, with consequent activation of proteases, lipases and DNAs which begin to degrade all cellular components. Under these stresses, cardiomyocytes within a few hours from the onset of ischemic damage die, and coagulative necrosis occurs in man within 12

hours of the onset of ischemic damage and continues as a prevalent process for 3-4 days (Kalogeris *et al.*, 2012).

For many years, scholars have agreed that the loss of CMs during an acute heart attack occurred only through necrosis. It has been observed that death from apoptosis also plays an important role in the progression of ischemic damage, especially in regions not affected by ischemia, but which will participate in the remodelling of the ventricular wall (Zhang *et al.*, 2001; Rodríguez, Lucchesi and Schaper, 2002).

The necrotic process, unlike apoptosis, triggers a rapid inflammatory response. In humans, inflammation appears within 12-16 hours of the ischemic event, with inflitration by neutrophil granulocytes first and then lymphocytes, plasma cells and macrophages (phase 2). Phase 3 coincides with the formation of the granulation tissue and in humans is completed within 2-3 weeks. This tissue is made up of macrophages, blood vessels formed by neoangiogenesis and "fibroblast-like" cells called myofibroblasts (Cleutjens *et al.*, 1999). The pre-existing collagen is degraded by proteolytic enzymes called matrix metalloproteases (MMP) such as MMP-1 (collagenase) and MMP-8 (gelatinase). Subsequently, inhibitory tissue proteins of the same MMPs intervene, and the deposition of new collagen (collagen types I and II) by the myofibroblasts begins (Cleutjens *et al.*, 1999). These cells express a protein pattern typical of smooth muscle cells, including Smooth Muscle Actin, SMA, and for this reason, they show a dual nature of actively proliferating and contractile cells.

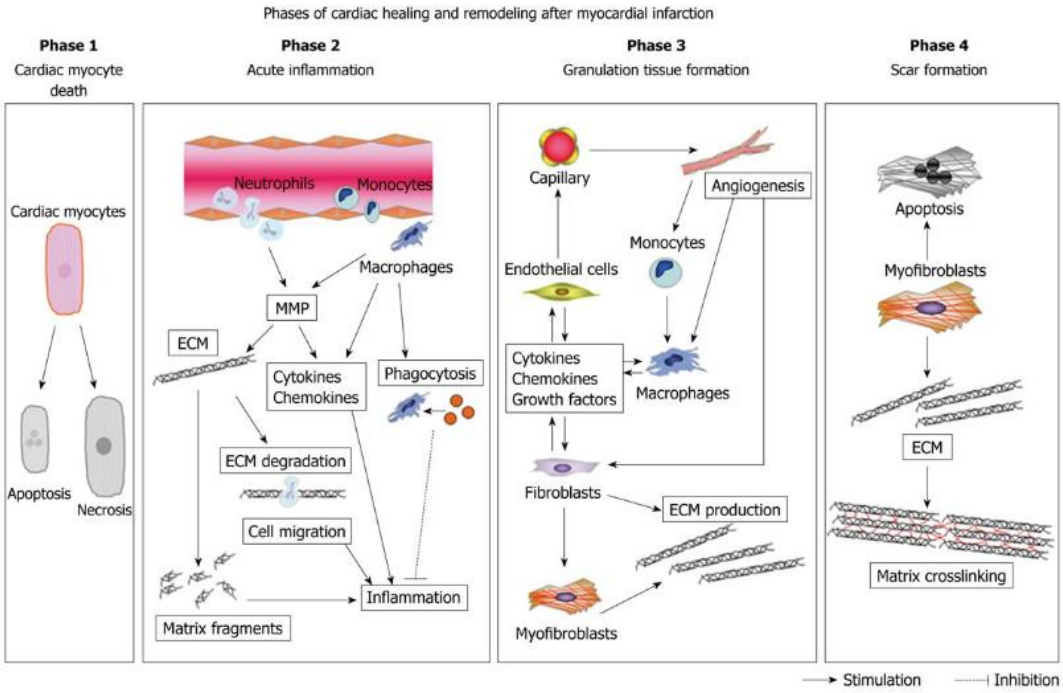

Fig.4.1. Phases of cardiad healing and remodeling after MI (Matsui et al . Matricellular proteins in myocardial infarction. 2010).

Myofibroblasts are the main protagonists of the remodelling process (phase 4, **Fig. 4.1**) which will lead to the replacement of the granulation tissue with the scar tissue destined to permanently remain in place of the myocardium.

1.4.3 Cellular therapies

Despite major advances in the management of ischemic heart disease, as it was mentioned above, myocardial ischemia remains a leading cause of morbidity and mortality worldwide (Lalu *et al.*, 2018). Therapies aim at preventing maladaptive myocardial remodelling, prolong survival of patients and mitigate the consequences of MI. Unfortunately, there are no drug treatment which generate new contractile tissue or reverse the ischemic myocardium. Based on the novel knowledge about undifferentiated cells, namely pluripotent stem cells, which are able to differentiate into various cytotypes, there are new strategies applying stem cells in possible tissue reparation (Lalu *et al.*, 2018). In recent years, stem cell transplantation has emerged as a promising therapeutic strategy for acute and chronic ischemic cardiomyopathy (Higuchi *et al.*, 2017). Several clinical trials are registered in the ClinicalTrial.gov

database, including trials in acute myocardial infarction using Human Pluripotent Stemm cels (hPSCs), Human Induced Pluripotent Stemm cells (hiPSCs) and Human Embryonic Stem cells (hESCs) (Higuchi *et al.*, 2017). These cell types have a high capacity to differentiate into several cell types, including CM, and they show strong functional integration with the myocardium (ref). Clinical trials were performed with patches contacting the stem cells, which were implanted into patients as well as with intracoronary injection of stem cells into a reperfused ischemic area (Higuchi *et al.*, 2017). Studies in this trials indicated that cells improved the ejection fraction, recovered the dysfunctional cardiac wall, increased vascular genesis, and decreased fibrosis in heart disease models (Guo *et al.*, 2020). Unfortunately, treatment by these cell types was accompanied by several problems. First of all ethical, relative to the societal perception of hESCs, and physiological, as cells with high proliferative capacity and undifferentiated can undergo neoplastic transition. (Lalu *et al.*, 2018). Along with hESCs, there are other cell types in use, namely Skeletal Myofibroblast (SMs), Mesenchymal Stem cells (MSCs), Bone Marrow Mononuclear cells (BMMNCs), and Hematopoietic Stem cells HSCs. SMs are the subject of most research on cell sheet for the treatment of acute MI. This is due to advantages such as autologous transplantation, ischemia resistance, nonmyocyte lineage differentiation, and high proliferative potential (Guo *et al.*, 2020). SMs improved cardiac function with fibrosis suppression, increased systolic function, increased wall thickness, and enhanced neovascularization, indicating the sufficiency and feasibility of SMs for cell sheet-based therapy in clinical MI (Guo *et al.*, 2020). Speaking about disadvantages there is limited potency of de novo cardiomyogenesis and arrhythmic risk.

1.4.4. Drug therapies

The fundamentals of pharmacologic treatment of myocardial infarction are aimed at different objectives depending on the disease phase. Initially, therapy is directed towards breaking up blood clots, prevent platelets from gathering and sticking to the plaque, and prevent further ischemia (Heart Association, 2020). After survived MI, therapy aims to avoid or slow down myocardial remodelling, which in time

occurs globally in the heart as result of the reduced muscle mass and function (Garza, 2015).

During the last 25 years, trials of treatments to prevent myocardial remodelling have established that beta-adrenergic receptor blockers and ACE inhibitors are the cornerstone of therapy when applicable (McMurray *et al.*, 2005). The landscape of possible medical options to treat HF is, however, rather unchanged, and novel therapeutic concepts are needed to treat efficiently this global burden. Beside the standardized pharmaceuticals, which are aimed at protecting the cardiomyocyte from excessive workload and degeneration, the cardiac sympathetic neurons may represent valuable alternative targets, as well demonstrated by the effects of vagal (parasympathetic) stimulation in HF (Hadaya and Ardell, 2020).

Preservation of cardiac mechanics is a long-sought goal, and it has become evident that the first physiopathology consequence of both chronic and acute myocardial ischemia, although with different mechanisms, are the interstitial collagen infiltration and subsequent diastolic defects (Nagueh, 2020). Although in chronic coronary artery disease, the extent and distribution of collagen is clearly different from replacement fibrosis following ischemic death of CMs in acute MI (Suthahar *et al.*, 2017), in both cases hardening of the myocardial interstitium reflects on reduced diastolic function and increased filling pressure.

Sympathetic neurons have the potential to modulate function and biology of cardiac fibroblasts and may be potential regulators of fibroblast activation and collagen deposition. This would be in line with the protective effect of beta-adrenergic antagonist against cardiac fibrosis in postischemic cardiomyopathy (Castaldi *et al.*, 2014). Neuromodulation would be an attractive option to maintain the healthy cardiac interstitium, and drugs which may enable this would be most welcome.

2. AIMS OF STUDY IV

To compare the dynamics of intercellular communication between cSNs and cardiac fibroblasts.

To define the role of sympathetic neurotransmitters in the regulation of cardiac fibroblast proliferation and differentiation.

To analyze the effect of removing sympathetic neurons on the tissue fibrotic response upon myocardial infarction

3. METHODS IV

3.1 Animal models

FBs and CMs isolated from neonatal (P1-P3) Sprague-Dawley rat hearts were used. All experimental procedures were performed according to the European Commission guidelines and have been approved by the local ethical committee and the Italian authority (Ministero della Salute), in compliance of Italian Animal Welfare Law (Law n.116/1992 and subsequent modifications), as well as of the guidelines of UK Home Office Animal (Scientific Procedures) Act of 1986 in London, UK.

3.2 Primary culture of neonatal fibroblasts

Cultured neonatal cardiomyocytes (CMs) were obtained from newborn (P1-P3) rat hearts and isolated following the protocol described previously (see Methods of Chapter I).

At the end of the digestion cycles, isolated cells were mixed and seeded in a 10 cm Petri dish (BD Falcon) and maintained in the incubator at 37°C for 1 hour. At the "pre-plating" stage cardiac fibroblasts were separated from CMs by faster adhesion to the dish. Fibroblasts were detached from the dish by covering them with 0.25% Trypsin-EDTA, applied for 5 minutes at 37°C. FBs suspension was centrifuged at 1250 rpm for 10 min. The supernatant was removed, and cells were re-suspended in 5 mL of first day medium. The total number of cells obtained was determined diluting cells in 0.2% Trypan Blue and counting viable cells in a Bürker chamber. FBs were then plated on laminin (20 ng/mm^2) - coated glass coverslips at a density of 50 cells/mm^2 for live imaging and immunofluorescence analysis. Then, 24 hours after isolation, cells were washed by ADS Buffer and the medium was replaced on the second day medium.

For FBs, New medium (see Tab.1 from Chapter I) was used during culturing.

3.3 Superior cervical ganglia neuron isolation

Sympathetic neurons were obtained from newborn (P1-P3) rat hearts and isolated following the protocol described previously (see Methods of Chapter II). The culture medium described in Chapter I (see Tab.1 of Chapter I) was used.

3.4 Co-cultures of SNs and CFs

Freshly isolated rat neonatal fibroblasts and sympathetic neurons were mixed at the ratio 1:5 (Neurons:CFs) and seeded at glass coverslips coated with laminin 0.1 μg/mm^2 at the density 50 cells/mm^2 for fibroblasts and 10 cells/mm^2 for neurons respectively.

Co-cultures were cultured with the "New protocol" (see Tab.1 of Chapter I), for the first day medium additional 100 ng/mL nerve growth factor (NGF) was added and replaced with second day culture medium after 24 hours.

3.5 Immunofluorescence analysis

Fibroblast-sympathetic neuron (CF/SN) co-culture were stained following the protocol described earlier (see Methods of Chapter I) The primary and secondary antibodies used in this study are listed in **Table8**.

Table 8. Primary and Secondary antibody used in this study.

Target	Supplier	Dilution	Host species
α-actinin	Sigma	1:200	Mouse
TOH	Sigma	1:1000	Rabbit
VIM	Invitrogen	1:1000	Chicken
αSMA	Invitrogen	1:1000	Mouse
KI67	Abcam	1:500	Rabbit

3.6 Scanning Ion Conductance Microscopy (SICM)

This method was described in the Chapter I.

3.7 Live imaging of cAMP dynamics

The protocol for cAMP dynamics in living fibroblasts was the same as described for CMs in the Methods section (Chapter I).

Sympathetic neurons co-cultured with FBs were activated by superfusing 1 μM nicotine in the bath. NE (100nM) and IBMX (50μM) were used as control for fibroblast activation. The analysis was performed with ImageJ, and changes of cAMP were measured in the cell cytosol by measuring the ratio between 480nm

and 545nm fluorescence emission signals upon excitation at 430nm, after background subtraction.

3.8 Calculating KI67 and αSMA positive cells

To calculate the number KI67 positive cells the software ImageJ was used. For the calculation α-SMA, positive cells the following algorithm was chosen from the control images, approximately 10 cells with the highest α-SMA immunoreactivity were identified and the average intensity of the signal was calculated. Then, the number of positive α-SMA cells in all conditions including treated with SD208, NE and NPY were calculated automatically with ImageJ by setting threshold as defined in the control experiments.

3.9 Mouse pharmacological heart denervation

Mice underwent intraperitoneal injection of 6-hydroxydopamine hydrochloride (6-OH-DA, Sigma Aldrich H4381-1G, 100mg/kg) (0.9% NaCl + 0.1% ascorbic acid). 6-OH-DA is a neurotoxin used to selectively destroy dopaminergic and noradrenergic neurons, as it enters the neurons via the dopamine and noradrenaline reuptake transporters and leads to neurodegeneration due to oxidative stress. Controls were represented by mice injected with vehicle solution. For irreversible sympathetic denervation, 6-OH-DA injection started at birth and repeated according to the scheme detailed in Fig.4.2

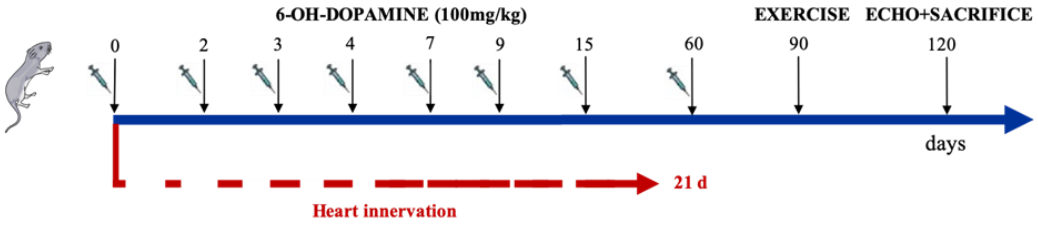

Fig.4.2 Protocol of pharmacologic sympathetic denervation in neonatal mice.

3.10 LAD ligation

3 months old CD1 mice were anaesthetized with isoflurane (2%). The neck area and the left side of the ribcage were shaved and disinfected using 80% ethanol. Left-sided thoracotomy between the 3rd and the 4th ribs was performed, the heart was isolated, and the pericardial sac carefully removed. The LAD was located between the pulmonary artery and the left auricle and ligated with a suture thread. The thoracic incision was closed after positioning a thoracic catheter (28G, venous catheter) between the 4th and the 5th rib (Kolk *et al.*, 2009).

3.11 Statistical analysis

All data are expressed as the mean ± SEM. Experimental groups were compared using unpaired (paired when appropriate) T-test, $P < 0.05$ was considered statistically significant.

4. RESULTS IV

4.1 Co-cultured sympathetic neurons extend processes forming a network with several cell-to-cell interactions.

Healthy sympathetic neurons are detected with IF in the myocardial interstitium. Neuronal processes show the typical pearl necklace morphology. Immunofluorescence analysis of rat heart slices (**Fig.4.3**) shows that neurons are distributed throughout the interstitial spaces and interact directly with cardiomyocytes at neuronal varicosities.

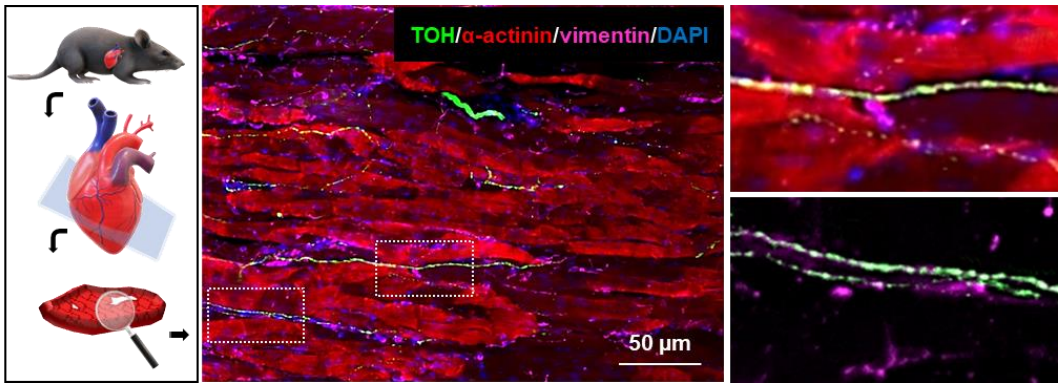

Fig.4.3 Representative confocal IF image of a rat heart slice. SNs were stained to TOH (green), CM to a-actinin (red), CFs to vimentin (magenta). Nuclei were counterstained with DAPI.

Neuronal processes can make close contact with myocardial fibroblasts as with cardiomyocytes (**Fig.4.4 A**). Moreover, sympathetic neurons, co-cultured with CFs develop with the same phenotype observed in co-culture with CMs (**Fig.4.4 B**), suggesting that both cell types are able to feed neurons with sufficient neurotrophic signalling. Neuronal varicosities appear near cardiac FBs, mimicking the phenotype of intact tissue in the heart.

The IF staining of CFs (**Fig.4.4 A**) showed that almost all cells in the culture are immunoreactive to α-smooth muscle actin (a-SMA). Although a-SMA is a frequently used marker of myofibroblasts (MFB), its specificity has been largely debated (Sun *et al.*, 2016; Park and Tallquist, 2018). Additional morphologic parameters and protein expression analysis, used to characterize and define the

profile fibroblasts and myofibroblasts, identified so-called “proto-MFB”, which are positive to α-SMA but do not show assembled myosin fibres (Baum and Duffy, 2011). As it is well agreed that a biological feature of MFB is the capacity to contract, it follows the ordered assembly of myosin filaments is a requirement (Mayer and Leinwand, 1997; Czubryt, 2019). We adhere to this latter definition, and define myofibroblasts interstitial cells, with assembled α-SMA actin fibers and which make up around 20% of the fibroblast culture. For simplicity, in the thesis, both cells are referred to with the inclusive definition “fibroblasts” except for paragraph 4.4 of this chapter.

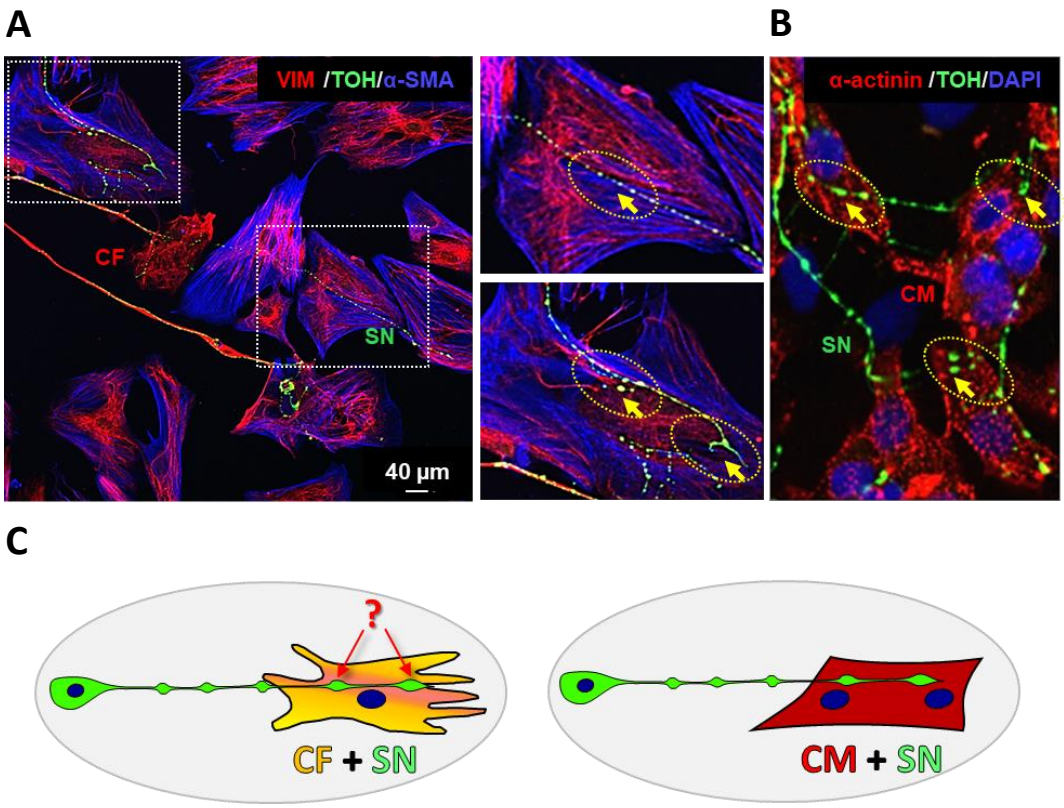

Fig.4.4 Sympathetic neurons co-cultured with FBs shows similar phenotype as co-cultured with CMs. Representative confocal IF images of cells in-vitro**. A)** CFs co-cultured with SNs (SNs, CFs, and MFBs were stained to TOH (green), to vimentin (red), and to α-SMA (blue), respectively). **B)** CMs co-cultured with SNs (right SNs and CMs were stained to TOH (green) and to a-actinin (red), respectively). Nuclei were counterstained with DAPI. **C)** Schematic representation of vesicles, which appear in both co-cultures with cardiomyocytes and fibroblasts.

4.2 Contact sites between cardiac SNs and cardiac FBs are smaller compared to SN-CM contacts.

To gain deeper insight into the characteristics of the neuron/CF contact site, we determined the cell surface profile using scanning ion conduction microscopy (SICM), which allows reconstructing the surface topography of living cells at high resolution. To increase our understanding of SN-CF interaction, we scanned the intercellular interaction of sympathetic neurons cultured with CFs. The volume of varicosities in contact with CFs is much lower than that of varicosities contacting CMs.

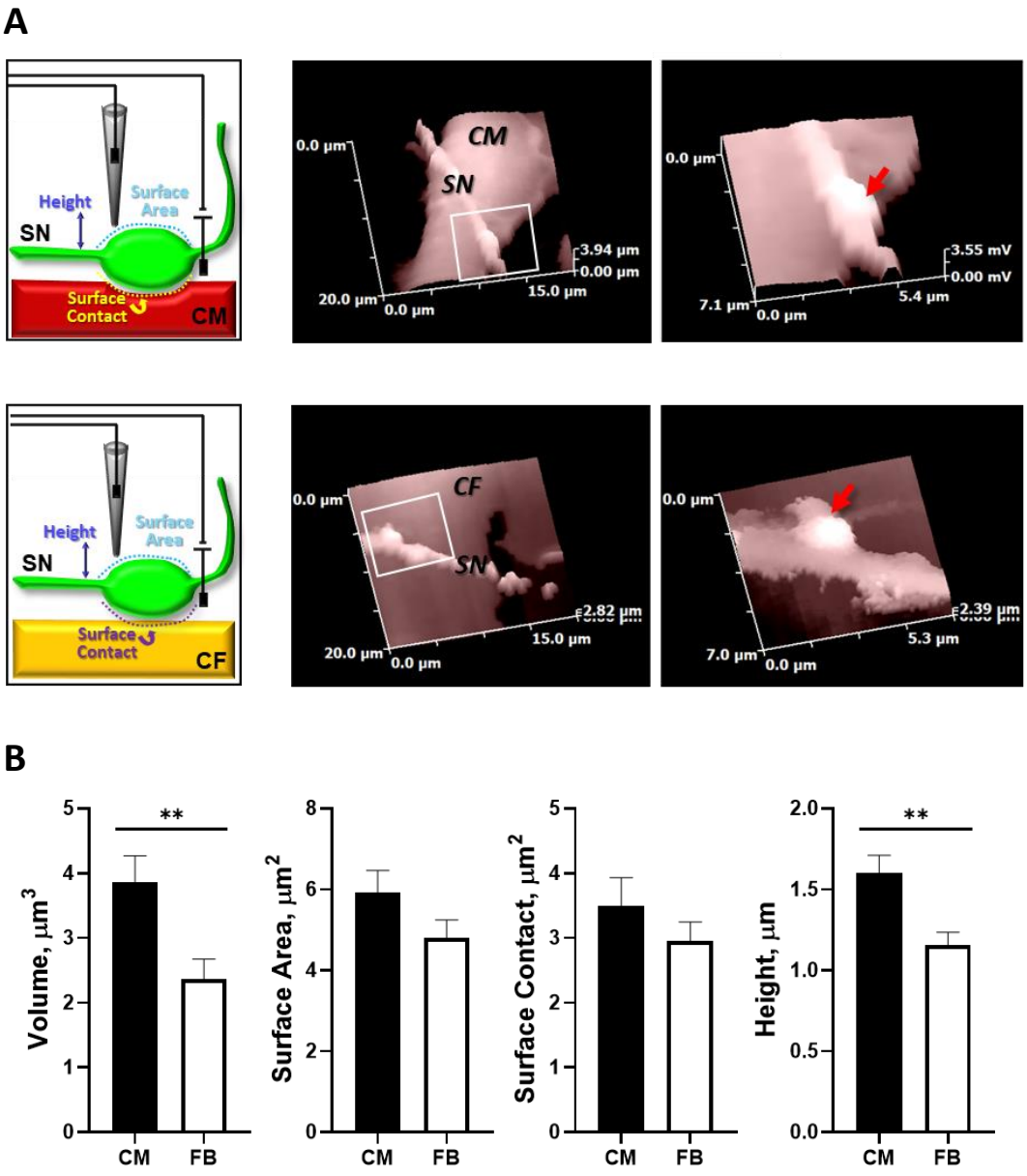

Fig.4.5 Comparison of contact sites between SNs and FBs or CMs scanned by SICM. **A)** Representative 20×20 and 7×7 μm SICM surface scans of SN-CM or SN-CF contact sites obtained in the absence of NGF **B)** Summary graphs of the Volume of connected neuron = 3.9± 0.4 and 2.4± 0.3μm^3, Surface area =5.9±0.6 and 4.8±0.4 μm^2, Surface contact = 3.5±0.4 and 2.9±0.3 μm^2, Height =1.6±0.1 and 1.2±0.1 μm with cardiomyocytes or fibroblasts, respectively. (*, $p<0.05$, from 3 different isolations, bars represent SEM).

On **Fig.4.5** representative scans of contact sites between sympathetic neurons and fibroblast or cardiomyocytes are shown. Quantitative analysis of the SICM experiments allowed to estimate the characteristics of the neuronal contact site, with either of the two cell types. Volume, surface, area, and height of the cell profile at the contact site were analysed for both co-cultures (**Fig.4.5 B)**, data are reported for CMs and CFs. We have established, in the preliminary experiments, that neurons cannot be easily scanned due to the loose adhesion of processes to the substrate. Thus, the method assumes that non-anchored neuron cannot be scanned.
The results show that SN do establish a connection with CFs.

4.3 cAMP imaging in cardiac fibroblasts co-cultured with sympathetic neurons.

Based on the previous results obtained by imaging methods, we aimed to determine whether the interaction between neurons and cardiomyocytes or fibroblasts underlay active signalling sites. We thus compared the dynamics of intercellular communication, by using real time cAMP imaging in CMs or FBs expressing the FRET-based cAMP probe H187, and co-cultured with SNs. Neuronal activation, by inducing the release of noradrenaline from varicosities, is expected to activate adrenergic receptors on the target cell and lead to an increase in intracellular cAMP. Nicotine (1µM) was used to activate SN. (**Fig.4.6 A-B)**

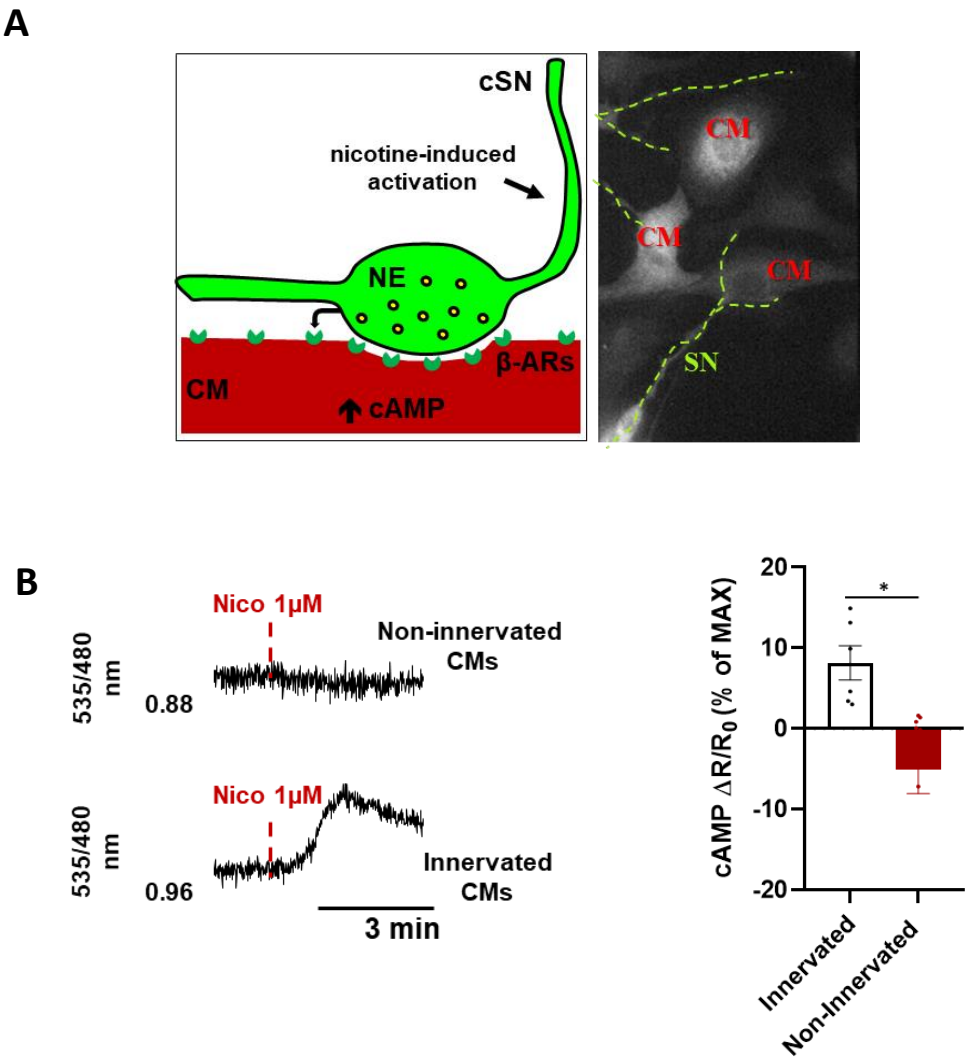

C

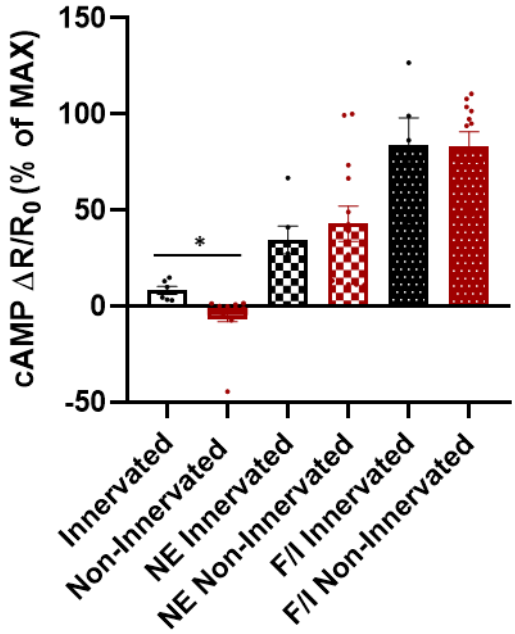

Fig.4.6 A) Representative image of neonatal CMs co-cultured with neurons infected by H187 virus. **B-C)** Neuronal stimulation elicits cAMP increase in innervated cardiomyocytes. Representative traces of cAMP changes in Epac1-camps expressing CMs, upon SN activation induced by 1uM nicotine, measured in innervated or non-innervated CMs, NE (1µM) and F/I (50µM) were used as control. Statistics of cAMP responses in corresponding groups (left/ down). Error bars indicate the SEM (* $p<0.05$; n =10.)

Neurons in contact with CMs, as previously shown by our laboratory, establish an interaction which warrants direct cell-cell communication. In support of this, activation of a SNs by nicotine caused an increase in cAMP only in the innervated CMs, while no changes were observed in non-innervated cells (**Fig.4.6 B-C**). This data supports that a structured, intercellular contact underlays the SNs to CM communication.

We thus explored the dynamics of SN-CF communication, by performing the neuronal activation assay on SN-CF co-cultures. Remarkably, SN activation did not generate cAMP increase in target FB, although cells responded to NE, added directly to the bathing medium (**Fig.4.7**). This data, together with the different morphology of SN-CF and SN-CM contact sites, indicates that the structured contact between neurons and CF is different than that established with CM.

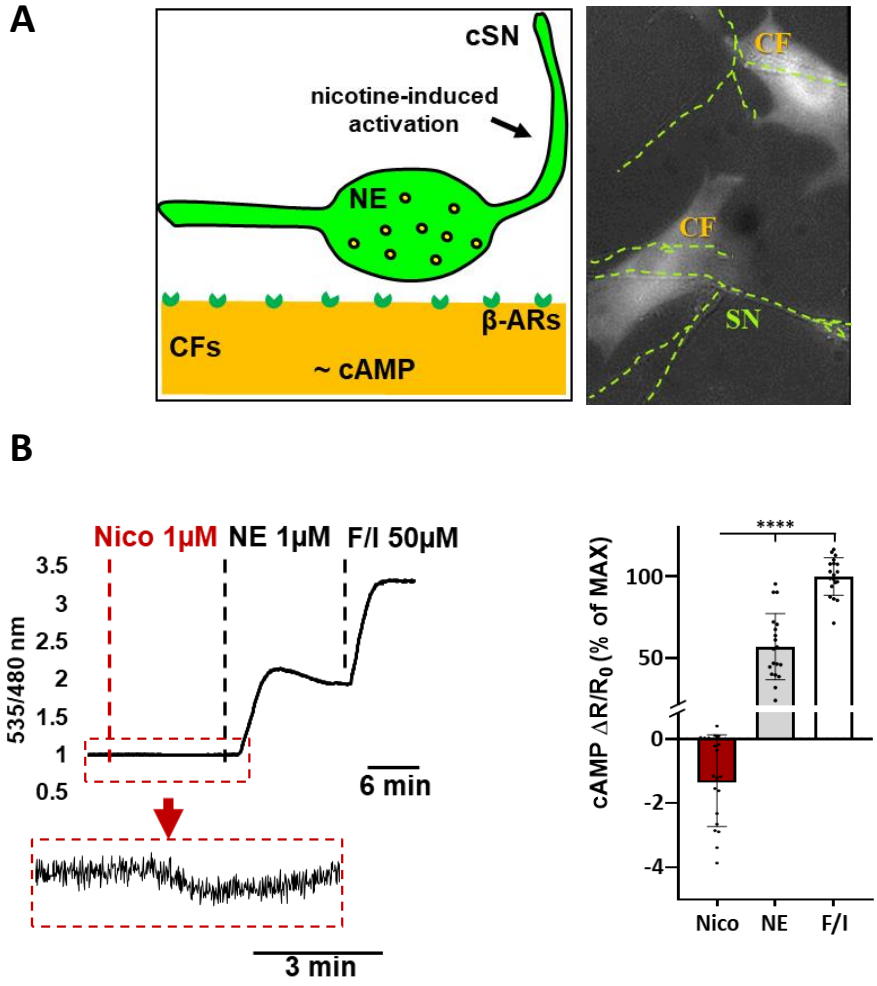

Fig4.7 A) Representative images of neonatal CFs co-cultured with neurons infected by H187 virus. **B)** cAMP imaging in neuronal cardiac fibroblasts co-cultured with neurons. Representative traces of cAMP changes in FBs, upon SN activation induced by 1uM nicotine. Statistics of cAMP responses (down). Error bars indicate the SEM (**** $p<0.001$; n =20 from 3 different isolation).

4.4 NPY increases the fraction of proliferating and differentiating cardiac fibroblasts.

We next aimed to determine the effect of the two sympathetic neurotransmitters, NE and NPY, on fibroblast proliferation. We thus treated cultured FBs with NE, NPY or a combination of both for 24 hours **(Fig.4.8 A).**

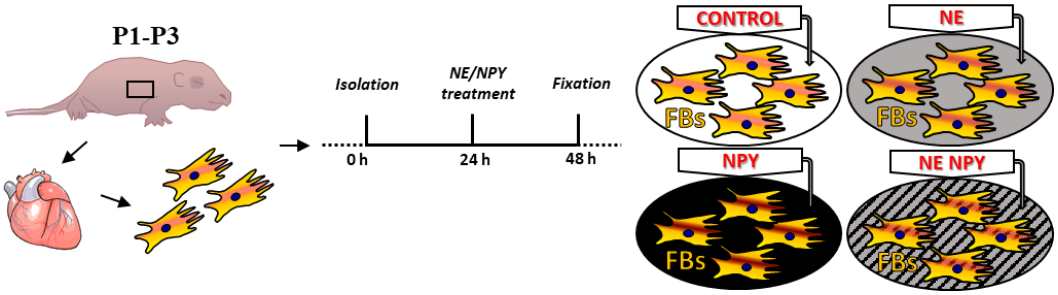

Fig4.8 Protocol of treating FBs NE and NPY, isolated from neonatal rats.

Cells were then fixed and stained with an antibody to KI67, a marker of cell proliferation. The percentage of KI67 positive cells over the total number of FBs was quantified. The graph **(Fig.4.9)** shows that incubation with NPY induced cell proliferation, indicating that sympathetic neurotransmitters may affect CF function.

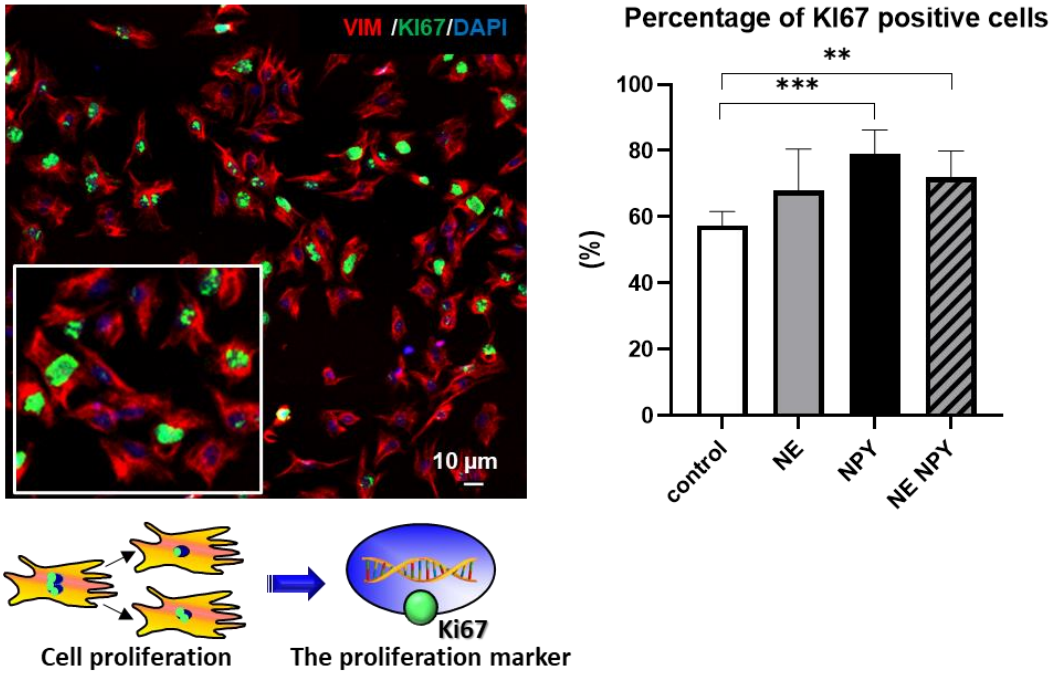

Fig.4.9 NPY increases the fraction of proliferating cardiac fibroblasts. Representative confocal IF analysis (**left**) of CFs stained to vimentin (red), proliferating FBs labelled by KI67 (green). Nuclei were counterstained with DAPI. Percentage of proliferating CFs (**right**), Control: 57±2, NE: 68±6, NPY 79±3, NE/NPY 72±4, %; ** p<0.01, *** P<0.001, error bars represent SEM, ~1000 cells for each condition were analysed.

To avoid the confounding effect due to the dynamic nature of CF in culture, which easily transition to activated, collagen secreting myofibroblasts, we used the kinase inhibitor SD208.

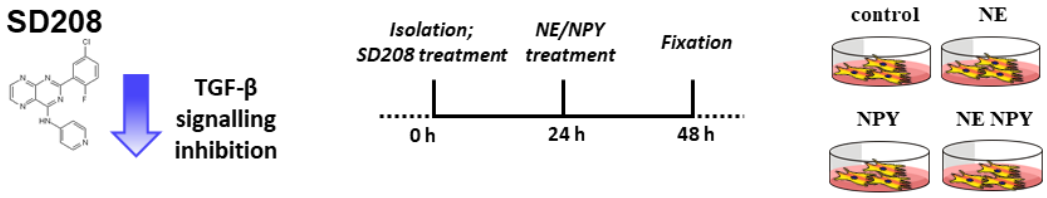

Fig.4.10 Protocol of treating FBs with SD208, NE and NPY.

NE and NPY increased the fraction of proliferating cardiac fibroblasts in the presence of SD208 (1 μM/L) by 12% and 19% respectively.

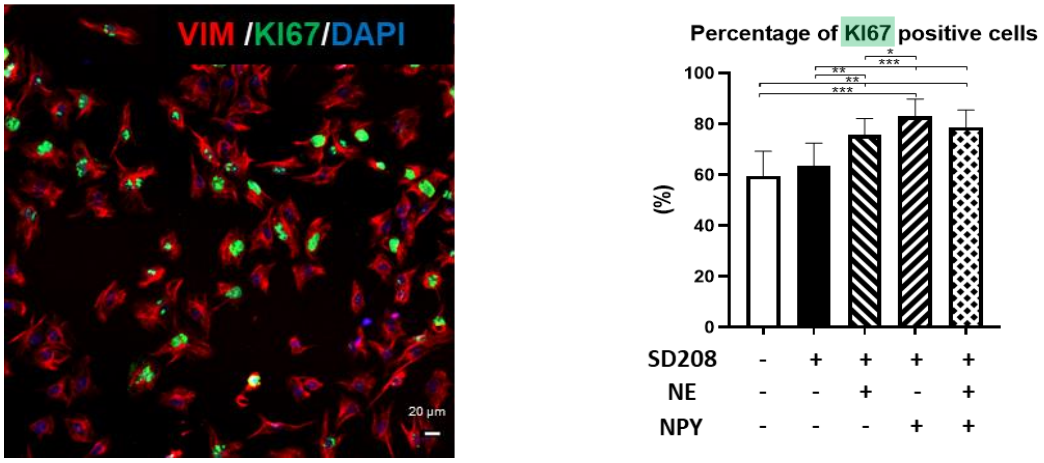

Fig.4.11 NPY increases the fraction of proliferating cardiac fibroblasts in the presence SD208. Representative confocal IF analysis (down left) of FBs stained to vimentin (red), proliferating FBs labelled with KI67 (green). Nuclei were counterstained with DAPI. Percentage of proliferating FBs (down right), 60±5, 63±3, 76±2, 83±2, 78±2, % for Control, SD208, SD208 with NE, NPY, NE/NPY, respectively. (* p<0.05, ** p<0.01, *** p<0.001; error bars represent SEM; ~800 cells were analysed for each condition; from 2 different isolations).

Also, even in the presence of SD208, NPY increases the fraction of differentiating cardiac FBs by 17% (**Fig.4.12**).

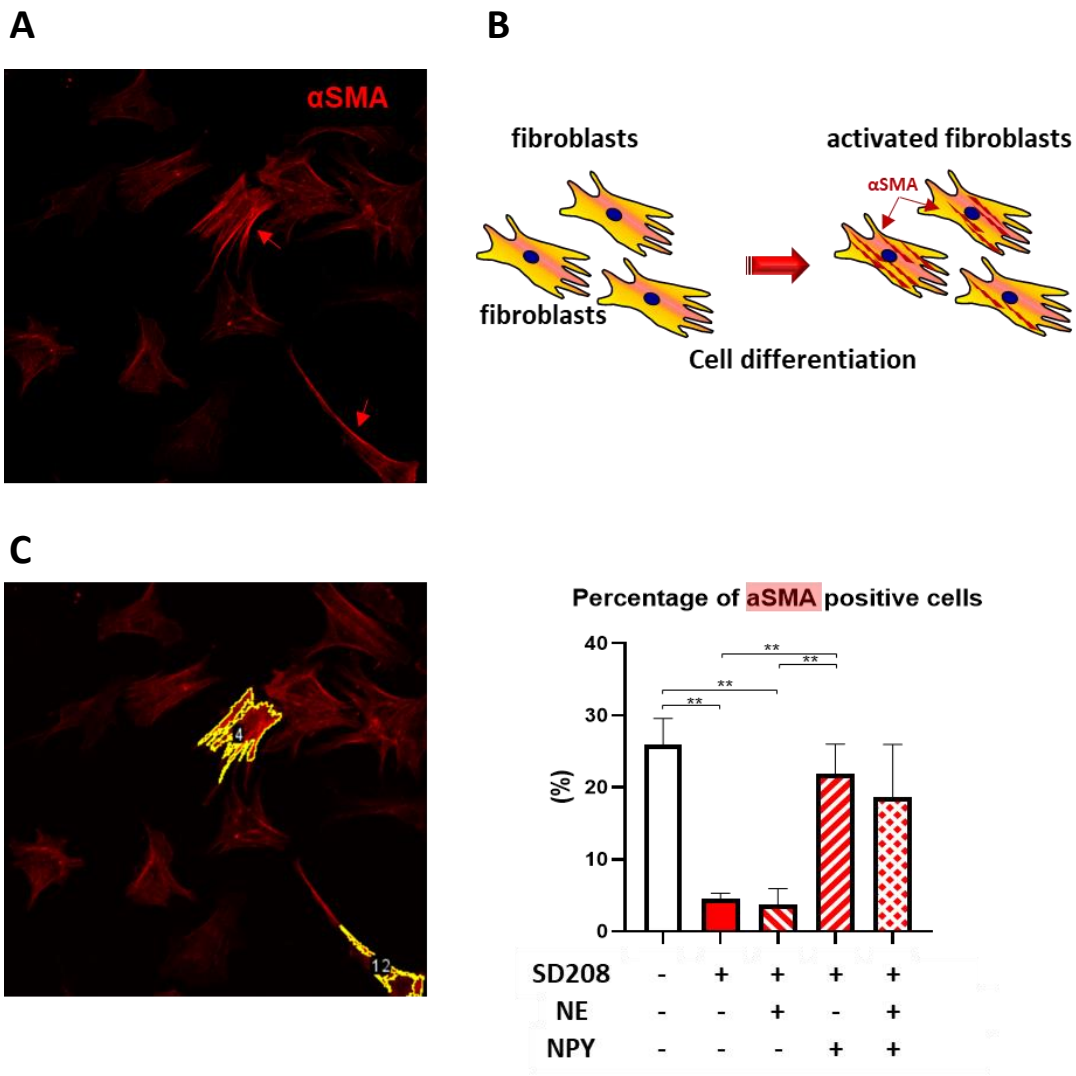

Fig.4.12 NPY increases the fraction of differentiating cardiac fibroblasts in the presence SD208. **A)** Representative confocal IF image of CFs stained to αSMA **B)** Diagram illustrates myofibroblast differentiation. **C)** Example of selected differentiated CFs (left). Percentage of differentiating CFs (right) , 26±7, 5±2, 4±2, 22±4, 19±7, % for Control, SD208, SD208 with NE, NPY, NE/NPY, respectively. Data presented as mean ± SEM.; * p<0.05, ** p<0,01 and *** p<0.001; ~ 400 cells were analysed for each condition, from 1 isolation.

4.5 Denervation induced by 6-OH-DA decrease heart fibrosis.

To assess the role of sympathetic neuron regulation in the in vivo context, we performed an exploratory experiment using pharmacologic heart denervation, in mice undergone ligation of the LAD and MI. For denervation, mice were treated with 6-OH-DA(6-Hydroxydopamine) an analogous of NE which is taken up by SNs and lead to their disruption due to oxidative stress. The control group was administered the vehicle (saline), while denervated mice received 6-OH-DA repeated in a 1-2-8-day regimen.

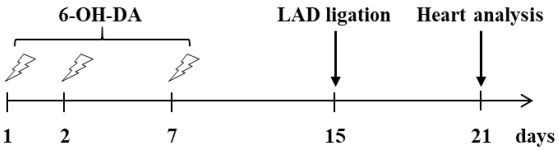

Fig.4.13 Protocol of pharmacologic sympathetic denervation in neonatal mice.

Treatment leads to degeneration of peripheral sympathetic neurons, as shown by the disappearance of anti-tyrosine hydroxylase immunoreactivity in myocardial sections (Zaglia *et al.*, 2013).

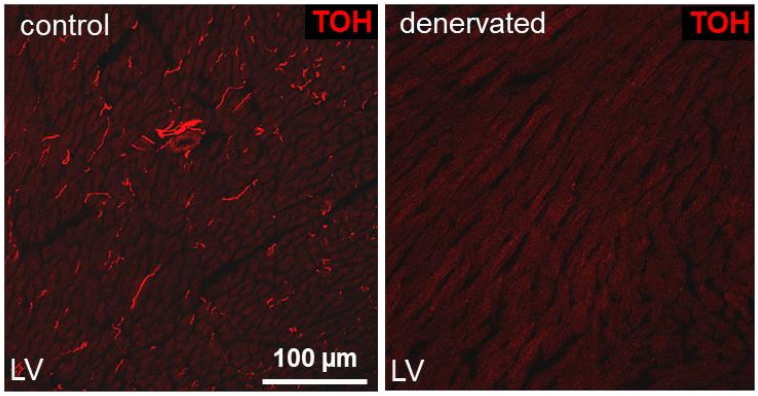

Fig.4.14 Confocal IF analysis of heart slices from WT and treated by 6-OH-DA mice stained to TOH (red) (Zaglia *et al.*, 2013).

Control and denervated mice underwent LAD (Left Anterior Descending) coronary artery ligation. There was no difference in survival rates after LAD ligation between control and denervated hearts. Infarct size was quantified by the tetrazolium method and was comparable in denervated and control mice. Myocardial histology was assessed 1 week after MI. At this time point, collagen deposition is evident in the

infarcted area. The size of infarct scar was quantified and the extent of cardiac fibrosis in denervated compared to control mice, was smaller (**Fig. 4.15**).

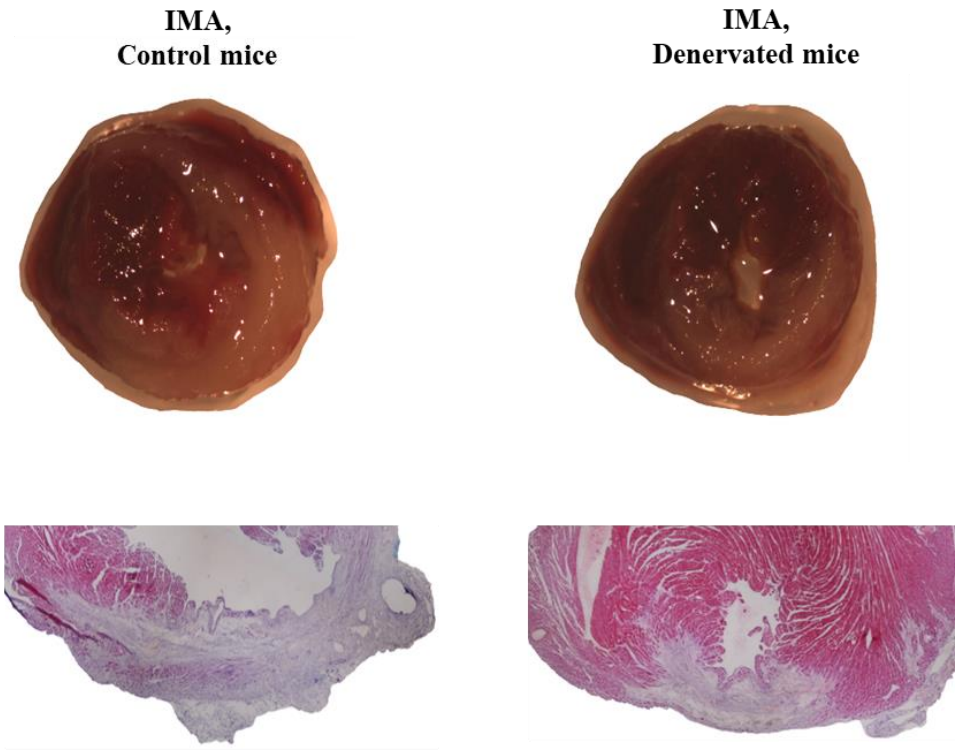

Fig.4.15 Denervation induced by 6-OH-DA decrease heart fibrosis. Fibrotic tissue visualized by haematoxylin and eosin staining in WT and denervated heart slices. n= 6 mice.

5. DISCUSSION IV

Among the plethora of different cell types which form the heart, research has invested most efforts in the study of the biology of CMs, and the consequences of their injury or dysfunction in pathologic instances. In the recent decades, however, it has been progressively acknowledged that other myocardial cells, including cardiac fibroblasts, allegedly the most abundant cells in the heart, have emerging roles in both cardiovascular physiology and pathology.

The number of functions attributed to cardiac fibroblasts is continuously increasing. In physiologic conditions, in healthy heart, CFs are main regulators of ECM dynamics, through collagen secretion (Villarreal *et al.*, 2009). Notably, the secretome of CF includes a large spectrum of small non-peptide molecules (e.g. hormones, cytokines) (Ceccato *et al.*, 2020) as well as larger proteins such as collagen (Butt, Laurent and Bishop, 1995), which represent the medium (paracrine) and long range (endocrine) means of CFs communication on other cell types. In addition, CFs have been shown (Zhang, Su and Mende, 2012) to cross-talk with neighboring cells through direct interaction, in a regulatory mechanism which might implicate cell-cell adhesion and signaling proteins, as well as direct cytoplasmic connections operated by gap junctional proteins (Ottaviano and Yee, 2011; Howard and Baudino, 2014).

In several cardiac pathologies, the disease mechanism may lead to adaptative changes in cardiac fibroblasts, causing evident alterations in the tissue, which can be caused by either fibroblast activation to replace injured tissue/cell death, or fibroblast activation by intrinsic or extrinsic factors increasing collagen secretion and interstitial fibrosis (Klionsky *et al.*, 2016; Travers *et al.*, 2016). The first instance is frequently observed upon ischemic death of infarcted cardimoyoctes, which is followed by the inflammatory response which, in the process of tissue repair, activates collagen deposition by activated fibroblasts. Given that the extent of fibrotic remodeling of the infarcted myocardium as well as the thickness of the cardiac interstitial matrix impact on heart diastolic relaxation, and indirectly on cardiac pump function, understanding the mechanisms which regulate cardiac fibroblast behavior is of utmost importance in molecular cardiovascular medicine.

We here show that cardiac fibroblasts in the myocardium interact with the sympathetic neuron in correspondence of the neuronal active neurotransmitter release sites (i.e. varicosities). The previous observation (Mias *et al.*, 2013) that fibroblasts in culture express and release NGF, indispensable for SN survival, and that the two cell type establish direct connections, suggests that the SN neurotransmitter outflow may influence CF function.

The analysis of the cell-to-cell interaction site, which was performed with SICM, an advanced methodology offering the unique advantage of reconstructing the surface profile of living cells non-invasively, has uncovered significant differences between the neuronal interaction with cardiomyocytes, which was discussed in more detail in the preceding chapters of this thesis, and that with CF. Remarkably, the volume of the varicosities interacting with CF was smaller than the average volume of CM-interacting ones. As previously discussed regarding the specific neuro-cardiac junction, and in chapter III, we have discovered that, by establishing a structured contact with target cells at the NCJ, neuron-cardiomyocyte communication occurs rapidly, at high efficiency and potently. The morphologic aspects of the SN/CF interaction support that neuro-fibroblast interaction is underlain by different properties. Our experiments assaying signalling coupling between SN and CF show that the effect of neuronal activation on cAMP responses of connected CF support that intercellular SN-CF signalling does not follow the same dynamics. In fact, neuronal activation did not evoke significant activation of beta-AR responses in CF. Although CF express a different adrenoceptor profile than CMs, relying mostly on β_2ARs, which could justify different sensitivity of the two cell types to neuronal stimulation. The comparable effect of stimulation with the same amount of exogenous NE suggests that differences could be in the different intercellular arrangement of the SN/CM and SN/CF couples. Additional experiments, addressing the expression level of adrenoceptors in CF and CM, and assessment of the CF response o neuronal stimulation in the presence of specific receptor blockers will be performed to gain better insight on these aspects. Taken together, our results suggest however the preliminary inference that the structured junctions which exist between cSNs and cardiomyocytes are qualitatively different than those with cardiac fibroblasts. This is in line with our previous observation that

while SN/CM interaction is stable in time, SN/CF contact sites are transitory and dynamic (Pianca *et al.*, 2019). However, as shown by Olga G. Shcherbakova *et al.* (2007) post-synaptic membrane remodelling, tethering adrenoceptors and signalling adapting proteins (i.e. AKAPs, SAP97) in CMs at the site of contact with the neuronal process has a functional role in the response to neuronal activation. Therefore, it is likely that in the limited interaction time between SN and CFs, adaptation of the adrenoceptor signalling complexes to the presence of the neuron does not have enough time to accomplish, thus explaining the reduced sensitivity to SN activation. Our evidence indicates that the unconventional sympathetic neurotransmitter, NPY, has a role in regulating cardiac fibroblast proliferation and differentiation. At the present time, we cannot determine the dynamics and molecular mechanisms regualating NPY release by SNs and its interaction with CFs. However, the data points towards a role of sympathetic neurons in the regulation of the cardiac matrix, which was not described until very recently, and identifies the molecular mediator of such interaction. Given that activation of the SNS is well known to occur immediately after myocardial infarction, and is maintained elevated throughout the cardiac postischemic remodelling (Kolettis *et al.*, 2015), it is remarkable, and in line with the evidence accrued in vitro, to observe that ablation of SN responses was effective in reducing the extent of myocardial fibrotic remodelling. Evidence thus supports that sympathetic neurons play a maladaptive role in the fibrotic response to myocardial ischemia (Borovac *et al.*, 2020). When considered together with the in vitro data presented above, while more experiments using specific receptor antagonists or agonists are needed, it is tempting to speculate that in a condition associated to sympathetic neuron activation, input by NPY might stimulate fibroblast proliferation and fuel myocardial fibrosis. Complementarily, these results suggest that interfering with sympathetic neurotranmitter receptors different from the commonly used adrenergic receptor blockers might alleviate the degree of postischemic myocardial remodelling.

REFERENCES

Aloe, L. *et al.* (2016) 'Nerve growth factor: role in growth, differentiation and controlling cancer cell development', *Journal of Experimental and Clinical Cancer Research*. BioMed Central Ltd., p. 116. doi: 10.1186/s13046-016-0395-y.

Andres, R. *et al.* (2001) 'Multiple effects of artemin on sympathetic neurone generation, survival and growth', *Development*, 128(19), pp. 3685–3695.

Angeli, S. *et al.* (2014) 'A high-resolution cardiovascular magnetic resonance diffusion tensor map from ex-vivo C57BL/6 murine hearts', *J Cardiovasc Magn Reson*. 2014/10/18, 16(1), p. 77. doi: 10.1186/s12968-014-0077-x.

Anmann, T. *et al.* (2014) 'Formation of highly organized intracellular structure and energy metabolism in cardiac muscle cells during postnatal development of rat heart', *Biochimica et Biophysica Acta - Bioenergetics*, 1837(8), pp. 1350–1361. doi: 10.1016/j.bbabio.2014.03.015.

Antzelevitch, C. *et al.* (1991) 'Heterogeneity within the ventricular wall. Electrophysiology and pharmacology of epicardial, endocardial, and M cells', *Circ Res*. 1991/12/01, 69(6), pp. 1427–1449. Available at: http://circres.ahajournals.org/content/69/6/1427.full.pdf.

Bailey, J. C., Lathrop, D. A. and Pippenger, D. L. (1977) 'Differences between proximal left and right bundle branch block action potential durations and refractoriness in the dog heart', *Circ Res*. 1977/05/01, 40(5), pp. 464–468.

Baker, J. G. (2005) 'The selectivity of β-adrenoceptor antagonists at the human β1, β2 and β3 adrenoceptors', *British Journal of Pharmacology*, 144(3), pp. 317–322. doi: 10.1038/sj.bjp.0706048.

Bamji, S. X. *et al.* (1998) 'The p75 neurotrophin receptor mediates neuronal apoptosis and is essential for naturally occurring sympathetic neuron death', *Journal of Cell Biology*, 140(4), pp. 911–923. doi: 10.1083/jcb.140.4.911.

Bass, A. *et al.* (2001) 'Ontogenetic development of energy-supplying enzymes in rat and guinea-pig heart', *Physiological Research*, 50(3), pp. 237–245.

Basser, P. J., Mattiello, J. and LeBihan, D. (1994) 'MR diffusion tensor spectroscopy and imaging', *Biophys J*, 66(1), pp. 259–267. doi: 10.1016/S0006-3495(94)80775-1.

Basso, C. *et al.* (2009) ‘Arrhythmogenic right ventricular cardiomyopathy’, *The Lancet*. Elsevier, pp. 1289–1300. doi: 10.1016/S0140-6736(09)60256-7.

Baum, J. and Duffy, H. S. (2011) ‘Fibroblasts and myofibroblasts: What are we talking about?’, *Journal of Cardiovascular Pharmacology*. NIH Public Access, pp. 376–379. doi: 10.1097/FJC.0b013e3182116e39.

BAXTER, M. I. and NISBET, R. H. (1963) ‘FEATURES OF THE NERVOUS SYSTEM AND HEART OF ARCHACHATINA REVEALED BY THE ELECTRON MICROSCOPE AND BY ELECTROPHYSIOLOGICAL RECORDING*’, *Journal of Molluscan Studies*, 35(4), pp. 167–177. doi: 10.1093/oxfordjournals.mollus.a064915.

Becker, A. E. and De Wit, A. P. (1979) ‘Mitral valve apparatus. A spectrum of normality relevant to mitral valve prolapse’, *Br Heart J*, 42(6), pp. 680–689. Available at: http://www.ncbi.nlm.nih.gov/pubmed/534585.

Bers, D. M. (2002) ‘Cardiac excitation-contraction coupling’, *Nature*, 415(6868), pp. 198–205. doi: 10.1038/415198a.

Betts (2017) *Anatomy & Physiology*. Texas: OpenStax.

Bierl, M. A. *et al.* (2005) ‘“Mature” nerve growth factor is a minor species in most peripheral tissues’, *Neuroscience Letters*, 380(1–2), pp. 133–137. doi: 10.1016/j.neulet.2005.01.029.

Błyszczuk, P. *et al.* (2020) ‘Activated Cardiac Fibroblasts Control Contraction of Human Fibrotic Cardiac Microtissues by a β-Adrenoreceptor-Dependent Mechanism’, *Cells*, 9(5). doi: 10.3390/cells9051270.

Borovac, J. A. *et al.* (2020) ‘Sympathetic nervous system activation and heart failure: Current state of evidence and the pathophysiology in the light of novel biomarkers’, *World Journal of Cardiology*. Baishideng Publishing Group Co, pp. 373–408. doi: 10.4330/wjc.v12.i8.373.

Braunwald, E., Ross, J. and Sonnenblick, E. H. (1967) ‘Mechanisms of Contraction of the Normal and Failing Heart’, *New England Journal of Medicine*, 277(15), pp. 794–800. doi: 10.1056/NEJM196710122771505.

Brothers, S. P. and Wahlestedt, C. (2010) ‘Therapeutic potential of neuropeptide y (NPY) receptor ligands’, *EMBO Molecular Medicine*. Wiley-Blackwell, pp. 429–439. doi: 10.1002/emmm.201000100.

Brunello, L. *et al.* (2013) ‘Decreased RyR2 refractoriness determines myocardial synchronization of aberrant Ca2+ release in a genetic model of arrhythmia’, *Proc Natl Acad Sci U S A*. 2013/06/05, 110(25), pp. 10312–10317. doi: 10.1073/pnas.1300052110.

Brutsaert, D. L. (1989) ‘The endocardium’, *Annu Rev Physiol*, 51, pp. 263–273. doi: 10.1146/annurev.ph.51.030189.001403.

Butt, R. P., Laurent, G. J. and Bishop, J. E. (1995) ‘Collagen production and replication by cardiac fibroblasts is enhanced in response to diverse classes of growth factors’, *European Journal of Cell Biology*, 68(3), pp. 330–335. Available at: https://pubmed.ncbi.nlm.nih.gov/8603686/ (Accessed: 9 February 2021).

Cao, J. M. *et al.* (2000) ‘Nerve sprouting and sudden cardiac death’, *Circ Res*. 2000/04/14, 86(7), pp. 816–821. Available at: http://circres.ahajournals.org/content/86/7/816.full.pdf.

Carafoli, E. (1991) ‘Calcium pump of the plasma membrane’, *Physiol Rev*. 1991/01/01, 71(1), pp. 129–153.

Carafoli, E., Garcia-Martin, E. and Guerini, D. (1996) ‘The plasma membrane calcium pump: Recent developments and future perspectives’, *Experientia*. Experientia, pp. 1091–1100. doi: 10.1007/BF01952107.

Castaldi, A. *et al.* (2014) ‘MicroRNA-133 modulates the beta1-adrenergic receptor transduction cascade’, *Circ Res*. 2014/05/09, 115(2), pp. 273–283. doi: 10.1161/CIRCRESAHA.115.303252 CIRCRESAHA.115.303252 [pii].

Ceccato, T. L. *et al.* (2020) ‘Defining the Cardiac Fibroblast Secretome in a Fibrotic Microenvironment’, *Journal of the American Heart Association*, 9(19), p. e017025. doi: 10.1161/JAHA.120.017025.

Chan, T. S. *et al.* (2018) ‘Upregulation of Krebs cycle and anaerobic glycolysis activity early after onset of liver ischemia’, *PLoS ONE*, 13(6). doi: 10.1371/journal.pone.0199177.

Chen, L. S. *et al.* (2007) ‘New perspectives on the role of autonomic nervous system in the genesis of arrhythmias’, *Journal of Cardiovascular Electrophysiology*. J Cardiovasc Electrophysiol, pp. 123–127. doi: 10.1111/j.1540-8167.2006.00590.x.

Cheng, H., Lederer, W. J. and Cannell, M. B. (1993) ‘Calcium sparks: Elementary events underlying excitation-contraction coupling in heart muscle’, *Science*, 262(5134), pp. 740–

744. doi: 10.1126/science.8235594.

Choate, J. K., Klemm, M. and Hirst, G. D. S. (1993) ‘Sympathetic and parasympathetic neuromuscular junctions in the guinea-pig sino-atrial node’, *Journal of the Autonomic Nervous System*, 44(1), pp. 1–15. doi: 10.1016/0165-1838(93)90374-4.

Clapham, D. E. and Neer, E. J. (1997) ‘G protein beta gamma subunits’, *Annu Rev Pharmacol Toxicol*, 37, pp. 167–203. doi: 10.1146/annurev.pharmtox.37.1.167.

Cleutjens, J. P. M. *et al.* (1999) ‘The infarcted myocardium: Simply dead tissue, or a lively target for therapeutic interventions’, *Cardiovascular Research*. Cardiovasc Res, pp. 232–241. doi: 10.1016/S0008-6363(99)00212-6.

Collinet, C. and Lecuit, T. (2013) ‘Stability and dynamics of cell-cell junctions’, in *Progress in Molecular Biology and Translational Science*. Elsevier B.V., pp. 25–47. doi: 10.1016/B978-0-12-394311-8.00002-9.

Conforti, L., Tohse, N. and Sperelakis, N. (1991) ‘Influence of sympathetic innervation on the membrane electrical properties of neonatal rat cardiomyocytes in culture’, *Journal of Developmental Physiology*, 15(4), pp. 237–246. Available at: https://pubmed.ncbi.nlm.nih.gov/1940151/ (Accessed: 8 February 2021).

Crnkovic, S. *et al.* (2014) ‘NPY/Y1 receptor-mediated vasoconstrictory and proliferative effects in pulmonary hypertension’, *British Journal of Pharmacology*, 171(16), pp. 3895–3907. doi: 10.1111/bph.12751.

Crowley, C. *et al.* (1994) ‘Mice lacking nerve growth factor display perinatal loss of sensory and sympathetic neurons yet develop basal forebrain cholinergic neurons’, *Cell*, 76(6), pp. 1001–1011. doi: 10.1016/0092-8674(94)90378-6.

Czubryt (2019) ‘Cardiac Fibroblast to Myofibroblast Phenotype Conversion—An Unexploited Therapeutic Target’, *Journal of Cardiovascular Development and Disease*, 6(3), p. 28. doi: 10.3390/jcdd6030028.

Davies, A. M. (2009) ‘Extracellular signals regulating sympathetic neuron survival and target innervation during development’, *Autonomic Neuroscience: Basic and Clinical*. Auton Neurosci, pp. 39–45. doi: 10.1016/j.autneu.2009.07.011.

Deppmann, C. D. *et al.* (2008) ‘A model for neuronal competition during development’, *Science*, 320(5874), pp. 369–373. doi: 10.1126/science.1152677.

Devic, E *et al.* (2001) ‘Beta-adrenergic receptor subtype-specific signaling in cardiac

myocytes from beta(1) and beta(2) adrenoceptor knockout mice', *Mol Pharmacol*. 2001/08/15, 60(3), pp. 577–583. Available at: http://molpharm.aspetjournals.org/content/60/3/577.full.pdf.

Devic, Eric *et al.* (2001) 'β-Adrenergic receptor subtype-specific signaling in cardiac myocytes from β1 and β2 adrenoceptor knockout mice', *Molecular Pharmacology*, 60(3), pp. 577–583. Available at: https://pubmed.ncbi.nlm.nih.gov/11502890/ (Accessed: 8 February 2021).

Dumont, Y. and Quirion, R. (2006) 'An overview of neuropeptide Y: pharmacology to molecular biology and receptor localization.', *EXS*. EXS, pp. 7–33. doi: 10.1007/3-7643-7417-9_2.

Eghbali, M. *et al.* (2005) 'Molecular and functional signature of heart hypertrophy during pregnancy', *Circulation Research*, 96(11), pp. 1208–1216. doi: 10.1161/01.RES.0000170652.71414.16.

Ehler, E., Moore-Morris, T. and Lange, S. (2013) 'Isolation and culture of neonatal mouse cardiomyocytes', *Journal of Visualized Experiments*, (79), p. 50154. doi: 10.3791/50154.

Epa, W. R., Markovska, K. and Barrett, G. L. (2004) 'The p75 neurotrophin receptor enhances TrkA signalling by binding to Shc and augmenting its phosphorylation', *Journal of Neurochemistry*, 89(2), pp. 344–353. doi: 10.1111/j.1471-4159.2004.02344.x.

Fabiato, A. (1983) 'Calcium-induced release of calcium from the cardiac sarcoplasmic reticulum', *Am J Physiol*. 1983/07/01, 245(1), pp. C1--14.

Fagan, A. M. *et al.* (1996) 'TrkA, but not TrkC, receptors are essential for survival of sympathetic neurons in vivo', *Journal of Neuroscience*, 16(19), pp. 6208–6218. doi: 10.1523/jneurosci.16-19-06208.1996.

Fan, D. *et al.* (2012) 'Cardiac fibroblasts, fibrosis and extracellular matrix remodeling in heart disease', *Fibrogenesis and Tissue Repair*. BioMed Central, p. 15. doi: 10.1186/1755-1536-5-15.

FAWCETT, D. W. and SELBY, C. C. (1958) 'Observations on the fine structure of the turtle atrium.', *The Journal of biophysical and biochemical cytology*, 4(1), pp. 63–72. doi: 10.1083/jcb.4.1.63.

Ferrara, N. *et al.* (2014) 'β-adrenergic receptor responsiveness in aging heart and clinical

implications', *Frontiers in Physiology*. Frontiers Media SA. doi: 10.3389/fphys.2013.00396.

Frade, J. M., Rodriguez-Tebar, A. and Barde, Y. A. (1996) 'Induction of cell death by endogenous nerve growth factor through its p75 receptor', *Nature*, 383(6596), pp. 166–168. doi: 10.1038/383166a0.

Francis, N. *et al.* (1999) 'NT-3, like NGF, is required for survival of sympathetic neurons, but not their precursors', *Developmental Biology*, 210(2), pp. 411–427. doi: 10.1006/dbio.1999.9269.

Franke, W. W. *et al.* (2006) 'The area composita of adhering junctions connecting heart muscle cells of vertebrates. I. Molecular definition in intercalated disks of cardiomyocytes by immunoelectron microscopy of desmosomal proteins', *Eur J Cell Biol*, 85(2), pp. 69–82. doi: 10.1016/j.ejcb.2005.11.003.

Franzoso, M., Zaglia, T. and Mongillo, M. (2016) 'Putting together the clues of the everlasting neuro-cardiac liaison', *Biochim Biophys Acta*, 1863, pp. 1904–1915. doi: 10.1016/j.bbamcr.2016.01.009.

Freeman, K. *et al.* (2014) 'In situ three-dimensional reconstruction of mouse heart sympathetic innervation by two-photon excitation fluorescence imaging', *Journal of Neuroscience Methods*, 221, pp. 48–61. doi: 10.1016/j.jneumeth.2013.09.005.

Fu, Q., Wang, Q. and Xiang, Y. K. (2017) 'Insulin and β Adrenergic Receptor Signaling: Crosstalk in Heart', *Trends in Endocrinology and Metabolism*. Elsevier Inc., pp. 416–427. doi: 10.1016/j.tem.2017.02.002.

Fukuda, K. *et al.* (2015) 'Cardiac innervation and sudden cardiac death', *Circ Res*, 116(12), pp. 2005–2019. doi: 10.1161/CIRCRESAHA.116.304679.

Gallicano (2001) 'Rescuing desmoplakin function in extra-embryonic ectoderm reveals the importance of this protein in embryonic heart, neuroepithelium, skin and vasculature', *Development*, 128, pp. 929–941.

Garza, M. A. (2015) 'Cardiac remodeling and physical training post myocardial infarction', *World Journal of Cardiology*, 7(2), p. 52. doi: 10.4330/wjc.v7.i2.52.

Gericke, M. T. *et al.* (2009) 'Receptors for NPY and PACAP differ in expression and activity during adipogenesis in the murine 3T3-L1 fibroblast cell line', *British Journal of Pharmacology*, 157(4), pp. 620–632. doi: 10.1111/j.1476-5381.2009.00164.x.

Grässel, S. and Muschter, D. (2017) ‘Peripheral nerve fibers and their neurotransmitters in osteoarthritis pathology’, *International Journal of Molecular Sciences*. MDPI AG. doi: 10.3390/ijms18050931.

Grillo, M. A. (1966) ‘Electron microscopy of sympathetic tissues.’, *Pharmacological Reviews*. Pharmacol Rev, pp. 387–399. Available at: https://pubmed.ncbi.nlm.nih.gov/5323767/ (Accessed: 8 February 2021).

Grisan, F. *et al.* (2020) ‘Studying β1 and β2 adrenergic receptor signals in cardiac cells using FRET-based sensors’, *Progress in Biophysics and Molecular Biology*, 154, pp. 30–38. doi: 10.1016/j.pbiomolbio.2019.06.001.

Grisham, M. B. and Granger, D. N. (1988) ‘Neutrophil-mediated mucosal injury - Role of reactive oxygen metabolites’, *Digestive Diseases and Sciences*, 33(3 Supplement). doi: 10.1007/BF01538126.

Gros, D. *et al.* (1994) ‘Restricted distribution of connexin40, a gap junctional protein, in mammalian heart’, *Circ Res*. 1994/05/01, 74(5), pp. 839–851. Available at: http://circres.ahajournals.org/content/74/5/839.full.pdf.

Guo, R. *et al.* (2020) ‘Stem cell-derived cell sheet transplantation for heart tissue repair in myocardial infarction’, *Stem Cell Research and Therapy*. BioMed Central Ltd. doi: 10.1186/s13287-019-1536-y.

Guo, Y. and Pu, W. T. (2020) ‘Cardiomyocyte maturation: New phase in development’, *Circulation Research*. Lippincott Williams and Wilkins, pp. 1086–1106. doi: 10.1161/CIRCRESAHA.119.315862.

Guyton and Hall (2006) *TEXTBOOK of Medical Physiology*. 11th edn. Elsevier Inc.

Haass, M. and Kübler, W. (1997) ‘Notice and sympathetic neurotransmission’, *Cardiovascular Drugs and Therapy*. Springer New York LLC, pp. 657–665. doi: 10.1007/BF00053022.

Hadaya, J. and Ardell, J. L. (2020) ‘Autonomic Modulation for Cardiovascular Disease’, *Frontiers in Physiology*. Frontiers Media S.A., p. 617459. doi: 10.3389/fphys.2020.617459.

Hanna, A. and Frangogiannis, N. G. (2019) ‘The Role of the TGF-β Superfamily in Myocardial Infarction’, *Frontiers in Cardiovascular Medicine*. Frontiers Media S.A., p. 140. doi: 10.3389/fcvm.2019.00140.

Harary, I. and Farley, B. (1963) ‘In vitro studies on single beating rat heart cells. II. Intercellular communication’, *Experimental Cell Research*, 29(3), pp. 466–474. doi: 10.1016/S0014-4827(63)80009-9.

Harrington, A. W. *et al.* (2011) ‘Recruitment of actin modifiers to TrkA endosomes governs retrograde NGF signaling and survival’, *Cell*, 146(3), pp. 421–434. doi: 10.1016/j.cell.2011.07.008.

Harrington, A. W. and Ginty, D. D. (2013) ‘Long-distance retrograde neurotrophic factor signalling in neurons’, *Nature Reviews Neuroscience*. Nat Rev Neurosci, pp. 177–187. doi: 10.1038/nrn3253.

Healy, L. J., Jiang, Y. and Hsu, E. W. (2011) ‘Quantitative comparison of myocardial fiber structure between mice, rabbit, and sheep using diffusion tensor cardiovascular magnetic resonance’, *Journal of Cardiovascular Magnetic Resonance*, 13(1). doi: 10.1186/1532-429X-13-74.

Heart Association, A. (2020) *What is a Heart Attack?*

Henderson, C. A. *et al.* (2017) ‘Overview of the muscle cytoskeleton’, *Comprehensive Physiology*, 7(3), pp. 891–944. doi: 10.1002/cphy.c160033.

Hendry, I. A. *et al.* (1974) ‘The retrograde axonal transport of nerve growth factor’, *Brain Research*, 68(1), pp. 103–121. doi: 10.1016/0006-8993(74)90536-8.

Higuchi, A. *et al.* (2017) ‘Stem cell therapies for myocardial infarction in clinical trials: Bioengineering and biomaterial aspects’, *Laboratory Investigation*. Nature Publishing Group, pp. 1167–1179. doi: 10.1038/labinvest.2017.100.

Hoerter, J. A., Kuznetsov, A. and Ventura-Clapier, R. (1991) ‘Functional development of the creatine kinase system in perinatal rabbit heart’, *Circulation Research*, 69(3), pp. 665–676. doi: 10.1161/01.RES.69.3.665.

Honma, Y. *et al.* (2002) ‘Artemin is a vascular-derived neurotropic factor for developing sympathetic neurons’, *Neuron*, 35(2), pp. 267–282. doi: 10.1016/S0896-6273(02)00774-2.

Howard, C. M. and Baudino, T. A. (2014) ‘Dynamic cell-cell and cell-ECM interactions in the heart’, *Journal of Molecular and Cellular Cardiology*. Academic Press, pp. 19–26. doi: 10.1016/j.yjmcc.2013.10.006.

Howe, C. L. *et al.* (2001) ‘NGF signaling from clathrin-coated vesicles: Evidence that

signaling endosomes serve as a platform for the Ras-MAPK pathway', *Neuron*, 32(5), pp. 801–814. doi: 10.1016/S0896-6273(01)00526-8.

Hoyt, R. H., Cohen, M. L. and Saffitz, J. E. (1989) 'Distribution and three-dimensional structure of intercellular junctions in canine myocardium', *Circ Res*. 1989/03/01, 64(3), pp. 563–574.

Huxley, H. E. (1969) 'The mechanism of muscular contraction', *Science*. Science, pp. 1356–1366. doi: 10.1126/science.164.3886.1356.

Ieda, M. *et al.* (2007) 'Sema3a maintains normal heart rhythm through sympathetic innervation patterning', *Nat Med*, 13, pp. 604–612. doi: 10.1038/nm1570.

Isu, G. *et al.* (2020) 'Fatty acid-based monolayer culture to promote in vitro neonatal rat cardiomyocyte maturation', *Biochimica et Biophysica Acta - Molecular Cell Research*, 1867(3). doi: 10.1016/j.bbamcr.2019.118561.

Janowski, E. *et al.* (2006) 'Diversity of Ca2+ signaling in developing cardiac cells', in *Annals of the New York Academy of Sciences*. Blackwell Publishing Inc., pp. 154–164. doi: 10.1196/annals.1380.014.

Jiang, Y. *et al.* (2004) 'Three-dimensional diffusion tensor microscopy of fixed mouse hearts', *Magn Reson Med*. 2004/08/31, 52(3), pp. 453–460. doi: 10.1002/mrm.20191.

Kalogeris, T. *et al.* (2012) 'Cell Biology of Ischemia/Reperfusion Injury', in *International Review of Cell and Molecular Biology*. Elsevier Inc., pp. 229–317. doi: 10.1016/B978-0-12-394309-5.00006-7.

Karemaker, J. M. (2017) 'An introduction into autonomic nervous function', *Physiological Measurement*. Institute of Physics Publishing, pp. R89–R118. doi: 10.1088/1361-6579/aa6782.

Katz, A. (2011) *Physiology of the heart*. 5th edn. London: Lippincot Williams and Wilkins.

Kaye, D. M. *et al.* (2000) 'Reduced myocardial nerve growth factor expression in human and experimental heart failure.', *Circulation research*, 86(7). doi: 10.1161/01.res.86.7.e80.

Van Kempen, M. J. *et al.* (1996) 'Developmental changes of connexin40 and connexin43 mRNA distribution patterns in the rat heart', *Cardiovasc Res*. 1996/11/01, 32(5), pp. 886–900. Available at:

http://cardiovascres.oxfordjournals.org/content/cardiovascres/32/5/886.full.pdf.

Kimura, K., Ieda, M. and Fukuda, K. (2012) 'Development, maturation, and transdifferentiation of cardiac sympathetic nerves', *Circ Res*, 110, pp. 325–336. doi: 10.1161/CIRCRESAHA.111.257253.

Kirchhoff, S. *et al.* (2000) 'Abnormal cardiac conduction and morphogenesis in connexin40 and connexin43 double-deficient mice', *Circ Res*. 2000/09/02, 87(5), pp. 399–405. Available at: http://circres.ahajournals.org/content/87/5/399.full.pdf.

Kisch (1961) 'Electronmicroscopy of the frog's heart', *Exp Med Surg*, 19, pp. 104–42.

Klarenbeek, J. *et al.* (2015) 'Fourth-Generation Epac-Based FRET Sensors for cAMP Feature Exceptional Brightness, Photostability and Dynamic Range: Characterization of Dedicated Sensors for FLIM, for Ratiometry and with High Affinity', *PLOS ONE*. Edited by K. I. Anderson, 10(4), p. e0122513. doi: 10.1371/journal.pone.0122513.

Klemm, M., Hirst, G. D. S. and Campbell, G. (1992) 'Structure of autonomic neuromuscular junctions in the sinus venosus of the toad', *Journal of the Autonomic Nervous System*, 39(2), pp. 139–150. doi: 10.1016/0165-1838(92)90054-K.

Klionsky, D. J. *et al.* (2016) 'Guidelines for the use and interpretation of assays for monitoring autophagy (3rd edition)', *Autophagy*. 2016/01/23, 12(1), pp. 1–222. doi: 10.1080/15548627.2015.1100356.

Kolettis, T. M. *et al.* (2015) 'Central Sympathetic Activation and Arrhythmogenesis during Acute Myocardial Infarction: Modulating Effects of Endothelin-B Receptors', *Frontiers in Cardiovascular Medicine*, 2. doi: 10.3389/fcvm.2015.00006.

Kolk, M. V. V. *et al.* (2009) 'LAD-ligation: A murine model of myocardial infarction', *Journal of Visualized Experiments*, (32). doi: 10.3791/1438.

Korsching, S. and Thoenen, H. (1983) 'Nerve growth factor in sympathetic ganglia and corresponding target organs of the rat: Correlation with density of sympathetic innervation', *Proceedings of the National Academy of Sciences of the United States of America*, 80(11 I), pp. 3513–3516. doi: 10.1073/pnas.80.11.3513.

Kuruvilla, R. *et al.* (2004) 'A neurotrophin signaling cascade coordinates sympathetic neuron development through differential control of TrkA trafficking and retrograde signaling', *Cell*, 118(2), pp. 243–255. doi: 10.1016/j.cell.2004.06.021.

Kuruvilla, R., Ye, H. and Ginty, D. D. (2000) 'Spatially and functionally distinct roles of

the PI3-K effector pathway during NGF signaling in sympathetic neurons', *Neuron*, 27(3), pp. 499–512. doi: 10.1016/S0896-6273(00)00061-1.

Kwon, Y. J. *et al.* (2009) 'Phosphorylation of CREB, a cyclic AMP responsive element binding protein, contributes partially to lysophosphatidic acid-induced fibroblast cell proliferation', *Biochemical and Biophysical Research Communications*, 380(3), pp. 655–659. doi: 10.1016/j.bbrc.2009.01.159.

Lalu, M. M. *et al.* (2018) 'Safety and Efficacy of Adult Stem Cell Therapy for Acute Myocardial Infarction and Ischemic Heart Failure (SafeCell Heart): A Systematic Review and Meta-Analysis', *Stem Cells Translational Medicine*. John Wiley and Sons Ltd., pp. 857–866. doi: 10.1002/sctm.18-0120.

Landis, S. C. (1976) 'Rat sympathetic neurons and cardiac myocytes developing in microcultures: correlation of the fine structure of endings with neurotransmitter function in single neurons', *Proc Natl Acad Sci U S A*, 73, pp. 4220–4224. doi: 10.1073/pnas.73.11.4220.

Larsen, H. E., Lefkimmiatis, K. and Paterson, D. J. (2016) 'Sympathetic neurons are a powerful driver of myocyte function in cardiovascular disease', *Scientific Reports*, 6. doi: 10.1038/srep38898.

Leask, A. (2007) 'TGFβ, cardiac fibroblasts, and the fibrotic response', *Cardiovascular Research*. Oxford Academic, pp. 207–212. doi: 10.1016/j.cardiores.2006.07.012.

Lehnart, S. E. *et al.* (2004) 'Sudden death in familial polymorphic ventricular tachycardia associated with calcium release channel (ryanodine receptor) leak', *Circulation*. 2004/06/16, 109(25), pp. 3208–3214. doi: 10.1161/01.cir.0000132472.98675.ec.

Lehnart, S. E. *et al.* (2006) 'Stabilization of cardiac ryanodine receptor prevents intracellular calcium leak and arrhythmias', *Proc Natl Acad Sci U S A*. 2006/05/05, 103(20), pp. 7906–7910. doi: 10.1073/pnas.0602133103.

Leicht, M., Greipel, N. and Zimmer, H. G. (2000) 'Comitogenic effect of catecholamines on rat cardiac fibroblasts in culture', *Cardiovascular Research*, 48(2), pp. 274–284. doi: 10.1016/S0008-6363(00)00170-X.

Lessmann, V., Gottmann, K. and Malcangio, M. (2003) 'Neurotrophin secretion: Current facts and future prospects', *Progress in Neurobiology*. Elsevier Ltd, pp. 341–374. doi: 10.1016/S0301-0082(03)00019-4.

Levi-Montalcini, R. and Angeletti, P. U. (1968) ‘Nerve growth factor.’, *Physiological reviews*. Physiol Rev, pp. 534–569. doi: 10.1152/physrev.1968.48.3.534.

Levi-Montalcini, R. and Hamburger, V. (1951) ‘Selective growth stimulating effects of mouse sarcoma on the sensory and sympathetic nervous system of the chick embryo’, *Journal of Experimental Zoology*, 116(2), pp. 321–361. doi: 10.1002/jez.1401160206.

Lewin, G. R. and Mendell, L. M. (1993) ‘Nerve growth factor and nociception’, *Trends in Neurosciences*. Trends Neurosci, pp. 353–359. doi: 10.1016/0166-2236(93)90092-Z.

Li, H. H. *et al.* (2004) ‘Atrogin-1/muscle atrophy F-box inhibits calcineurin-dependent cardiac hypertrophy by participating in an SCF ubiquitin ligase complex’, *J Clin Invest*. 2004/10/19, 114(8), pp. 1058–1071. doi: 10.1172/jci22220.

Lijnen, P. and Petrov, V. (2002) ‘Transforming growth factor-β1-induced collagen production in cultures of cardiac fibroblasts is the result of the appearance of myofibroblasts’, *Methods and Findings in Experimental and Clinical Pharmacology*, 24(6), pp. 333–344. doi: 10.1358/mf.2002.24.6.693065.

Lin, B. L., Song, T. and Sadayappan, S. (2017) ‘Myofilaments: Movers and rulers of the sarcomere’, *Comprehensive Physiology*, 7(2), pp. 675–692. doi: 10.1002/cphy.c160026.

Lloyd, T. R. and Marvin, W. J. (1990) ‘Sympathetic innervation improves the contractile performance of neonatal cardiac ventricular myocytes in culture’, *Journal of Molecular and Cellular Cardiology*, 22(3), pp. 333–342. doi: 10.1016/0022-2828(90)91466-K.

Lockhart (2000) ‘Nerve growth factor collaborates with myocyte-derived factors to promote development of presynaptic sites in cultured sympathetic neurons.’, *J Neurobiol.*, 42, pp. 460–76.

Lockhart, S. T., Turrigiano, G. G. and Birren, S. J. (1997) ‘Nerve growth factor modulates synaptic transmission between sympathetic neurons and cardiac myocytes’, *J Neurosci*, 17, pp. 9573–9582. Available at: https://www.ncbi.nlm.nih.gov/pubmed/9391012.

Louch, W. E., Koivumäki, J. T. and Tavi, P. (2015) ‘Calcium signalling in developing cardiomyocytes: Implications for model systems and disease’, *Journal of Physiology*. Blackwell Publishing Ltd, pp. 1047–1063. doi: 10.1113/jphysiol.2014.274712.

Louch, W. E., Sheehan, K. A. and Wolska, B. M. (2011) ‘Methods in cardiomyocyte isolation, culture, and gene transfer’, *Journal of Molecular and Cellular Cardiology*. NIH

Public Access, pp. 288–298. doi: 10.1016/j.yjmcc.2011.06.012.

Luttrell, L. M. (2006) ‘Transmembrane signaling by G protein-coupled receptors’, *Methods Mol Biol*, 332, pp. 3–49. doi: 10.1385/1-59745-048-0:1.

Lyons, G. E. *et al.* (1990) ‘Developmental regulation of myosin gene expression in mouse cardiac muscle’, *Journal of Cell Biology*, 111(6 I), pp. 2427–2436. doi: 10.1083/jcb.111.6.2427.

Maxwell Cowan, W. *et al.* (1984) ‘Regressive events in neurogenesis’, *Science*, 225(4668), pp. 1258–1265. doi: 10.1126/science.6474175.

Mayer, D. C. G. and Leinwand, L. A. (1997) ‘Sarcomeric gene expression and contractility in myofibroblasts’, *Journal of Cell Biology*, 139(6), pp. 1477–1484. doi: 10.1083/jcb.139.6.1477.

McCully, B. H. *et al.* (2013) ‘Sympathetic cardiac hyperinnervation and atrial autonomic imbalance in diet-induced obesity promote cardiac arrhythmias’, *Am J Physiol Heart Circ Physiol*. 2013/09/10, 305(10), pp. H1530--7. doi: 10.1152/ajpheart.00196.2013.

McDermott, B. and Bell, D. (2007) ‘NPY and Cardiac Diseases’, *Current Topics in Medicinal Chemistry*, 7(17), pp. 1692–1703. doi: 10.2174/156802607782340939.

McMurray, J. *et al.* (2005) ‘Practical recommendations for the use of ACE inhibitors, beta-blockers, aldosterone antagonists and angiotensin receptor blockers in heart failure: Putting guidelines into practice’, *European Journal of Heart Failure*. Eur J Heart Fail, pp. 710–721. doi: 10.1016/j.ejheart.2005.07.002.

Mendis, S. *et al.* (2011) ‘World Health Organization definition of myocardial infarction: 2008-09 revision’, *International Journal of Epidemiology*, 40(1), pp. 139–146. doi: 10.1093/ije/dyq165.

Meng, W. and Takeichi, M. (2009) ‘Adherens junction: molecular architecture and regulation.’, *Cold Spring Harbor perspectives in biology*. Cold Spring Harb Perspect Biol. doi: 10.1101/cshperspect.a002899.

Meszaros, J. G. *et al.* (2000) ‘Identification of G protein-coupled signaling pathways in cardiac fibroblasts: Cross talk between G(q) and G(s)’, *American Journal of Physiology - Cell Physiology*, 278(1 47-1). doi: 10.1152/ajpcell.2000.278.1.c154.

Mias, C. *et al.* (2013) ‘Cardiac fibroblasts regulate sympathetic nerve sprouting and neurocardiac synapse stability’, *PLoS ONE*, 8(11). doi: 10.1371/journal.pone.0079068.

Michael, G. J. *et al.* (1997) 'Nerve growth factor treatment increases brain-derived neurotrophic factor selectively in TrkA-expressing dorsal root ganglion cells and in their central terminations within the spinal cord', *Journal of Neuroscience*, 17(21), pp. 8476–8490. doi: 10.1523/jneurosci.17-21-08476.1997.

Michaelevski, I. and Lotan, I. (2011) 'Role of neuronal potassium M-channels in sympathetic regulation of cardiac function', *Journal of Physiology*. J Physiol, pp. 2659–2660. doi: 10.1113/jphysiol.2011.210161.

Minichiello, L. and Klein, R. (1996) 'TrkB and TrkC neurotrophin receptors cooperate in promoting survival of hippocampal and cerebellar granule neurons', *Genes and Development*, 10(22), pp. 2849–2858. doi: 10.1101/gad.10.22.2849.

Miquerol, L. *et al.* (2010) 'Biphasic development of the mammalian ventricular conduction system', *Circ Res*. 2010/05/15, 107(1), pp. 153–161. doi: 10.1161/circresaha.110.218156.

MITCHELL, G. A. (1953) 'The innervation of the heart.', *British heart journal*, 15(2), pp. 159–171. doi: 10.1136/hrt.15.2.159.

Mocchetti, I. *et al.* (1989) 'Regulation of nerve growth factor biosynthesis by β-adrenergic receptor activation in astrocytoma cells: A potential role of c-Fos protein', *Proceedings of the National Academy of Sciences of the United States of America*, 86(10), pp. 3891–3895. doi: 10.1073/pnas.86.10.3891.

Mok, S. A., Lund, K. and Campenot, R. B. (2009) 'A retrograde apoptotic signal originating in NGF-deprived distal axons of rat sympathetic neurons in compartmented cultures', *Cell Research*, 19(5), pp. 546–560. doi: 10.1038/cr.2009.11.

Molloy, N. H., Read, D. E. and Gorman, A. M. (2011) 'Nerve growth factor in cancer cell death and survival', *Cancers*. Cancers (Basel), pp. 510–530. doi: 10.3390/cancers3010510.

Moseley, M. E. *et al.* (1993) 'Early detection of regional cerebral ischemia using high-speed MRI', *Stroke*, 24(12 Suppl), pp. I60--5. Available at: http://www.ncbi.nlm.nih.gov/pubmed/8249022.

Myles, R. C. *et al.* (2012) 'Local beta-adrenergic stimulation overcomes source-sink mismatch to generate focal arrhythmia', *Circ Res*. 2012/04/28, 110(11), pp. 1454–1464. doi: 10.1161/circresaha.111.262345.

Nagueh, S. F. (2020) ‘Heart failure with preserved ejection fraction: insights into diagnosis and pathophysiology’, *Cardiovascular Research*. doi: 10.1093/cvr/cvaa228.

NAPOLITANO, L. M. *et al.* (1965) ‘INTRINSIC INNERVATION OF THE HEART’, *The American journal of physiology*, 208, pp. 455–458. doi: 10.1152/ajplegacy.1965.208.3.455.

Netter (2019) *Netter’s Clinical Anatomy*. 4th edn. Elsevier Inc.

Nielsen, E. *et al.* (2009) ‘Normal right ventricular three-dimensional architecture, as assessed with diffusion tensor magnetic resonance imaging, is preserved during experimentally induced right ventricular hypertrophy’, *Anat Rec (Hoboken)*. 2009/03/24, 292(5), pp. 640–651. doi: 10.1002/ar.20873.

Nikolaev, V. O. *et al.* (2006) ‘Cyclic AMP imaging in adult cardiac myocytes reveals far-reaching β1-adrenergic but locally confined β2-adrenergic receptor-mediated signaling’, *Circulation Research*, 99(10), pp. 1084–1091. doi: 10.1161/01.RES.0000250046.69918.d5.

Nikolaev, V. O. *et al.* (2010) ‘β2-adrenergic receptor redistribution in heart failure changes cAMP compartmentation’, *Science*, 327(5973), pp. 1653–1657. doi: 10.1126/science.1185988.

Nindl, W. *et al.* (2004) ‘Expression of basic fibroblast growth factor isoforms in postmitotic sympathetic neurons: Synthesis, intracellular localization and involvement in karyokinesis’, *Neuroscience*, 124(3), pp. 561–572. doi: 10.1016/j.neuroscience.2003.11.032.

Nomura, M. *et al.* (2011) ‘Facilitated intracellular transport of TrkA by an interaction with nerve growth factor’, *Developmental Neurobiology*, 71(7), pp. 634–649. doi: 10.1002/dneu.20879.

North, A. C., Hargreaves, D. J. and McKendrick, J. (1999) ‘The influence of in-store music on wine selections’, *Journal of Applied Psychology*, 84(2), pp. 271–276. doi: 10.1037/0021-9010.84.2.271.

Novak, P. *et al.* (2009) ‘Nanoscale live cell imaging using hopping probe ion conductance microscopy’, *Nat Methods*, 6(4), pp. 279–281. doi: 10.1038/nmeth.1306.

Oben, J. A. *et al.* (2003) ‘Norepinephrine and neuropeptide Y promote proliferation and collagen gene expression of hepatic myofibroblastic stellate cells’, *Biochemical and*

Biophysical Research Communications, 302(4), pp. 685–690. doi: 10.1016/S0006-291X(03)00232-8.

Ogawa, S. *et al.* (1992) 'Direct contact between sympathetic neurons and rat cardiac myocytes in vitro increases expression of functional calcium channels', *J Clin Invest*, 89, pp. 1085–1093. doi: 10.1172/JCI115688.

Oh, Y. *et al.* (2016) 'Functional coupling with cardiac muscle promotes maturation of hPSC-derived sympathetic neurons', *Cell Stem Cell*, 19, pp. 95–106. doi: 10.1016/j.stem.2016.05.002.

Opie, L. H. (2004) *Heart Physiology : From Cell to Circulation*. 4th edn. Philadelphia: Lippincott Williams and Wilkins.

Ottaviano, F. G. and Yee, K. O. (2011) 'Communication signals between cardiac fibroblasts and cardiac myocytes', *Journal of Cardiovascular Pharmacology*. J Cardiovasc Pharmacol, pp. 513–521. doi: 10.1097/FJC.0b013e31821209ee.

Park, J. and Tallquist, M. D. (2018) 'Cardiac Fibroblast', in *Encyclopedia of Cardiovascular Research and Medicine*. Elsevier, pp. 420–433. doi: 10.1016/b978-0-12-809657-4.99828-4.

Paur, H. *et al.* (2012) 'High levels of circulating epinephrine trigger apical cardiodepression in a β 2-adrenergic receptor/Gi-dependent manner: A new model of takotsubo cardiomyopathy', *Circulation*, 126(6), pp. 697–706. doi: 10.1161/CIRCULATIONAHA.112.111591.

Pazyra-Murphy, M. F. *et al.* (2009) 'A retrograde neuronal survival response: Target-derived neurotrophins regulate MEF2D and bcl-w', *Journal of Neuroscience*, 29(20), pp. 6700–6709. doi: 10.1523/JNEUROSCI.0233-09.2009.

Pedroza, M. *et al.* (2016) 'STAT-3 contributes to pulmonary fibrosis through epithelial injury and fibroblast-myofibroblast differentiation', *The FASEB Journal*, 30(1), pp. 129–140. doi: 10.1096/fj.15-273953.

Pellieux, C. *et al.* (2000) 'Neuropeptide Y (NPY) potentiates phenylephrine-induced mitogen-activated protein kinase activation in primary cardiomyocytes via NPY Y5 receptors', *Proceedings of the National Academy of Sciences of the United States of America*, 97(4), pp. 1595–1600. doi: 10.1073/pnas.030533197.

Peters, N. S. (1996) 'New insights into myocardial arrhythmogenesis: distribution of gap-

junctional coupling in normal, ischaemic and hypertrophied human hearts', *Clin Sci (Lond)*. 1996/06/01, 90(6), pp. 447–452.

Pianca, N. *et al.* (2019) 'Cardiac sympathetic innervation network shapes the myocardium by locally controlling cardiomyocyte size through the cellular proteolytic machinery', *Journal of Physiology*, 597(14), pp. 3639–3656. doi: 10.1113/JP276200.

Picht, E. *et al.* (2007) 'SparkMaster: Automated calcium spark analysis with ImageJ', *American Journal of Physiology - Cell Physiology*, 293(3). doi: 10.1152/ajpcell.00586.2006.

Piquereau, J. *et al.* (2010) 'Postnatal development of mouse heart: Formation of energetic microdomains', *Journal of Physiology*, 588(13), pp. 2443–2454. doi: 10.1113/jphysiol.2010.189670.

Pittenger, G. and Vinik, A. (2003) 'Nerve growth factor and diabetic neuropathy', *Experimental Diabesity Research*. Taylor and Francis Ltd., pp. 271–285. doi: 10.1155/EDR.2003.271.

Pons, J. *et al.* (2008) 'Interactions of multiple signaling pathways in neuropeptide Y-mediated bimodal vascular smooth muscle cell growth', *Canadian Journal of Physiology and Pharmacology*, 86(7), pp. 438–448. doi: 10.1139/Y08-054.

Prando, V. *et al.* (2018) 'Dynamics of neuroeffector coupling at cardiac sympathetic synapses', *The Journal of Physiology*, 596(11), pp. 2055–2075. doi: 10.1113/JP275693.

PRICE, Z. *et al.* (1959) 'Ultrastructure of the dog cardiac muscle cell.', *Circulation research*, 7, pp. 858–865. doi: 10.1161/01.RES.7.6.858.

Priori, S. G. *et al.* (2015) '2015 ESC Guidelines for the management of patients with ventricular arrhythmias and the prevention of sudden cardiac death: The Task Force for the Management of Patients with Ventricular Arrhythmias and the Prevention of Sudden Cardiac Death of the Europe', *Eur Heart J*. 2015/09/01. doi: 10.1093/eurheartj/ehv316.

Protas, L. *et al.* (2003) 'Neuropeptide Y is an essential in vivo developmental regulator of cardiac ICa,L', *Circ Res*, 93(10), pp. 972–979. doi: 10.1161/01.RES.0000099244.01926.56.

Protas, L. and Robinson, R. B. (1999) 'Neuropeptide Y contributes to innervation-dependent increase in I(Ca, L) via ventricular Y2 receptors', *Am J Physiol*, 277(3 Pt 2), pp. H940--6. Available at: http://www.ncbi.nlm.nih.gov/pubmed/10484414.

Putcha, G. V., Deshmukh, M. and Johnson, E. M. (1999) 'BAX translocation is a critical event in neuronal apoptosis: Regulation by neuroprotectants, BCL-2, and caspases', *Journal of Neuroscience*, 19(17), pp. 7476–7485. doi: 10.1523/jneurosci.19-17-07476.1999.

Quaife-Ryan, G. A. *et al.* (2017) 'Multicellular transcriptional analysis of mammalian heart regeneration', *Circulation*, 136(12), pp. 1123–1139. doi: 10.1161/CIRCULATIONAHA.117.028252.

Randall, W. C. *et al.* (1968) 'Patterns of sympathetic nerve projections onto the canine heart', *Circ Res*, 22(3), pp. 315–323. Available at: http://www.ncbi.nlm.nih.gov/pubmed/5639044.

Reece (2011) *Campbell biology*. Boston: Benjamin Cummings / Pearson, ©2011.

Reuter, H. *et al.* (2005) 'Na+-Ca2+exchange in the regulation of cardiac excitation-contraction coupling', *Cardiovascular Research*. Cardiovasc Res, pp. 198–207. doi: 10.1016/j.cardiores.2005.04.031.

Riccio, A. *et al.* (1997) 'An NGF-TrkA-mediated retrograde signal to transcription factor CREB in sympathetic neurons', *Science*, 277(5329), pp. 1097–1100. doi: 10.1126/science.277.5329.1097.

Rodríguez, M., Lucchesi, B. R. and Schaper, J. (2002) 'Apoptosis in myocardial infarction', *Annals of Medicine*. Ann Med, pp. 470–479. doi: 10.1080/078538902321012414.

Ruohonen, S. T. *et al.* (2008) 'Transgenic mice overexpressing neuropeptide y in noradrenergic neurons: A novel model of increased adiposity and impaired glucose tolerance', *Diabetes*, 57(6), pp. 1517–1525. doi: 10.2337/db07-0722.

Sakai, K. *et al.* (2017) 'Functional innervation of human induced pluripotent stem cell-derived cardiomyocytes by co-culture with sympathetic neurons developed using a microtunnel technique', *Biochemical and Biophysical Research Communications*, 494(1–2), pp. 138–143. doi: 10.1016/j.bbrc.2017.10.065.

Salameh, A. and Dhein, S. (2005) 'Culture of neonatal cardiomyocytes', in *Practical Methods in Cardiovascular Research*. Springer Berlin Heidelberg, pp. 568–576. doi: 10.1007/3-540-26574-0_29.

Sands, G. B. *et al.* (2005) 'Automated imaging of extended tissue volumes using confocal

microscopy', *Microscopy Research and Technique*, 67(5), pp. 227–239. doi: 10.1002/jemt.20200.

Schmitt, B. *et al.* (2009) 'Three-dimensional alignment of the aggregated myocytes in the normal and hypertrophic murine heart', *J Appl Physiol (1985)*. 2009/07/25, 107(3), pp. 921–927. doi: 10.1152/japplphysiol.00275.2009.

Seidah, N. G. *et al.* (1996) 'Cellular processing of the nerve growth factor precursor by the mammalian pro-protein convertases', *Biochemical Journal*, 314(3), pp. 951–960. doi: 10.1042/bj3140951.

Seki, S. *et al.* (2003) 'Fetal and postnatal development of Ca2+ transients and Ca2+ sparks in rat cardiomyocytes', *Cardiovascular Research*, 58(3), pp. 535–548. doi: 10.1016/S0008-6363(03)00255-4.

Settanni, G., Cattaneo, A. and Carloni, P. (2003) 'Molecular dynamics simulations of the NGF-TrkA domain 5 complex and comparison with biological data', *Biophysical Journal*, 84(4), pp. 2282–2292. doi: 10.1016/S0006-3495(03)75034-6.

Shao, Y. *et al.* (2002) 'Pincher, a pinocytic chaperone for nerve growth factor/TrkA signaling endosomes', *Journal of Cell Biology*, 157(4), pp. 679–691. doi: 10.1083/jcb.200201063.

Shcherbakova, O G *et al.* (2007) 'Organization of beta-adrenoceptor signaling compartments by sympathetic innervation of cardiac myocytes', *J Cell Biol*, 176, pp. 521–533. doi: 10.1083/jcb.200604167.

Shcherbakova, Olga G. *et al.* (2007) 'Organization of β-adrenoceptor signaling compartments by sympathetic innervation of cardiac myocytes', *Journal of Cell Biology*, 176(4), pp. 521–533. doi: 10.1083/jcb.200604167.

Shelton, D. L. and Reichardt, L. F. (1984) 'Expression of the β-nerve growth factor gene correlates with the density of sympathetic innervation in effector organs', *Proceedings of the National Academy of Sciences of the United States of America*, 81(24 I), pp. 7951–7955. doi: 10.1073/pnas.81.24.7951.

Simpson, P. and Savion, S. (1982) 'Differentiation of rat myocytes in single cell cultures with and without proliferating nonmyocardial cells. Cross-striations, ultrastructure, and chronotropic response to isoproterenol', *Circulation Research*, 50(1), pp. 101–116. doi: 10.1161/01.RES.50.1.101.

Smeyne, R. J. *et al.* (1994) ‘Severe sensory and sympathetic neuropathies in mice carrying a disrupted Trk/NGF receptor gene’, *Nature*, 368(6468), pp. 246–249. doi: 10.1038/368246a0.

Sreejit, P., Kumar, S. and Verma, R. S. (2008) ‘An improved protocol for primary culture of cardiomyocyte from neonatal mice’, *In Vitro Cellular and Developmental Biology - Animal*, 44(3–4), pp. 45–50. doi: 10.1007/s11626-007-9079-4.

Sun, K. H. *et al.* (2016) ‘α-smooth muscle actin is an inconsistent marker of fibroblasts responsible for force-dependent TGFβ activation or collagen production across multiple models of organ fibrosis’, *American Journal of Physiology - Lung Cellular and Molecular Physiology*, 310(9), pp. L824–L836. doi: 10.1152/ajplung.00350.2015.

Suthahar, N. *et al.* (2017) ‘From Inflammation to Fibrosis—Molecular and Cellular Mechanisms of Myocardial Tissue Remodelling and Perspectives on Differential Treatment Opportunities’, *Current Heart Failure Reports*. Current Science Inc., pp. 235–250. doi: 10.1007/s11897-017-0343-y.

Takeuchi, A. *et al.* (2012) ‘Sympathetic neurons modulate the beat rate of pluripotent cell-derived cardiomyocytes in vitro’, *Integrative Biology (United Kingdom)*, 4(12), pp. 1532–1539. doi: 10.1039/c2ib20060k.

Takeuchi, A. *et al.* (2013) ‘Microfabricated device for co-culture of sympathetic neuron and iPS-derived cardiomyocytes’, in *Proceedings of the Annual International Conference of the IEEE Engineering in Medicine and Biology Society, EMBS*. Annu Int Conf IEEE Eng Med Biol Soc, pp. 3817–3820. doi: 10.1109/EMBC.2013.6610376.

Tan, C. M. J. *et al.* (2018) ‘The role of neuropeptide Y in cardiovascular health and disease’, *Frontiers in Physiology*. Frontiers Media S.A., p. 1281. doi: 10.3389/fphys.2018.01281.

Thaemert, J. C. (1969) ‘Fine structure of neuromuscular relationships in mouse heart’, *The Anatomical Record*, 163(4), pp. 575–585. doi: 10.1002/ar.1091630409.

Toni, T., Dua, P. and Van Der Graaf, P. H. (2014) ‘Systems pharmacology of the NGF signaling through p75 and TrkA receptors’, *CPT: Pharmacometrics and Systems Pharmacology*, 3(12). doi: 10.1038/psp.2014.48.

Totland, M. Z. *et al.* (2020) ‘Regulation of gap junction intercellular communication by connexin ubiquitination: physiological and pathophysiological implications’, *Cellular*

and Molecular Life Sciences. Springer, pp. 573–591. doi: 10.1007/s00018-019-03285-0.

Trautwein, W. and Uchizono, K. (1963) 'Electron microscopic and electrophysiologic study of the pacemaker in the sino-atrial node of the rabbit heart', *Zeitschrift für Zellforschung und Mikroskopische Anatomie*, 61(1), pp. 96–109. doi: 10.1007/BF00341523.

Travers, J. G. *et al.* (2016) 'Cardiac fibrosis: The fibroblast awakens', *Circulation Research*. Lippincott Williams and Wilkins, pp. 1021–1040. doi: 10.1161/CIRCRESAHA.115.306565.

Tsien (1979) 'Cellular and subcellular mechanisms of cardiac pacemaker oscillations', *J Exp Biol*, 81, pp. 205–215.

Veeraraghavan, R., Poelzing, S. and Gourdie, R. G. (2014) 'Intercellular electrical communication in the heart: a new, active role for the intercalated disk', *Cell Commun Adhes*, 21(3), pp. 161–167. doi: 10.3109/15419061.2014.905932.

Vermij, S. H., Abriel, H. and van Veen, T. A. B. (2017) 'Refining the molecular organization of the cardiac intercalated disc', *Cardiovascular research*, pp. 259–275. doi: 10.1093/cvr/cvw259.

Villarreal, F. *et al.* (2009) 'Regulation of cardiac fibroblast collagen synthesis by adenosine: Roles for Epac and PI3K', *American Journal of Physiology - Cell Physiology*, 296(5). doi: 10.1152/ajpcell.00291.2008.

Wang, X. H. and Poo, M. M. (1997) 'Potentiation of developing synapses by postsynaptic release of neurotrophin-4', *Neuron*, 19(4), pp. 825–835. doi: 10.1016/S0896-6273(00)80964-2.

Wehrens, X. H. *et al.* (2003) 'FKBP12.6 deficiency and defective calcium release channel (ryanodine receptor) function linked to exercise-induced sudden cardiac death', *Cell*. 2003/07/03, 113(7), pp. 829–840.

Weidmann, S. (1966) 'Cardiac muscle: the functional significance of the intercalated disks', *Ann N Y Acad Sci*, 137(2), pp. 540–542. Available at: http://www.ncbi.nlm.nih.gov/pubmed/5229813.

Weingart, R. (1974) 'The permeability to tetraethylammonium ions of the surface membrane and the intercalated disks of sheep and calf myocardium', *J Physiol*, 240(3), pp. 741–762. Available at: http://www.ncbi.nlm.nih.gov/pubmed/4416405.

Wengrowski, A. M. *et al.* (2015) 'Optogenetic release of norepinephrine from cardiac sympathetic neurons alters mechanical and electrical function', *Cardiovascular Research*. doi: 10.1093/cvr/cvu258.

Wiesmann, C. and De Vos, A. M. (2001) 'Nerve growth factor: Structure and function', *Cellular and Molecular Life Sciences*. Birkhauser Verlag Basel, pp. 748–759. doi: 10.1007/PL00000898.

Williams, G. S. *et al.* (2013) 'Mitochondrial calcium uptake', *Proc Natl Acad Sci U S A*. 2013/06/14, 110(26), pp. 10479–10486. doi: 10.1073/pnas.1300410110.

Wlesmann, C. *et al.* (1999) 'Crystal structure of nerve growth factor in complex with the ligand- binding domain of the TrkA receptor', *Nature*, 401(6749), pp. 184–188. doi: 10.1038/43705.

Wong, S. T. *et al.* (2001) 'Adenylyl Cyclase 3 Mediates Prostaglandin E2-induced Growth Inhibition in Arterial Smooth Muscle Cells', *Journal of Biological Chemistry*, 276(36), pp. 34206–34212. doi: 10.1074/jbc.M103923200.

Wyatt, S. *et al.* (1997) 'Sympathetic neuron survival and TrkA expression in NT3-deficient mouse embryos', *EMBO Journal*, 16(11), pp. 3115–3123. doi: 10.1093/emboj/16.11.3115.

Wyatt, S. *et al.* (1999) 'Selective regulation of trkC expression by NT3 in the developing peripheral nervous system', *Journal of Neuroscience*, 19(15), pp. 6559–6570. doi: 10.1523/jneurosci.19-15-06559.1999.

Xie, Y. *et al.* (2010) 'So little source, so much sink: requirements for afterdepolarizations to propagate in tissue', *Biophys J*. 2010/09/08, 99(5), pp. 1408–1415. doi: 10.1016/j.bpj.2010.06.042.

Yang, H. Q. *et al.* (2019) 'β2-Adrenergic Stimulation Compartmentalizes β1 Signaling into Nanoscale Local Domains by Targeting the C-Terminus of β1-Adrenoceptors', *Circulation Research*, 124(9), pp. 1350–1359. doi: 10.1161/CIRCRESAHA.118.314322.

Yang, K. *et al.* (2008) ' Neuropeptide Y is produced in visceral adipose tissue and promotes proliferation of adipocyte precursor cells via the Y1 receptor ', *The FASEB Journal*, 22(7), pp. 2452–2464. doi: 10.1096/fj.07-100735.

Zaglia, T. *et al.* (2013) 'Cardiac sympathetic neurons provide trophic signal to the heart via beta2-adrenoceptor-dependent regulation of proteolysis', *Cardiovasc Res*, 97, pp.

240–250. doi: 10.1093/cvr/cvs320.

Zaglia, T. *et al.* (2014) ‘Atrogin-1 deficiency promotes cardiomyopathy and premature death via impaired autophagy’, *J Clin Invest*. 2014/05/03, 124(6), pp. 2410–2424. doi: 10.1172/JCI66339 66339 [pii].

Zaglia, T. and Mongillo, M. (2017) ‘Cardiac sympathetic innervation, from a different point of (re)view’, *The Journal of Physiology*, 595(12), pp. 3919–3930. doi: 10.1113/JP273120.

Zaika, O., Zhang, J. and Shapiro, M. S. (2011) ‘Functional role of M-type (KCNQ) K(+) channels in adrenergic control of cardiomyocyte contraction rate by sympathetic neurons’, *J Physiol*, 589, pp. 2559–2568. doi: 10.1113/jphysiol.2010.204768.

Zhang, M. *et al.* (2001) ‘Cardiomyocyte grafting for cardiac repair: Graft cell death and anti-death strategies’, *Journal of Molecular and Cellular Cardiology*, 33(5), pp. 907–921. doi: 10.1006/jmcc.2001.1367.

Zhang, P., Su, J. and Mende, U. (2012) ‘Cross talk between cardiac myocytes and fibroblasts: From multiscale investigative approaches to mechanisms and functional consequences’, *American Journal of Physiology - Heart and Circulatory Physiology*. Am J Physiol Heart Circ Physiol. doi: 10.1152/ajpheart.01167.2011.

Zipes, D. P. (2008) ‘Heart-brain interactions in cardiac arrhythmias: role of the autonomic nervous system’, *Cleve Clin J Med*. 2008/06/11, 75 Suppl 2, pp. S94--6.

Zukowska-Grojec, Z. and Vaz, A. C. (1988) ‘Role of neuropeptide Y (NPY) in cardiovascular responses to stress’, *Synapse*, 2(3), pp. 293–298. doi: 10.1002/syn.890020319.

Zurn, A. (1992) ‘Fibroblast growth factor differentially modulates the neurotransmitter phenotype of cultured sympathetic neurons’, *Journal of Neuroscience*, 12(11), pp. 4195–4201. doi: 10.1523/jneurosci.12-11-04195.1992.

PHD COURSE ACTIVITIES

PUBLICATIONS

Abstracts:

- M Mongillo, M Franzoso, V Prando, *L Dokshokova*, A Di Bona, C Basso, J Gorelik, L Vitiello, T Zaglia "The neuro-cardiac junction defines an extracellular microdomain required for neurotrophic signalling", Eur. Heart J Vol 41, Issue Supp2 (2020) doi.org/10.1093/ehjci/ehaa946.3589
- V Prando, S Bertoli, G Favaro, M Guescini, V Di Mauro, A Di Bona, F lo Verso, R Soares, *L Dokshokova*, P Da Costa Martins, M Capri, S Salvioli, C Franceschi, D Catalucci, M Mongillo, M Sandri, T Zaglia "Circulating muscle-derived MIR-206 links skeletal muscle dysfunction to cardiac autonomic denervation", Vasc. Pharmacol Vol 132 (2020) doi.org/10.1016/j.vph.2020.106742

Manuscripts in preparation

- M Ronfini, V Prando, A Scalco, *L Dokshokova*, E Lazzeri, I Costantini, L Alàn, N Pianca, A Di Bona, A Incensi, F S Pavone, L Sacconi, V Donadio, V Carelli, L Scorrano, T Zaglia, M Mongillo “The mitochondrial Optic atrophy factor-1 (Opa1) is required to sustain cardiac sympathetic innervation”.
- *L Dokshokova*, M Franzoso, A Di Bona, V Prando, O Marin, C Basso, J Gorelik, L Vitiello, T Zaglia, M Mongillo “The neuro-cardiac junction defines an extracellular microdomain required for neurotrophic signalling”.
- *L Dokoshkova*, A Campo, G Borile, N Moro, V Prando, I Barison, T Zaglia, M Mongillo “Development of a protocol for in vitro maturation of neonatal cardiomyocytes”.

PRESENTATIONS

Poster sessions:

- New culture protocol promotes in vitro maturation of neonatal cardiomyocytes - 2018 Preganziol (TV), Italy

- Improved culture protocol promotes structural and functional maturation of neonatal rat ventricular myocytes in vitro - 2019, 16th Annual Retreat" VIMM RETREAT", Treviso, Italy
- The neuro-cardiac junction defines an extracellular microdomain required for neurotrophic signalling - 2019 XXIII ISHR World Congress, Beijing China

Oral presentation:

- Advanced methods to study sympathetic neurons/cardiac cells interactions 2019, 18th Annual Retreat" VIMM RETREAT", Treviso, Italy

ACKNOWLEDGMENTS

To begin with, I would like to genially thank Prof. Giuseppe Faggian for the presented opportunity to be at the University of Verona, for his wise advice and incredible help in any situation. I would like to extremely thank Prof. Marco Mongillo for his incredible impact on my knowledge and scientific progress and his constant invaluable help and unimaginable contribution to the whole of this work. I want to say infinite thanks to Prof. Julia Gorelik, who gave me the opportunity to be on the edge of advanced science, who incredibly supported me throughout my scientific career and to her wise leadership, helped me to improve. I want to say a huge thanks to Dr.ssa Tanya Zaglia for the incredible help in my scientific work and in my life, for a large number of enthusiastic scientific ideas and tips that helped me to compose an interesting integral story from my scientific data. A huge thanks I want to say to Dr. Sanchez Alonso-Mardones, a man who has an incredible talent to be a superhuman and knows how to do everything, all kinds of methods and techniques, who has excellent logical thinking, which helped me to cut off all unnecessary and focus on the main goals and thanks for the constant help and incredible work on even the smallest details.

I would like to thank a lot Dr. Antonio Campo who was one of the first who introduce me to the work with living cells and made a huge contribution to the work on the novel medium for neonatal cardiomyocytes. I would like to thank a lot Dr. Mauro Franzoso for his great contribution to the study of NGF signalling.

I want to say a huge thank to my colleagues in the laboratory of Prof. Marco Mongillo and Dr.ssa Tania Zaglia who have become my true friends. I want to thank for constant help in the laboratory and general life Anna Di Bona, Arianna Scalco, Marco Ronfini, Nicol Moro, Veronica Vita, Silvia Bertoli, Valentina Prando.

I want to say a huge thank to my colleague in the laboratory of Prof. Julia Gorelik. I want to thank for the constant support and help Peter Wright, Benedict Reilly-O'Donnell, Anita Alvarez Laviada, Roman Medvedev, Neda Mohamadi, Pamela Swiatlowska, Elisa Ferraro, Qianqian Song, Sasha Judina, Alveera Hasan, Zoe Kwan, and others. I want to say a special thank, to Ivan Diakonov for his help in the laboratory and for the isolation of healthy cardiomyocytes. I want to thank Wong Tsz Fung Marcus for his huge contribution with $\beta_{1/2}$ blocking experiments.

Also, I would like to say a special thanks to Laura Fedele, for obtaining the amazing data of action potential.
I would like to thank an important people for me, my family, who supported me from every moment of my life, and who correctly set goals in childhood, so I was able to fulfil my dream and find myself in the world of science.